GDAŃSK UNIVERSITY OF TECHNOLOGY

The author of the doctoral dissertation: Przemysław Gnatowski
Scientific discipline: Chemical Sciences

DOCTORAL DISSERTATION

Title of doctoral dissertation: Development of biodegradable polyurethanes with hydrogel coatings for the controlled delivery of active substances

Title of doctoral dissertation (in Polish): Opracowanie biodegradowalnych poliuretanów z powłokami hydrożelowymi do kontrolowanego uwalniania substancji aktywnych

Supervisor *signature*	Second supervisor *signature*
dr hab. inż. Justyna Kucińska-Lipka	prof. dr hab. n. med. Andrzej Tadeusz Skorek
Auxiliary supervisor n.a *signature*	Cosupervisor n.a. *signature*
n.a.	n.a.

Gdańsk, year 2026

GDAŃSK UNIVERSITY OF TECHNOLOGY

STATEMENT

The author of the doctoral dissertation: Przemysław Gnatowski

I, the undersigned, declare that I am aware that in accordance with the provisions of Art. 27 (1) and (2) of the Act of 4th February 1994 on Copyright and Related Rights (Journal of Laws of 2021, item 1062), the university may use my doctoral dissertation entitled:

Development of biodegradable polyurethanes with hydrogel coatings for the controlled delivery of active substances

for scientific or didactic purposes.[1]

Gdańsk,..... .....
signature of the PhD student

Aware of criminal liability for violations of the Act of 4th February 1994 on Copyright and Related Rights and disciplinary actions set out in the Law on Higher Education and Science (Journal of Laws 2021, item 478), as well as civil liability, I declare, that the submitted doctoral dissertation is my own work.

I declare, that the submitted doctoral dissertation is my own work performed under and in cooperation with the supervision of dr hab. inż. Justyna Kucińska-Lipka, the second supervision of prof. dr hab. n. med. Andrzej Tadeusz Skorek.

This submitted doctoral dissertation has never before been the basis of an official procedure associated with the awarding of a PhD degree.

All the information contained in the above thesis which is derived from written and electronic sources is documented in a list of relevant literature in accordance with Art. 34 of the Copyright and Related Rights Act.

I confirm that this doctoral dissertation is identical to the attached electronic version.

Gdańsk,..... .....
signature of the PhD student

I, the undersigned, agree to include an electronic version of the above doctoral dissertation in the open, institutional, digital repository of Gdańsk University of Technology.

Gdańsk,..... .....
signature of the PhD student

[1] Art 27. 1. Educational institutions and entities referred to in art. 7 sec. 1 points 1, 2 and 4–8 of the Act of 20 July 2018 – Law on Higher Education and Science, may use the disseminated works in the original and in translation for the purposes of illustrating the content provided for didactic purposes or in order to conduct research activities, and to reproduce for this purpose disseminated minor works or fragments of larger works.

2. If the works are made available to the public in such a way that everyone can have access to them at the place and time selected by them, as referred to in para. 1, is allowed only for a limited group of people learning, teaching or conducting research, identified by the entities listed in paragraph 1.

GDAŃSK UNIVERSITY OF TECHNOLOGY

DESCRIPTION OF DOCTORAL DISSERTATION

The Author of the doctoral dissertation: Przemysław Gnatowski
Title of doctoral dissertation: Development of biodegradable polyurethanes with hydrogel coatings for the controlled delivery of active substances

Title of doctoral dissertation in Polish: Opracowanie biodegradowalnych poliuretanów z powłokami hydrożelowymi do kontrolowanego uwalniania substancji aktywnych

Language of doctoral dissertation: English

Supervisor: Justyna Kucińska-Lipka

Second supervisor*: Andrzej Tadeusz Skorek

Date of doctoral defense:

Keywords of doctoral dissertation in Polish: poliuretany, hydrożele, kurkumina, nos, kortykosteroidy

Keywords of doctoral dissertation in English: polyurethanes, hydrogels, curcumin, nose, corticosteroids

Summary of doctoral dissertation in Polish: Niniejsza praca doktorska skupia się na opracowaniu nowego biodegradowalnego systemu uwalniania leków opartego na poliuretanach do zastosowania w medycynie regeneracyjnej. Stworzony system ma zapewnić miejscowe, kontrolowane uwalnianie substancji aktywnych w celu przyspieszenia gojenia tkanek i zminimalizowania powikłań pooperacyjnych, umożliwiając jednocześnie personalizację systemu przy użyciu m.in. druku 3D. W ramach pracy badawczej zsyntezowano i scharakteryzowano 10 typów bazowych poliuretanów alifatycznych na bazie diizocyjanianu heksametylenu, różniących się użytą mieszaniną poliolową, oraz siedem typów bazowych hydrożeli na bazie agaru. Wybrane materiały następnie modyfikowano przy użyciu m.in. kolagenu, diosminy, kurkuminy czy też kortykosetoridu. Właściwości otrzymanych poliuretanów porównano z wydrukami z handlowo dostępnych filamentów do druku 3D. W ramach pracy wytworzono biodegradowalny system typu rdzeń-powłoka do jednoczesnego dostarczania dwóch substancji, oparty na poliuretanie poliestro-eterowym (ET2:ET1:ES1) modyfikowanym kortykosteroidem oraz hydrożelu na bazie agaru modyfikowanym kurkuminą. Niniejsza praca wykazuje, że dostosowanie właściwości materiałowych oraz kontrolowanie uwalniania substancji aktywnych może być alternatywą dla standardowych metod podawania leków po zabiegu chirurgicznym.

Summary of doctoral dissertation in English: This doctoral thesis focuses on the development of a novel biodegradable, polyurethane-based drug delivery system for applications in regenerative medicine. The system is designed to provide localized, controlled release of active substances to accelerate tissue healing and minimize postoperative complications, while also allowing for system customization through techniques such as 3D printing. The research involved synthesizing and characterizing 10 types of base aliphatic polyurethanes derived from hexamethylene diisocyanate, differing in their polyol mixtures, and seven types of base agar-based hydrogels. The chosen materials were subsequently modified with active substances such as collagen, diosmin, curcumin, and a corticosteroid. The properties of the resulting polyurethanes were compared with printouts from commercially available 3D printing filaments. Ultimately, biodegradable core-shell system for the simultaneous delivery of two substances was fabricated, utilizing a corticosteroid-modified ET2:ET1:ES1 polyester-ether polyurethane and a curcumin-modified AG0.6/PVA0.4 hydrogel. This work demonstrates that tailoring material properties and controlling the release of active substances offers an alternative to standard postoperative drug delivery methods.

Acknowledgments

Several people played a decisive role on the path leading to the completion of my PhD, and I would like to express my sincere gratitude to:

My Supervisor, Justyna Kucińska-Lipka, DSc, PhD, for giving me a chance despite the doubts of others, and for guiding me when I struggled to fit into the conventional academic framework;

My Second Supervisor, prof. Andrzej Skorek, MD, for his guidance in shaping the research topic and grounding it in clinical practice;

Maciej Sienkiewicz, PhD, for helping me to develop my practical skills and generously sharing his experience with implementation projects;

prof. Helena Janik and Mohammad Reza Saeb, PhD, for their mentoring and for helping shape me as scientist;

Hubert Cieśliński, DSc, PhD, for his expertise with antibacterial testing and for hours of inspiring, meaningful discussion;

Ewa Augustin, DSc, PhD and Agnieszka Kurdyn, for carrying out cytotoxicity assessment;

All colleagues and doctoral candidates at the Department of Polymer Technology, for the shared knowledge, collaboration and daily laughs;

My research Team - Paweł Szarlej, PhD, Edyta Piłat-Wójcik, Olga Zawadzka, Klaudia Gawin, Wojciech Malottki - or the daily camaraderie and support with challenges large and small;

My Grandma Wiera, for her unwavering faith in me, even without needing to know what a PhD entails;

My Siblings - Arleta, Basia, Rafał and Aneta - for their grounding presence, life lessons and for pulling me back whenever I drifted too deep into abstract science;

My Parents, for more than words can capture: my Mom, Joanna, for sharing fascination with biology and medicine, and my Dad, Krzysztof, for shaping my engineering mindset from my earliest days;

And last, but by no means least, my beloved wife, Malwina, with whom I began this path and with whom I now conclude this chapter. Thank you for walking with me through the good, the hard and the ordinary days, for being my anchor, and for reminding me every day that a rich world exists beyond the University and all the downsides related to it.

A po nocy przychodzi dzień,
A po burzy spokój

Budka Suflera - Jest taki samotny dom

Table of contents

Table of contents 5

Abbreviations 6

1. Introduction 9

2. Research hypothesis and objectives 12

3. Thesis scope and novelty 13

4. Literature review 16

5. Materials and methods 106

6. Development of biodegradable polyurethane matrices 121

7. 3D modelling and evaluation of commercial filaments 133

8. Hydrogel formulation 148

9. Composite implant development 165

10. Conclusions and future outlook 172

11. Scientific achievements 178

12. References 184

List of figures 207

List of tables 215

Abbreviations

AI - Artificial Intelligence

BDA - 1,4-butanediamine

BDI - 1,4-butane diisocyanate

BDO - 1,4-butanediol

CA - cinnamaldehyde,

CFU - colony-forming units,

DABCO - 1,4-diazabicyclo[2.2.2]octane

DAS - dialdehyde starch

DBTDL - dibutyltin dilaurate

DBU - 1,8-diazabicycloundec-7-ene

DDS - drug delivery system,

DEG - diethylene glycol

ECM - extracellular matrix ECM

ED - ethylenediamine

EDTA - ethylenediaminetetraacetic acid

EG - ethylene glycol

FDM – fused deposition modelling

FDM - fused deposition modelling,

FQLs - fluoroquinolones

GA - glutaraldehyde

Gel-MA - gelatin methacrylate,

GelMA - methacrylated gelatin

H_{12}MDI - 4,4’-dicyclohexylmethane diisocyanate

HA - Hyaluronic acid

HA-MA - Hyaluronic acid methacrylate

HDI - 1,6-hexamethylene diisocyanate

HMDA - hexamethylenediamine

IPDI - isophorone diisocyanate

iPSCs - pluripotent stem cells

LDI – L-lysine-based diisocyanates

MDA - 4,4’-methylenedianiline

MDI - 4,4’-methylenediphenyl diisocyanate

ML - Machine Learning

MRI - magnetic resonance imaging

NHCs - N-heterocyclic carbenes

NIPUs - non-isocyanate polyurethanes

NP – nanoparticle,

PAA - poly(acrylic acid),

PAAm - polyacrylamide,

PCL - poly(ε-caprolactone)

PDO - 1,3-propanediol

PE – poly(ethylene)

PEG - poly(ethylene glycol)

PEGDA - poly(ethylene glycol) diacrylate

PEG-DA - poly(ethylene glycol)-diacrylate,

PGA - poly(glycolic acid)/poly(glycolide)

pHEMA - poly(2-hydroxyethyl methacrylate),

PHMG - polyhexamethylene guanidine hydrochloride,

PLA - poly(lactic acid)/poly(lactide)

PLGA - poly(lactic-co-glycolic acid),

PMMA - poly(methyl methacrylate)

PNIPAAm - poly(N-isopropylacrylamide),

PPG - polypropylene glycol

PTFE – poly(tetrafluoroethylene)

PTMEG - poly(tetrahydrofuran)/poly(tetramethylene ether) glycol/poly(tetramethylene oxide)

PU – polyurethane

PVA - poly(vinyl alcohol)

PVP - poly(vinyl pyrrolidone),

SLA - stereolithography,

SMP - Shape-memory polymer

TBD - 1,5,7-triazabicyclodec-5-ene

TDA - 2,4-toluene diamine

TDI - toluene diisocyanate

THF - tetrahydrofuran

TPU – thermoplastic polyurethane

WBPU - waterborne polyurethanes

1. Introduction

The development of biodegradable polyurethanes with hydrogel coatings for the controlled delivery of active substances addresses a primary challenge in medicine and localized pharmacotherapy. Designing such multifunctional therapeutic devices requires structural matrices capable of safe integration and gradual degradation within biological systems. As such devices are designed to have direct contact with the living tissues, the base materials, polyurethanes and hydrogels, have to meet the requirements for biomaterials. The field categorizes these materials into three generations: bioinert, bioactive and biodegradable [1]. Novel therapeutic devices should ideally belong to third-generation of biomaterials, demonstrating non-toxicity, integration with host tissues and degradation while being replaced by natural cellular structures. The application of such advanced biomaterials is particularly crucial in surgical interventions. Although, providing structural support is the most important aspect of the therapeutic device, it is only one aspect of patient recovery.

Ensuring the success of an implant and promoting complete tissue regeneration heavily relies on effective postoperative care, which frequently requires the simultaneous administration of pharmacological agents. Despite numerous active agents for disease treatment being evaluated, their direct application in postoperative care remains difficult. Achieving therapeutic drug concentrations at specific target sites presents a persistent clinical obstacle [2]. This limitation arises primarily from distinct biological and physical distribution barriers that depend on the administration route. Drugs administered using traditional methods disperse throughout the entire organism, which often leads to subtherapeutic concentrations at the targeted tissue and increases the risk of off-target toxicity, placing a particular burden on the kidneys and liver. On the other hand, conventional locally applied formulations, are subject to physiological barriers such as rapid clearance by interstitial fluids, enzymatic degradation or limited tissue retention, which typically prevent sustained drug activity at the surgical site [3].

Standard delivery routes currently fail to satisfy comprehensive patient and medical requirements [3]. Oral administration offers ease of use but yields poor absorption rates, low bioavailability and may trigger gastrointestinal complications [4]. Parenteral routes provide stable absorption and high bioavailability but disrupt patient functioning requiring frequent medical interventions or the attachment of specialized devices [5]. Inhalation offers rapid delivery but remains highly patient-dependent, as concurrent conditions may severely decrease absorption efficiency [6]. Transdermal systems provide stable absorption but restrict the types of transportable drugs and fail to deliver substances to deeply located tissues [7]. Consequently, patients require pain-free, non-disruptive methods that promote rapid recovery. Physicians require delivery systems that ensure stable bioavailability, minimize systemic organ burden and operate independently of patient compliance, overcoming transport disturbances.

Implantable drug delivery devices offer a viable alternative to conventional administration routes, directly addressing the aforementioned clinical requirements. Such devices allow for

localized drug delivery, which ensures achieving high, therapeutic concentrations of active substances, while simultaneously limiting systemic toxicity. The most used topical agents include glucocorticosteroids, antibacterials, anesthetics and selected cytostatics, which are often expected to have anti-inflammatory, antibacterial, analgesic or antiproliferative effects by modulating signaling pathways strictly within the affected tissue. This approach is employed in fields such as dermatology, ophthalmology, pulmonology and interventional oncology. Increasing local bioavailability allows for a reduction in the total therapeutic dose, thereby directly optimizing the treatment's safety profile.

Although early non-degradable concepts emerged in the late 1980s, current research prioritizes biodegradable systems that eliminate the need for secondary surgical removal or subsequent surgeries, decreasing therapy costs and improving patient comfort [8]. To overcome these delivery barriers and provide stable mechanical support, achieving organ-level shape modification, tailored polymeric matrices are required. Due to the combination of unique properties and susceptibility to modification, thermoplastic polyurethanes (TPUs) are commonly used polymers in the field of medical applications and possess a well-established history in the medical sector. Commercial formulations, such as Pellethane™ [9], Tecoflex™ [10], Estane™ [11] and BioSpan™ [12], function primarily as biostable materials for long-term implantation and typically rely on aromatic diisocyanates. However, regenerative medicine requires novel aliphatic PU structures that degrade congruently with new tissue formation, avoiding the release of toxic aromatic byproducts [13]. The structure of thermoplastic polyurethanes consists of alternating rigid and flexible segments which, under specific thermodynamic conditions, undergo phase separation, generating a nanodomain morphology. Tailoring this segmented structure allows to precisely control mechanical properties and facilitates advanced manufacturing techniques, such as fused deposition modeling (FDM) [14]. Although FDM enables the creation of patient-specific geometries, currently available commercial filaments often lack the required bioactivity, fail to provide controlled drug delivery or exhibit unexpected cytotoxicity [15]. Consequently, addressing these limitations requires the development of custom, biofunctionalized polymeric systems.

To optimize biocompatibility and regulate degradation kinetics, polyurethanes often require structural or surface modifications. Integrating natural polymers, nanoparticles or active pharmacological agents into the polymer matrix can induce bioactivity [16]. In the proposed research, the customized polyurethane functions as a stable, degradable matrix for targeted active substance release. This localized delivery mechanism ensures appropriate therapeutic dosing, increases bioavailability and minimizes systemic side effects.

The primary function of drug-eluting stents is the continuous, controlled release of a therapeutic substance. While polyurethanes provide necessary structural support, bare polymer matrices often face limitations in accommodating multiple therapeutic agents with distinct physicochemical properties. To overcome this challenge, hydrogel coatings can be applied to the polyurethane surface. Hydrogels, characterized by their highly porous, hydrophilic networks, mimic the natural extracellular matrix (ECM) and establish a highly biocompatible interface with

host tissues [17]. Furthermore, specific hydrogel formulations can incorporate secondary polymers to stabilize hydrophobic active substances within an aqueous environment [18]. This hybrid architecture, combining a solid polyurethane core with a soft hydrogel shell, facilitates the simultaneous incorporation and controlled release of two distinct pharmacological agents.

This dissertation proposes a dual-delivery implant system designed to release both a corticosteroid and curcumin. In postoperative care, corticosteroids act to suppress local inflammation and prevent tissue hyperplasia. Concurrently, curcumin promotes collagen deposition and exhibits antibacterial effects. Employing the hydrogel coating for an initial release phase and the degrading polyurethane core for long-term sustained release provides a synergistic therapeutic effect. This localized dual-delivery mechanism aims to accelerate tissue healing, mitigate postoperative complications and bypass the limitations of conventional systemic administration methods.

2. Research hypothesis and objectives

The primary objective of this doctoral dissertation is to design, synthesize and evaluate a biodegradable, dual-drug eluting implant system for application in regenerative medicine. To achieve it, the multifunctional system based on the novel aliphatic polyurethane matrix and a curcumin-loaded hydrogel coating was developed. This system aims to provide localized, controlled release of active substances to accelerate tissue healing and minimize postoperative complications.

The hypothesis of this research states that **applying a curcumin-loaded, polymer-stabilized hydrogel coating to an aliphatic polyurethane core creates a functional dual-delivery system capable of sequential active substance release**. Furthermore, this hypothesis postulates that the **composite architecture provides an initial antibacterial release from the hydrogel shell**, followed by a sustained release of a secondary pharmacological agent from the degrading polyurethane core, without compromising the mechanical integrity or cytocompatibility of the implant.

To test this hypothesis and achieve the primary objective, the research methodology encompasses the following specific tasks:

- Synthesize and characterize novel biodegradable aliphatic polyurethanes. This includes tailoring the polyol mixture to achieve specific mechanical properties, target degradation profiles and processability suitable for medical applications.
- Fabricate implant prototypes using FDM to determine the influence of the implant design on the viability of processing using this method.
- Evaluate the structural, thermal and biological suitability of commercially available medical-grade filaments for FDM. This task focused on assessing the advantages of the newly developed polyurethane material to the current market solutions regarding printability and cytocompatibility.
- Formulate and optimize aqueous hydrogel bioinks capable of stabilizing hydrophobic active substances. This task focuses on utilizing secondary polymers (such as poly(vinyl alcohol) and poly(vinylpyrrolidone)) as interfacial mediators to incorporate curcumin into an agar matrix without the use of toxic organic solvents.
- Assess the biological response to the developed materials. This includes performing cytotoxicity assays on the raw polymers, the hydrogel coatings and the final implant, as well as testing the antimicrobial efficacy of the curcumin-loaded hydrogels.
- Characterize the dual-release pharmacokinetics of the composite system. This task aims to quantify the initial release profile of curcumin from the outer hydrogel layer and the sustained release profile of a corticosteroid from the degrading polyurethane core.

3. Thesis scope and novelty

The scope of this research includes the entire material development process, from the evaluation of existing commercial baselines to the fabrication of a novel composite implant. Specifically, the project begins with a deep literature survey focused on the current developments in biomaterial-based drug delivery systems (DDS) and the role of polyurethane materials in this field. The particular emphasis placed on the polyurethane synthesis and structure-properties relations allowed to design and synthesize custom aliphatic polyurethanes (PUs) with the tailored degradation profiles. To assess the possibility of application of newly developed material in DDS field, a case study on the drug eluting nasal stent was proposed and conducted. This particular application was chosen due to the high clinical prevalence of postoperative complications following nasal and paranasal sinus surgery, including mucosal inflammation, tissue hyperplasia and bacterial contamination. Furthermore, the intricate and patient-specific geometry of the nasal cavity necessitates patient-specific structural support, making it an optimal candidate for customized fused deposition modeling (FDM). Evaluating the system in this specific anatomical context provides a rigorous benchmark for assessing material processing, localized dual-drug elution, degradation kinetics and mucosal cytocompatibility. The effectiveness of novel PU material was compared with commercially available filaments for fused deposition modeling (FDM), evaluating their structural, thermal and biological suitability for nasal septum implants.

Concurrently, due to observed limitations, the scope covers the formulation of aqueous hydrogel bioinks. This involves utilizing secondary polymers as interfacial mediators to stabilize hydrophobic active substances (curcumin) within an agar matrix. Finally, the project scope culminates in assembling these two distinct material systems into a core-shell architecture, followed by a comprehensive *in vitro* evaluation of its dual-release pharmacokinetics, degradation behavior and cytocompatibility.

This dissertation introduces several novel contributions to the fields of biomaterials and targeted drug delivery:

- **Development of a biodegradable core-shell dual-delivery system.** According to the current literature, this research represents the first attempt to create a biodegradable implant combining a thermoplastic polyurethane core with a hydrogel shell for the simultaneous, sequential delivery of a corticosteroid and curcumin. This architecture uniquely addresses the need for both immediate antibacterial action and long-term anti-inflammatory therapy.
- **Green formulation of hydrophobic drugs in aqueous inks.** The research introduces a novel, water-based method for incorporating hydrophobic curcumin into hydrophilic agar networks. By utilizing poly(vinyl alcohol) and poly(vinylpyrrolidone) as interfacial mediators, the methodology avoids toxic organic solvents, preserving the hydrogel’s biocompatibility and printability.

- **Influence of processing on release kinetics.** This work advances the understanding of how advanced manufacturing techniques (such as modification during synthesis versus traditional dip coating) influence the internal morphology of polyurethane matrices and, consequently, the degradation and drug elution profiles.
- **Medical 3D printing.** By establishing that commercial “medical-grade” filaments possess significant biological and functional shortcomings for internal mucosal contact, including the observed cytotoxicity, this work provides a strong rationale for custom aliphatic polyurethane synthesis. Custom materials demonstrate how precise control over soft segments yields superior matrices for personalized FDM printing without releasing toxic aromatic degradation products.

Some of the core findings presented in this thesis have been peer-reviewed and published in international scientific journals. Structure of the dissertation follows a logical progression from material baseline assessment to the development and evaluation of a novel dual-drug delivery implant. The dissertation work cycle was summarized in Figure 1 and is organized as follows:

- Chapter 4 (Literature review): Provides the theoretical background on biomaterials, polyurethane chemistry and hydrogel-based drug delivery systems, identifying the current gaps in postoperative care. This chapter partially adapts material published in [19–23].
- Chapter 5 (Materials and methods): Details the synthesis protocols, hydrogel formulation techniques and characterization methods utilized throughout the project.
- Chapter 6 (Development of biodegradable polyurethane matrices): Analyzes the impact of different polyols on the properties of aliphatic polyurethanes. This chapter incorporates findings published in [24,25].
- Chapter 7 (Evaluation of commercial filaments): Presents the case study of modelling nasal implant and the assessment of existing FDM materials. This chapter incorporates findings published in [24,26].
- Chapter 8 (Hydrogel formulation): Discusses the stabilization of curcumin in aqueous agar networks using secondary polymers.
- Chapter 9 (Composite implant development): Evaluates the complete core-shell system.
- Chapter 10 (Conclusions and future perspectives): Summarizes the primary findings and suggests directions for future clinical applications.

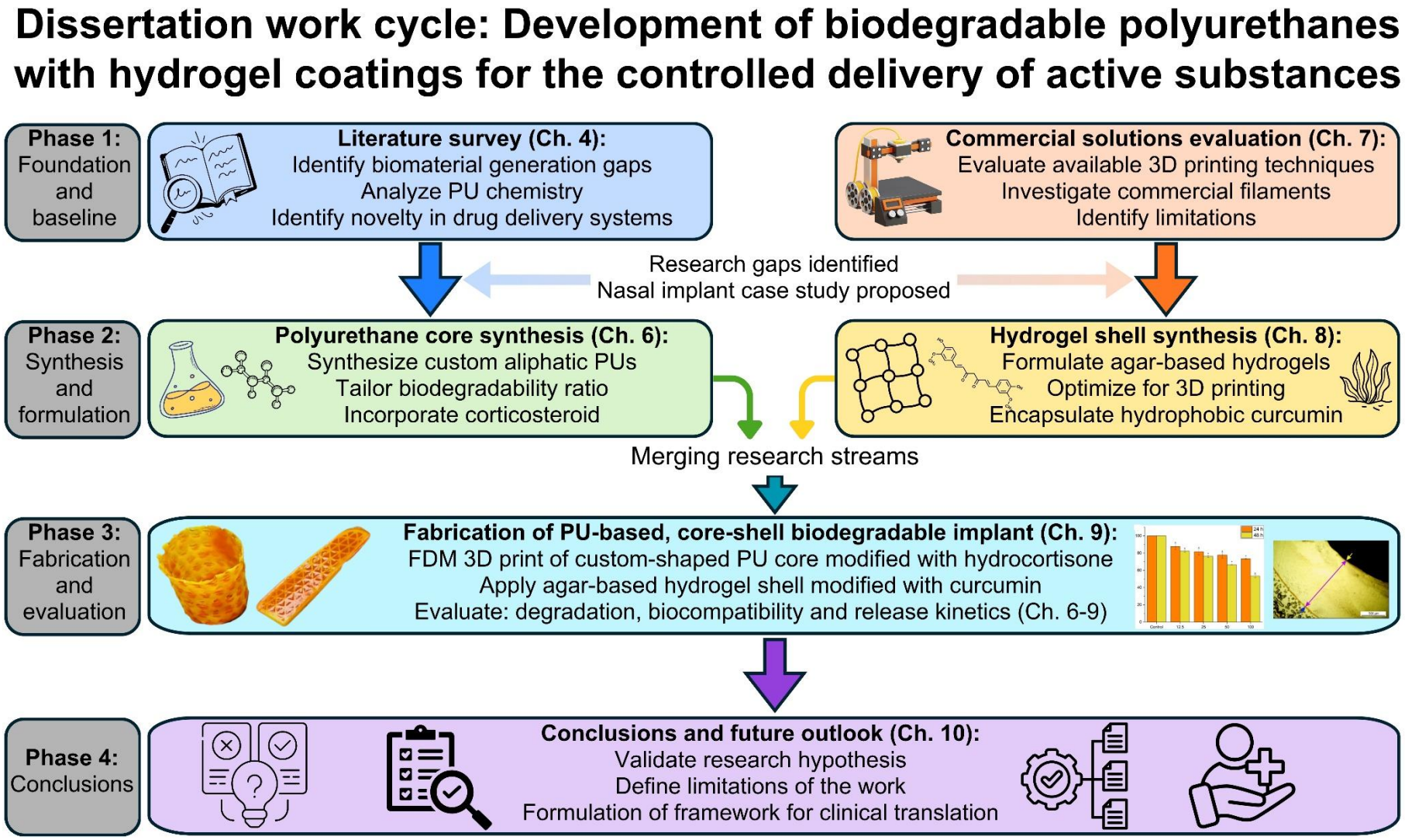


Figure 1 The summary of the dissertation work cycle – from research gaps identification to validation of the research hypothesis. Created with Canva.

4. Literature review

4.1. Evolution of polymeric biomaterials

Polymeric biomaterials interact directly with biological systems to treat, augment or replace specific tissues and organ functions [1]. The scientific consensus regarding the definition of a biomaterial progressed from characterizing these materials as purely pharmacologically inert substances to recognizing them as sophisticated systems intended to actively interact with living tissues [27]. In modern surgical practice, these polymers primarily provide essential mechanical support or facilitate targeted therapeutic outcomes. The development of biomaterials constitutes an evolutionary process driven by continuous advancements in materials science and an expanding comprehension of cell-material interactions at the biological interface [28].

Researchers categorize the evolution of synthetic biomaterials into distinct generations, which provides a systematic framework to analyze their historical and functional development (Figure 2). This classification traces a fundamental shift in the intended material performance. Early clinical applications accepted a passive role, where the host body accepted the foreign material with minimal immune reactivity [29]. Current research paradigms require an active role, where the biomaterial affects its surrounding biological environment and modulates specific cellular responses [30]. Changing focus of research is also evidenced by the number of articles published in the topic of biomaterials. Global research interest in the field of biomaterials has reached an unprecedented scale, with the number of published papers exceeding 150 000 in 2025 alone (Figure 3). This remarkable output establishes the biomaterials discipline as one of the most prominent and rapidly evolving areas in modern science. Despite the observed constant, exponential growth of interest in the general topic, it is obvious that it is driven by bioactive biomaterials (~86 000 entries in 2025) (Figure 4). However, it must be noted that the apparent popularity of the second generation may be somewhat misleading. Although the classification into generations has long been established, researchers frequently use terminology characteristic of second-generation biomaterials to describe third-generation materials, which can be misleading. The increasing number of scientific articles featuring keywords characteristic of specific generations clearly delineates the timeline of their emergence within the scientific community: 2nd generation ~1980, 3rd generation ~2000, 4th generation ~2010. This continuous transition from bioinert to bioactive polymers establishes the theoretical foundation for modern resorbable surgical implants and dual-action composite systems (Figure 5). However, long before the formal categorization of these synthetic generations, early surgical practices relied on naturally derived polymers to address basic clinical needs.

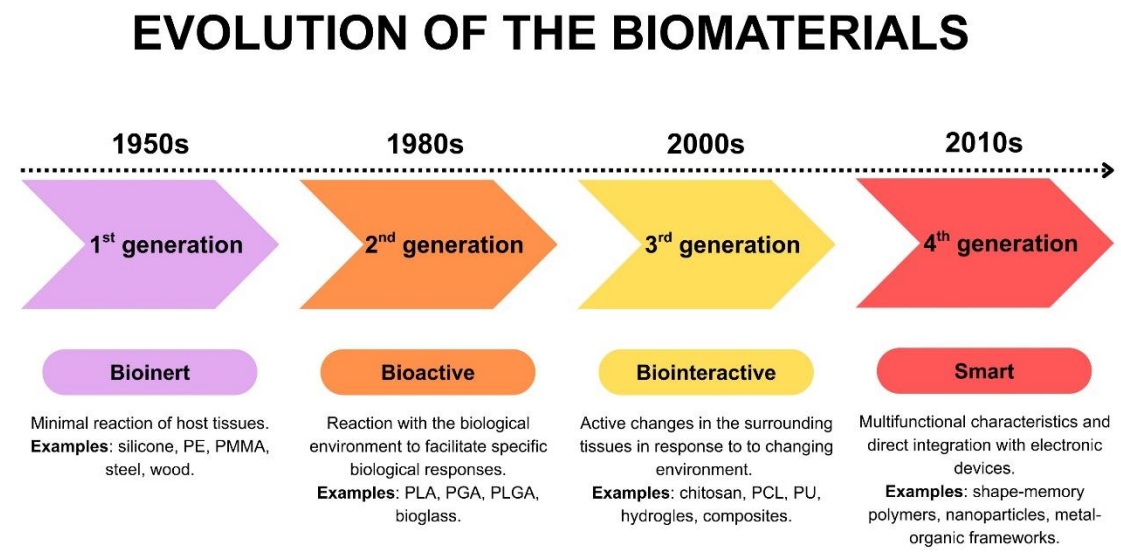


Figure 2 Schematic representation of biomaterials evolution through generations.

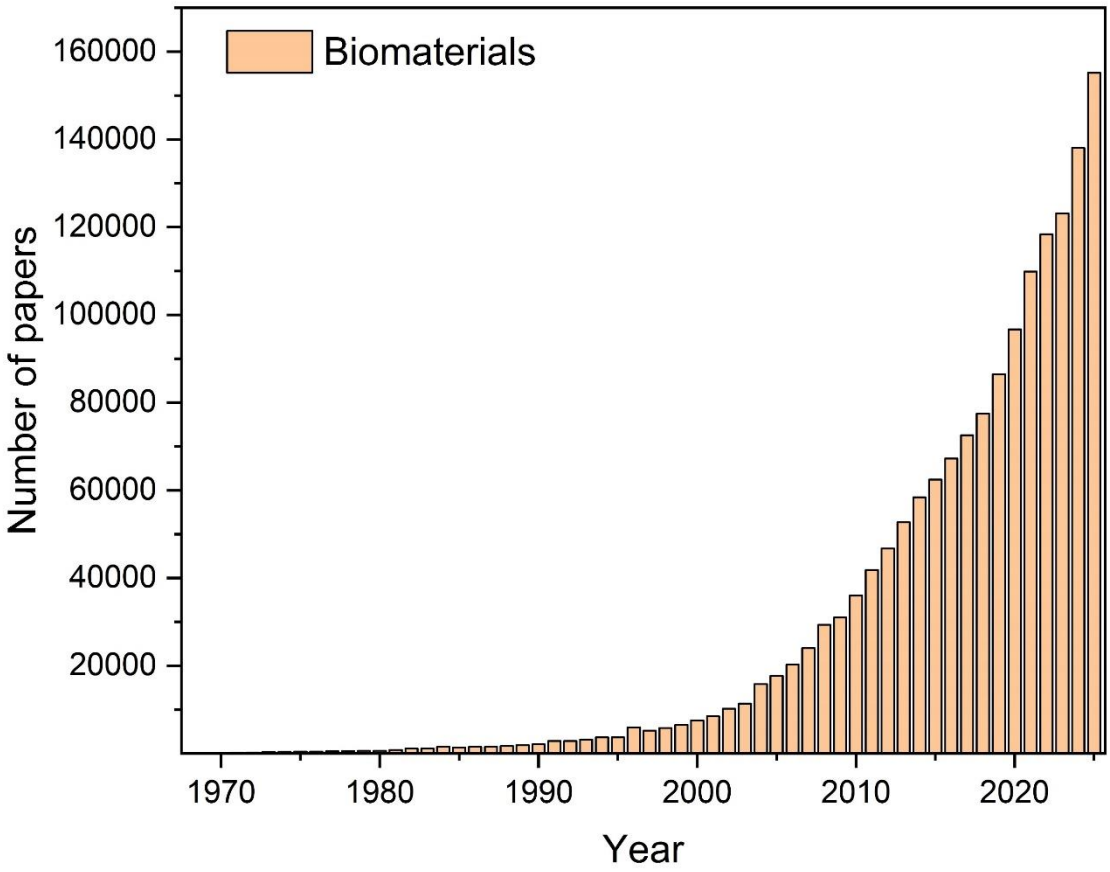


Figure 3 Evolution of research interest in biomaterials. Data base: Scopus within Article title, abstract and keywords. Search query: ("biomaterial" OR "biomedical material*").*

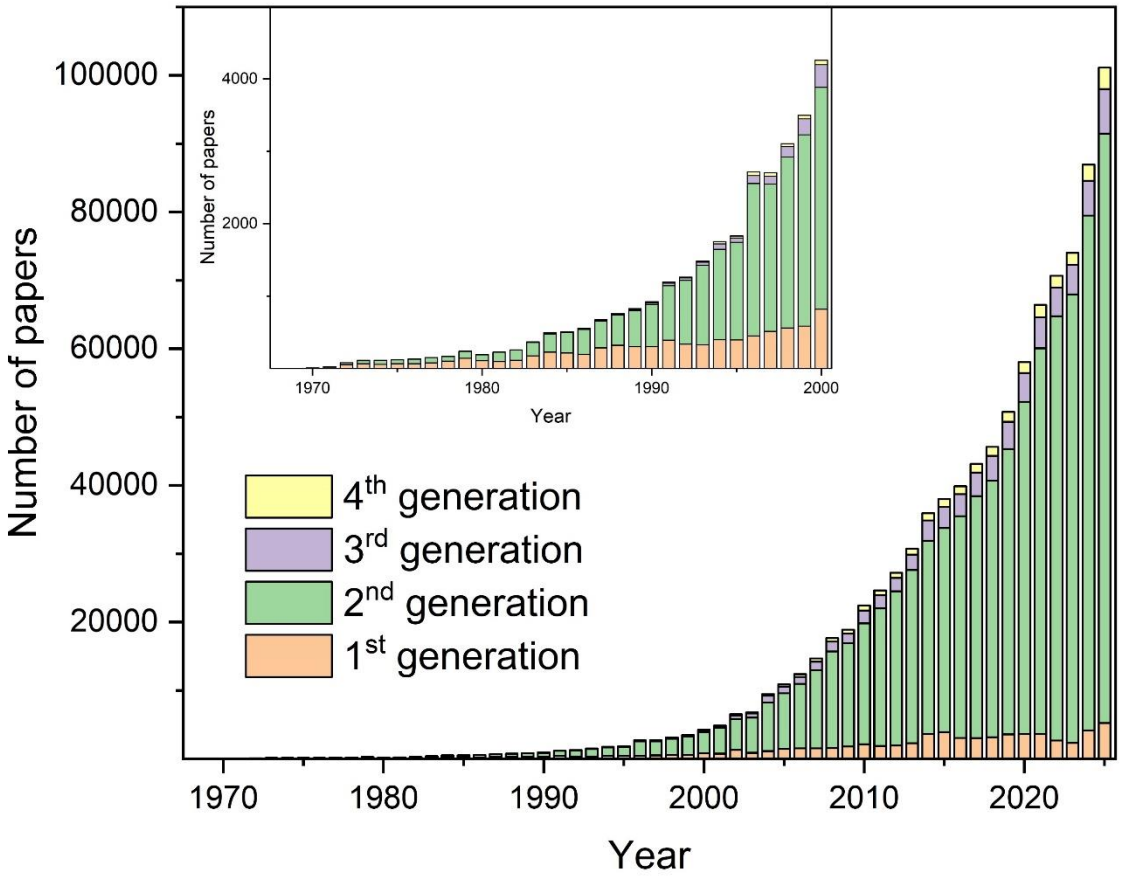


Figure 4 Evolution of biomaterials generations depicted by the changing research interest. Data base: Scopus within Article title, abstract and keywords. Search queries: 1st generation: ("biomaterial" OR "biomedical material*") AND ("first generation" OR "1st generation" OR "bioinert*" OR "inert*" OR "minimal host response" OR "biocompatible"). 2nd generation: ("biomaterial*" OR "biomedical material*") AND ("second generation" OR "2nd generation" OR "bioactive" OR "bioresorbable" OR "biodegradable" OR "bioglass" OR "hydroxyapatite" OR "calcium phosphate" OR "osteo*" OR "osseo*"). 3rd generation: ("biomaterial*" OR "biomedical material*") AND ("third generation" OR "3rd generation" OR "biointeractive" OR "regenerative" OR "biomimetic" OR "tissue engineering" OR "scaffold*" OR "extracellular matrix" OR "ECM" OR "molecular signaling" OR "stem cell*" OR "cellular response"). 4th generation: ("biomaterial*" OR "biomedical material*") AND ("fourth generation" OR "4th generation" OR "smart" OR "electronic*" OR "autonomous" OR "programmable" OR "stimuli-responsive" OR "Theranostic*" OR "nano" OR "cyber" OR "piezoelectric*" OR "sensor" OR "shape-memory" OR "shape memory").*

4.1.1. Historical precursors to biomaterials

The application of polymeric materials in surgical and medical interventions predates modern synthetic chemistry by millennia. Early medical practitioners utilized naturally occurring polymers, such as bitumen, resins and cellulose, to treat wounds and replace missing anatomical structures. Archaeological evidence demonstrates the use of a bitumen paste to form a hemispherical ocular prosthesis in the Bronze Age settlement of Shahr-i Sokhta around 2900 BC [31]. Historical texts suggest that ancient clinicians recognized the rudimentary bioactive properties of these materials. For instance, Assyrian records from the second millennium BC indicate the external application of bitumen to manage localized infections [32]. Subsequent

classical physicians, including Pedanius Dioscorides, recorded the capacity of bitumen to reduce inflammation and promote tissue adhesion [33].

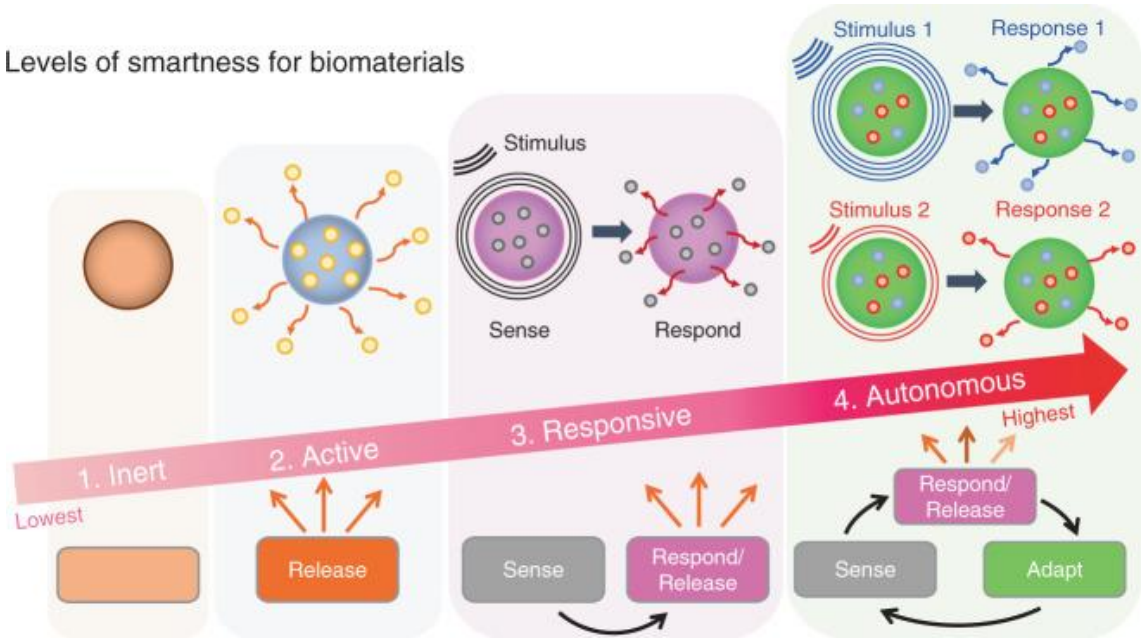


Figure 5 The progression of biomaterials smartness level – from inert materials to fully autonomous systems with closed cycle of sense-response-adapt interactions. Adapted from: [34] under CC BY 4.0 license.

Other naturally derived polymers served functional roles in wound management. Sumerian texts document the use of terebinth (*Pistacia terebinthus*) resin for dermal repair [35]. Furthermore, cellulose-based polymers, specifically linen and cotton, have functioned as suture materials for millennia [36]. These practices established the foundational concept of utilizing pliable, non-metallic materials to support tissue healing.

The introduction of natural rubber from *Hevea brasiliensis* expanded the functional applications of early polymers. Indigenous populations in the Americas processed rubber for various implements, including early prototypes of medical syringes [37]. Following its introduction to Europe in the sixteenth century, rubber found extended medicinal utility. However, its application remained limited by poor mechanical stability and chemical resistance until the development of the vulcanization process by Charles Goodyear in 1839 [38]. While vulcanized rubber provided improved structural integrity, sustained clinical use eventually revealed adverse biological responses, such as latex hypersensitivity [39]. This historical progression illustrates early attempts to balance material properties with biological compatibility. Resolving this tension between structural mechanics and host tissue response continues to direct the design of modern synthetic polymers and biodegradable polyurethanes.

4.1.2.First Generation: Bioinertness and structural permanence

The formal classification of first-generation synthetic biomaterials emerged predominantly in the 50s and 60s of the last century, establishing bioinertness and structural permanence as the first requirements for surgical implants. In 1974, during the sixth “Annual International Biomaterial

Symposium” in USA, the scientific community established a strict consensus, defining a biomaterial exclusively as a “systematically, pharmacologically inert substance designed for implantation within or incorporation with a living system” [40]. At these early stages, researchers and clinicians prioritized the absence of negative biological responses over any potential bioactive effects. The primary surgical objective involved replacing damaged tissue with a permanent, non-reactive substitute that could coexist with surrounding host tissues without altering innate biological functions or physical properties.

Following that, the rigorous procedure of evaluating any foreign material for biomedical use in terms of its immunogenicity and cytotoxicity, as these parameters dictated the severity of the localized tissue reaction, was implemented to the medical practice. To achieve these clinical objectives, synthetic polymers that exhibited minimal chemical reactivity within the host organism were selected. Consequently, early surgical applications relied heavily on synthetic polymers such as poly(methyl methacrylate) (PMMA), poly(tetrafluoroethylene) (PTFE) and poly(ethylene) (PE) due to their exceptional chemical stability and mechanical durability [41]. Clinicians applied these bioinert polymers extensively in purely structural roles, including artificial joints, bone cements and basic prosthetics. For example, PMMA successfully replaced fragile glass and celluloid to become the standard material for ocular prostheses [42].

While first-generation polymers provided essential restoration of mechanical and/or esthetical function, their design fundamentally restricted their long-term clinical efficacy. These materials operate in a strictly passive role; they do not actively interact with the biological environment at the molecular or cellular level. Because they lack the capacity to integrate dynamically with the host, the body often recognizes the permanent synthetic structure as a foreign entity. The host biological response typically attempts to isolate the implant, which often results in the formation of a dense fibrous capsule at the material-tissue interface (Figure 6). Although minimizing scar tissue remained a primary goal of early bioinert designs, the inevitable long-term presence of a non-integrating polymer increased the risks of implant fatigue, chronic inflammation and eventual mechanical failure [43]. This inherent limitation in structural permanence drove the subsequent scientific transition toward materials capable of physiological interaction and controlled degradation.

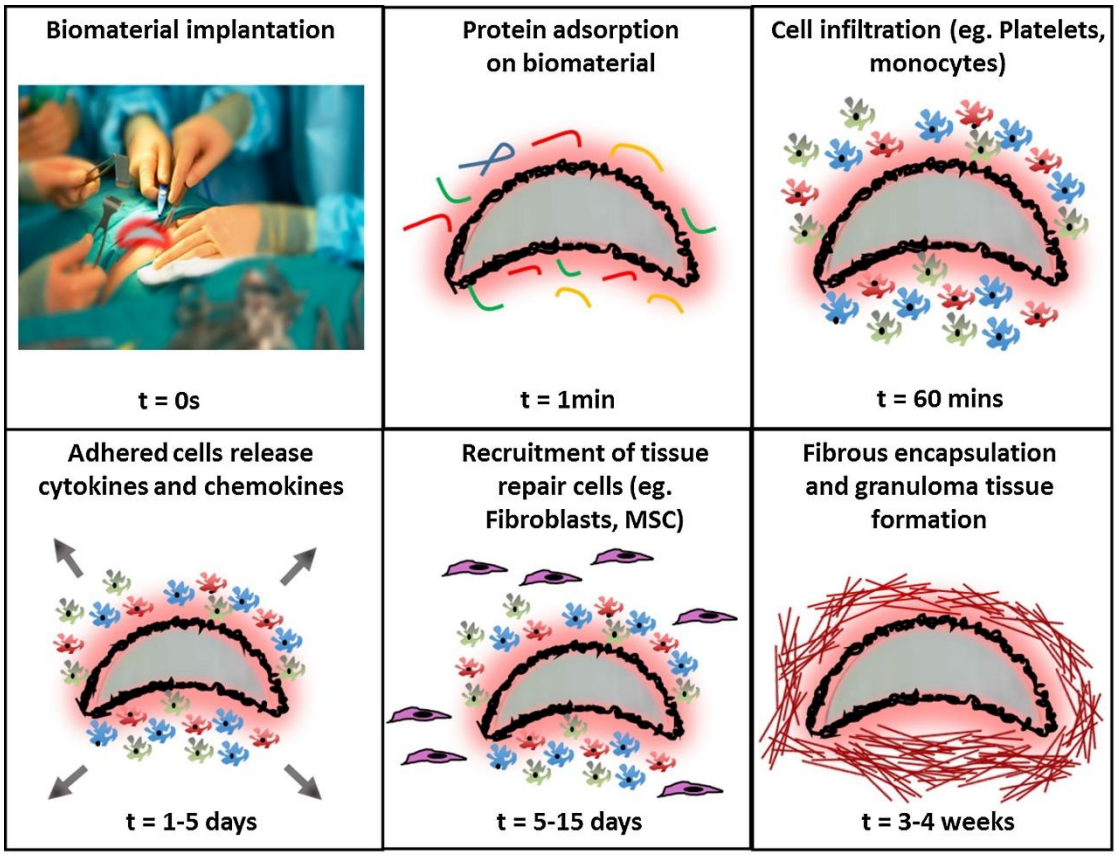


Figure 6 The evolution of host biological response to inert implants. Following inert biomaterial implantation, vascular protein adsorption triggers the recruitment and adhesion of innate immune cells like macrophages and platelets. These cells secrete signaling molecules that recruit fibroblasts and stem cells, ultimately leading to collagen deposition and fibrous encapsulation of the implant. Adapted from: [44] under CC BY-NC-ND 4.0 license.

4.1.3.Second generation: Bioactivity and controlled degradation

The observed clinical limitations of bioinert materials prompted a fundamental paradigm shift in surgical biomaterial design. Thanks to advances in the knowledge of biological mechanisms at bio-interfaces, researchers realized that passive structural substitution was not sufficient in long-term applications and initiated the development of second-generation biomaterials [27]. This classification encompasses bioactive and bioresorbable polymers that actively interact with the physiological environment while simultaneously undergoing controlled degradation. The focus of biomaterials development shifted decisively from a “passive” role to a “bioactive” role. Rather than merely evading the host immune response, these new materials possessed the explicit ability to interact with the biological environment to facilitate specific biological responses. This behavior is depicted in Figure 7. The transition to this second generation represents a critical evolution in surgical practice, as it can be described as the dawn of application-specific materials engineering, when engineers began to design polymers intended to elicit specific, desirable biological responses from the host tissue rather than merely evading immune detection.

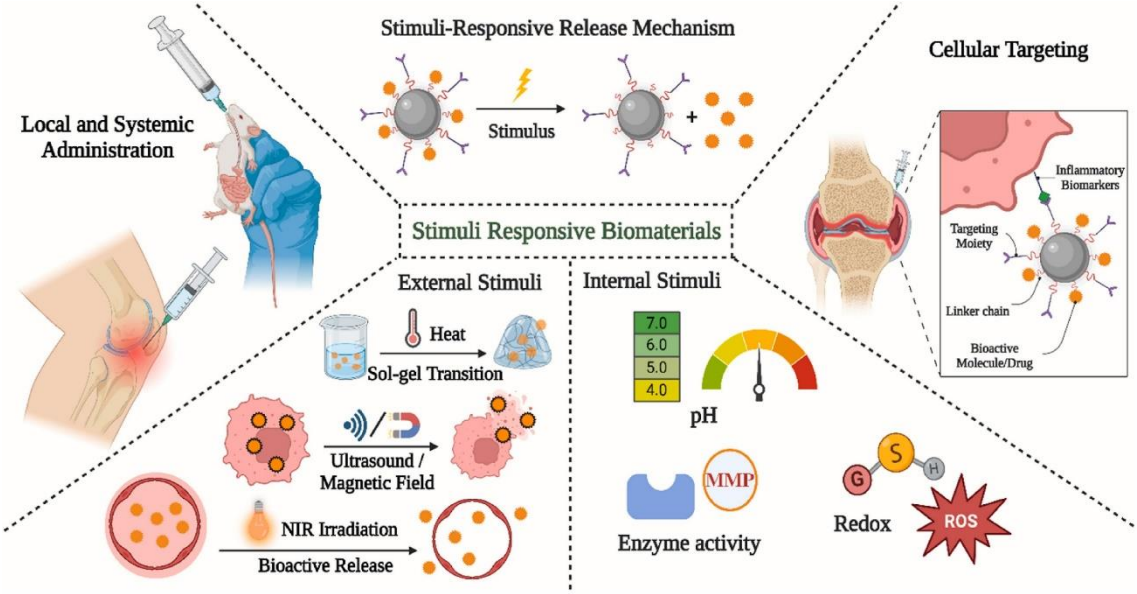


Figure 7 Second generation of biomaterials can adapt dynamically to various stimuli, including pH, light, ultrasound and enzymatic triggers, highlighting their responsive behavior in both internal and external environments. Adapted from: [45] under CC BY-NC-ND 4.0 license.

The origin of the shift into bioactive characteristics traces back to the creation of the first bioactive glass. This established standard of using inert polymers, metals or ceramics changed when Professor Larry L. Hench created and patented bioglass in 1969 and this initial bioactive glass, specifically designated as Bioglass 45S5 has been in clinical use since 1985. The invention of Bioglass demonstrated that a synthetic material could form a direct, cohesive chemical bond with living host tissue [46]. This concept proved highly radical for its era. In fact, an official 1974 scientific consensus still defined a biomaterial strictly as an inert substance, completely excluding bioactive compounds five years after Hench obtained his patent [47]. Historical records suggest that minimizing scar tissue remained the dominant priority at the time, but the clinical success of Bioglass eventually forced researchers to acknowledge that interfacial reactions could successfully drive positive outcomes.

To synthesize materials that exhibit this required bioactivity, two primary methodological approaches are employed [48]. The first approach involves altering the surface structure of the biomaterial to increase surface roughness and porosity. Additionally, the internal architecture of the scaffold must remain tissue-specific, requiring precise control over pore size, shape and interconnectivity to allow proper transport of nutrients to infiltrating cells, actively interacting with the surrounding tissues. These topographical modifications enhance initial protein adsorption and facilitate subsequent cellular adhesion, proliferation and differentiation [49]. Alternatively, manufacturers can apply bioactive ceramic coatings directly onto the polymer surface to stimulate integration with the surrounding ECM and attachment of cells. The examples of different surface modifications were presented in Figure 8.

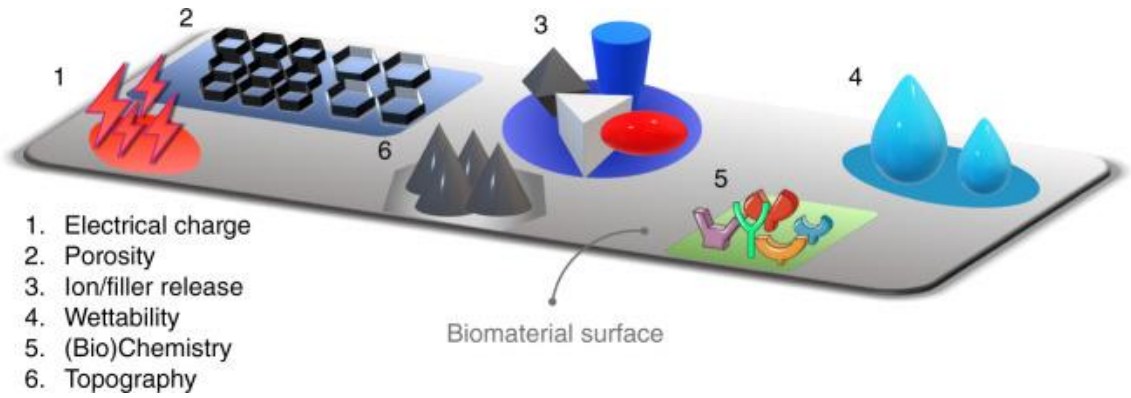


Figure 8 The strategies of surface modifications/ used to improve the degree of interactions on the host-biomaterial interface. Adapted from: [34] under CC BY 4.0 license.

Alongside this emphasis on bioactivity, the second generation also formalized the requirement for controlled degradation. Second-generation biomaterials demonstrated better biocompatibility, biodegradability and the capacity to actively promote tissue regeneration compared to their first-generation predecessors [50]. Prior clinical procedures relied on permanent synthetic structures that often required subsequent surgical extraction. The integration of bioresorbable properties meant that the implant could interact with the biological environment to facilitate biological responses while also being able to degrade safely within the physiological environment. The development of biodegradable polymers perfectly met the expected behavior by providing temporary mechanical support that gradually declines as the host tissue repairs itself. Synthetic absorbable polymers, such as poly(glycolic acid) (PGA) and poly(lactic acid) (PLA), degrade primarily through hydrolysis [51]. The physiological environment cleaves the polymer chains into non-toxic metabolites and body readily metabolizes and excretes these degradation byproducts, preventing localized systemic toxicity [52]. Consequently, biodegradable polymers provide distinct medical, financial and psychological advantages by eliminating the risks and costs associated with extraction surgeries. Furthermore, these systems maintain prolonged drug exposure, thereby offering superior local disease control in the management of chronic conditions characterized by frequent recurrences.

Furthermore, the implementation of biodegradable scaffolds directly addresses the mechanical complications associated with permanent implants. Solid metallic implants often cause stress shielding, a phenomenon where the rigid implant absorbs the majority of physiological loads, leading to adjacent bone resorption and tissue weakening [53]. Biodegradable polymers exhibit lower initial stiffness and elastic moduli compared to metallic counterparts. Because the polymer degrades over time, it progressively transfers the mechanical load to the regenerating host tissue, which stimulates natural cellular remodeling processes [54]. The stiffness and elastic modulus of a polymer scaffold must carefully match the properties of the native tissue at the implantation site. Proper mechanical alignment ensures that the scaffold maintains high initial strength to support tissue integration before dissolution and the subsequent loss of its functional shape [54].

The expansion of second-generation materials also included the extensive integration of naturally derived biodegradable polymers. Natural polymers provide high inherent biocompatibility and favorable degradation profiles. For example, sodium alginate, extracted from brown seaweed, forms highly hydrophilic and bioactive hydrogels suitable for soft tissue regeneration [55]. Similarly, chitosan, derived from the deacetylation of crustacean chitin, functions as a highly biocompatible and biodegradable scaffold. Studies demonstrate that chitosan exhibits intrinsic antimicrobial properties and supports cellular adhesion, making it highly valuable for early tissue engineering applications [56].

Despite demonstrating significant advancements over first-generation bioinert implants, second-generation biomaterials presented distinct physical constraints. Clinical evaluations show that these early bioactive and biodegradable systems exhibited severe limitations regarding their stability, physical durability and intrinsic mechanical strength [57]. A biomaterial must sustain its mechanical integrity long enough to facilitate complete tissue regeneration. However, early resorbable polymers occasionally degraded faster than the native tissue could regenerate, compromising functional repair or lacked the structural robustness required for load-bearing surgical applications [58]. These persistent mechanical and stability limitations subsequently drove the scientific community to conceptualize and develop more advanced third-generation or bio-interactive materials.

4.1.4.Third generation: Biointeractive and biodegradable systems

During the late 90s, biomaterial researchers shifted their focus to combine the advantages of previously introduced materials, creating functional complex systems. The third generation of biomaterials actively combines inherent bioactivity with predictable biodegradability and the ability to react to changing environment, giving it unique ability to not only perform structural functions, but also actively change the surrounding tissues [27]. To achieve this instructive capacity, these materials are designed to stimulate cellular responses at the molecular level, which facilitates accelerated and highly organized tissue regeneration. A one of characteristic of third-generation materials involves their direct structural and biochemical mimicry of the native extracellular matrix, especially in case of wound dressings. To replicate this complex physiological environment, the molecular architectures of both synthetic and natural polymers can be modified, ensuring precise interactions with host cells and controlled degradation profiles [59].

4.1.4.1. Solid materials

Synthetic polyesters, such as PLA and poly(e-caprolactone) (PCL), frequently serve as the structural foundation for biomedical implants due to their high tensile strength and predictable hydrolytic degradation. However, these synthetic polymers inherently lack the specific biological sequences required to promote direct cellular adhesion. To overcome this limitation and force interaction with the body, advanced surface modifications and covalent functionalization can be employed [60]. For example, researchers utilize metal-free click chemistry to functionalize electrospun poly(L-lactide) (PLLA) scaffolds with the Tyr-Ile-Gly-Ser-Arg (YIGSR) peptide, a

sequence derived from the natural protein laminin. Studies demonstrate that presenting this specific peptide on the synthetic surface significantly increases the attachment of neural cells and promotes directed neurite extension [61]. Similarly, PCL surfaces are frequently functionalized with Arg-Gly-Asp (RGD) peptide sequences, which act as universal cell-binding sites to stimulate robust receptor-mediated cellular adhesion and proliferation [62]. Comparison between different modifies substrates is presented in Figure 9.

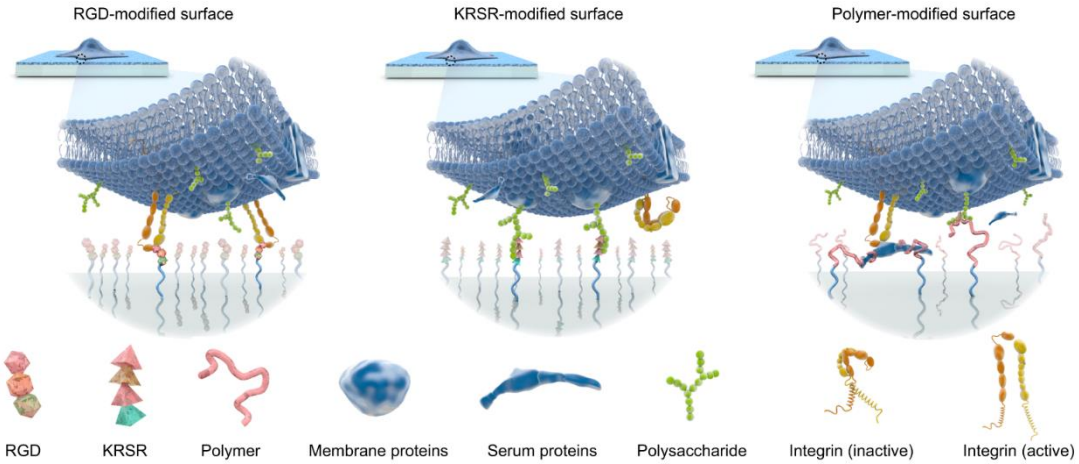


Figure 9 Mechanisms of cellular adhesion on surfaces functionalized with RGD peptides, KRSR sequences and β-amino acid polymers. Adapted from: [63] under CC BY 4.0 license.

While modified polyesters offer excellent structural support, their degradation occasionally releases acidic metabolites that alter the local physiological pH and provoke localized inflammatory responses [64]. To resolve these biochemical limitations, researchers engineered biodegradable polyurethanes as a highly adaptable class of third-generation biomaterials. PUs function as segmented block copolymers, containing alternating hard and soft segments that determine their specific mechanical toughness and elasticity [65]. The chemical composition of these segments is specifically modified to synthesize variants that match the exact mechanical compliance of various host tissues, thereby preventing mechanical failure and stress shielding. To ensure optimal interaction with the host immune system, modern modifications focus on eliminating toxic byproducts. One of the approaches is synthesizing amino acid-modified polyurethanes and waterborne polyurethanes (WBPU) [14]. Evidence demonstrates that these specifically modified polyurethane scaffolds undergo controlled degradation without causing a local accumulation of acidic substances, presenting a distinct biological advantage over bioresorbable polyesters [66]. Furthermore, natural polymers, such as cellulose and chitosan, can be incorporated directly into the polymer chain as chain extenders, which drastically enhances the inherent biocompatibility and cellular recognition of the synthetic core [67,68].

4.1.4.2. Hydrogel materials

Beyond rigid structural support, third-generation systems require a highly interactive, hydrated interface to modulate cellular behavior, a requirement fulfilled by hydrogel-building polymers. While natural polymers provide exceptional inherent bioactivity, they frequently lack the structural durability required for surgical implants, necessitating targeted chemical modifications. Hyaluronic acid (HA) functions as a primary component of native connective tissues and its presence actively promotes targeted cell growth, proliferation and differentiation. However, its high water solubility results in rapid physiological resorption, limiting its applications to only short-term implants [69]. To stabilize the molecule while retaining its biological signaling capacity, researchers created hyaluronic acid methacrylate (HA-MA), enabling the formation of covalent cross-links upon exposure to light, yielding a robust, bio-interactive hydrogel [70]. Examples of HA-MA hydrogels usage in advanced, biointeractive materials were presented in Figure 10.

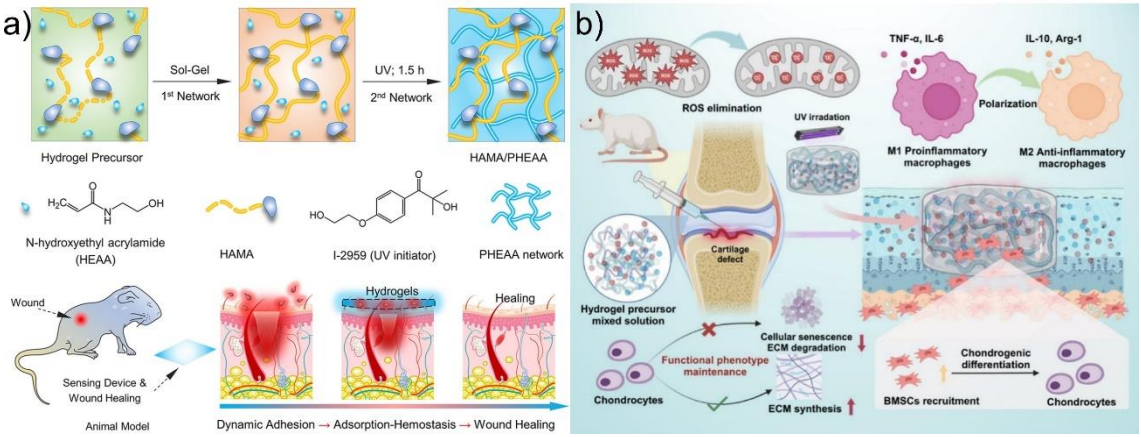


Figure 10 Examples of HA-MA hydrogels usage in biointeractive materials. a) Schematic representation of HA-MA/ poly(N-hydroxyethyl acrylamide) hydrogel synthesis for wound dressing applications. The insets provide the chemical structures for the HEAA monomer, HA-MA biomacromolecules and the I-2959 photoinitiator, alongside the resulting network architecture. Adapted from: [71] under CC BY 4.0 license. b) RGD-modified HA-MA hydrogel co-loaded with cartilaginous inducer Kartogenin (KGN) and anti-aging protein Klotho (HAMA-RGD@KGN/Klotho, HRKK) hydrogel to ameliorate the adverse joint microenvironment and enhance cartilage regeneration. Adapted from: [72] under CC BY 4.0 license.

Other example of natural polymer useful in hydrogel formation is alginate, a polysaccharide extracted from algae, which provides a highly biocompatible environment frequently utilized to encapsulate living cells due to its gentle gelation mechanism in the presence of divalent cations, such as calcium [73]. However, native alginate lacks mammalian cell-adhesive sites and resists degradation in the human body, as mammals lack the specific alginate lyase enzymes required to cleave its polymer chains [74]. To resolve this downside, researchers covalently couple RGD peptide sequences to the alginate backbone, which successfully overrides the inert nature of the polysaccharide and stimulates the adhesion and spreading of encapsulated cells [75]. Furthermore, to facilitate physiological clearance, the polymer can be treated with oxidative reagents or gamma irradiation to proactively reduce its molecular weight, ensuring the degradation byproducts fall below the threshold required for safe renal excretion [76].

Due to downsides of natural polymers, synthetic ones are widely used thanks to their superior mechanical properties and control over the structure. One of the examples is the poly(ethylene glycol) (PEG) representing a universally utilized synthetic polymer in this regard due to its structural consistency and precise chemical control [77]. However, as pure PEG resists protein adsorption, lacks cell-binding spots and resists physiological degradation, it has to undergo multiple structural modifications to be successfully implemented as third generation biomaterial. First, to create a stable network, researchers derivatize PEG with reactive acrylate groups to form poly(ethylene glycol) diacrylate (PEGDA), which allows for precise photo-cross-linking during scaffold fabrication [78]. To force the material to degrade safely within the body, chemists incorporate hydrolytically unstable oligomers, such as those derived from PLA or PGA, directly into the PEGDA backbone [79]. Alternatively, biologically responsive degradation mechanisms can be designed by inserting specific peptide sequences into the polymer chain that cleave only in the presence of specific cell-secreted proteolytic enzymes [80]. Finally, to enable direct cellular interaction, specific peptide sequences (like RGD) can be covalently attach to the PEG network, overriding its natural resistance to cell attachment and transforming it into an instructive matrix [81].

Similarly, poly(vinyl alcohol) (PVA) requires specific modifications to function as an effective third-generation biomaterial. PVA provides high water solubility and elasticity, but researchers must induce crystallinity and stability to utilize it in real-life environments [82]. The physical structure of PVA can be modified through repeated freezing and drying (freeze-thaw) cycles, which induces dense hydrogen bonding between the 1,3-diol backbone subunits [83]. Alternatively, they are treating PVA by e.g., glutaraldehyde (GA), glyoxal or dialdehyde starch (DAS) treatments to chemically crosslink the hydroxyl groups, creating the stable, continuous hydrogel networks [82]. These targeted modifications significantly increase the mechanical properties of the hydrogel, allowing to utilize modified PVA to successfully mimic the elastic properties of human cartilage. To ensure the material eventually resorbs, PVA can be further functionalized with hydrolytically cleavable polyesters, granting control over its degradation timeline [84].

4.1.4.3. Composite materials

The ultimate manifestation of third-generation biomaterials integrates diversely modified polymers with other materials into unified, bio-interactive composite systems. Single-component materials frequently lack the capacity to simultaneously provide mechanical rigidity and a soft, cellularly instructive interface. Studies demonstrate the clinical efficacy of dual-component approach across various polymer types [85]. For example, researchers successfully fabricated rigid PCL scaffolds and subsequently coated them with a soft PEG hydrogel layer [86]. This specific composite design allowed the structural core to provide necessary physical support while the hydrogel coating actively altered cellular behavior and inhibited unwanted tissue mineralization. Applying this architectural strategy yields an implant capable of withstanding

dynamic physiological loads while presenting an adaptable, biologically recognizable surface to the host. Different types of PEG coatings were presented in Figure 11.

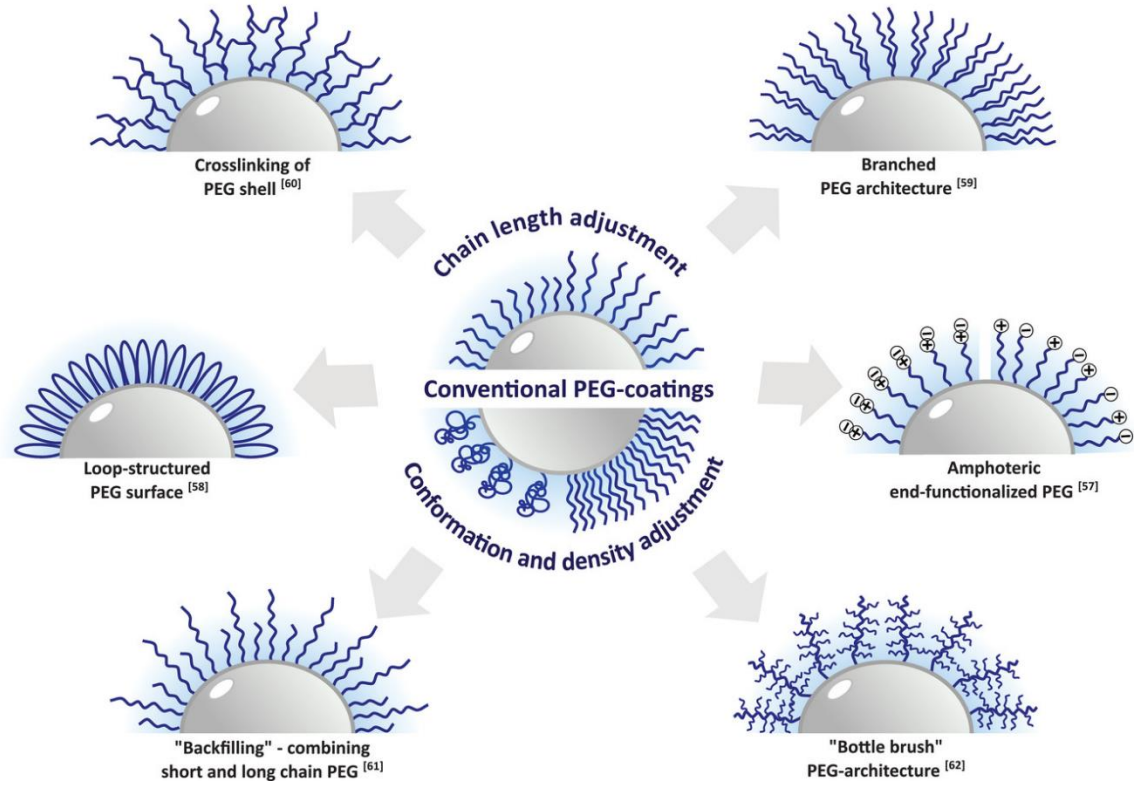


Figure 11 Emerging strategies for optimizing nanocarrier stealth emphasizing PEG conformation (e.g., linear vs. branched), terminal group functionalization and the development of "sheddable" coatings to balance long circulation with efficient cellular uptake. Adapted from: [87] under CC BY-NC-ND 4.0 license.

Beyond facilitating direct cellular attachment, the highly hydrated hydrogel layer serves as a specialized reservoir for the localized delivery of active pharmacological substances, growth factors or encapsulated cells directly into the surgical site [76]. Hydrogel matrix are designed to release its therapeutic payload via diffusion, swelling or targeted enzymatic degradation [88]. The aqueous environment of the hydrogel protects sensitive biological components from premature degradation and mechanical shear forces during implantation and delivering specific active agents at the scaffold surface directly accelerates complex healing mechanisms. Advanced core-shell fabrication techniques are frequently utilized to achieve this precise spatial distribution of materials. For instance, evidence shows the successful development of bioprinted core-shell structures that utilize a methacrylated gelatin (GelMA) shell surrounding a cell-laden chitosan core. This distinct layering strategy maintained high cellular viability and actively promoted prevascularization to accelerate wound closure [89]. Modification of such composite structure with active substances can promote specific, desirable cellular activities while actively inhibiting adverse biological reactions. For example, studies demonstrate that in chondroitin sulfate methacryloyl/GelMA core/shell structure, modifying a GelMA shell with celecoxib liposomes resulted in suppression of inflammatory agents' generation and rapid degradation of the hydrogel shell in response to the osteoarthritic microenvironment. Following the degradation of shell, core

started to degrade, releasing chondroitin sulfate promoting cartilage repair [90]. One of the most interesting approaches in core/shell structures is utilization of hydrogel/hydrogel architecture, where low-viscosity core serves as an antibiotic depot encapsulated within a structurally dense hydrogel shell. In one study, antibiotic-modified alginate core was utilized along with alginate-methylcellulose hydrogel shell, modified with Laponite nanoclay. The prepared modular platform demonstrated a potent antibacterial effect against *S. aureus* and *S. epidermidis*, offering a versatile strategy to simultaneously prevent soft tissue infections and promote wound regeneration in trauma patients [91].

While hydrogel-based systems excel in soft tissue regeneration and localized substance delivery, numerous surgical applications require load-bearing capabilities that surpass the mechanical limits of highly hydrated networks. To address these structural demands, non-hydrogel composite biomaterials were developed by integrating rigid biodegradable polymers with bioactive inorganic fillers. This strategy typically involves combining thermoplastic polyesters, such as poly(lactic acid) (PLA) or poly(e-caprolactone) (PCL), with bioceramics like hydroxyapatite (HAp), tricalcium phosphate or bioactive glasses [92]. Pure hydroxyapatite precisely mimics the mineral composition of natural bone and exhibits high osteoconductivity, but its inherent brittleness restricts its standalone use in load-bearing implants. Embedding HAp nanoparticles into a ductile polymer matrix resolves this mechanical limitation. The polymer matrix prevents premature structural failure, while the ceramic particles act as reinforcing elements that significantly increase the compressive modulus of the resulting scaffold. Furthermore, the inclusion of basic bioceramics actively mitigates biochemical complications associated with polyester degradation [93]. For example, incorporating hydroxyapatite into a PLA matrix successfully neutralizes the acidic degradation by-products of polylactide, preventing localized tissue inflammation and supporting high cell viability *in vivo* [94]. Researchers also utilize bioactive glasses within these robust composites. These glasses possess the unique capacity to undergo an ion exchange reaction with surrounding body fluids to form a biologically active layer of carbonate apatite, promoting a direct, cohesive bond with native bone tissue [95]. Beyond polymer matrices, biodegradable metal-ceramic composites are constructed to fulfill similar clinical needs [96]. In one study, researchers have developed a programmable bone screw synthesized from a PU matrix reinforced with hydroxyapatite (HA) and surface-modified with RGD peptides (Figure 12). This resulting screw offered mechanical compatibility with cancellous bone, featuring a Young's modulus of approximately 250 MPa. *In vivo* studies demonstrated that such approach outperforms traditional metal screws by reducing inflammatory responses and accelerating the growth of new bone tissue and collagen fibers [97]. Studies demonstrate that introducing hydroxyapatite and fluoroapatite particles into a biodegradable magnesium matrix improves both the corrosion resistance and the surface bioactivity of the metal, promoting direct interaction with osteoblast cells. By carefully modulating the mass ratios, particle sizes and distribution of these inorganic additives within solid matrices, mechanically robust composites tailored specifically for orthopedic implants and rigid structural repair can be produced [98]. Ultimately, the capacity for

precise biochemical modulation transforms the composite implants from a static structural substitute into a dynamic participant in the regenerative process.

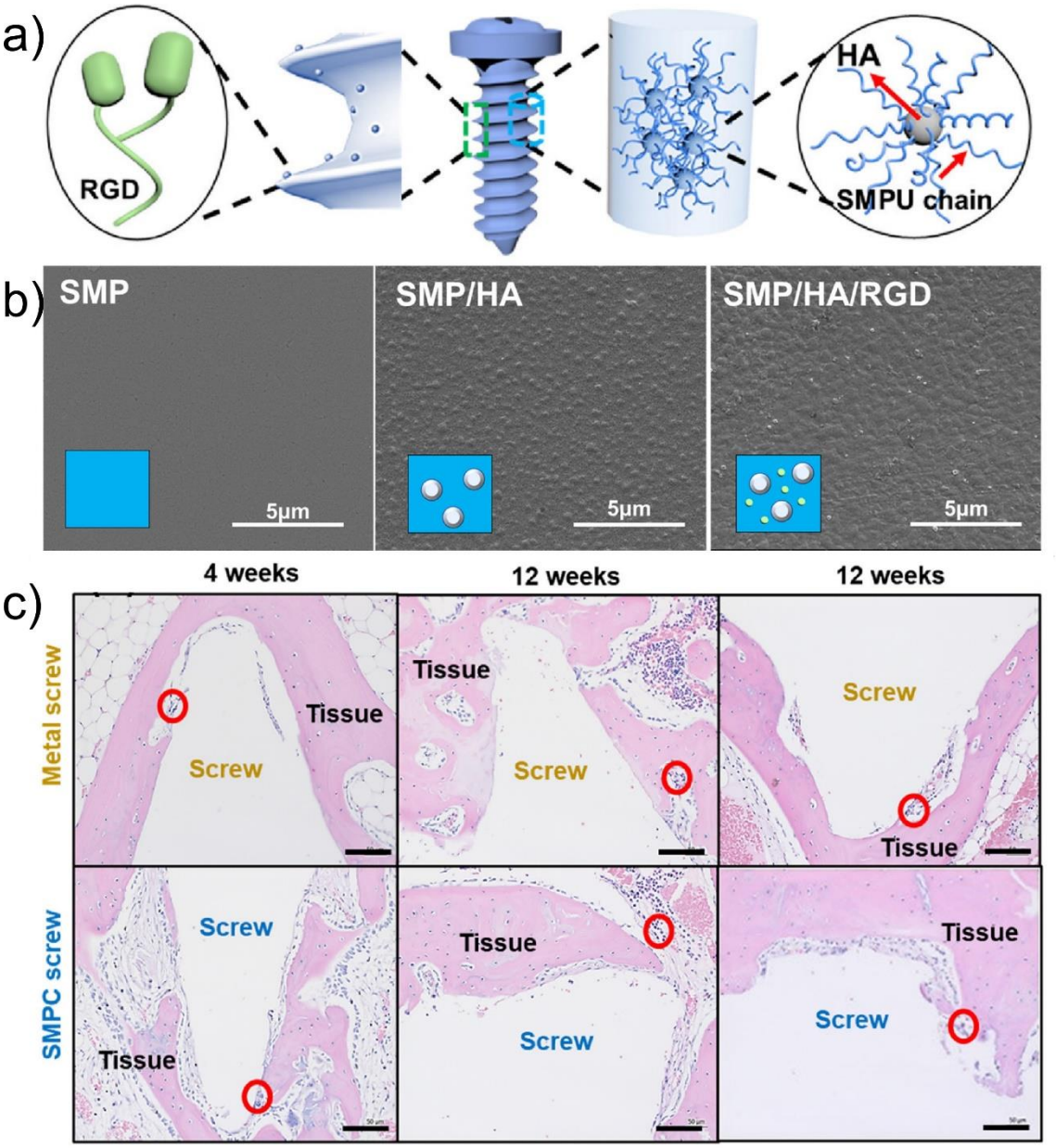


Figure 12 The composite screw prepared utilizing PU as base material, HA as an osseointegrating agent and RGD modification for improved cell signaling. a) schematic visualization of screw components. b) SEM surface images revealing surface size development due to the even distribution of the composite components neat polymer. c) Histological investigation of the screws after implantation showing lower number of inflammatory cells in case of composite screw. Reprinted from Acta Biomaterialia, 103, Yuanchi Zhang, Jinlian Hu, Ruiqi Xie, Yuhe Yang, Jie Cao, Yunhu Tu, Yi Zhang, Tingwu Qin, Xin Zhao, A programmable, fast-fixing, osteo-regenerative, biomechanically robust bone screw, Pages 293-305, Copyright (2020), with permission from Elsevier [97].

4.1.5. Fourth generation? Autonomous, smart intelligent systems and bioelectronics

The most recent progression in biomaterial research involves the development of bioelectronic materials, sometimes classified as fourth-generation biomaterials [27]. While earlier generations focused on structural mimicry and biochemical signaling, researchers base this novel class of materials on the fundamental principles of bioelectricity, which influence various functions in biological systems. These biomaterials exhibit multifunctional characteristics and allow for direct integration with electronic devices to detect and regulate bioelectric signals within the host body [99]. Rather than merely releasing a static dose of a pharmacological agent, bioelectronic materials actively monitor the electrical activity of the surrounding tissue. This continuous monitoring enables the implant to respond to specific physiological states, providing highly controlled electrical stimulation to direct tissue repair [100].

The application of bioelectronics relies on the established understanding that cells communicate and coordinate structural repair through electrical impulses. Studies show that endogenous bioelectrical signals directly regulate critical cellular functions, including cell migration, apoptosis, differentiation and proliferation [101]. By interfacing directly with these communication pathways, fourth-generation biomaterials can issue precise electrical directives to the host tissue. Consequently, evidence suggests that bioelectronic materials may promote precise, controlled tissue regeneration by actively modulating these bioelectrical signals at the molecular level [102]. This capability allows to move beyond passive scaffolding and create systems that instruct complex physiological processes, such as synchronized muscle contraction or neural bridging, directly at the implant site.

To systematically classify the capabilities of these advanced systems, researchers proposed a redefined framework for material responsiveness, categorizing functionality into four distinct stages: inert, active, responsive and autonomous [102]. Furthermore, literature now explicitly distinguishes between “smart” and “intelligent” biomaterials to clarify their functional limits [103]. Smart biomaterials apply previously acquired knowledge to respond to specific, predefined changes in their environment. They operate based on engineered stimulus-response mechanisms, acting essentially as biological switches. In contrast, intelligent biomaterials possess an innate capacity to acquire knowledge and adapt to their environment. This distinction means that an intelligent material must evaluate unpredictable physiological conditions and modify its behavior without relying solely on pre-programmed pathways, representing a significant increase in functional complexity.

Concurrently, the progression of interactive biomaterials has led to the conceptualization of autonomous systems, which represent the highest defined level of material responsiveness within this fourth generation. Researchers consider autonomous biomaterials to be self-sufficient entities capable of independently adjusting their physical properties and therapeutic functions in response to dynamic changes in the surrounding biological environment [104]. This autonomy is achieved by utilizing multifunctional nanoparticles, including metal-organic frameworks, designed

to integrate multiple chemical and physical stimuli simultaneously. These advanced systems target specific anatomical regions to monitor physiological health and actively intervene in biological events. Autonomous biomaterials operate as programmable and reconfigurable systems, executing a broad range of functions without requiring manual external intervention [21,105]. By combining the synergistic effects of multiple active additives, these materials function as dynamic entities that alter their environment through continuous autonomous feedback.

The physical foundation for many of these autonomous functions relies on advanced structural polymers capable of macroscopic mechanical transformations. Shape-memory polymers (SMPs) function as a highly relevant class of smart scaffolds within this generation [106]. Most common SMPs are PCL, PLA, PU and poly(lactic-co-glycolic acid) (PLGA). These materials exhibit programmable reconfigurability, maintaining a temporary physical form until exposure to a predefined stimulus, such as thermal or electrical energy, triggers their return to a permanent structure. Researchers widely recognize specific polyesters and PUs for their diverse biomedical applications utilizing these shape-memory capabilities. Furthermore, dual-functional biomaterials that possess both shape-memory and self-healing properties can be synthesized [107]. This dual functionality grants the polymer network the ability to autonomously repair structural or chemical damage sustained during dynamic physiological loading, significantly increasing the long-term mechanical reliability of the surgical implant.

The clinical application of these autonomous and bioelectronic systems offers distinct advantages in highly complex medical fields, particularly neural engineering and precision medicine. In neural engineering, multifunctional nanoparticles communicate directly with the nervous system to precisely deliver therapeutic agents to targeted anatomical sites [108]. Additionally, photo-responsive biomaterials allow engineers to dynamically alter the extracellular matrix or release specific biomolecules upon targeted light exposure [109]. Moreover, to support continuous monitoring and intervention, the integration of self-powered tissue batteries with these dynamic biomaterials is being investigated [100]. This theoretical capacity to process environmental information, adapt automatically and generate internal power provides a foundation for highly personalized surgical therapies.

Personalized medicine is a concept that aims to tailor diagnostic and therapeutic strategies to individual patient profiles, helping to maximize therapeutic efficacy, while minimizing systemic adverse effects. By including the patient-specific molecular, cellular and physiological differences during therapy design process, such approach improves treatment accuracy and shortens recovery time. However, clinical implementation presents disadvantages, including elevated fabrication costs, complex regulatory pathways, significant challenges in long-term device biocompatibility and need for change in medical staff mindset. Despite these constraints, the primary advantage of personalized medicine remains the capacity to transition from generic protocols to adaptive interventions that directly address patient specific conditions [110].

The “biocooperation” is emphasized as an emerging strategy where biology is not merely a template to copy, but a partner to engage with. In this framework, biological mechanisms such

as the coagulation cascade or macrophage migration serve as active partners in the material's functional evolution [111]. For example, "cellular backpacks" utilize the innate homing capabilities of macrophages to transport therapeutic agents to injury sites, effectively turning living cells into autonomous delivery vehicles [112]. This convergence of synthetic logic and biological machinery represents the definitive shift from instructive to truly cooperative fourth-generation systems. The recent trends in fourth generation biomaterials research were summarized in Figure 13.

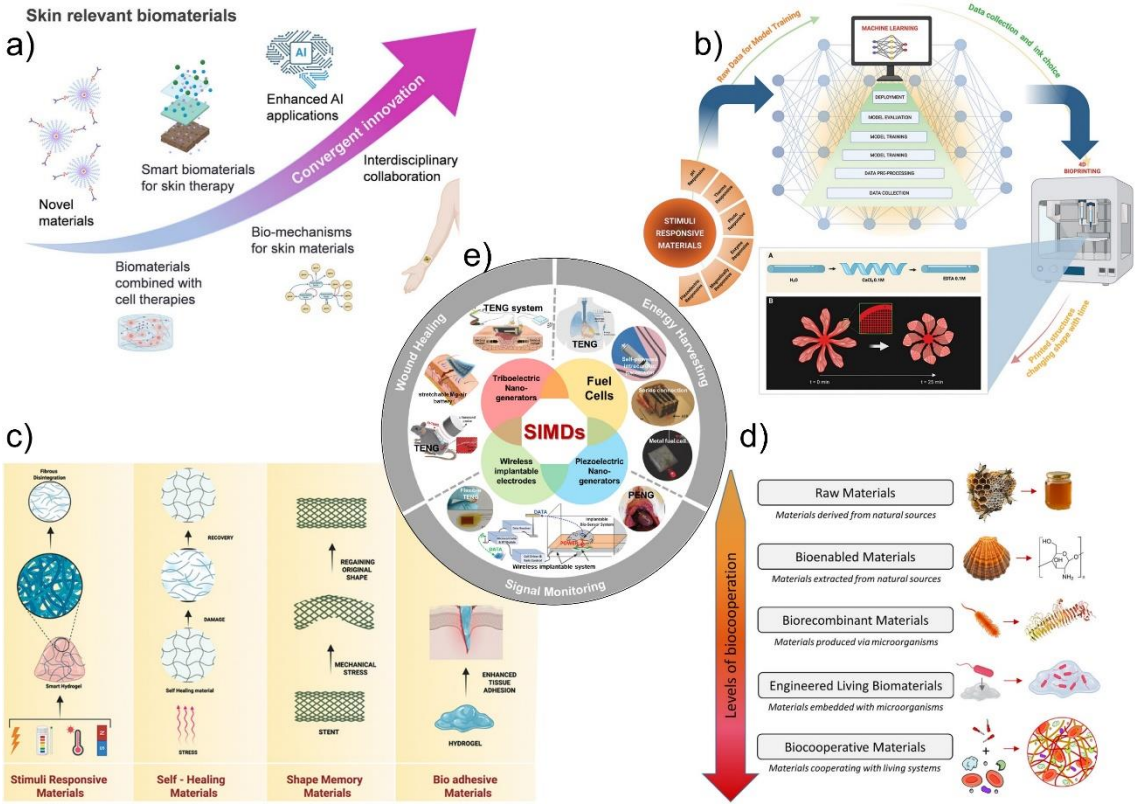


Figure 13 Recent trends in biomaterials research. a) Six major focus areas to guide future development of biomaterials: novel materials. Adapted from: [113]. b) Future direction towards the design of stimuli responsive materials with help of machine learning. c) Representation of main material types utilized in modern biomaterials research. Adapted from: [103]. d) The evolution of biocooperation level through the integration of rationally designed synthetic materials with natural agents. Adapted from: [114]. e) Implantable self-powered medical devices (SIMDs) for biomedical applications. Adapted from: [110]. All images were adapted under applicable Creative Commons license.

4.1.6. The future of biomaterials

The evolution of biomaterials has progressed from a fundamental desire to replace missing tissue to the ambitious goal of perfectly mimicking and seamlessly integrating with human biology. Throughout this transformative journey, polymers have consistently driven the innovation due to their remarkable versatility and tunable properties. A summary of the key advantages, disadvantages, applications and modification methods of the most popular polymers is presented in Table 1. Currently, the field is firmly positioned within the fourth generation of biomaterial development. These "smart" or autonomous biomaterials represent a paradigm shift from passive

structural support to dynamic, programmable functionality. The current state of the art is heavily defined by the convergence of materials science with nanotechnology, bioelectronics and advanced biofabrication. Innovations such as piezoelectric scaffolds, multi-stimuli-responsive nanocomposite hydrogels and 3D/4D bioprinting are enabling the creation of implants that communicate two-way with the host's nervous or immune systems, facilitating real-time adaptation and accelerated tissue regeneration.

Looking into the future of biomaterials, the current trends in the field point toward the emergence of a fifth generation of biomaterials, characterized by extreme biological complexity and true autonomy [115]. Future research directions will be likely largely focused on erasing the remaining boundaries between synthetic materials and living tissues. Key future directions include:

- Artificial Intelligence (AI) and Machine Learning (ML). The integration of AI into biomaterials research is poised to revolutionize material design. Machine learning algorithms will increasingly be used to predict cell-material interactions, optimize scaffold geometries and tailor degradation kinetics, shifting the field from trial-and-error *in vitro* experimentation to highly precise, data-driven engineering [116].
- "Living" biomaterials and synthetic biology. The next frontier involves engineering materials that possess the full, multi-layered complexity of the ECM. By embedding engineered living cells, programmable genetic circuits and dynamic molecular signaling pathways directly into the material matrix, these systems will not merely support regeneration but actively manage it, adapting morphologically and biochemically as the tissue heals [117].
- Hyper-personalized medicine. Advances in patient-specific 3D bioprinting, combined with the patient's own induced pluripotent stem cells (iPSCs) and genomic data, will enable the routine fabrication of customized bio-implants. This will be particularly vital for complex applications like neural system repair and immune-modulating cancer therapeutics [118].

In summary, the future of biomaterials lies at the intersection of molecular biology, materials science and computational engineering. As the field moves beyond smart materials toward fully living, AI-optimized regenerative systems, biomaterials will no longer be viewed as foreign implants, but rather as seamless extensions of the human body.

Table 1 Key advantages, disadvantages, applications and modification methods of the selected most popular polymeric biomaterials

Polymer	Key advantages	Key disadvantages	Applications	Modification methods	References
Poly(lactic acid)/ poly(lactide) (PLA)	- Originates from bio-based sources. - Exhibits high tensile strength and modulus. - Degrades into naturally occurring lactic acid.	- Remains rigid at body temperature. - Demonstrates low inherent cell affinity. - Undergoes autocatalytic hydrolytic degradation in dense formulations.	- Cardiovascular applications. - Bone scaffolds and orthopedic implants. - Neural degenerative disorder treatments.	- Copolymerization with trimethylene carbonate (1,3-dioxan-2-one) to reduce T_g. - Blending with poly(ε-caprolactone) to improve ductility. - Coating with hydroxyapatite to induce osseointegration.	[15,26,94,119,120]
Poly(glycolic acid) (PGA)	- Degrades faster than poly(lactic acid). - Provides high mechanical strength. - Retains high crystallinity.	- Resists dissolution in many standard solvents. - Causes different macrophage activation. - Requires specific processing due to high melting point.	- Vascular grafts. - Suture anchors. - Nerve conduits.	- Unidirectional stretching to produce anisotropic 3D porous scaffolds. - Melt-spinning into multifilament fibers, permitting the fabrication of high-strength fibers. - Surface coating with tetrafluoroethylene or silicones to reduce tissue drag and limits mechanical trauma to the tissue during wound closure	[54,121–123]

Polymer	Key advantages	Key disadvantages	Applications	Modification methods	References
Poly(ε-caprolactone) (PCL)	- Exhibits high ductility and elongation. - Possesses a low glass transition temperature (-60 °C). - Extrudes at mild temperatures for 3D printing.	- Degrades at a slow rate (up to 3 years). - Shows highly anisotropic degradation. - Has low thermal stability.	- Cardiac aortic valves. - Orthopedic and dental implants. - Vascular tissue engineering.	- Chemical cross-linking to establish a permanent network for shape-memory properties. - Blending with PLA to enhance rigidity. - Electrospinning with silk fibroin or polyaniline to promote cell growth.	[124–128]
Poly(lactic-co-glycolic acid) (PLGA)	- Enables tuning of degradation pace. - Maintains robust mechanical properties. - Yields nontoxic degradation products.	- Produces acidic degradation products that can alter local pH. - Undergoes bulk erosion. - Frequently requires blending or functionalization to overcome hydrophobicity.	- Cardiac patches. - Fracture fixation. - Nerve conduits.	- Adjusting stoichiometric ratio of lactide to glycolide to tune degradation kinetics. - Blending with PEG block copolymers to increase hydrophilicity. - Creating porous scaffolds to facilitate cellular ingrowth.	[129–132]

Polymer	Key advantages	Key disadvantages	Applications	Modification methods	References
Poly(ethylene glycol) (PEG) / Poly(ethylene oxide) (PEO)	- Dissolves readily in water. - Offers versatile functionalization options. - Resists protein adsorption.	- Lacks high mechanical strength. - Resists enzymatic degradation. - Requires oxidation for structural breakdown.	- Bone graft scaffolds. - Drug delivery devices. - Hydrogel bioinks.	- Derivatization with reactive acrylate groups, allowing attachment of drugs (PEG-DA). - Incorporation of hydrolytic oligomers (PLA/PGA) into the backbone to accelerate degradation. - Copolymerizing with poly(propylene oxide) to control swelling.	[78,80,125,133]
Poly(vinyl alcohol) (PVA)	- Provides high elasticity. - Demonstrates high water solubility. - Exhibits low protein adsorption.	- Requires oxidative catalysts for complete *in vivo* degradation. - Requires cross-linking to form stable hydrogels. - Lacks mechanical strength.	- Vascular grafts. - Cardiac patches. - Neural cell regeneration.	- Freezing-drying or aldehyde treatment to cross-link pendant -OH groups. - Functionalization with hydrolytically cleavable polyesters to increase degradability. - Electrospinning as a blend with hydroxyapatite to improve bioactivity.	[82,84,134–136]

Polymer	Key advantages	Key disadvantages	Applications	Modification methods	References
Polyurethanes (PU)	- Highly tunable material. - Degradation byproducts are essential amino acids (limiting cytotoxicity). - Limited inflammatory response *in vivo*.	- Synthesized with potentially toxic cross-linking agents depending on formulation. - Can degrade during sterilization (ethylene oxide). - Susceptibility to oxidation or hydrolysis based on soft segment chemistry.	- Tissue engineered vascular grafts, - Wound dressings. - Surgical adhesion barriers.	- Incorporation of natural polymer chain extenders to improve biocompatibility. - Integration of enzyme-sensitive linkages to promote targeted enzymatic degradation. - Substitution with polycarbonate or siloxane-based macrodiols to increase the resistance to *in vivo* hydrolysis and oxidative degradation.	[9,15,65,67,68]
Hyaluronic acid (HA)	- Possesses inherent bioactivity. - Promotes cell proliferation and differentiation. - Retains water to support wound healing.	- Resorbs rapidly in biological environments. - Lacks mechanical integrity. - Insufficient cell adhesion.	- Cardiac repair and heart valves. - Cartilage regeneration. - Central nervous system regeneration.	- Functionalization with methacrylate end groups (HA-MA) for photo-cross-linking. - Dual-hydrogel networks with alginate to increase hydrolytic stability. - Integration with MXenes for 3D bioprinting.	[70,71,137–139]

Polymer	Key advantages	Key disadvantages	Applications	Modification methods	References
Chitosan	- Shares structural similarity with the extracellular matrix. - Exhibits inherent antibacterial properties. - Highly tunable material.	- Resists dissolution in water at neutral pH. - Yields low mechanical strength. - Risks endotoxic contamination depending on formulation.	- Cardiac muscle repair. - Wound dressings. - Neural implants.	- Modification with glycidyltrimethylammonium chloride, succinic anhydride or lactobionic acid to improve solubility at neutral pH. - Cross-linking via aldehyde-functionalized polymers into hydrogel adhesives capable of self-healing. - Cross-linking via diisocyanates to produce tissue adhesives.	[56,68,89,140–142]
Alginate	- Undergoes fast physical gelation under physiological conditions. - Demonstrates high biocompatibility. - Functions as a low-cost material.	- Lacks native cell-binding motifs. - Resists enzymatic degradation in mammalian systems. - Loses structural integrity via physical ion-exchange.	- Blood vessel engineering. - Cancer models. - Central nervous system regeneration.	- Ionic cross-linking using multivalent cations (Ca^{2+}, Ba^{2+}, Sr^{2+}). - Gamma radiation or oxidation treatment to reduce molecular weight, accelerating degradation. - Covalent functionalization with peptides to induce cell-binding.	[73,76,142–144]

Polymer	Key advantages	Key disadvantages	Applications	Modification methods	References
Collagen	- Functions as the primary structural component of the mammalian extracellular matrix. - Contains inherent cell-binding sequences (e.g., RGD, GFOGER). - Undergoes natural degradation into nontoxic byproducts.	- Exhibits relatively weak mechanical strength. - Carries a risk of an immune or inflammatory response when sourced from animal tissues (bovine/porcine). - Presents batch-to-batch variability and potential for pathogen transmission.	- 3D bioprinting bioinks for skin tissue engineering. - Bone cell transplantation scaffolds. - Sciatic nerve regeneration matrices.	- Blending with synthetic polymers or other biopolymers (e.g., silk fibroin or oxidized cellulose) to enhance the mechanical properties. - Coating with human fibrinogen and thrombin to induce cell-binding. - Chemical cross-linking (e.g., utilizing a citric acid derivative) to increase the mechanical strength and decrease degradation rate.	[121,142,145–147]
Agar/agarose	- Undergoes a rapid, thermo-reversible sol-gel transition upon cooling. - High biocompatibility and tolerance in biological environments. - Permits tuning of gel stiffness via concentration adjustments.	- Lacks native cell-binding motifs. - Yields low mechanical strength. - Resists enzymatic degradation in mammalian systems.	- Nerve guidance conduits. - Self-healing tissue adhesives and wound dressings. - Hydrogel bioinks for 3D bioprinting.	- Functionalization with peptides to induce bioactivity. - Modification of functional groups attached to sugar residues to alter the gelling temperature. - Thermal cross-linking via freeze-thaw to induce a conformational transition from a random-coil to a helical 3D network.	[148–154]

4.2. Polyurethane biomaterials - chemistry and medical applications

Polyurethanes represent a group of synthetic polymers characterized by tunable mechanical strength and thermal stability. This polymer was developed by Otto Bayer et al. in late 1930s and widely introduced into the global market in 1950s [155]. Although polyurethanes function as essential components of modern medical implants, they occupy a specific niche in current literature, accounting for approximately 200 publications in 2025 (0.12% of the biomaterials sector). Data analysis reveals a trend toward hybrid research - the total keyword count across different generations outweighs the absolute number of papers. This suggests that contemporary research frequently combines characteristics from various stages of biomaterial evolution (Figure 14). Historically, PUs have been widely adopted for permanent blood-contacting medical devices, including pacemaker leads, vascular grafts and artificial heart valves [156]. Their high mechanical durability and favorable biocompatibility allowed them to successfully fulfill the role of 1st generation inert biomaterials. Currently, PUs successfully serve in different sectors of tissue engineering, for instance skeletal muscle engineering, cardiac tissue engineering and cartilage tissue engineering [157], where researchers utilize PUs inherent modifiability, creating advanced interactive and smart biomaterials of 3rd and 4th generation. These modifications typically aim to improve biological integration and fine-tune degradation kinetics of the base polyurethanes to meet the strict requirements for both *in vivo* or *in vitro* applications. Standard modification routes incorporate natural polymers, such as chitosan, collagen or hyaluronic acid, to increase the hydrophilicity of the matrix. Furthermore, researchers formulate functionalized polyurethanes by integrating active pharmacological drugs directly into the matrix, transforming the structural support into an active drug delivery system [158].

The distinct functional advantages of polyurethanes originate directly from their molecular structure. PUs function as segmented block copolymers characterized by the presence of urethane linkages within the main polymer chain. In case of TPU, the structure consists of alternating rigid and flexible blocks. The flexible soft segments, typically derived from macrodiols (e.g., polyethers, polyesters or polycarbonates), provide elastomeric characteristics and strongly influence the overall degradation rate. The rigid hard segments, formed by diisocyanates and short-chain extenders, supply structural strength through extensive hydrogen bonding between urethane groups. Under specific thermodynamic conditions, phase separation occurs between these incompatible blocks, generating a distinct nanodomain morphology. This the dispersed hard domains function as physical cross-links and reinforcing filler particles, allowing the material to behave as an elastomer at physiological temperatures while remaining processable at elevated temperatures [159].

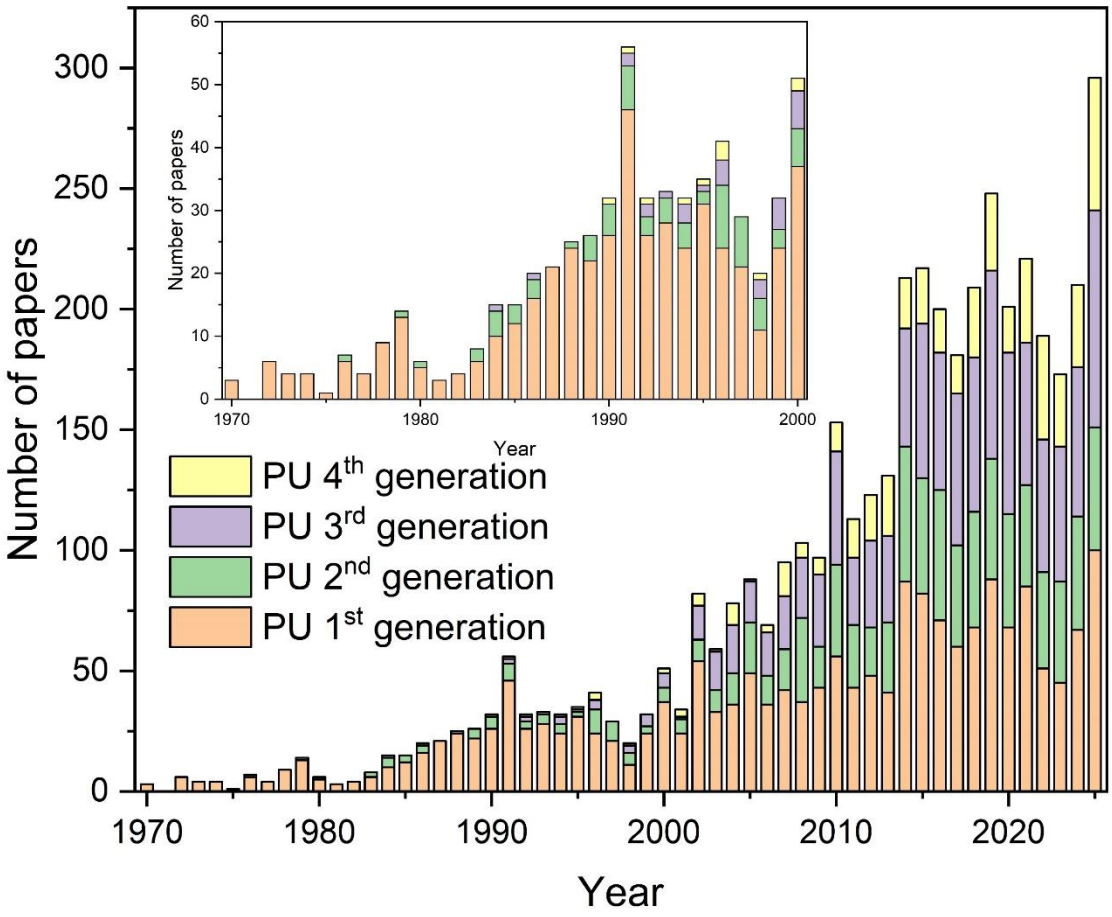


Figure 14 Evolution the polyurethanes share in biomaterials generations depicted by the changing research interest. Data base: Scopus within Article title, abstract and keywords. Search queries: 1st generation: ("biomaterial" OR "biomedical material*") AND ("polyurethane*" OR "polyesterurethane*" OR "polyetherurethane*" OR "thermoplastic polyurethane*") AND ("first generation" OR "1st generation" OR "bioinert*" OR "inert*" OR "minimal host response" OR "biocompatible"). 2nd generation: ("biomaterial*" OR "biomedical material*") AND ("polyurethane*" OR "polyesterurethane*" OR "polyetherurethane*" OR "thermoplastic polyurethane*") AND ("second generation" OR "2nd generation" OR "bioactive" OR "bioresorbable" OR "biodegradable" OR "bioglass" OR "hydroxyapatite" OR "calcium phosphate" OR "osteo*" OR "osseo*"). 3rd generation: ("biomaterial*" OR "biomedical material*") AND ("polyurethane*" OR "polyesterurethane*" OR "polyetherurethane*" OR "thermoplastic polyurethane*") AND ("third generation" OR "3rd generation" OR "biointeractive" OR "regenerative" OR "biomimetic" OR "tissue engineering" OR "scaffold*" OR "extracellular matrix" OR "ECM" OR "molecular signaling" OR "stem cell*" OR "cellular response"). 4th generation: ("biomaterial*" OR "biomedical material*") AND ("polyurethane*" OR "polyesterurethane*" OR "polyetherurethane*" OR "thermoplastic polyurethane*") AND ("fourth generation" OR "4th generation" OR "smart" OR "electronic*" OR "autonomous" OR "programmable" OR "stimuli-responsive" OR "Theranostic*" OR "nano" OR "cyber" OR "piezoelectric*" OR "sensor" OR "shape-memory" OR "shape memory").*

By manipulating the chemical composition and relative proportions of these segments, the physical characteristics of polyurethanes can be customized to match precise clinical requirements. Modifying the ratio of hard segments to soft segments allows to synthesize polyurethanes that range from highly compliant elastomers to rigid structural plastics.

Furthermore, the specific chemical nature of the chain extender directly influences the resulting mechanical stiffness [159]. Studies indicate that incorporating aliphatic chain extenders yields softer polymers, whereas utilizing aromatic chain extenders produces more rigid materials [14]. This tunability proves critical in biomaterial engineering, as the implant must exhibit a mechanical compliance that closely replicates the native properties of the target host tissue to prevent stress shielding and mechanical failure. Consequently, analyzing the synthetic mechanisms and the specific roles of individual precursors provides the necessary foundation for evaluating polyurethanes as advanced biomaterials.

4.2.1. Polyurethane synthesis for medical applications

Polyurethanes comprise a diverse class of synthetic polymers defined by the presence of urethane linkages within their main chain. These materials are synthesized through a step-growth polyaddition reaction, which primarily involves the reaction between molecules containing two or more isocyanate groups and compounds bearing multiple reactive hydroxyl or amine functional groups [159]. The synthesis of medical-grade TPUs usually requires three primary precursors: a diisocyanate, a high molecular weight macrodiol and a low molecular weight chain extender. The summary of commonly used raw materials in synthesizing PUs was presented in Figure 15. Researchers frequently conduct this synthesis via a two-step prepolymer method to maintain strict control over the final polymer architecture, although single-step polymerization methods still remain viable [156]. During the two-step process, the diisocyanate first reacts with the macrodiol to form an isocyanate-terminated prepolymer. Subsequently, adding the short-chain diol or diamine extends the polymer chain and completes the macromolecular structure [160]. The summary of the most common reactions between isocyanate and H-labile groups was presented in Figure 16.

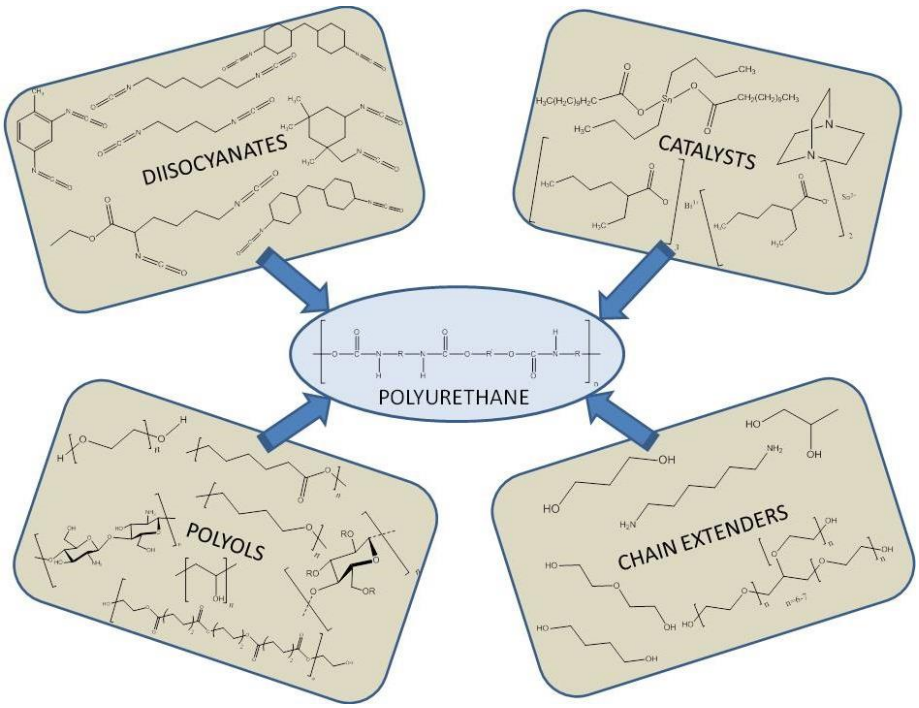


Figure 15 The summary of commonly used raw materials in synthesizing PUs for each of the main materials groups: diisocyanates, catalysts, polyols and chain extenders.

These specific synthetic pathways directly establish the characteristic microphase-separated morphology of polyurethanes. The macrodiols form the flexible soft segments, providing elastomeric compliance, whereas the diisocyanates and chain extenders combine to construct the rigid hard segments, supplying structural durability. Because these segments exhibit thermodynamic incompatibility, they separate into distinct microdomains during synthesis. By evaluating the specific reaction mechanisms of these precursors and systematically selecting the starting monomers, scientists can tune the resulting the final physical and chemical properties to match the distinct mechanical, chemical and biological demands of target host tissues.

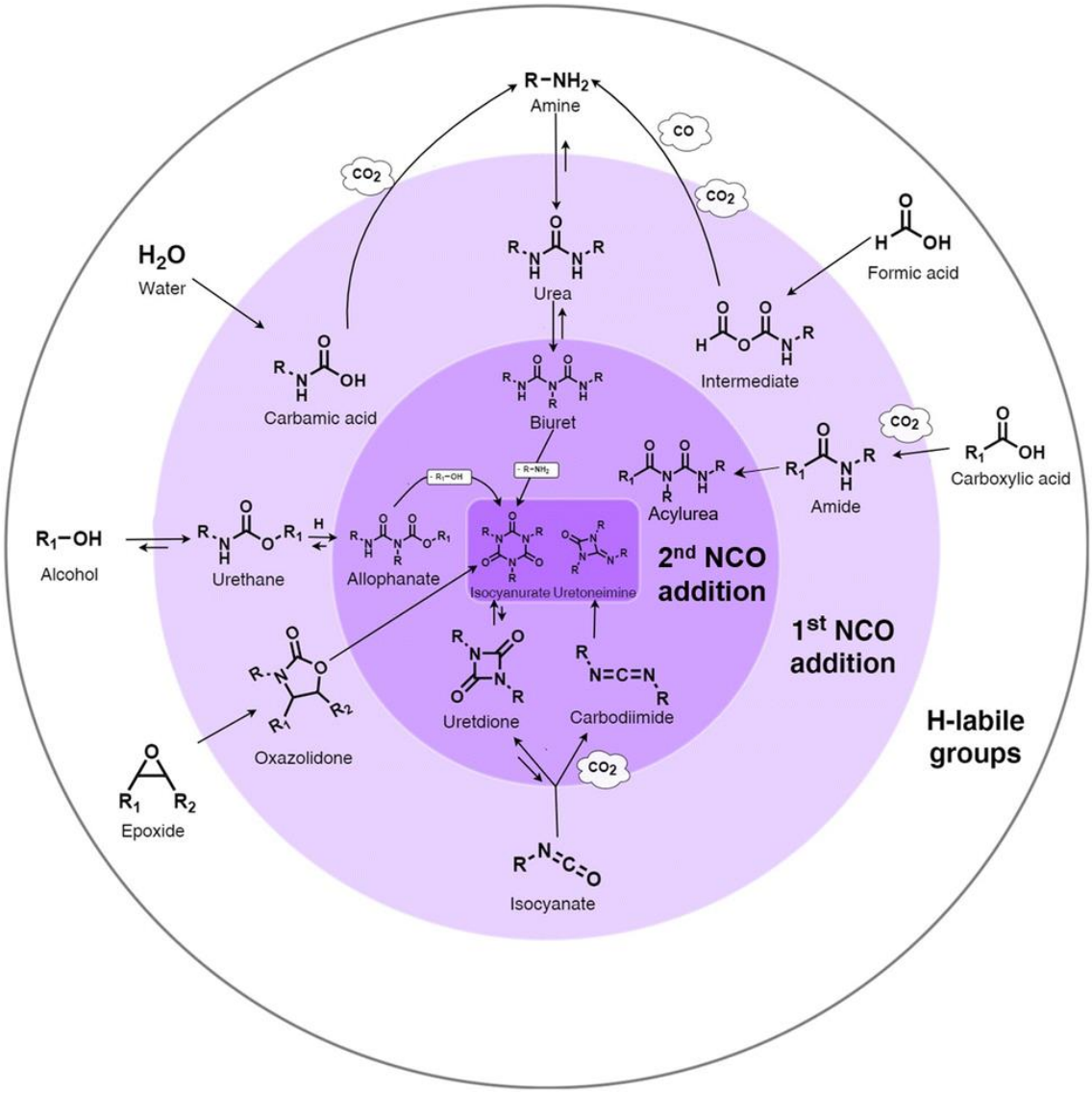


Figure 16 The summary of the most common reactions between isocyanate and H-labile groups. Adapted from: [161] under CC BY 3.0 license.

4.2.1.1. Hard segments

Polyurethanes derive their distinct mechanical properties from a unique microphase-separated morphology, within which the rigid hard segments play a foundational role. Hard segments, composed of diisocyanates and low molecular weight chain extenders, undergo phase

separation and aggregate into ordered, often crystalline microdomains dispersed throughout the continuous amorphous soft phase. The specific geometrical configuration of the diisocyanate and chain extender drives the ease of polymeric chains alignment to form these ordered structures. Ultimately, the content and structure of hard segments determine the upper range of the material's operating temperature and provide overall structural strength, hardness and impact resistance required for medical implants [160].

When engineering polyurethanes for biomedical applications, researchers carefully select the diisocyanate precursor, as it defines both the mechanical performance and the biological safety of the final device. Historically, industrial formulations frequently utilized aromatic diisocyanates, such as 4,4'-methylenediphenyl diisocyanate (MDI) and toluene diisocyanate (TDI), due to their high reactivity and the robust rigidity they bring to the polymer network. However, it has to be noted that the *in vivo* degradation of aromatic polyurethanes yields toxic and potentially carcinogenic by-products, specifically 4,4'-methylenedianiline (MDA) and 2,4-toluene diamine (TDA), which present severe health risks. Despite these concerns, aromatic diisocyanates like MDI [162], TDI [163,164] or HYPOL 2002 (TDI/hexamethylene diisocyante-based prepolymer) [165], are still in use in the medical field, threating with potential cytotoxic effects on living tissues. The application of these aromatic diisocyanates in PU biomaterials research is probably dictated by the chosen method of classical foaming to obtain PU foam dressings for further modifications. Aromatic diisocyanates are commonly used for this purpose due to their higher reactivity compared to aliphatic compounds [166].

Consequently, to address these health risks, resorbable polyurethanes are usually synthetized using aliphatic or cycloaliphatic diisocyanates, which degrade into safe, non-cytotoxic metabolic intermediates. Standard alternatives include 1,6-hexamethylene diisocyanate (HDI) [167], 1,4-butane diisocyanate (BDI) [168], isophorone diisocyanate (IPDI) [169] and 4,4'-methylenebis(cyclohexyl isocyanate) (H_{12}MDI) [170]. Systems based on HMDI were reported to have strong H-bonding among hard segments and lower phase separation between soft and hard segments in comparison to HDI and IPDI-based systems [171,172]. Furthermore, to actively control the resorption timeline, lysine-based diisocyanates (LDI) is frequently incorporated [173,174]. The asymmetrical structure of LDI disrupts the tight packing of the hard domains, while its pendant hydrolysable ester groups accelerate water penetration and subsequent polymer breakdown. The comparison of diisocyanate types used in PU synthesis was presented in Table 2.

Small molecule chain extenders complete the hard segment sequence, significantly influencing the degree of phase separation and the internal architecture of the rigid microdomains. Researchers primarily employ simple aliphatic diols, such as 1,4-butanediol (BDO) [173,175–178], ethylene glycol (EG) [179], diethylene glycol (DEG) [180], polypropylene glycol (PPG) [163], 1,3-propanediol (PDO) [181]. To facilitate the formation of highly ordered hard segments corresponding diamines are often used, including ethylenediamine (ED), 1,4-butanediamine

(BDA) [182] and hexamethylenediamine (HMDA) [183]. The comparison of chain extender types used in PU synthesis was presented in Table 3.

The structural integrity provided by the hard segments relies heavily on extensive intermolecular secondary interactions, predominantly hydrogen bonding [159]. During the reaction of isocyanates with hydroxyl or amine groups, the urethane and urea linkages are formed, which contain highly reactive sites. Hydrogen bonds form primarily between the secondary amine groups and the carbonyl oxygen atoms present within these linkages. With bond energies ranging between 20 and 50 kJ/mol, hydrogen bonds represent the strongest secondary forces in the polyurethane matrix, acting as robust physical cross-links that reinforce the organized, crystalline domains [159]. Analytical studies utilizing infrared spectroscopy demonstrate that at room temperature, approximately 90% of the amino groups located in the rigid segments participate in hydrogen bonding. As the temperature increases and approaches the glass transition temperature of the rigid segments, the extent of hydrogen bonding gradually decreases. However, approximately 30% to 40% of these bonds remain intact even at temperatures up to 200 °C [184]. This dense network of physical cross-links restricts the mobility of the polymer chains under applied stress, directly translating into the high tensile strength and stiffness observed in segmented polyurethanes.

The specific chemical structure and alkyl chain length of these extenders define the distance and alignment between the urethane or urea groups, thereby determining the efficiency of the hydrogen-bonded network. Modulating the chain extender structure allows chemists to adjust the arrangement and size of the hard segment clusters distributed within the soft phase [185]. The uniform distribution optimizes energy dissipation upon mechanical deformation, significantly improving the tensile strength, toughness and crack resistance of the biomaterial.

Table 2 Common diisocyanates in polyurethane synthesis

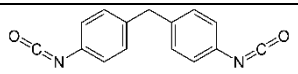
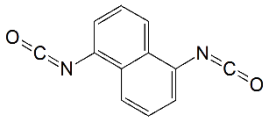
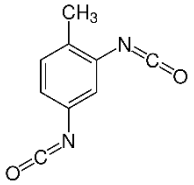
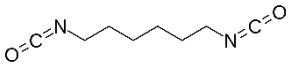
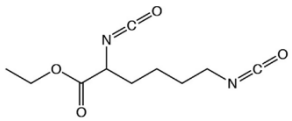
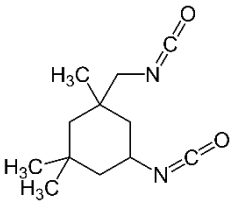
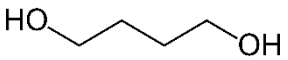
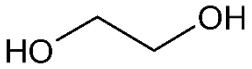
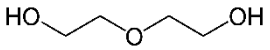
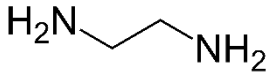
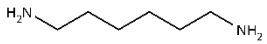
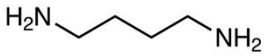
Type	Examples	Advantages	Disadvantages	Medical applications [156,158,186]
Aromatic	 4,4'-methylenediphenyl diisocyanate (MDI)  1,5-naphthalene diisocyanate (NDI)  Toluene diisocyanate (TDI)	- Produce PUs with high tensile strength and rigidity. - High chemical reactivity. - Excellent thermal stability.	- Generate toxic degradation by-products (MDA, TDA). - Potentially *in vivo* carcinogenic. - Restricted to strictly biostable devices.	- Permanent pacemaker leads. - Biostable artificial heart valves. - Long-term electronic encapsulants.
Aliphatic / Cycloaliphatic	 1,6-hexamethylene diisocyanate (HDI)  Lysine diisocyanate (LDI)  Isophorone diisocyanate (IPDI)	- Yield non-toxic metabolic products. - Excellent biocompatibility. - Controlled hydrolytic degradation.	- Lower chemical reactivity than aromatics. - Produce PUs with reduced initial stiffness. - Require precise catalytic control during synthesis.	- Biodegradable tissue scaffolds. - Resorbable wound dressings. - Controlled drug delivery matrices.

Table 3 Common chain extenders in polyurethane synthesis

Type	Examples	Advantages	Disadvantages	Medical applications [156,158,186]
Diols	 1,4-butanediol (BDO)  Ethylene glycol (EG)  Diethylene glycol (DEG)	- Form highly ordered crystalline microdomains. - Excellent thermal processability. - Maintain predictable hydrolytic degradation profiles.	- Exhibit slower reaction kinetics. - Generate weaker hydrogen bonds. - Induce exceedingly slow degradation in non-functionalized forms.	- Compliant vascular grafts. - Temporary skeletal support structures. - Resorbable surgical sutures.
Diamines	 Ethylenediamine (ED)  Hexamethylenediamine (HMDA)  1,4-butanediamine (BDA)	- Form exceptionally strong urea linkages. - High intermolecular hydrogen bonding density. - Efficient mechanical energy dissipation.	- React rapidly, which complicates manufacturing. - Produce highly rigid domains slowing degradation. - Require purification to prevent residual monomer toxicity.	- Load-bearing orthopedic components. - High-fatigue cardiac implants. - Wear-resistant joint surface replacements.

4.2.1.2. Soft segments

The flexible soft segments within the thermoplastic polyurethane backbone primarily govern the elastomeric characteristics and degradation kinetics of the resulting biomaterial. Synthetically, researchers utilize high molecular weight macrodiols (usually in range of 400 – 8 000 g/mol) to form these extended, flexible domains. During the step-growth polymerization process, these macrodiols alternate with the rigid hard segments, driving the thermodynamic microphase separation that defines polyurethane morphology [159]. The soft segments organize into amorphous continuous phases that allow for chain mobility and extension under mechanical stress, which imparts the necessary elasticity and toughness. The chemical composition and molecular weight of the macrodiol dan be utilized to precisely tune the hydrophilic-hydrophobic balance, the rate of *in vivo* degradation and the mechanical flexibility. The three principal classes of macrodiols utilized in biomedical polyurethanes include polyethers, polyesters and polycarbonates, each offering distinct advantages and limitations depending on the clinical application [160]. The comparison of polyol types used in PU synthesis was presented in Table 4.

Historically, polyether-based macrodiols, such as poly(tetrahydrofuran) (PTMEG) (also called poly(tetramethylene ether) glycol or poly(tetramethylene oxide)) and PEG, gained prominence due to their exceptional flexibility and high resistance to hydrolytic degradation [156]. The ether linkages within the polymer main chain withstand water penetration, making them suitable candidates for environments subject to constant moisture. Furthermore, incorporating PEG significantly increases the hydrophilicity of the polyurethane matrix, which facilitates water uptake and creates an environment resistant to non-specific protein adsorption and bacterial adhesion [159]. This specific antifouling property proves highly beneficial in the design of blood-contacting devices and wound dressings. However, clinical evaluations demonstrate that polyether-based polyurethanes remain susceptible to oxidative degradation. *In vivo*, the presence of reactive oxygen species, released e.g., by macrophages during the inflammatory response, leads to the oxidation of ether bonds, resulting in surface cracking and eventual mechanical failure of the implant over long-term exposure [187]. Consequently, polyurethanes synthesized with pure polyether soft segments are frequently limited to short-term or highly specific applications, where oxidative stress remains low.

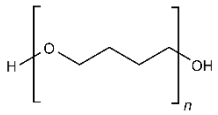
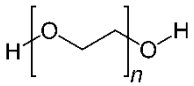
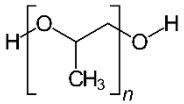
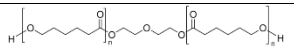
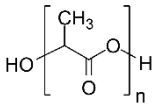
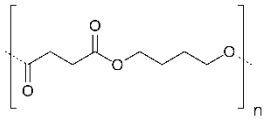
To address the need for fully resorbable implants, researchers shifted focus toward polyester-based macrodiols, including PCL, PLA and PGA diols [160]. The ester linkages within these soft segments readily undergo hydrolytic and enzymatic degradation in physiological environments, allowing the entire polyurethane construct to degrade into non-cytotoxic metabolic intermediates [187]. Among these, PCL represents the most widely utilized polyester macrodiol due to its favorable mechanical compliance and controlled, relatively slow degradation rate, which closely matches the regeneration timeline of many tissues [126,188]. Studies indicate that the concentration of ester groups directly correlates with the rate of hydrolytic degradation, as increasing the density of ester bonds accelerates the breakdown process. Furthermore, the acidic by-products generated during ester hydrolysis act as autocatalysts, further accelerating the

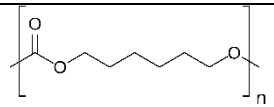
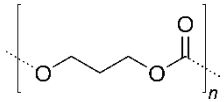
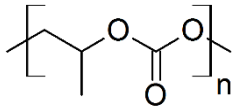
polymer's degradation [187]. By combining different polyester macrodiols, such as PLA, PCL or PEG copolymers or mixtures, polyurethanes with highly specific degradation profiles tailored for temporary tissue engineering scaffolds and controlled drug delivery vehicles can be obtained [11,167,175].

For applications demanding exceptional long-term biostability, such as artificial heart valves and orthopedic joint replacements, engineers utilize polycarbonate diols to synthesize the soft segments [189]. Polycarbonate-based polyurethanes emerged as a solution to the respective oxidative and hydrolytic vulnerabilities of polyether and polyester segments. The carbonate linkages exhibit robust resistance to both reactive oxygen species and water-mediated cleavage, providing superior *in vivo* longevity [160]. Experimental evidence indicates that polycarbonate polyurethanes maintain their mechanical integrity and surface morphology significantly longer than their polyether counterparts when subjected to enzymes or macrophage-induced oxidative stress [190,191]. Additionally, these materials present mechanical, chemical and biological properties that equal or exceed those of traditional segmented polyurethanes, making them the standard choice for chronic, load-bearing medical implants [192].

The structural characteristics of the soft segment also play a critical role in establishing the biomimetic properties necessary for successful tissue integration. The natural extracellular matrix operates as a highly hydrated, flexible gel that provides mechanical support and regulates cell behavior. To replicate this function, the synthetic soft segments must facilitate a similar degree of mechanical compliance and water absorption. Highly flexible macrodiols yield scaffolds with low elastic moduli, appropriately mimicking soft tissues such as nerves, blood vessels and skeletal muscle [193]. On the other hand, selecting shorter or more constrained macrodiols increases the stiffness, making the substrate suitable for cartilage or bone regeneration [194]. Furthermore, the specific hydrophilicity of the soft segment governs the initial protein adsorption upon implantation, subsequently allowing cell adhesion, proliferation and differentiation. By meticulously designing the soft segment architecture, polyurethanes can trigger the biological response and promote the formation of functional host tissue.

Table 4 Common polyols in polyurethane synthesis

Type	Examples	Advantages	Disadvantages	Medical applications [156,158,186]
Polyethers	 Poly(tetrahydrofurane) (PTMEG)  Poly(ethylene glycol) (PEG)  Poly(propylene glycol) (PPG)	- Provide exceptional mechanical flexibility. - High resistance to hydrolysis. - Antifouling surface properties	- Undergo rapid oxidative degradation. - Develop surface cracks during extended implantation. - Lower inherent tensile strength and tear resistance	- Short-term blood-contacting catheters. - Moisture-regulating wound dressings. - Temporary extracorporeal tubing.
Polyesters	 Poly(ε-caprolactone) diol (PCL)  Poly(lactic acid) (PLA)  Polybutylene succinate (PBS)	- Undergo predictable hydrolytic and enzymatic cleavage. - Degrade into strictly non-cytotoxic metabolic intermediates. - Offer highly tunable degradation kinetics based on ester density.	- Generate acidic by-products that autocatalyze further degradation. - Products require strict moisture-free storage conditions. - Lack of sufficient biostability for permanent implant applications.	- Biodegradable tissue engineering scaffolds. - Controlled therapeutic drug delivery systems. - Fully resorbable surgical sutures.

Type	Examples	Advantages	Disadvantages	Medical applications [156,158,186]
Polycarbonates	 Poly(hexamethylene carbonate) (PHMC)  Poly(trimethylene carbonate) (PTMC)  Poly(propylene carbonate) (PPC)	- Exceptional resistance to oxidative degradation, hydrolysis and chronic physiological stress. - Superior mechanical toughness and ultimate tensile strength. - Long-term hemocompatibility and a minimal inflammatory tissue response.	- Demand significantly higher processing temperatures during manufacturing. - Involve more complex and costly synthetic precursors. - Resist bioresorption and exhibit strong hydrophobicity	- Long-term load-bearing orthopedic implants. - Biostable artificial heart valves. - Long-term implantable biosensors.

4.2.1.3. Catalysis

In the absence of catalytic activation, the primary step-growth polyaddition between isocyanate groups and active hydrogen precursors proceeds at an exceptionally slow rate (Figure 17a). Furthermore, attempting to accelerate these uncatalyzed reactions by applying elevated temperatures frequently induces undesirable side reactions, disrupting the macromolecular architecture. This kinetic profile makes uncatalyzed synthesis highly impractical for efficient biomaterial manufacturing, as it demands extended reaction times to achieve sufficient polymer molecular weights [159]. Thus, the step-growth polyaddition of diisocyanates and diols requires precise kinetic control, which chemists achieve through specific catalytic systems.

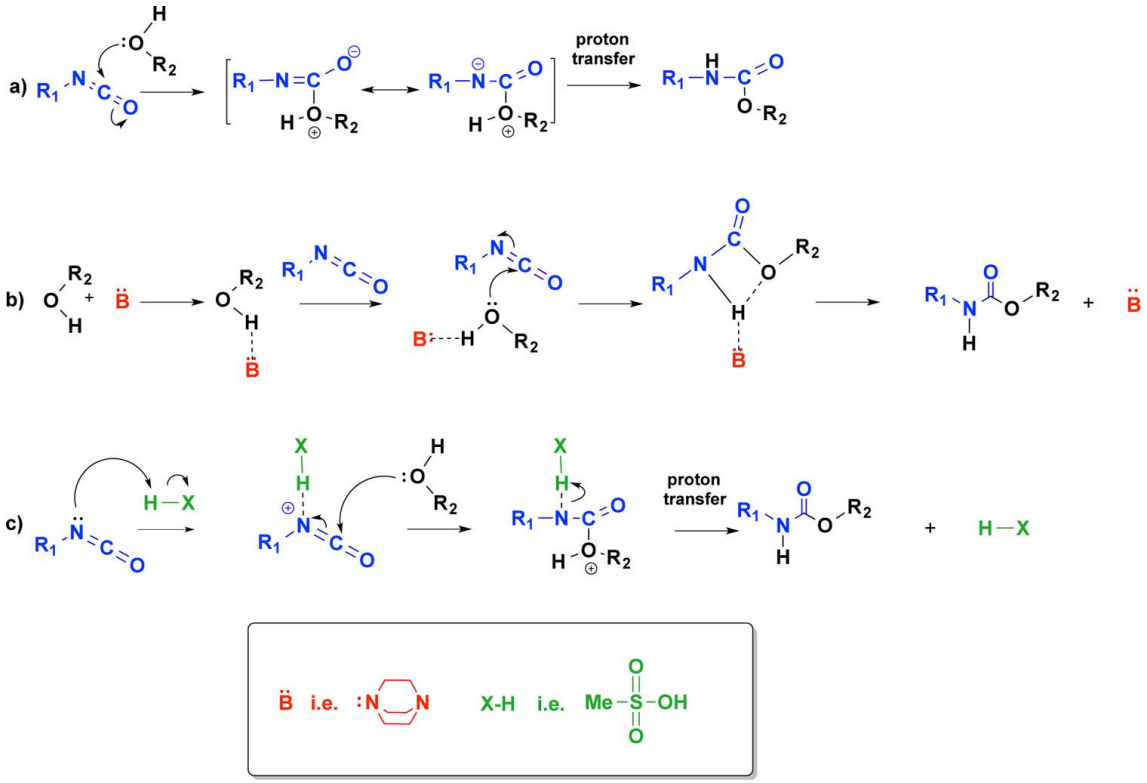


Figure 17 Mechanisms of polyurethane synthesis in the a) absence of catalyst, b) presence of a base (nucleophilic) catalyst, c) presence of an acid (electrophilic) catalyst. Adapted from: [195] under ACS AuthorChoice License.

Historically, the PU industry relied heavily on organometallic compounds, predominantly organotin derivatives, such as dibutyltin dilaurate (DBTDL), acting as Lewis acids [196]. Kinetic data suggest they operate via a mechanism where the isocyanate nitrogen coordinates with a tin alkoxide intermediate (preceded by alcoholysis of the tin catalyst), forming the intermediate N-stannylurethane. It then is followed by alkoxide anion transfer and subsequent alcoholysis to generate the urethane linkage and tin alkoxide [197]. The organotin-catalyzed reaction scheme of PU synthesis was depicted in Figure 18. While highly efficient, organotin catalysts present severe limitations for biomedical and advanced structural applications. Residual heavy metals remain physically entrapped within the polymer matrix, complicating purification and posing

significant toxicity risks [198]. Consequently, contemporary research focuses on developing metal-free organocatalysts to synthesize safer biomaterials, categorizing these alternatives primarily into organic bases and organic acids.

Tertiary amines represent the most traditional class of basic organocatalysts utilized in polyurethane synthesis. Among these, 1,4-diazabicyclo[2.2.2]octane (DABCO) serves as the industrial standard [160]. The activation mechanism relies on the strong basicity of the amine, which typically abstracts a proton from the alcohol to increase its nucleophilicity, facilitating its direct attack on the electrophilic carbon of the isocyanate [199]. General reaction scheme of polyurethane synthesis with base catalyst was depicted in Figure 17b. Tertiary amines effectively catalyze both the isocyanate-hydroxyl reaction to form urethanes and the isocyanate-water reaction to form polyurea and carbon dioxide [200]. This dual activity proves highly advantageous for producing polyurethane foams, where simultaneous gelling and blowing processes are necessary [201]. However, for solid elastomers, this lack of selectivity requires chemists to seek catalysts with higher basicity and strict specificity for the hydroxyl reaction.

Certain clinical and industrial applications, such as reaction injection molding, require latent catalysts that remain inactive at room temperature but initiate polymerization upon thermal activation. Researchers synthesized stable guanidinium salts by neutralizing strong bases like 1,8-diazabicycloundec-7-ene (DBU) with organic carboxylic acids, such as benzoic acid. These salts provide extended pot lives at ambient conditions and selectively decompose at elevated temperatures to release the active basic catalyst [202]. The transition toward organocatalysis addresses the safety and environmental requirements of biomaterial engineering. By carefully selecting specific organic acids or bases, the polymerization kinetics can be precisely controlled, accommodating sensitive functional monomers and eliminate heavy metal toxicity from the final medical device [203].

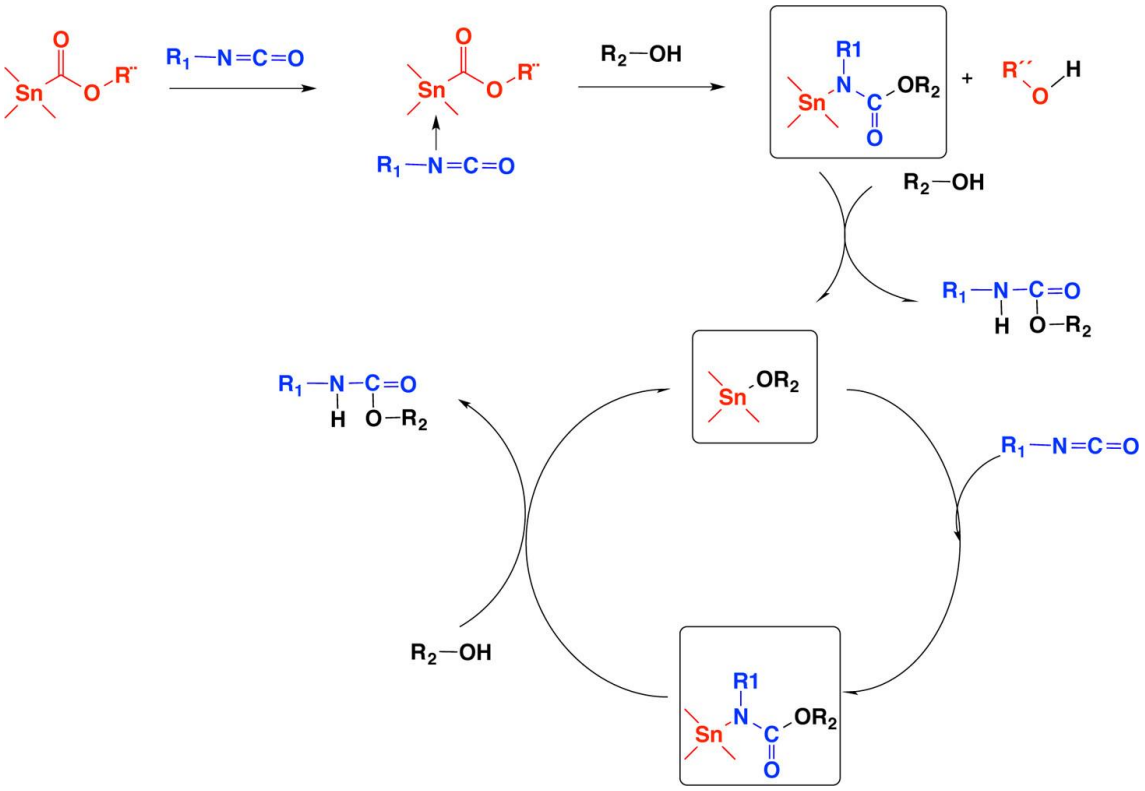


Figure 18 Scheme of polyurethane synthesis reaction catalyzed by organotin. Adapted from: [195] under ACS AuthorChoice License.

4.2.2. Polyurethane biocompatibility and biodegradation mechanisms

Polyurethanes thanks to their tunable structure are exceptional candidates for diverse biomedical applications, including implants, scaffolds and DDSs. When designing these materials, two critical parameters must be strictly evaluated: biocompatibility and biodegradation. Biocompatibility refers to the capacity of living tissues to interact directly with the PU surface without triggering adverse systemic responses, such as acute inflammation, toxicity or allergic reactions. Although medical-grade PUs generally demonstrate excellent biocompatibility, safety concerns persist regarding the potential leaching of unreacted isocyanate monomers, organometallic catalysts or additives into the physiological environment [204].

Alongside biocompatibility, researchers continuously evaluate the biodegradation profile of PUs. Biodegradation is the ability of the polymer network to decompose within a biological environment. Depending on the clinical target, PUs are designed to either resist degradation for long-term biostability (such as in cardiovascular implants) or undergo controlled breakdown for short-term applications (such as in drug delivery vehicles or resorbable tissue scaffolds) [205]. Within the human body, the degradation process inevitably releases various by-products, including small-chain hydroxyls, carboxylic acids or polyamines [206]. Consequently, the degradation kinetics must be precisely regulated to prevent local tissue toxicity or the accumulation of carcinogenic compounds.

Both biocompatibility and biodegradation depend heavily on the chemical composition of the PU backbone. The selection of specific monomers for the hard segments and soft segments influences the PUs hydrophilicity, crystallinity and surface energy. These physicochemical properties govern how the material interacts with cells and proteins at the tissue interface, while simultaneously determining the polymer's susceptibility to various *in vivo* degradation pathways [207]. The following subsections analyze the specific mechanisms of surface interactions and the distinct biological and chemical degradation pathways that govern PU performance in medical applications.

4.2.2.1. Surface interactions

The interactions between biomaterial and living tissue, including cell adhesion, proliferation and migration on the polymer surface, strictly influences the success or failure of the medical device. To optimize integration, PU surfaces must be designed to mimic the tissue-specific ECM architecture and its specific physicochemical properties, such as surface roughness, wettability and free energy. Lack of such interactions frequently triggers local infections, chronic inflammation or severe foreign body responses.

Studies show that cell-biomaterial adhesion relies on both long-range physical interactions (van der Waals forces, electric repulsions) and short-range chemical interactions (hydrogen bonds, hydrophobic interactions). These forces can be directly altered by adjusting the hydrophobic/hydrophilic balance and the ratio of hard to soft segments in PU material. For example, it was observed that endothelial cells exhibit distinct behaviors depending on the PU composition: they proliferate into a continuous single layer on polyester-based PUs [208] but restrict their growth to limited areas on polyether-based PUs [209].

In case of biodegradable polyurethane scaffolds for tissue engineering applications, cell adhesion is usually desirable to achieve therapeutic effect. Cells fundamentally rely on integrin-mediated interactions with the extracellular matrix to attach, proliferate and differentiate. Because synthesized PU networks frequently exhibit high hydrophobicity, they tend to resist favorable protein adsorption, which subsequently limits initial cell attachment [210]. Experimental data demonstrate that applying plasma treatment or chemical hydrolysis to the PU surface increases surface wettability and roughness, generating a physical environment more suitable for cellular integration [211]. Alternatively, blending the synthetic PU with natural polymers, including collagen, gelatin or chitosan, provides endogenous binding sites that mimic the native extracellular matrix, actively supporting cell adhesion and tissue remodeling [212].

While strong cell adhesion benefits tissue engineering scaffolds, it is not desirable in blood-contacting applications, such as cardiovascular implants and catheters. In these environments, the non-specific adsorption of proteins (like fibrinogen and albumin) and the subsequent adhesion of platelets must be actively suppressed to prevent thrombosis and embolism [213]. To achieve thromboresistance, researchers utilize different strategies (Figure 19). One of them is to synthesize polyurethane ionomers by incorporating anionic, cationic or

zwitterionic groups into the polymer backbone. Experimental data demonstrate that zwitterionic PUs, particularly those containing carboxybetaine or sulfobetaine moieties, exhibit exceptional non-fouling properties [214]. These zwitterionic groups feature uniformly distributed, oppositely charged units that minimize the dipole moment and promote strong hydration via ionic solvation. This hydration layer acts as a physical and energetic barrier, effectively repelling proteins and cells. Similarly, studies indicate that incorporating hydrophilic PEG chains [215] or heparin-mimicking sulfate groups to the PU surface [216] significantly decreases platelet deposition and thrombus formation.

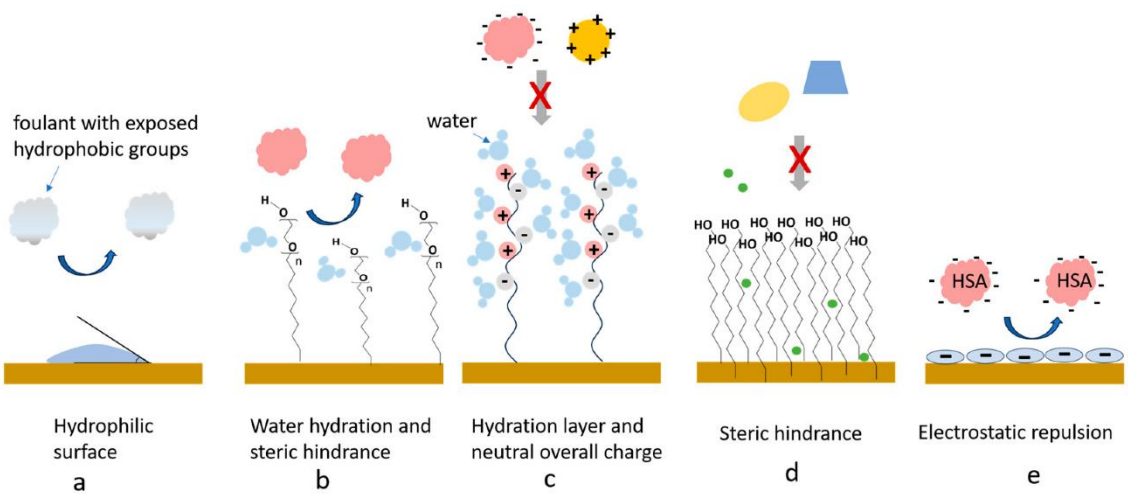


Figure 19 The main strategies of counteracting non-specific adsorption of proteins: a) surface hydrophobization, b) attachment of long, hydrophilic polymers, c) usage of zwitterionic polymers, d) creating steric hindrance or e) surface negatively charging. Adapted from: [217] under CC BY 4.0 license.

4.2.2.2. Degradation pathways

Within the physiological environment, polyurethanes face a complex combination of degradation mechanisms. Researchers categorize these breakdown processes primarily into hydrolytic, oxidative and enzymatic pathways. The most important biodegradation reactions of polyurethanes were depicted in Figure 20. The degradation kinetics strictly depend on the chemical composition of the soft and hard segments, which describes whether the polymer functions as a biostable implant or a bioresorbable scaffold.

Hydrolytic degradation occurs when water penetrates the polymer matrix and cleaves susceptible chemical bonds. Water molecules can react with the ester linkages in the PU's soft segments, causing chain scission that generate shorter fragments with hydroxyl and carboxyl end groups. The accumulation of these acidic carboxyl groups locally lowers the pH, which subsequently acts as an autocatalyst to accelerate further polymer breakdown [218]. Consequently, this process causes a rapid loss of molecular weight and mechanical integrity. This process is frequently utilized to control biodegradation for tissue engineering applications, when PCL or PLA are used as polyols. Conversely, when long-term biostability is required, polyether-based or polycarbonate-based soft segments are preferred due to their superior resistance to hydrolysis.

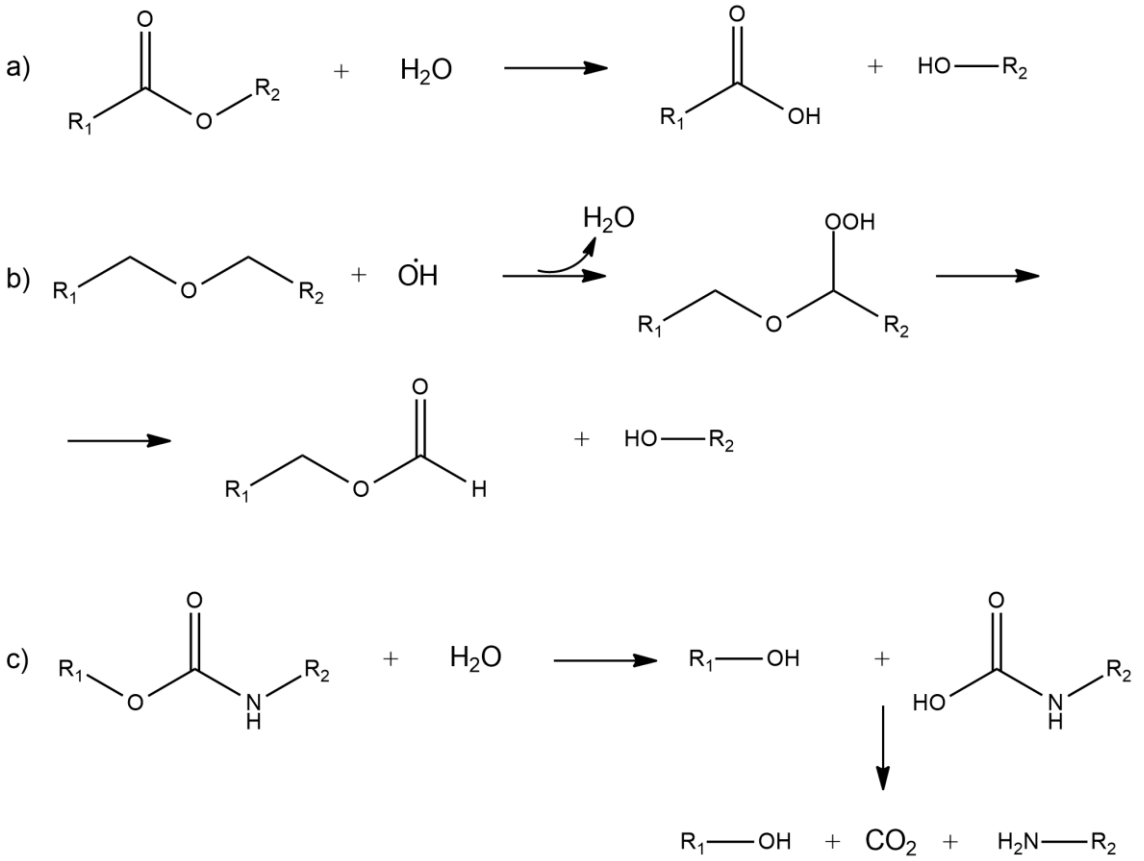


Figure 20 Schematic representation of the most important biodegradation reactions of polyurethanes: a) polyol ester bond hydrolysis, b) polyol ether bond oxidation, c) urethane bond hydrolysis.

Although polyether-based PUs resist hydrolysis, they exhibit significant susceptibility to oxidative degradation *in vivo* [219]. This process is mainly driven by the host immune response. Following implantation, monocyte-derived macrophages attach to the biomaterial surface and release highly reactive oxygen species, including oxygen radicals and hydrogen peroxide [220]. These oxidative agents attack the ether bonds within the soft segment. Experimental data indicate that this localized chemical oxidation, combined with physiological mechanical stress, induces environmental stress cracking [221]. This phenomenon manifests as deep surface cracks that eventually cause structural failure of the medical device. To mitigate oxidative degradation, polyethers can be replaced by siloxanes or polycarbonates, which demonstrate enhanced oxidative stability compared to standard polyether networks.

In parallel with hydrolysis and oxidation, biological enzymes actively participate in polymer breakdown. Aqueous enzymes, such as cholesterol esterase and various proteolytic enzymes like papain, interact directly with the polymer surface [210]. Moreover, enzymatic degradation frequently operates synergistically with oxidative pathways, as PUs subjected to prior oxidation by macrophage-derived radicals exhibit significantly higher susceptibility to subsequent enzymatic cleavage [222]. While cholesterol esterase primarily targets the soft segment linkages, proteolytic enzymes can cleave the urethane and urea bonds within the hard segment domains [223].

The chemical breakdown of the polyurethane network ultimately releases degradation by-products into the surrounding physiological space. Soft segment degradation typically yields small-chain hydroxyls, carboxylic acids, aldehydes or ketones, which, apart from inducing local pH changes, typically do not have negative impact on the host's body [218]. However, hard segment breakdown presents more critical safety challenges. The enzymatic or hydrolytic cleavage of urethane bonds produces polyamines [223]. If manufacturers synthesize the polyurethane using conventional aromatic diisocyanates, such as toluene diisocyanate or methylene diphenyl diisocyanate, the resulting degradation products include toluene diamine and methylene dianiline [224]. Experimental evidence suggests that these specific aromatic amines are highly cytotoxic and potentially carcinogenic, precluding their use in bioresorbable applications. Thus, to resolve this toxicity issue, strictly aliphatic diisocyanates should be utilized, including HDI or IPDI, for any polyurethane designed to degrade within the body. The aliphatic polyamines generated from these structures demonstrate significantly lower toxicity and are safely metabolized or cleared by the liver and kidneys [225].

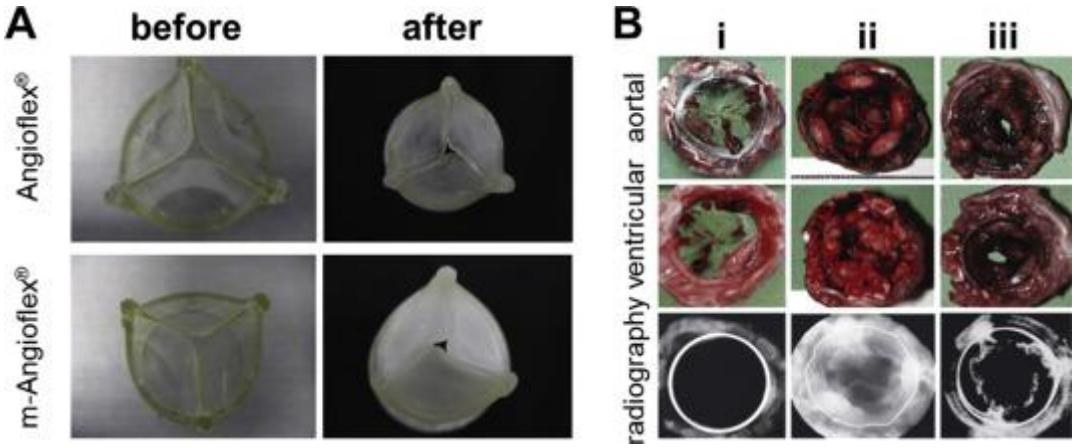


Figure 21 Comparison of calcification susceptibility of different polyurethane heart valves. A) polyether-based polyurethane Angioflex® and it's bisphosphonate-modified version valves before and after calcification. B) (i) Polycarbonate-based polyurethane (ADIAM®) after 20 weeks of implantation, (ii) porcine-based Mosaic® after 10 days and (iii) bovine-based Perimount® after 30 days (animals died after the indicated time for ii and iii implants). Adapted from: [226] under CC BY-NC-ND 4.0 license.

Finally, in blood-contacting applications such as cardiovascular implants, polyurethanes frequently undergo calcification. In this process, cellular debris and localized thrombi facilitate the deposition of calcium sediments onto the polymer surface [227]. While this mechanism alters the surface chemistry more than the bulk structure, the progressive accumulation of calcium causes severe hardening, loss of material elasticity and eventual macroscopic fractures that severely limit the lifespan of the medical device and eventually causes host's death. To suppress this detrimental calcium diffusion and extend implant viability, surface modifications and specific structural compositions are continuously investigated. The polycarbonate-based PUs show superior resistance to calcification and were successful introduced to the market as the ADIAM® [228] (Figure 21B). Another approach is introduction of siloxanes into the PU structure, e.g. in form of hybrid polysiloxane/polyether-based polyurethanes (Angioflex®) that demonstrate

superior resistance to calcification [227] (Figure 21A). Other modifications include application of metal chelating agents like ethylenediaminetetraacetic acid (EDTA) and citric acid or trivalent cations such as Al^{3+} and Fe^{3+}, which are highly effective at blocking calcium-binding sites and disrupting mineral crystallization.

4.2.3. Polyurethane structure tuning and modifications

To meet the strict mechanical and biological demands of dynamic physiological environments, the properties of polyurethane networks have to be precisely adjusted. Medical devices are subjected to cyclic loading, enzymatic attacks and complex cellular interactions, necessitating materials that adapt to these exact conditions. The versatile chemistry of PUs allows for comprehensive modifications at multiple levels. Researchers modify the base PU materials through direct chemical structural engineering, physical blending with natural macromolecules, integration of nanoparticles or the localized loading of bioactive compounds. The summary of the most common modification routes was presented in Figure 22. These four main modification strategies act synergistically to define the final physicochemical profile, determining how the material behaves under physiological stress and interacts with living tissue over its functional lifespan.

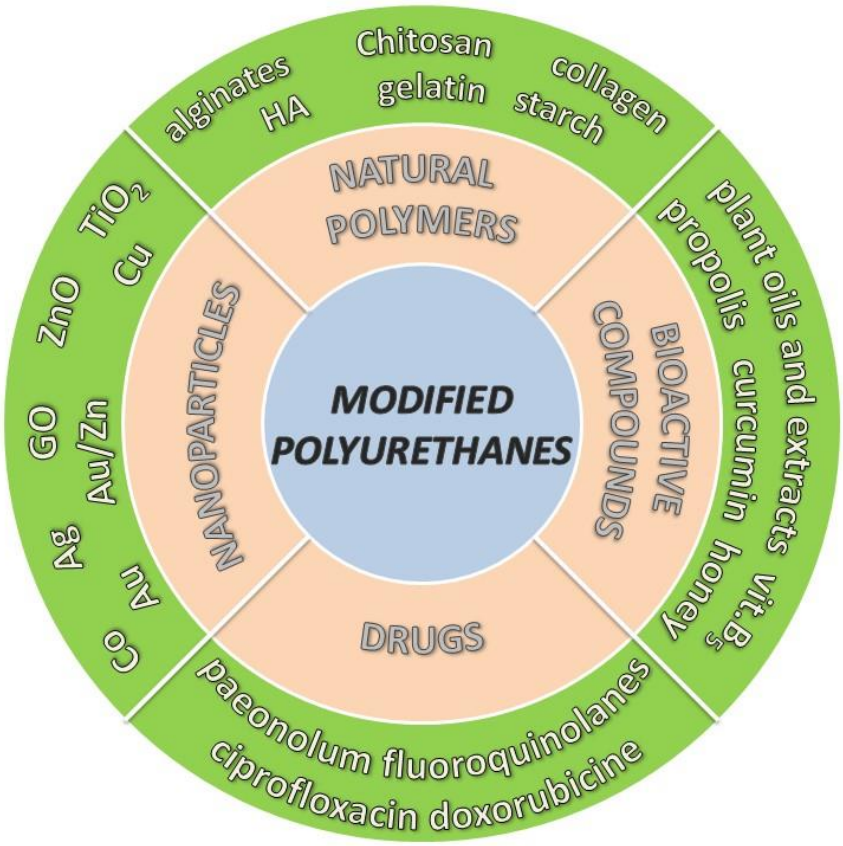


Figure 22 Four main groups of most used polyurethane modification methods useful in biomaterials manufacturing: natural polymers, bioactive compounds, drugs and nanoparticles. For each group, the mostly used compounds were described.

4.2.3.1. Chemical structural engineering

Due to PU's chemistry, the fundamental method for altering PU-based material behavior involves the direct manipulation of its monomeric composition and chain architecture. The structure, defined mainly by phase separation between hard and soft segments, can be directly engineered by modifying the stoichiometric ratio of isocyanates, polyols and chain extenders. Experimental data demonstrate that increasing the hard segment concentration increases the crystalline domain fraction, which yields materials with higher tensile strength, enhanced abrasion resistance and a greater Young's modulus [160]. On the other hand, expanding the soft segment length enhances the mobility of the polymer chains, yielding networks with superior elasticity and elongation at break [159]. This ratio also fundamentally controls shape-memory capabilities. Studies show that tuning the glass transition temperature of the soft segment relative to physiological temperatures allows researchers to program polyurethanes that maintain a temporary shape during surgical insertion and recover their permanent architecture upon exposure to body heat [229].

Beyond the chemical identity of the macrodiol (described in previous sections), the specific arrangement and length of the soft segments fundamentally alter the phase separation and, consequently, the bulk mechanical properties of the polyurethane. According to the Flory-Huggins phase separation theory, the block length of the copolymers heavily defines the extent to which the hard and soft domains segregate [230,231]. By carefully adjusting the polymerization parameters, such as the prepolymerization time, monomer feed ratio or reaction temperature, the sequence length of the soft segments can be controlled. Studies demonstrate that modulating the segment arrangement in traditional formulations yields elastomers with significantly enhanced tensile strength and exceptional toughness [232].

Apart from the microstructure adjustments, scientists synthesize polyurethanes with specialized functional groups or building blocks integrated directly into the polymer backbone. The examples of such polyurethane structural tuning were presented in Figure 23. Studies indicate that incorporating stimuli-responsive moieties, such as disulfide, hydrazine, ketal or diselenide linkages, produces dynamic networks capable of changing their conformation in response to specific pH variations or reducing environments [233]. For instance, the reductive cleavage of disulfide bonds within the polyurethane chain allows for the controlled, triggered disassembly of the polymer matrix in glutathione-rich tumor microenvironments [234]. Furthermore, researchers engineer self-healing polyurethanes by introducing dynamic covalent bonds or reversible non-covalent interactions, such as metal-ligand coordination and dense hydrogen bonding arrays [235]. This capability allows the material to autonomously repair structural micro-damage, which significantly extends the functional lifespan of load-bearing implants. Additionally, modifying the soft segment by partially substituting standard macrodiols with specific end-functionalized polymers, such as hydroxyl-terminated polyacrylates, effectively suppresses cavitation during deformation, thereby improving the material's fatigue resistance and self-healing capacity [236]. Such precise structural engineering at the macromolecular level

utilizing the most recent advances in synthetic chemistry (atom transfer radical polymerization - ATRP, reversible addition-fragmentation chain transfer - RAFT, group transfer polymerization – GTP, click chemistry) will allow researchers to develop ultra-tough biomaterials capable of withstanding the dynamic mechanical environments of cardiac and muscular tissues in future.

Recent advancements in polymer processing have expanded the functional capabilities of biodegradable polyurethanes. The development of waterborne polyurethanes (WBPU) enables the fabrication of highly flexible scaffolds that induce no apparent acute rejection or inflammation *in vivo*. Evidence demonstrates that these specific polyurethane scaffolds undergo controlled degradation without causing a local accumulation of acidic substances [67]. This presents a distinct biological advantage over traditional biodegradable polyesters, such as PLA or PGA, which often release acidic metabolites that alter the pH of surrounding tissues and provoke localized inflammatory responses [66]. Furthermore, researchers synthesize specialized polyurethane variants that exhibit shape-memory properties [68]. These responsive materials possess the capability to maintain a temporary physical form and subsequently revert to their permanent structure upon exposure to specific stimuli.

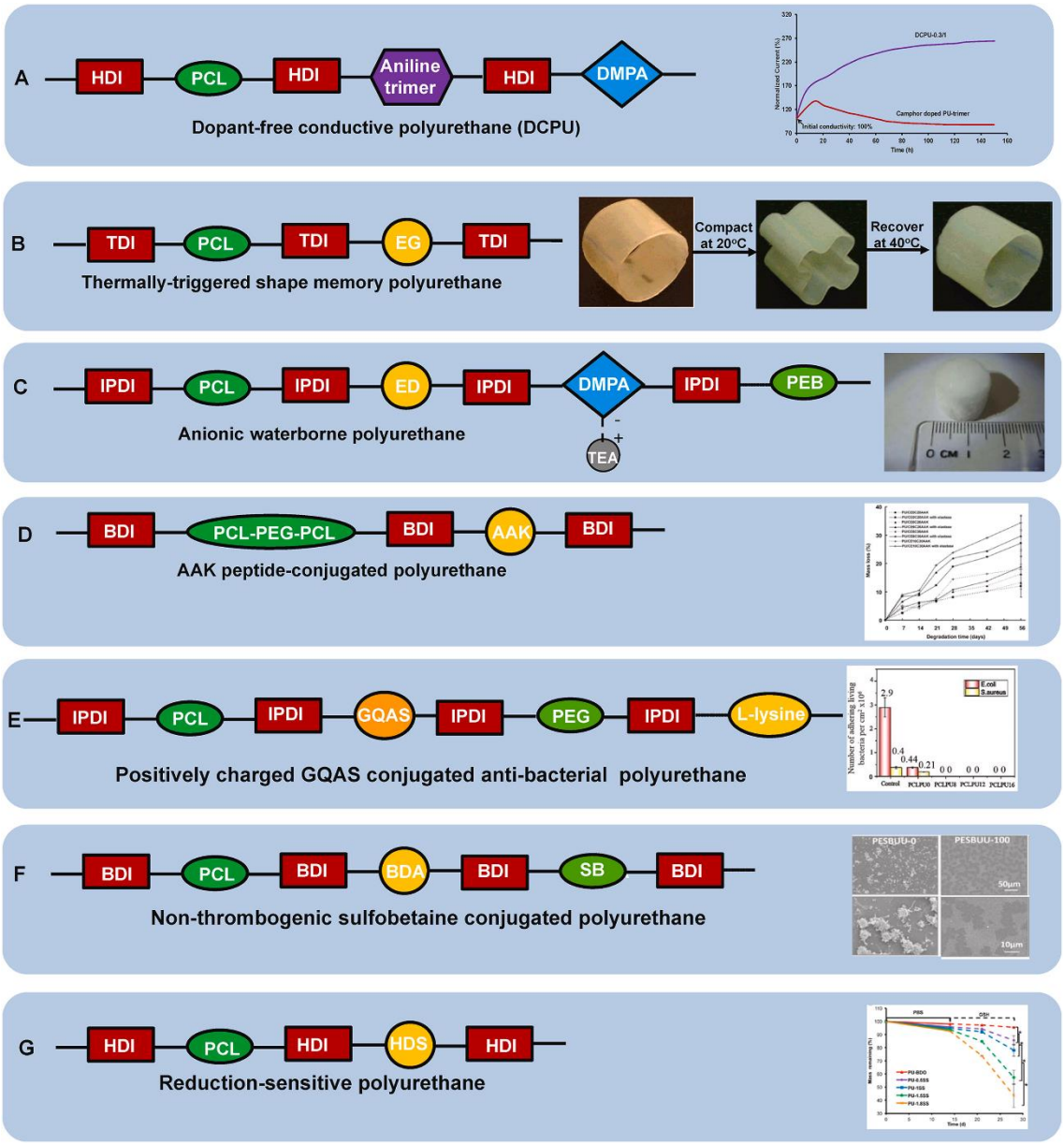


Figure 23 Examples of polyurethane structure tuning and modifications. On the left there are presented structural designs and on the right the exemplary features. Modifications for: A) electrical conductivity, B) temperature induced shape-memory, C) solubility in water, D) enzymatic degradation susceptibility, E) antibacterial properties, F) reduction of thrombogenesis, G) reduction degradation susceptibility. Adapted from: [205], under CC BY-NC-ND 4.0 license.

4.2.3.2. Blending with natural polymers

Utilizing naturally derived polyols or blending with natural polymers is viable strategy to promote biological recognition and robust cellular integration of PU-based materials. Researchers successfully integrate biomacromolecules, including polysaccharides (such as starch, cellulosic derivatives, chitin and alginate) [237,238] or precursor molecules produced by microorganisms [239] into the soft segment domains. This approach combines the tunable mechanical integrity and biostability of the synthetic network with the inherent bioactivity, hemocompatibility and enzymatic degradability of natural macromolecules. The exemplary techniques of creating such

blends and/or composites were presented in Figure 24. However, successful blending requires precise thermodynamic control as the synthetic and natural polymers exhibit inherently different polarities and molecular weights, causing macroscopic phase separation during processing [240]. To mitigate this incompatibility, different strategies are utilized, including optimizing solvent selection, controlling processing temperatures or introducing chemical cross-linkers, to ensure a thermodynamically stable, homogeneously dispersed composite material.

Polysaccharides represent a primary class of natural additives utilized to modify polyurethane materials. Chitosan, a chitin derivative, is often used to impart inherent antimicrobial properties to the polyurethane matrix. Experimental data indicate that blending thermoplastic polyurethanes with chitosan via melt extrusion or solvent casting produces semi-crystalline structures with significantly enhanced surface wettability [241]. The abundant amine and hydroxyl groups on the chitosan backbone form dense inter-chain hydrogen bonds with the urethane linkages, which stabilizes the blend and prevents the rapid dissolution of the polysaccharide in physiological fluids. Furthermore, studies show that incorporating alginates alters the water vapor transmission rate of polyurethane films, optimizing the moisture environment to facilitate rapid granulation tissue formation in dermal wound dressings [242].

Another often utilized natural polymer is hyaluronic acid, which plays a critical role in native tissue repair and angiogenesis. Evidence suggests that enriching PU electrospun scaffolds with HA significantly accelerates the proliferation and migration of fibroblast cells at the material interface [243]. In physiological models, these specific blends demonstrate accelerated wound closure rates and reduced inflammatory responses compared to neat polyurethane controls. However, HA is susceptible to rapid enzymatic degradation by native hyaluronidases, thus mild chemical cross-linking techniques are often applied during the blending process, extending the functional lifetime of the bioactive component within the synthetic matrix [244].

Another approach to further integrate PU-based materials with the native physiological environment, protein-based biopolymers, predominantly collagen and its denatured derivative, gelatin can be utilized. These natural proteins supply critical endogenous binding domains that synthetic polyurethanes lack. Studies demonstrate that electrospinning polyurethane alongside gelatin produces micro-fibrous and nano-fibrous scaffolds that accurately mimic the topological architecture of the extracellular matrix [245]. Thanks to the gelatin component, which exposes specific amino acid sequences (RGD motif), the human endothelial cells and osteoblasts adhere more rapidly and display enhanced differentiation markers on polyurethane-gelatin blends than on unmodified polyurethane surfaces.

Finally, researchers can utilize cellulose-derived materials, including cellulose nanowhiskers or carboxymethyl cellulose, to simultaneously modulate the mechanical profile and degradation kinetics of the blends. While large-scale blending with cellulose alters the macroscopic hydrophilicity of PU-based materials, integrating highly crystalline cellulose domains into the PU soft segments acts as a physical reinforcement mechanism [246]. This addition increases the tensile modulus and restricts the free volume of the polymer chains. Additionally,

these structural changes allow to precisely tune the degradation rate as the hydrophilic cellulose-based domains degrade rapidly via enzymatic action. This process gradually increases the porosity of the implant to permit cellular infiltration, while the synthetic polyurethane framework maintains the required mechanical support until native tissue fully regenerates [247].

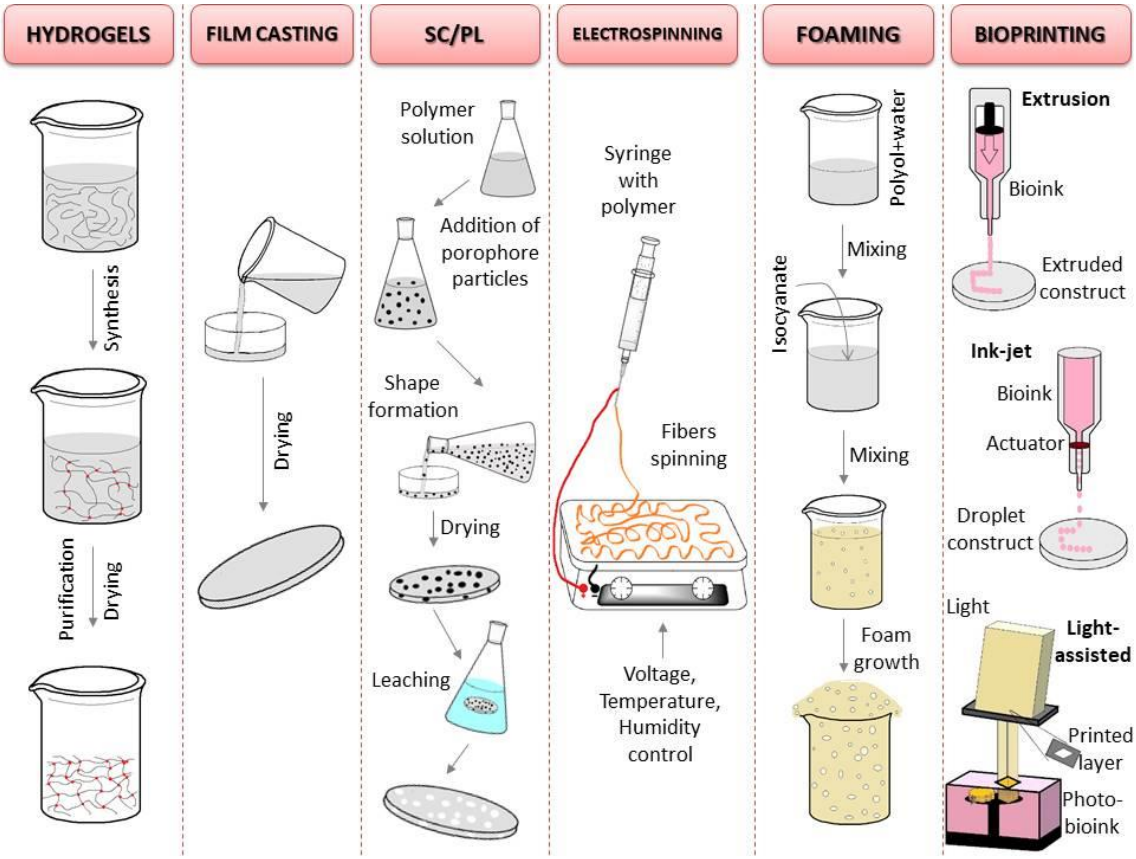


Figure 24 Graphical representation of main fabrication methods for small-scale manufacturing of PU-based blends and composites useful in tissue engineering: hydrogels formation, film casting, SC/PL, electrospinning, foaming and bioprinting.

4.2.3.3. Loading with drugs and natural active substances

Designing infection-resistant biomaterials has been widely focused on by numerous research groups. Ideal infection-resistant material should provide the following features: providing a moist environment in the wound site to improve the healing process, enable new tissue formation without scar tissue formation, a broad spectrum of antimicrobial activity, effective absorption of wound exudates enabled permeability for gases and delivery of therapeutics and/or nutrients (and at the same moment removal of metabolites) for cells growth and proliferation and also tissue regeneration and remodeling. These strict requirements can be fulfilled partially by the proper design of PU-materials, which can provide mechanical support, physicochemical properties, thermal stability and biodegradation.

Bacterial adhesion represents another critical challenge at the tissue-material interface. Bacteria, such as *Staphylococcus aureus*, rapidly adhere to biomaterial surfaces (often within minutes) preferentially binding to hydrophobic segments. Once attached, they form highly

resistant biofilms that cause severe implant-associated infections and degrade the PU matrix. To prevent biofilm formation, active bactericidal compounds can be integrated directly into the PU matrix, such as fluoroquinolones (FQLs) [175]. FQLs represent an essential group of chemotherapeutic compounds with a broad spectrum of activity against various pathogenic microorganisms resistant to aminoglycosides, penicillin, cephalosporins, tetracyclines and other antibiotics. For example, ciprofloxacin exhibits activity against aerobic Gram-negative and Gram-positive bacteria, while is especially active against *P. aeruginosa*, aminoglycoside-resistant bacteria and beta-lactamase-producing organisms [167]. Other common antibiotics include chloramphenicol [248], mupirocin [249], doxorubicin [250] or clindamycin [251]. Other studies demonstrate that modifying the PU soft segments with iodine-based compounds produces strong contact-killing properties due to the oxidation and subsequent release of iodine, which effectively inhibit bacterial proliferation [252,253].

Furthermore, researchers evaluate natural additives to enhance both antimicrobial resistance and biocompatibility. As previously described, creating blends of PU with polysaccharides, such as chitosan, yields hybrid composites that exhibit significant antibacterial capabilities. Similarly, experimental data show that enriching polyurethane matrices with natural organic extracts provides remarkable antimicrobial properties suitable for clinical wound healing applications. The exemplary studies utilizing natural active substances were summarized in Table 5. One of such examples is cinnamaldehyde (CA), the main component of cinnamon oil, a natural compound extracted from the cinnamon leaf and bark [250]. Another example is honey, which was used historically in traditional medicine for wound treatment thanks to its inherent antimicrobial and antioxidant properties. Recent research in this regard, focuses on the propolis - a resinous compound, which is called bee glue. The bioactive constituents of propolis are flavonoids, phenolic components, amino acids and some inorganic compounds. The addition of propolis to PU-based materials induce anti-inflammatory effect, antibacterial, antifungal, antiviral and antioxidant properties [254,255].

On of the most important natural antibacterial agents in the modern medicine is curcumin, known of its effect against both Gram-positive and Gram-negative bacteria species. Moreover, curcumin was observed to show antioxidant, antitumor and anti-inflammatory activities [173]. However, due to its hydrophobic nature, curcumin has poor aqueous solubility, resulting in low bioavailability itself. This problem may be solved by proper polymer fabrication or processing, e.g., electrospinning. Although addition of curcumin is an interesting approach, the number of quality studies regarding its introduction to PU materials is largely limited. Other popular substances used for antibacterial properties are essential oils. Lavender oil, murivenna oil, sesame oil, turmeric oil (where curcumin is an active compound) or channa striatus (also called snakehead fish oil) represent good antibacterial activity and anti-inflammatory effects [256–260] when introduced into PU-based materials.

Despite their enormous research interest, natural substances inherently exhibit significant batch-to-batch chemical variability depending on their geographic origin and extraction methods,

which tends to complicate the rigorous standardization required by regulatory agencies. Furthermore, these bioactive compounds frequently demonstrate poor thermal and chemical stability, restricting their ability to survive the high-temperature processing conditions necessary to manufacture synthetic polymer devices. Consequently, although experimental models suggest promising antimicrobial efficacy, manufacturers struggle to translate these heterogeneous formulations into reproducible, clinically approved products that satisfy strict medical device regulations.

Table 5 Examples of polyurethane-based biomaterials modified with natural active substances.

Fabrication method	Polyurethane type	Additive/modifier	Main results	Refs.
Freeze drying	Synthesized from PCL, HDI, dimethylol propionic acid, triethylamine	Soy protein isolate	Controllable tensile and compressive strength (~0.5-6 MPa); superior water absorption; enhanced proliferation of fibroblast cells by 40%; biodegradability and wound regeneration after 7 months of implantation	[261]
Two-step polymerization procedure	Synthesized from α, ω-dihydroxy(ethylene-butylene adipate), HDI, 1,4-butanodiol and ascorbic acid	Polylactide, ciprofloxacin	Suitable tensile strength ~800 kPa; 45% degradation after 15 days; good antimicrobial properties (up to 22 mm of inhibition zone diameter)	[175]
Electrospinning	Tecoflex® EG-80A	Turmeric oil	Great blood compatibility with very low percentage of lysis of red blood cells; enhanced proliferation of fibroblast cells by 20%; hydrophilic surface	[259]
	Tecoflex® SG-80A	Gelatin/Amnion	High tensile strength; biocompatibility and bioactivity surpassing seeded tissue culture after 14 days; wound healing capability after 14 days	[262]
	Cardio Technology PU M_w=110 kDa	Salicylic acid	Enhanced proliferation of fibroblast cells by 30% with improved attachment; antimicrobial properties; facile fabrication	[263]
	Tecoflex® SG-80A and Carbothane® PC-3575A	Silk fibroin	Great viability and attachment of human foreskin fibroblasts; high mechanical and physical properties	[264]
	Skythane® X595A-11	Propolis	Great cell adhesion; hydrophilicity; cytocompatibility	[265]
Flim casting	Synthesized from castor oil, CAPA 7201, diethylene glycol and HDI	-	Suitable tensile strength (4 MPa); good water absorption and vapors transmission; biocompatibility and significant acceleration of wound closure time	[266]
Foaming	Synthesized from polypropylene glycol, Dabco DC5810, Dabco 33-LV, T9 tin catalyst and TDI	Starch, cellulose derivatives, chitosan, alginate, gelatin, asiaticoside, silver NPs	High water absorption; appropriate vapors transmission; increased compression strength; no irritations and significantly accelerated wound closure time and epithelialization	[267]
Bioprinting	Synthesized from PCL, poly(D, L-lactide), IPDI, dimethylolpropionic acid and ethylenediamine	Gelatin, sodium bicarbonate	High printing resolution (~210 μm); tunable viscosity and degradation rate; high proliferation rate (>220%); accelerated wound closure time and epithelialization	[268]

4.2.4. Polyurethane commercial medical applications

Polyurethanes transition from laboratory research to commercial medical applications due to their tunable mechanical resilience and demonstrated hemocompatibility. Conventional medical-grade polyurethanes, including commercial formulations like Pellethane™ and Tecoflex™, typically utilize aromatic diisocyanates. These polymers function primarily as biostable materials for long-term implantation: cardiovascular devices, advanced wound management systems, load-bearing orthopedic implants and flexible bioelectronics. However, as described in previous sections, upon *in vivo* degradation, aromatic polyurethanes may release toxic byproducts, such as aromatic diamines. Therefore, modern tissue engineering explicitly requires the use of aliphatic diisocyanates to ensure the safe resorption of the implant and its degradation products. Modification of PUs in terms of biocompatibility and mimicking potential by blending PUs with other biopolymers, incorporation of nanoparticles into PUs and advancing fabrication techniques could be also considered. Such modifications, targeted at the application of resulting materials in wound healing were briefly summarized in Table 6. The most often reported commercial PU was Tecoflex™, which is due to its characteristics. Tecoflex™ is a group of aliphatic, medical grade polyether-based PUs of hard segments derived from HDI. It represents excellent flexibility, good biodegradability, biocompatibility, barrier properties and oxidation stability. Moreover, Tecoflex™ is thermoplastic and can be processed with a variety of techniques, methods and technologies. Thus, it is so widely used in current medical research on skin engineering products.

As stated before, cardiovascular engineering represents the most established commercial sector for biomedical PUs. The dynamic physiological environment of the human circulatory system requires materials that resist cyclic fatigue and limit thrombogenesis. Manufacturers utilize biostable polyurethanes to fabricate pacemaker lead insulation, central venous catheters or synthetic vascular grafts. Historically, polyether-based formulations faced failures due to *in vivo* oxidative degradation and environmental stress cracking. To resolve this structural vulnerability, the industry transitioned to polycarbonate-based polyurethanes, such as ChronoFlex™, which demonstrate superior oxidative stability and long-term biostability [269]. Similarly, manufacturers utilize siloxane-modified polyurethanes, such as Elast-Eon™, to further enhance the chemical degradation resistance of cardiovascular leads [270]. For highly specialized structural components, engineers employ Angioflex™ – PU specifically formulated to resist calcification and mechanical fatigue in artificial heart valve leaflets and ventricular assist devices [227].

Another area of high PU-based materials utilization is the wound dressings segment. In dermal repair, the commercial market relies heavily on PU foams and transparent semi-permeable films. Effective wound management necessitates regulating the local moisture environment and preventing bacterial infiltration. Products like Allevyn™ utilize highly absorbent polyurethane foams to manage excessive inflammatory exudate while maintaining a moist wound bed [271]. This physical mechanism accelerates granulation tissue formation without adhering directly to the regenerating tissue, which prevents mechanical trauma during dressing changes.

Commercial semi-permeable films, such as Tegaderm™, provide selective surface permeability. They permit oxygen and water vapor transmission but actively block liquid water and environmental pathogens [272]. For advanced tissue regeneration, manufacturers offer fully biodegradable polyurethane matrices, such as NovoSorb®. This specific material functions as a resorbable dermal template for severe burn injuries, degrading completely via hydrolysis as native cellular infiltration progresses [273]. The list of commercial products found on the WoundSource, an annual wound care product reference guide, based on these PUs was presented in Table 7.

The commercial integration of PUs into orthopedics focuses on bone cements, gap fillers and structural soft tissue scaffolds. Traditional acrylic-based bone cements frequently exhibit high exothermic curing temperatures that cause local tissue necrosis [274]. To mitigate thermal damage, companies developed PU-based bone adhesives, such as Kryptonite™ [275]. These commercial alternatives cure via distinctly less exothermic reactions while providing equivalent mechanical fixation and permitting subsequent bone ingrowth. Additionally, the industry produces degradable polyurethane scaffolds for soft tissue reinforcement. For example, Artelon® is a commercial degradable polyurethane-urea matrix utilized by orthopedic surgeons to augment tendon and ligament repairs [276]. These structural scaffolds support the required mechanical loads immediately after surgery, while gradually transferring stress from the degrading polyurethane scaffold to the newly formed mineralized tissue, preventing stress shielding and promoting healthy bone remodeling.

Finally, manufacturers apply highly calibrated PUs coatings to commercial drug-eluting stents [277]. These coatings regulate the sustained release of anti-restenosis pharmaceuticals, such as paclitaxel, which inhibits local smooth muscle cell proliferation and prevents subsequent vessel occlusion. In parallel, the commercial landscape continuously expands toward flexible bioelectronics. Polyurethane elastomers, including medical-grade Tecoflex®, frequently serve as structural substrates or encapsulating layers for wearable sensors and implantable neural electrodes [278]. The inherent mechanical compliance of the polyurethane network minimizes the stiffness mismatch between rigid electronic components and soft biological tissues. This interface optimization suppresses chronic inflammatory responses and maintains long-term signal fidelity in complex medical devices.

4.2.5.Current state of polyurethane-based biomaterials

Polyurethane-based biomaterials are widely used and have an established position in biomedical field due to their segmented architecture, which permits precise control over final material properties. Proper engineering of flexible soft segments (composed of polyesters, polyethers or polycarbonates) and rigid hard segments (composed of diisocyanates and chain extenders) can result in the increased compliance with diverse soft and hard native tissues.

Historically, biostable PUs served as first-generation biomaterials, being commonly utilized in blood-contacting devices, including pacemaker leads and vascular grafts. Susceptibility to macrophage-mediated environmental stress cracking in polyether formulations led to the

adoption of polycarbonate-based soft segments that exhibit oxidative resistance and reduced calcification. Utilization of biodegradable polyesters (PLA, PGA, PCL) and aliphatic diisocyanates (HDI, IPDI, LDI) allowed for creation of hydrolytically degradable biomaterials of second-generation, that degrade into non-cytotoxic metabolic intermediates. To create fully third-generation PU-based biomaterials, functionalization strategies have to be employed to enhance biointeractivity, usually utilizing ECM peptides, natural biopolymers (chitosan, hyaluronic acid) or inorganic nanoparticles (hydroxyapatite) to drive cell proliferation and osteointegration. Furthermore, PUs can be used to form dynamic matrices for fourth-generation stimuli-responsive systems, including shape-memory scaffolds and bioelectronics.

Despite these structural and clinical advancements, several research gaps still remain. The most important one is the fact that despite the known toxicity, many commercial and experimental formulations still utilize aromatic diisocyanates (MDI, TDI) due to their high reactivity, risking the release of carcinogenic diamines during *in vivo* degradation. The translation to aliphatic isocyanates is slow, as it is often associated with significantly slower reaction kinetics and initial mechanical stiffness, requiring usage of metal catalysts (such as organotin compounds). In turn, it limits the positive effect, because most of the popular catalysts can exhibit cytotoxicity, forcing usage challenging purification protocols or implementation of less-common and costly catalytic systems. The second gap is directly related to possible cytotoxicity of PU-based materials. To improve the biocompatibility, natural polymers and extracts are often utilized. However, it is inevitably connected with the significant batch-to-batch chemical variability. Additionally, these compounds often exhibit low thermal stability, often excluding usage standard industrial processing or sterilization techniques. The third knowledge gap is associated with the complicated environment, directly influencing the polyurethane degradation. The real, *in vivo* degradation of PUs is often much faster than predicted, due to synergy of hydrolysis, oxidation and enzymatic effect of human body fluids, resulting in the mismatch between polymer resorption and new tissue buildup. The last identified gap is underdevelopment of real-time responsive and autonomous devices. Although shape-memory, electroconductive or sensitive PU-based implants are known and work *in vitro*, their integration into certified medical systems capable of continuous sensing or adaptive drug delivery is still missing.

These identified research gaps, together with the very low research interest in PU-based biomaterials, suggest that advancing knowledge in synthesis of non-toxic, biodegradable and bioactive polyurethanes can be an area worthy of research interest.

Table 6 Commercially available polyurethanes and their chemical modification, processing and targeted application in skin engineering.

Commercial PU type	Modifier	Processing	Application	Ref.
Biatain	Ciprofloxacin-bismuth complex	Foaming	Antibacterial wound dressing	[279]
Estane 5714F1	Fibrin and platelet lysate	Electrospinning	Diabetic wounds	[280]
HYPOL 2002	Tetramethylorthosilane	Foaming	Enhanced wound healing	[165]
PU (2363-80AE)	Chitooligosaccharide and dopamine	Film casting	Acute and chronic dermal wounds	[281]
Selectophore (81367-5 G)	Chitosan	Electrospinning	Skin regeneration	[282]
Tecoflex EG 80A	Sodium bicarbonate and pantothenic acid	Electrospinning	Chronic wounds treatment	[283]
	Turmeric oil	Electrospinning	Wound dressing	[259]
	Propolis	SC/PL	Wound dressing	[255]
	Sesame oil, honey, propolis	Electrospinning	Skin tissue engineering	[284]
	Garlic extract	Electrospinning	Wound dressings	[285]
	Ginger extract	Electrospinning	Wound healing	[286]
	Dietary grapes extract	Electrospinning	Skin tissue engineering	[287]
	Murivenna oil	Electrospinning	Wound dressing	[257]
	Starch and hyaluronic acid	Electrospinning	Skin tissue engineering	[243]
	Channa striatus	Electrospinning	Wound dressing	[260]
Tecoflex EG 85A	Dextran, curcumin	Electrospinning	Antibacterial membranes	[288]
Tecoflex LM 95A	Hyaluronic acid, glycerol, gelatin, fibrinogen	Bioprinting	Biomask for facial skin reconstruction	[289]
Tecophilic HP 60D 35	Hemicyanine dye and polyvinylpyrrolidone	Electrospinning	Sensors for bacterial infections	[290]
	Ciprofloxacin and hemicyanine dye	Electrospinning	Detecting and curing wound infections	[291]
Tecophilic SP 80 A150, Tecophilic HP 60 D20	Carbopol 981NF Carbopol 907	Film casting	Anisotropic wound dressings	[292]
Texin Rx85A	Starch	Electrospinning	Wound dressing	[293]
Texin RxT85A	Polydimethylsiloxane	Electrospinning	Skin tissue engineering	[294]

Table 7 Commercially available PU wound dressings (films or foams) found on the WoundSource, an annual wound care product reference guide.

Name	Description
Advazorb Lite	Soft and comfortable, non-adherent, hydrophilic polyurethane foam dressing.
Advzorb	Soft and comfortable hydrophilic polyurethane foam dressing with breathable backing.
Cardinal Health™	Thin hydrocolloid with semi-permeable film backing.
CovaWound™ Foam	Non-adherent dressing composed of soft, comfortable, highly absorbent polyurethane foam with breathable polyurethane film and an adhesive, breathable polyurethane boarder. The outer layer protects against eschar formation and is also waterproof, protecting against external contamination, while maintaining moist environment
CovaWound™ Silicone	Self-adherent soft silicone foam dressing with boarder. This atraumatic dressing consists of soft silicone adhesive that does not stick to the surface of the wound or cause epidermal stripping or pain upon removal. The absorbent core is made of polyurethane foam, nonwoven fabric and vapor-permeable membrane, which acts as a barrier to liquids and microorganisms.
GEMCORE360°™	Hydrocolloid film backed dressing, sterile, self-adhesive wound dressing. It consists of a thin absorbent wound contact layer of hydrocolloid with a backing layer of semi-permeable, low-friction, waterproof polyurethane film, which provides a bacterial barrier.
Kendall®	Window transparent film dressing made of semi-permeable polyurethane film, which allows moisture and oxygen transmission, while protecting against infection.
Lyofoam® Max	Polyurethane foam sterile dressing providing an appropriate wound environment to support optimal healing of lightly to moderately exudating wounds.
Lyofoam® MaxT	Polyurethane foam sterile dressing specially shaped with a “cross-cut” that permits close fitting around external tubes/cannulas or pins.
P-DERM®	Polyurethane adhesives form a thin and flexible wound covering providing a soft wound covers composed of cross-linked polymers reinforced with or bonded to mesh or fabric.
Suprasorb® F	Transparent film dressing. Thin, flexible, breathable made of polyurethane. Provides protection from external fluids and contaminants, maintains a moist wound.

4.3. Hydrogel matrices for localized drug delivery

Hydrogels are an essential part of the modern medicine, being applied in nearly all its branches – from cooling pads on pillows and mattresses, through the wound dressings and contact lenses, finishing on the advanced, degradable drug delivery systems [295]. Hydrogels constitute a class of three-dimensional, highly hydrated polymeric networks, defined by their unique capacity to absorb and retain significant volumes of water or biological fluids without dissolving. Thanks to these potent properties, hydrogels are a very popular research topic, accounting for approximately 3200 publications in 2025 (~2% of the biomaterials sector). Similarly to the PUs, data analysis reveals a trend toward hybrid research - the total keyword count across different generations nearly doubles the absolute number of papers, suggesting contemporary research combines characteristics from various stages of biomaterial evolution (Figure 25). Literature first identifies colloidal gel preparations in 1894, formulated using inorganic salts [296], but the modern foundation of biomedical hydrogels were established in 1960, when Wichterle and Lim have synthesized crosslinked poly(2-hydroxyethyl methacrylate) (pHEMA) for ophthalmic use in soft contact lenses [297]. This milestone marks the first generation of hydrogel biomaterials, where research was primarily focused on evaluating macroscopic properties, maximizing swelling capacity and improving mechanical durability through optimized chemical crosslinking. Following these initial structural advancements, in the late 90s, the field started transitioning toward materials engineered to respond dynamically to the surrounding environment. Since then, researchers have developed stimuli-responsive networks that undergo reversible phase transitions or volume alterations when exposed to specific physiological triggers, including fluctuations in temperature, local pH or ionic concentration [21].

The unique properties of hydrogels originate from the thermodynamic affinity between the aqueous solvent and hydrophilic functional groups distributed along the polymer backbone [23]. Functional groups such as hydroxyl, carboxyl, amino and amide domains facilitate hydrogen bonding with water molecules, driving solvent diffusion into the polymer matrix, causing its swelling [18]. Concurrently, structural crosslinks within the polymer matrix, consisting of either permanent covalent bonds, reversible ionic interactions or transient physical entanglements, counter this thin behavior, maintaining the structural integrity of the entire polymer network [298]. The equilibrium between thermodynamic swelling forces and elastic network reaction governs the final hydration state of the material. Thanks to the high water content, hydrogels can closely approximate the physical characteristics of native biological tissues, making them highly relevant for biomedical engineering. Furthermore, the soft, elastic nature of the hydrated network reduces mechanical friction and minimizes irritation upon contact with tissues, which allows broad utilization in diverse anatomical sites.

Apart from the swelling degree, the spatial arrangement of the crosslinked polymer chains generates a distinct porous architecture, which determines the material's permeability, directly controlling the diffusion of fluids through the hydrogel matrix. The ultimate porosity and average mesh size of the network can be controlled by modulating the crosslinking density during

synthesis, allowing hydrogels to encapsulate diverse therapeutic agents, including small molecule drugs, macromolecular proteins and intact mammalian cells [88]. Following encapsulation, the porous network is responsible the release kinetics of these active substances, providing a mechanism for sustained, controlled administration [152].

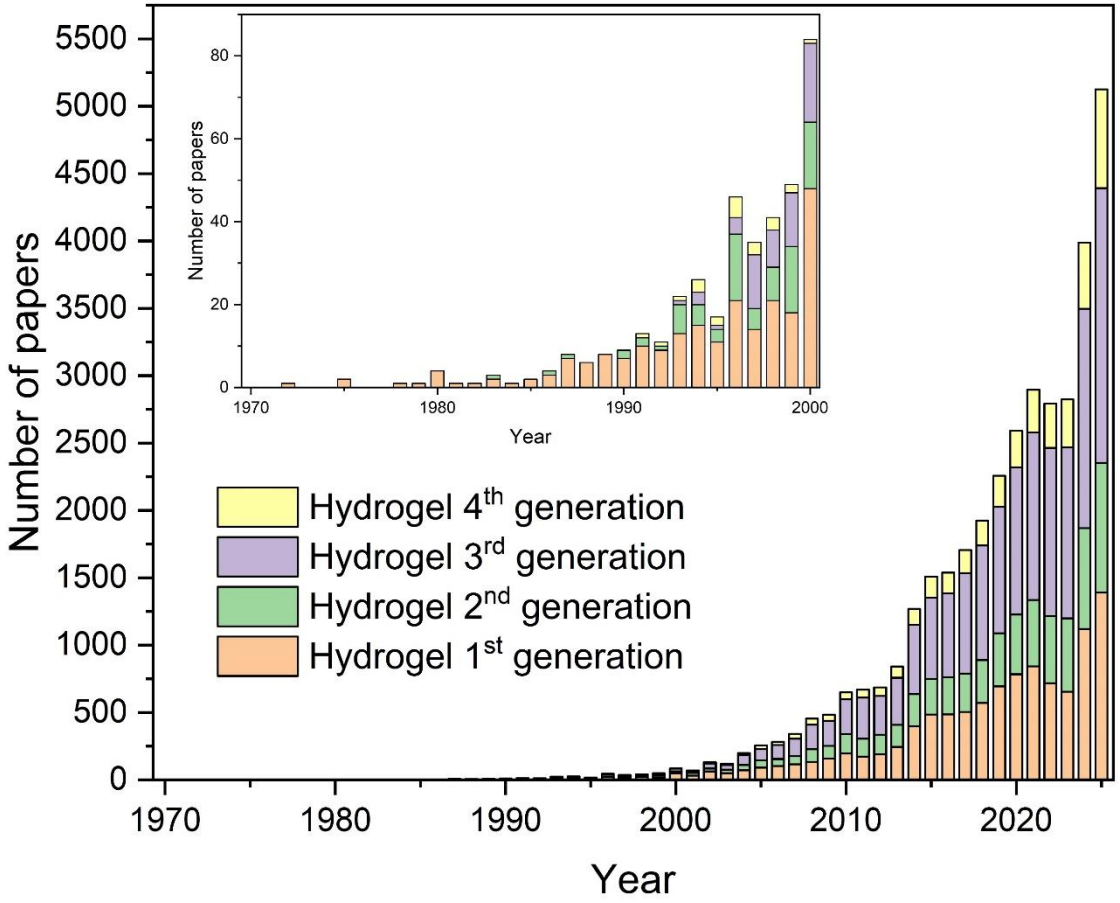


Figure 25 Evolution the hydrogels share in biomaterials generations depicted by the changing research interest. Data base: Scopus within Article title, abstract and keywords. Search queries: 1st generation: ("biomaterial" OR "biomedical material*") AND ("hydrogel*" OR "microgel*" OR "nanogel*" OR "polymeric gel*") AND ("first generation" OR "1st generation" OR "bioinert*" OR "inert*" OR "minimal host response" OR "biocompatible"). 2nd generation: ("biomaterial*" OR "biomedical material*") AND ("hydrogel*" OR "microgel*" OR "nanogel*" OR "polymeric gel*") AND ("second generation" OR "2nd generation" OR "bioactive" OR "bioresorbable" OR "biodegradable" OR "bioglass" OR "hydroxyapatite" OR "calcium phosphate" OR "osteo*" OR "osseo*"). 3rd generation: ("biomaterial*" OR "biomedical material*") AND ("hydrogel*" OR "microgel*" OR "nanogel*" OR "polymeric gel*") AND ("third generation" OR "3rd generation" OR "biointeractive" OR "regenerative" OR "biomimetic" OR "tissue engineering" OR "scaffold*" OR "extracellular matrix" OR "ECM" OR "molecular signaling" OR "stem cell*" OR "cellular response"). 4th generation ("biomaterial*" OR "biomedical material*") AND ("hydrogel*" OR "microgel*" OR "nanogel*" OR "polymeric gel*") AND ("fourth generation" OR "4th generation" OR "smart" OR "electronic*" OR "autonomous" OR "programmable" OR "stimuli-responsive" OR "Theranostic*" OR "nano" OR "cyber" OR "piezoelectric*" OR "sensor" OR "shape-memory" OR "shape memory").*

Current research priorities integration of tunable physicochemical properties that scientists modify using advanced techniques such as click chemistry, chemoenzymatic synthesis and plasma-assisted crosslinking [299]. Such precise synthetic control enables the formulation of tunable materials that adapt their properties over time, mimicking the dynamic heterogeneity of the native ECM. By approximating the structural complexity of living tissues, these advanced hydrogels facilitate complex *in vitro* organoid culture [23], functional tissue engineering [79] and specialized antibacterial formulations [150].

4.3.1.Source materials for hydrogel synthesis

Hydrogel biomaterials can be divided into three primary categories based on the origin of their constituent polymers: natural, synthetic and hybrid systems. The selection of the source material defines the resulting physicochemical characteristics, degradation kinetics and biological interactions of the hydrogel. In Table 8, the comparison of hydrogel source was presented.

4.3.1.1. Natural polymers

Naturally derived hydrogels are extracted from natural resources and inherently mimic the structure and function of the native extracellular matrix. Researchers divide these biopolymers into two main subclasses: proteins and polysaccharides.

Protein-based hydrogels utilize macromolecules such as collagen, gelatin, fibrin and elastin. Collagen, the primary structural protein in mammalian connective tissues, forms hydrogels that exhibit low antigenicity and excellent biocompatibility. Clinical formulations rely heavily on collagen for tissue engineering and augmentation. Specifically, clinicians implant non-injectable collagen hydrogels to repair damaged tendons and ligamentous tissues. Commercial devices based on collagen were successfully implemented in different areas of medicine. In example, the Permacol™, porcine-derived implant, utilized in soft tissue closures, demonstrated the clinical utility of these matrices in supporting rotator cuff regeneration [300]. A large number or collagen-based hydrogels, like CosmoDerm®, ComsoPlast® or Artefill®, function as dermal fillers to correct soft tissue contour deficiencies, wrinkles and scars [301]. Furthermore collagen is often utilized in wound dressings, where Apligraf®, an implantable hydrogel incorporating collagen with fibroblasts and keratinocytes, was developed to treat diabetic foot ulcers and venous leg ulcers [302].

Denaturation or hydrolysis of the collagen triple helix yields gelatin, a water-soluble derivative that maintains low immunogenicity and readily undergoes enzymatic breakdown. Manufacturers extract type A gelatin via acid hydrolysis of porcine skin, whereas type B gelatin results from the alkaline processing of animal bones. Researchers utilize both physical and chemical crosslinking methods to transform these distinct gelatin derivatives into stable hydrogel networks. Current research on gelatin is focused on validation of its properties for applications in drug delivery [90], wound dressings [303] and bioprinting [304]. In clinical practice, gelatin is widely utilized to create hemostatic matrices to seal bleeding during surgeries in anatomically complex surgical sites. Examples of such products are Surgiflo®, Borayerflo® or Floseal®

[305,306]. Advanced products based on gelatin are also developed, such as XEN45 - minimally invasive surgical implant, utilized primarily to reduce intraocular pressure in patients with refractory open-angle glaucoma and to prevent further optic nerve degeneration [307].

Fibrin, a protein involved in the coagulation cascade, allows for the formulation of autologous scaffolds when extracted directly from a patient's blood, which significantly reduces the risk of immunological incompatibility [308]. In the field of ophthalmology, fibrin was utilized to create fully biodegradable scaffolds for the sub-retinal transplantation of induced pluripotent stem cell-derived retinal pigment epithelium monolayers. These autologous matrices provide essential mechanical stability to fragile cell sheets during surgical delivery to treat macular degeneration, subsequently degrading completely *in vivo* to prevent chronic foreign-body inflammation [309]. Furthermore, clinical-grade natural fibrin-based sealants (such as Tisseel™) have been successfully repurposed in neuro-oncology as conformal matrices to line brain tumor resection cavities. Encapsulating therapeutic mesenchymal stem cells within these *in situ* forming fibrin hydrogels significantly increases localized cell retention and prolongs anti-tumor efficacy against residual glioblastoma multiforme cells compared to conventional liquid injections [310]. Following up the research, the attempts are made to commercialize advanced fibrin-based hydrogels. For example, CartiLife®, a fibrin microsphere hydrogel that encapsulates active chondrocytes used to repair articular cartilage defects, is currently in Phase III human clinical trials (NCT05051332) [311]. Despite these strong biological advantages, pure fibrin hydrogels often demonstrate insufficient mechanical strength for severe load-bearing applications when formulated without supplementary synthetic crosslinking.

Polysaccharide-based hydrogels employ carbohydrate polymers, including hyaluronic acid, alginate and chitosan. HA, an anionic glycosaminoglycan naturally present in synovial fluid, promotes cellular processes such as angiogenesis and cell proliferation. Because manufacturers can produce it on a massive scale via microbial fermentation, HA serves as the base for numerous clinical devices. Products such as Restylane® and Juvéderm™ are widely administered as dermal injections to correct facial wrinkles and volume deficits [312]. Additionally, HA formulations like Orthovisc and Monovisc provide pain relief through intra-articular injection for patients suffering from osteoarthritis [313].

Alginate, extracted from brown algae cell walls, consists of mannuronic and glucuronic acid blocks that readily undergo ionic gelation in the presence of divalent cations like calcium. This gelation mechanism supports clinical applications such as Algisyl-LVR™, an alginate hydrogel implant for advanced heart failure implanted using catheter-based delivery system [314]. Alginate also forms the structural basis for commercial wound dressings like Algisite™ and honey-containing Medihoney™, which absorb wound exudates and maintain a moist environment to accelerate the healing of lacerations, abrasions and minor burns [315].

Chitosan, a cationic polymer derived from arthropod chitin, provides inherent antibacterial characteristics and mucoadhesion, though it also presents weak mechanical properties. Despite numerous publications on chitosan-based hydrogels [316], there are only two approved commercially available devices. The first on is the HemCon® wound dressing, widely used in battlefield medicine, which is indicated to provide a hemostatic and antibacterial barrier for wounds [317]. The second one is BST-CARGEL®, an injectable, hydrogel used as an adjunct to microfracture surgery for the repair of focal articular cartilage lesions [318].

Agar and its purified derivative, agarose, represent another vital class of polysaccharide-based hydrogels extracted from marine algae. Agarose forms highly biocompatible, non-immunogenic matrices that successfully mimic the physical properties of the native extracellular matrix. Because of this structural similarity, agarose hydrogels are often used to transport essential cell growth factors directly to injured anatomical sites [148]. One of the examples is like Algeness®, a subdermal filler used in aesthetic and reconstructive medicine to provide deep volumetric tissue support [319]. Furthermore, the numerous pendant functional groups present along the agarose polymer backbone facilitate robust hydrogen bonding with diverse therapeutic agents [150–152]. However, despite the known beneficial properties of agar, its broader recognition in medicine remains largely undeveloped.

Table 8 Overview of materials utilized in the fabrication hydrogels depending on the source material origin. Originally published in [23]. PAA: poly(acrylic acid), PAAm: polyacrylamide, PNIPAAm: poly(N-isopropylacrylamide), Gel-MA: gelatin methacrylate, PEG-DA: poly(ethylene glycol)-diacrylate.

Source		**Material**	**Advantages**	**Disadvantages**
Natural	**Proteins**	Collagen	- Highly biocompatible and non-immunogenic - Stimulate cell adhesion, migration and proliferation - Similar structure to the ECM - Biodegradable - Available from renewable resources - Cost effective - High swelling ratio and water retention	- Poor mechanical properties (tensile strength < 20 kPa) - Difficult reproducibility - Poor processability - Low stability without extensive crosslinking
		Fibrin		
		Gelatin		
		Elastin		
		Collagen- Elastin		
		Silk		
	Polysaccharides	HA		
		Agarose		
		Chitosan		
		Collagen/Alginate		
		Collagen/Chitosan		
Synthetic		PEG	- Easily tuned properties - Good mechanical properties (tensile strength up to 1 MPa) - High transparency - More reproducible physical and chemical properties - Long-term stability	- Lack of cell-specific binding sites, resulting in lower cell adhesion, migration and proliferation - Problems with biodegradation - Limited biocompatibility and potential toxicity - Lower swelling ratio and water retention
		PVA		
		pHEMA		
		PVP		
		PAA		
		PAAm		
		PNIPAAm		
Hybrid		Gel-MA	- High biocompatibility - Tunable mechanical properties - Biodegradable - Medium stability	- Complex production process - Highly expensive
		HA-MA		
		Dopamine-modified alginate		
		PEG-fibrinogen		
		Gel-MA/PEG-DA		

4.3.1.2. Synthetic polymers

Since natural polymers often suffer from drawbacks such as poor mechanical properties, synthetic polymers, obtained through controlled organic chemical synthesis, can be used to ensure highly reproducible material properties and minimized structural inconsistencies. Additionally, these materials function offer precise control over mechanical, chemical and spatial properties [320]. However, the bio-inert nature of synthetic polymers presents a primary limitation in regenerative medicine. Because these materials lack endogenous cell adhesion sites, they cannot actively facilitate cellular attachment or matrix remodeling without incorporating modifications, such as integrin-binding peptides (e.g., RGD sequences).

Poly(ethylene glycol) is one of the most popular choices for creating synthetic-based hydrogels. Thanks to the hydroxyl groups distributed along a non-degradable, biocompatible polymer chain, the resulting highly hydrophilic and stable matrices can be obtained. PEG also offer unique properties, which can effectively shield encapsulated therapeutic agents from premature degradation and host immune responses, optimizing their physicochemical stability during delivery [80,125]. Furthermore, PEG excels as a structural matrix in bone tissue engineering due to its tunable swelling behavior and structural reliability [321]. It is also frequently applied for surgical sealing and tissue protection in products like ReSure® for sealing clear corneal incisions [322] or SpaceOAR to protect vulnerable perirectal tissues during prostate cancer radiotherapy [323].

In contrast to PEG, poly(vinyl alcohol), derived from the hydrolysis of poly(vinyl acetate), can form biodegradable hydrogels. The specific degree of hydrolysis and the polymer's molecular weight directly influence the resulting hydrophilicity and solubility of the PVA network. Additionally, PVA demonstrates exceptionally low protein adsorption, making it highly suitable for tissue adhesives and protective wound dressings. Furthermore, *in vitro* and *in vivo* studies indicate that PVA hydrogels seeded with adipose-derived stem cells successfully promote accelerated wound healing [119]. Unique properties of PVA allow the use of hydrogels made of this material both outside and inside the body. On the outside, PVA is often used to prepare wound dressings, often functionalized to prevent infections [167]. One of the commercialized products is Hydrofera Blue® - a bacteriostatic wound dressing complexed with organic pigments - methylene blue and gentian violet. The hydrophilic PVA matrix effectively absorbs wound exudate while maintaining a moist healing environment and the embedded pigments provide broad-spectrum antibacterial protection [324]. On the other hand, PVA hydrogels are used as implantable devices, for example Cartiva® was developed to treat osteoarthritis, relying on the compressive strength and high water content of the PVA hydrogel to act as a spacer, directly mimicking the biomechanical shock-absorbing properties of natural human cartilage [325].

Beyond these primary polymers, researchers utilize several other synthetic materials for targeted applications. Poly(vinyl pyrrolidone) (PVP) combines advantages of both PEG and PVA and serves as an effective synthetic matrix for specialized delivery systems. PVP readily complexes with diverse pharmacological drugs, significantly enhancing their aqueous solubility

and chemical stability prior to release [326]. Polyacrylamide (PAMm) offers high mechanical strength and stability, though its hydrolytic degradation releases acidic byproducts that may compromise local cell viability. Poly(N-isopropylacrylamide) (PNIPAAm) exhibits distinct thermoresponsive behavior, undergoing reversible phase transitions at specific temperatures to enable stimuli-responsive drug delivery. However, these polymers usually have to be combined with natural polymers to ensure the biocompatibility of the resulting system [327–329]. Finally, aliphatic polyesters such as PCL, PLA and PLGA provide controlled degradation profiles [240]. However, these ester-based hydrogels must be carefully monitored when applied internally, as their hydrolytic breakdown can result in release of acids that tend to lower the local tissue pH and induce inflammatory responses. Additionally, biostable synthetic polymers can be also affected by biodegradation to some extent, leading to release of potentially toxic byproducts, such as acrylamide derivatives, aldehydes and epoxides, indicating the need to address these challenges by creating hybrid systems [330].

4.3.1.3. Hybrid, composite and semi-synthetic networks

Purely natural and purely synthetic hydrogels each present inherent limitations in biomedical applications [330]. Thus, hydrogel feedstock is often composed of different types of polymers, their derivatives or composites. This strategy generates complex materials that balance the mechanical robustness and tunable parameters of synthetic polymers with the intrinsic bioactivity of natural matrices. The most popular natural and synthetic polymers used for creating hybrid hydrogels were summarized in Figure 26.

The simplest strategy for creating hybrid materials is simple blending of natural polysaccharides with synthetic polymers or structural proteins to formulate advanced wound dressings. For example, creation of composite agarose-based hydrogels allowed for creation of matrices with high level of versatility as their permeability profiles could be tailored at will by integrating macromolecules [331]. Commercial devices also rely on these blends. Aqua-Gel®, a radiation-crosslinked hydrogel wound dressing, has its matrix formulated primarily from synthetic PVP, PEG and natural agar. The resulting flexible, highly hydrated sheet provides an immediate cooling effect to burns and ulcers, protects exposed nerve endings to reduce pain and facilitates the autolytic debridement of necrotic tissue [332]. Interesting development is CARTIPATCH®, which is a blend of unmodified alginate, unmodified agarose and autologous chondrocytes. The hydrogel combines structural stability of agarose while utilizing the highly porous, water-retaining nature of alginate. This provides the embedded chondrocytes with an ideal 3D environment to proliferate, preventing them from dedifferentiating and allowing them to secrete fresh, healthy ECM [333].

The other strategy is the chemical modification of polymer backbones to introduce reactive functional groups, thereby enabling robust covalent crosslinking. For example, covalently crosslinked methacrylated gelatin commercially available as standardized bioinks such as PhotoGel® and the GelX® series, exhibits enhanced mechanical integrity, controlled swelling behavior and optimized drug release kinetics compared to physically crosslinked, unmodified

gelatin [304]. Similarly, the functionalization of hyaluronic acid with methacrylate or methacrylamide groups yields HA-MA, transforming a mechanically weak native polysaccharide into a rapidly photo-polymerizable hydrogel. In commercial formulations, such as PhotoHA®, upon exposure to ultraviolet or visible light in the presence of a photoinitiator, HA-MA forms a stable 3D matrix with highly tunable stiffness while retaining crucial endogenous signaling capabilities of HA, such as CD44 receptor binding, rendering it highly advantageous for 3D bioprinting applications [71]. This functionalization strategy extends to synthetic polymers, most prominently through the synthesis of poly(ethylene glycol) diacrylate (PEG-DA), widely available as the bioink.

Terminating polymer chains with reactive acrylate groups allow hybridization of synthetic and natural polymers, adding the necessary bioactivity for cellular attachment and tissue remodeling to otherwise bio-inert matrix [80]. For example, conjugating synthetic PEG chains with natural proteins or polysaccharides improves the structural stability of the natural components. Simultaneously, this conjugation introduces necessary cell-adhesive domains to the otherwise bio-inert PEG network [321]. Another benefit of this approach is the ability to adjust the ratio of natural to synthetic constituents, which can be used to customize the chemical, physical and biological functionality of the hybrid matrix for specific therapeutic applications. In clinical treatments GelrinC, a commercial hybrid hydrogel consisting of denatured fibrinogen crosslinked with synthetic PEG diacrylate, is used to treat focal cartilage lesions following microfracture surgery [334]. On the other hand, direct crosslinking of synthetic PVP with natural HA can produce rigid hydrogel microneedles. This enhanced mechanical strength ensures that the microneedles effectively penetrate the stratum corneum to deliver therapeutic agents directly into the underlying tissue. Once inserted, the PVP matrix dissolves in the interstitial fluid to deliver active therapeutics deep into the target tissue [335].

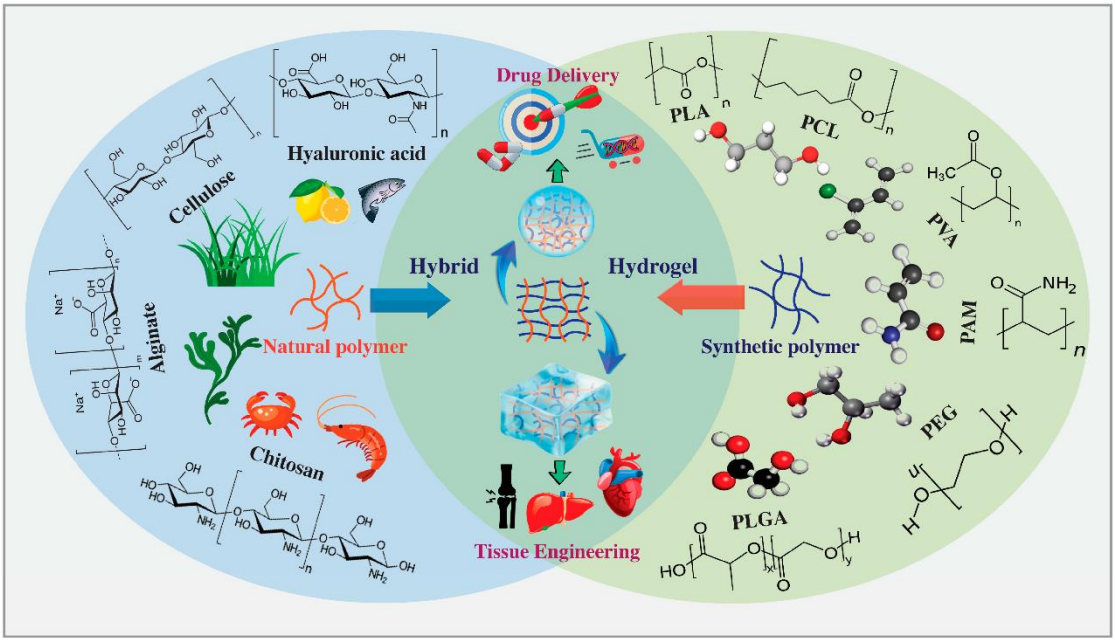


Figure 26 The most popular natural and synthetic polymers used for development of hybrid hydrogels. Adapted from: [336] under CC BY 4.0 license.

4.3.2. Crosslinking mechanisms of hydrogels

The macroscopic stability, mechanical performance and porosity of a hydrogel directly depend on its internal crosslinking density and specific bonding mechanism. Crosslinking transforms a liquid polymer solution into a cohesive gel state by physically restricting the independent thermodynamic movement of individual polymer chains. To successfully form a functional hydrogel, the constituent polymer network must meet two critical structural conditions. First, the polymers are required to have interactive sites to establish a stable, interconnected molecular topology that resists dissolution. Second, the resulting three-dimensional architecture must remain sufficiently hydrophilic and porous to encourage continuous access, diffusion and residence of water within the empty spaces. By modulating structural parameters during synthesis, the material's elastic modulus, degradation kinetics and transport capabilities can be precisely tuned to match specific physiological requirements. Based on the nature of these interchain connections, network formation processes can be categorized into three classes: physically crosslinked matrices, chemically crosslinked networks and interpenetrating polymer networks (IPNs). The approaches for hydrogel crosslinking were summarized in Figure 27.

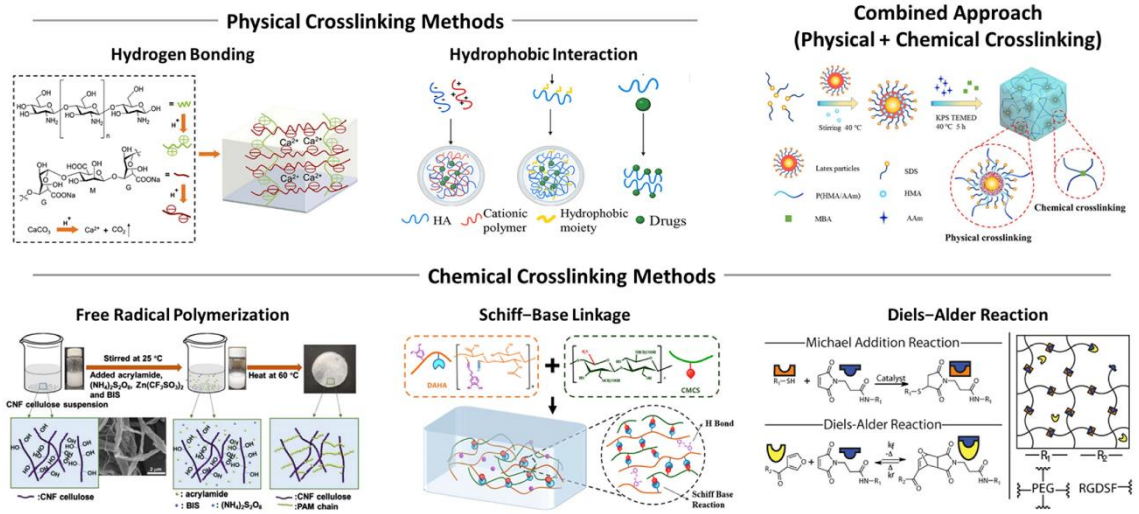


Figure 27 Comparison of different approaches for hydrogel crosslinking: physical, chemical and combined. Adapted from: [337] under CC BY 4.0 license.

4.3.2.1. Physical crosslinking methods

Physical gelation relies on transient, non-covalent interactions between adjacent polymer chains to establish a three-dimensional macromolecular network. Unlike chemical gelation, this process actively avoids the use of chemical crosslinking agents, photo-initiators or ultraviolet irradiation. Consequently, physical crosslinking demonstrates superior cytocompatibility, ensuring that the structural integrity of encapsulated cells and therapeutic proteins remains intact during synthesis [299]. Four primary reversible gelation mechanisms to formulate physical hydrogels can be distinguished: ionic interactions, hydrogen bonding, hydrophobic interactions and crystallization (Figure 28).

Ionic crosslinking occurs through electrostatic attraction between oppositely charged groups or via metal-ligand interactions. This mechanism frequently involves a phase-separation process known as coacervation, which is induced by modifying the environmental pH, ionic strength or temperature. During simple coacervation, a single polymer precipitates upon the introduction of a specific salt or coacervation agent containing di- or trivalent counter ions like Ca^{2+}, Mg^{2+} or Fe^{3+}. For example, the addition of divalent Ca^{2+} rapidly gelates alginate, while tripolyphosphate acts as an effective ionic agent to crosslink chitosan [299].

Polymers containing polar functional groups, such as hydroxyl, acylamino and carboxyl domains, can formulate hydrogels via hydrogen bonding. While individual hydrogen bonds remain weak, the presence of multiple hydrogen donors and acceptors along the polymer backbone generates the cumulative force required to maintain macroscopic gelation. For instance, natural polymers like gelatin, collagen, agar and starch rely heavily on hydrogen bonding for network formation [153]. However, pure hydrogen-bonded hydrogels often possess low crosslink density and high water content, which typically results in weak mechanical properties and difficulty during syringe injections.

Hydrophobic interactions drive physical gelation through specific thermal triggers or structural modifications. These hydrogels can be formed utilizing micelles as crosslinking agents or by directly grafting hydrophobic moieties onto a hydrophilic polymer precursor. Furthermore, heating or cooling specific polymer solutions induces gelation when the constituent chains possess helices or helix-like junction zones [330]. For example, mixing hot stock solutions of carrageenan and gelatin at 40 °C initiates complex formation of hydrogel due to random coil and hydrophobic interactions. As the temperature decreases, the complex transitions into a helix conformation and electrostatic interactions stabilize the final hydrogel [338]. Such thermo-reversible systems prove highly effective for encapsulating hydrophobic drugs within their micellar domains.

Finally, crystallization provides a unique physical crosslinking mechanism, where crystallites within the polymer chain function as the primary structural junction points of hydrogel matrix. This process can be executed at temperatures within the freezing range. During the initial freezing phase, liquid-liquid phase separation occurs, generating a distinct porous architecture and subsequent thawing creates both amorphous and crystalline regions within the matrix. This freeze-thaw method is mostly used to prepare PVA hydrogels [83]. Free water molecules occupy the voids established by the phase separation to form the amorphous zones, while the aggregation of crystallites defines the crystalline regions. Both regions act as functional crosslinking points, resulting in a thermoreversible material.

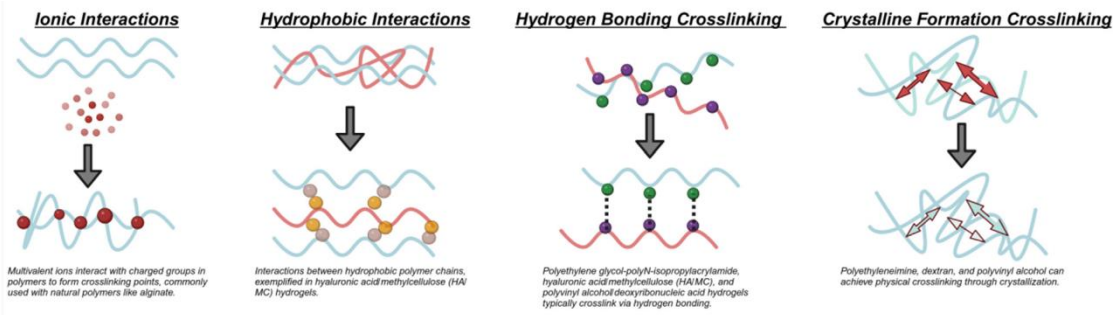


Figure 28 Physical crosslinking methods of hydrogels. Adapted from: [339] under CC BY 4.0 license.

While physically crosslinked hydrogels do not possess the toxicity associated with chemical synthesis, their behavior under dynamic physiological conditions requires careful evaluation. The clustering of molecules during physical gelation frequently generates free chain loops and lattice imperfections within the network [320]. Because the non-covalent bonds remain thermodynamically reversible, these lattice inconsistencies tend to cause relative structural instability. Upon implantation, exposure to fluctuating physiological fluids, localized pH changes and body temperature may induce rapid and unpredictable macroscopic disintegration [330]. Consequently, while physical hydrogels excel as temporary, biocompatible vehicles for controlled drug release, they generally lack the long-term load-bearing resilience required for permanent tissue engineering scaffolds unless reinforced by secondary chemical crosslinking mechanisms.

4.3.2.2. Chemical crosslinking methods

Chemical crosslinking of hydrogels involves the creation of permanent covalent bonds between polymer chains, generating highly stable and structurally robust three-dimensional networks. Multiple synthetic strategies are employed to establish these irreversible linkages, allowing precise modulation of the hydrogel's final properties. By selecting the appropriate chemical reaction, synthesis process can be customized to meet the specific requirements of the target tissue or encapsulated active substances. Five primary chemical crosslinking can be distinguished: usage of crosslinking agents, radical polymerization, photopolymerization, click chemistry and enzymatic crosslinking (Figure 29).

Fundamental mechanism for chemical crosslinking involves the direct application of bi-functional or poly-functional crosslinking agents. These reactive small molecules contain terminal groups that establish covalent bonds between specific functional domains on adjacent polymer chains. Glutaraldehyde represents the most classical and widely utilized crosslinker in this category. It functions by reacting predominantly with the primary amine groups present in natural polymers, such as collagen, gelatin and chitosan, to form highly stable Schiff base linkages [330]. While glutaraldehyde effectively generates rigid, structurally resilient and permanent hydrogel networks, its biomedical application presents strict limitations. Both unreacted glutaraldehyde molecules and their subsequent hydrolytic degradation byproducts exhibit significant dose-dependent cytotoxicity and can induce severe localized inflammatory responses upon implantation. Consequently, hydrogels crosslinked with these synthetic agents require

exhaustive, multi-step washing protocols to extract residual toxins prior to biological use. To mitigate these inherent toxicity risks, glutaraldehyde is increasingly substituted with naturally derived, lower-toxicity crosslinkers like genipin or employ zero-length crosslinking systems such as 1-ethyl-3-(3-dimethylaminopropyl)carbodiimide (EDC) [336]. EDC facilitates direct amide bond formation between the carboxyl and amine groups of the constituent polymers without remaining part of the final structural matrix, thereby eliminating the risk of toxic byproduct release.

Chemical bonding can be also performed without additional crosslinkers. The free radical polymerization, similarly, as in standard polymerization of bulk materials, utilizes specific chemical initiators that undergo homolytic dissociation or redox reactions to generate highly active free radicals. These radicals then target the carbon-carbon double bonds present in monomers, such as acrylates, vinyl lactams and amides, initiating rapid chain propagation until the reaction terminates via combination or disproportionation [340]. While free radical polymerization effectively produces solid matrices in a short timeframe, the resulting hydrogels frequently exhibit high spatial heterogeneity as the reaction proceeds in an uncontrolled manner, causing inconsistent crosslink density and leaving inaccessible double bonds trapped within the network. To resolve this, photopolymerization was developed, where visible or ultraviolet light is used to activate specific photoinitiators mixed within the liquid precursor solution. Thanks to the high level of control of light position, highly specific geometric structures can be produced, which is utilized in bioprinting technologies. It must be underlined that free radicals exhibit inherent cytotoxicity, as they interact with native biological tissues, thus alternative step-growth photochemistries must be implemented to produce biomedical hydrogels, such as the radical-mediated thiol-norbornene platform [298].

Recently, novel techniques for chemical crosslinking were developed. One of them is click chemistry, representing a class of highly efficient, versatile and specific step-growth reactions that generate minimal toxic byproducts. Unlike radical chain-growth methods, click reactions link complementary functional groups in a precise one-to-one stoichiometric ratio, which yields a structurally uniform and predictable molecular architecture right in the aqueous environments Prominent click mechanisms include strain-promoted azide-alkyne cycloaddition, Diels-Alder cycloaddition, oxime ligation and thiol-Michael additions [75,125]. Another route is utilization of specific biological catalysts to form permanent covalent bonds between polymer chains under mild physiological conditions. This strategy offers a living cells-friendly alternative to synthetic chemical crosslinkers or ultraviolet irradiation. Gelation typically occurs rapidly at normal body temperatures (36-37 °C), providing an ideal mechanism for *in situ* injectable hydrogel formulations designed for tissue engineering. Typical enzymes used for enzymatic crosslinking include horseradish peroxidase, tyrosinase, transglutaminase and specific DNA ligases, like T4 ligase [337].

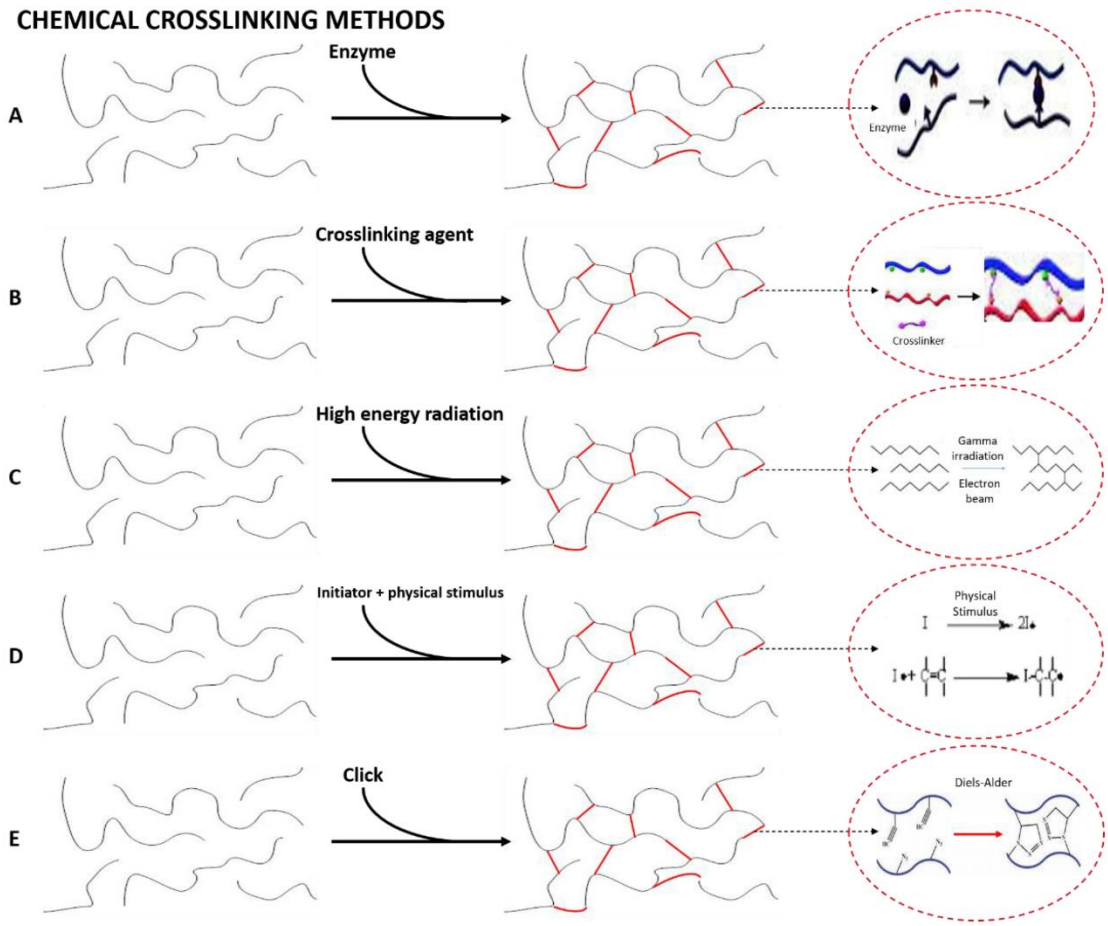


Figure 29 Main chemical crosslinking methods of hydrogels: A) enzymatic crosslinking, B) chemical reaction promoted by a cross-linking agent, C) high-energy radiation, D) free-radical polymerization and E) click reactions. Adapted from: [341] under CC BY 4.0 license.

4.3.2.3. Interpenetrating polymer networks

To overcome the inherent mechanical and biological limitations of conventional single-network hydrogels, interpenetrating polymer networks were developed. They are defined as a complex polymeric matrix comprising two or more distinct polymer networks that remain partially (semi-interpenetrating) or fully interpenetrating on a molecular scale. No covalent bonds are formed between the individual networks. Instead, they intertwine physically such that their separation strictly requires breaking the internal chemical bonds of the individual matrices. This unique topological configuration allows to combine the favorable physicochemical attributes of multiple polymers while resolving the mechanical deficiencies typically associated with individual hydrogel systems. A fully-IPN forms when both the primary and secondary polymer chains undergo independent crosslinking reactions, creating two distinct, continuous and intertwined three-dimensional matrices. In contrast, a semi-IPN features only one actively crosslinked matrix, whereas the secondary component consists of linear or branched polymer chains that physically entangle within the primary crosslinked framework. Semi-IPNs tend to retain greater kinetic flexibility, allowing the uncrosslinked chains to migrate or rearrange within the primary matrix

under physiological conditions, which facilitate tailored degradation profiles and controlled biological interactions.

Semi-IPNs are often used for engineering bioactive biomaterials of third generation. The mobile secondary chains provide a highly versatile platform for incorporating specific bioactive molecules, such as growth factors or antimicrobial agents, directly into the matrix without permanently locking them into the covalent structure, as is commonly done in conventional hydrogels. As the primary network swells in aqueous media, the secondary chains modulate the diffusion pathways, providing precise control over the macroscopic degradation rate and the subsequent release of encapsulated therapeutics.

The primary advantage of IPNs is their extraordinary potential to improve mechanical strength and fracture toughness in comparison to conventional hydrogels. It is especially effective for highly laden environments such as articular cartilage repair or artificial ligament construction. In such cases, the primary network can provide a densely crosslinked, rigid but brittle polymer that provides high initial mechanical strength and stiffness. The secondary network, usually composed of loosely crosslinked, flexible and ductile polymer, is then used for effective absorption of mechanical energy and prevention of catastrophic material failure, holding the structure together [342]. The forces causing entanglements in IPNs were presented in Figure 30. This synergistic coupling mechanism dissipates substantial amounts of mechanical energy during deformation across multiple interwoven chains rather than localizing it at a single focal point, resulting in increase of fracture energy by orders of magnitude reaching values as high as ~9000 J/m^2 with alginate-PAAm systems, even at high water contents [343].

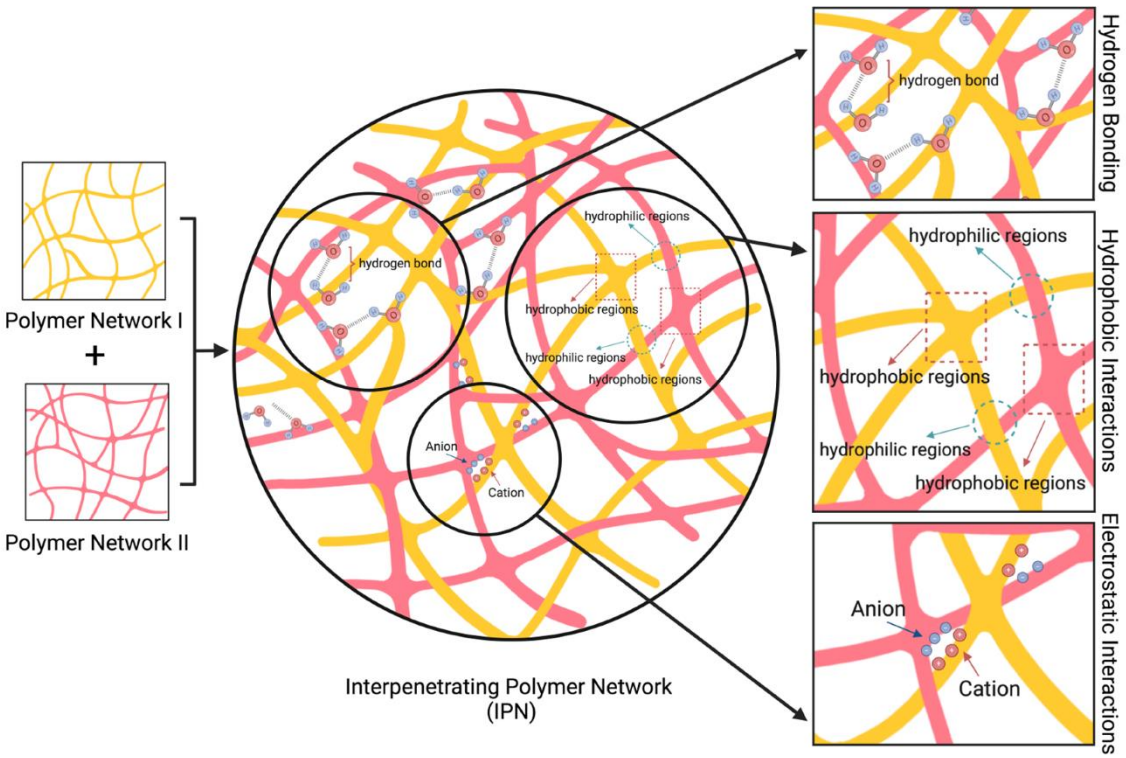


Figure 30 Interactions in interpenetrating polymer networks. Adapted from: [342] under CC BY 4.0 license.

4.3.3. Physicochemical and rheological properties of hydrogels

The clinical utility and usefulness of hydrogel biomaterials depend strictly on their physicochemical characteristics and thermodynamic stability under dynamic physiological conditions. Although the hydrogel chemical structure strongly influences its macroscopic material properties, including its swelling capacity, porosity, permeability and mechanical properties, they must be carefully evaluated, how the polymer network interacts with aqueous biological fluids and applied mechanical forces. Additionally, in more advanced applications stimuli-responsiveness is crucial for creating DDSs together with the proper rheological behavior essential in 3D bioprinting and injectable devices. Thanks to highly tunable characteristics of hydrogel materials, parameters like crosslinking density, monomer molecular weight, porosity or specific polymer-solvent interactions can be precisely tuned to match the exact requirements of the target anatomical site. For instance, load-bearing orthopedic applications require rigid, highly resilient networks, whereas injectable delivery vehicles necessitate soft, flexible and shear-thinning matrices [329,339]. Furthermore, modern, third generation biomaterials extend beyond static structural parameters, relying on smart polymeric systems engineered to actively adapt their physical state in response to complex environmental triggers. Therefore, a comprehensive analysis of hydrogel properties in relation to the final application or target tissue remains critical for optimizing their clinical performance, as shown in Figure 31.

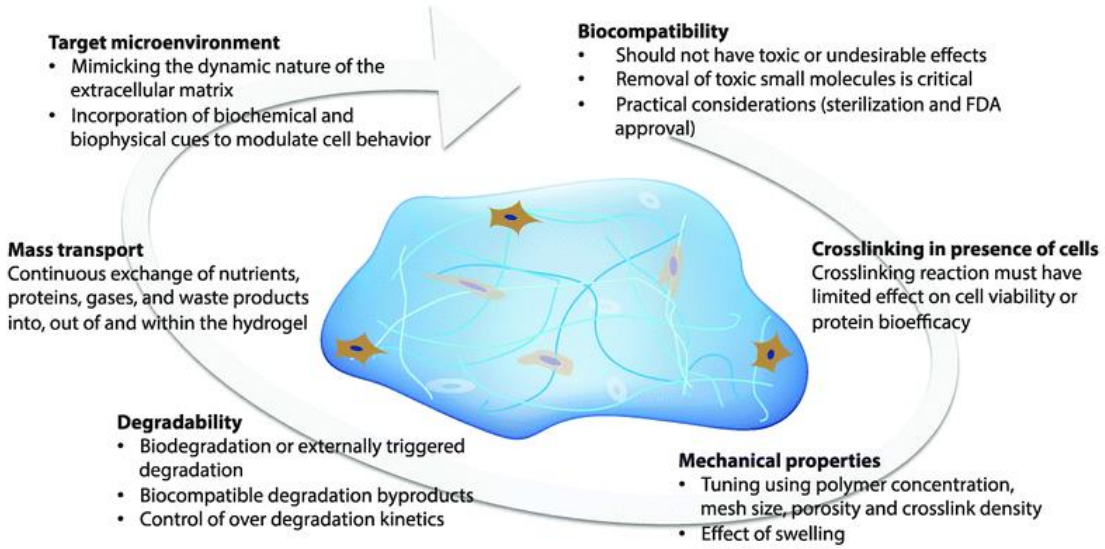


Figure 31 Structure-property relations in hydrogel design. Adapted from: [344] under CC BY-NC 3.0 license.

4.3.3.1. Swelling kinetics and thermodynamics

The defining characteristic of a hydrogel is its thermodynamic capacity to absorb and retain significant volumes of aqueous solvents without dissolving. When a completely dehydrated hydrogel (a xerogel) is exposed to a fluid, it absorbs the liquid and expands continuously until reaching a thermodynamic state defined as equilibrium swelling. According to Flory-Rehner theory, this equilibrium state results directly from a physical balance between two opposing thermodynamic forces [345,346]. First, the thermodynamic affinity between water molecules and

the hydrophilic polar groups along the polymer chains generates an osmotic driving force (ΔG_{mix}) that compels the solvent to penetrate and diffuse into the matrix. Second, as the network expands, the structurally crosslinked polymer chains stretch. This stretching exerts a cohesive, elastic restorative force (ΔG_{el}) that actively resists further volumetric expansion. The hydrogel stops swelling when the osmotic swelling forces are balanced with the elastic retraction forces. This behavior is quantified using the swelling ratio, which compares the mass of the swollen gel relative to its dry xerogel state. At this thermodynamic equilibrium, the chemical potential of the solvent inside the crosslinked polymer network must equal the chemical potential of the pure solvent outside the gel. The Flory-Rehner theory mathematically expresses this balance as the sum of two distinct chemical potential changes: the mixing contribution ($\Delta\mu_{mix}$) and the elastic contribution ($\Delta\mu_{el}$) (Eq. 1) [347]. This sum can be calculated by partial differentiation of the total free energy (ΔG_{tot}) or each of its constituents with respect to number of solvent molecules (n_1). When the total chemical potential ($\Delta\mu_{tot}$) is equal to zero, the equilibrium swelling state is reached, as the net flux of solvent molecules in and out of the material is zero.

$$\frac{\partial(\Delta G_{tot})}{\partial n_1} = \frac{\partial(\Delta G_{mix})}{\partial n_1} + \frac{\partial(\Delta G_{el})}{\partial n_1} = \Delta\mu_{tot} = \Delta\mu_{mix} + \Delta\mu_{el} \quad (1)$$

Additionally, the contribution of chemical potential change induced by mixing polymer and solvent with the elastic energy within the expanding polymer network due incorporation of solvent can be directly compared, leading to the Flory-Rehner equation [345,346] (Eq. 2). It allows the calculation of the most critical structural parameter of the hydrogel: the average molecular weight between crosslinks (M_c), allowing to deduce the internal crosslinking density of a biomaterial simply by measuring its macroscopic volumetric expansion in water.

$$\mathrm{M_c} = -\frac{\mathrm{d_p V_s}\left(\mathrm{V_{2,s}}^{\frac{1}{3}} - \frac{\mathrm{V_{2,s}}}{2}\right)}{\ln\left(1-\mathrm{V_{2,s}}\right) + \mathrm{V_{2,s}} + \chi\mathrm{V_{2,s}}^2} \quad (2)$$

In Eq 2, M_c is the average molecular weight between cross-links [g/mol], d_p is the density of hydrogel [g/cm^3], V_s is the molar volume of water [-], $V_{2,s}$ is a volume fraction of hydrogel [-].

Understanding and accurately predicting these swelling thermodynamics is strictly required for designing effective DDSs. The extent of equilibrium swelling directly influences the macroscopic porosity and the internal mesh size of the hydrogel architecture. When therapeutic agents, like small molecule drugs or macromolecular proteins, are encapsulated within a dehydrated xerogel, the dense polymer network physically traps the active substances. Upon administration, the xerogel starts absorbing physiological fluids, leading to the expansion of hydrogel network. In result, the internal pores progressively enlarge, systematically increasing the permeability of the matrix. This dynamic swelling process actively regulates the diffusion of the encapsulated therapeutics into the surrounding tissue.

This swelling-controlled mechanism allows for sustained release, maintaining optimal therapeutic drug levels over an extended period and preventing the rapid, uncontrolled expulsion of the drug to minimize systemic toxicity. Furthermore, targeted swelling behaviors can be utilized to protect sensitive active substances during transit through hostile physiological environments,

especially stomach. For example, in the oral administration of insulin, a specific matrices were designed that restrict swelling within the acidic environment of the stomach, protecting the encapsulated peptide from enzymatic degradation [348]. Once the system reaches the neutral pH of the intestine, altered environmental conditions trigger rapid swelling, opening the polymer mesh to safely release the insulin into the bloodstream.

The high water content achieved through equilibrium swelling ensures that the hydrogel closely mimics the physical mass transport properties of native biological tissues, providing a highly favorable microenvironment that supports efficient biological integration. However, this process is highly dependent on many factors, often influenced by external stimuli. The brief summary of swelling forces is presented in Figure 32.

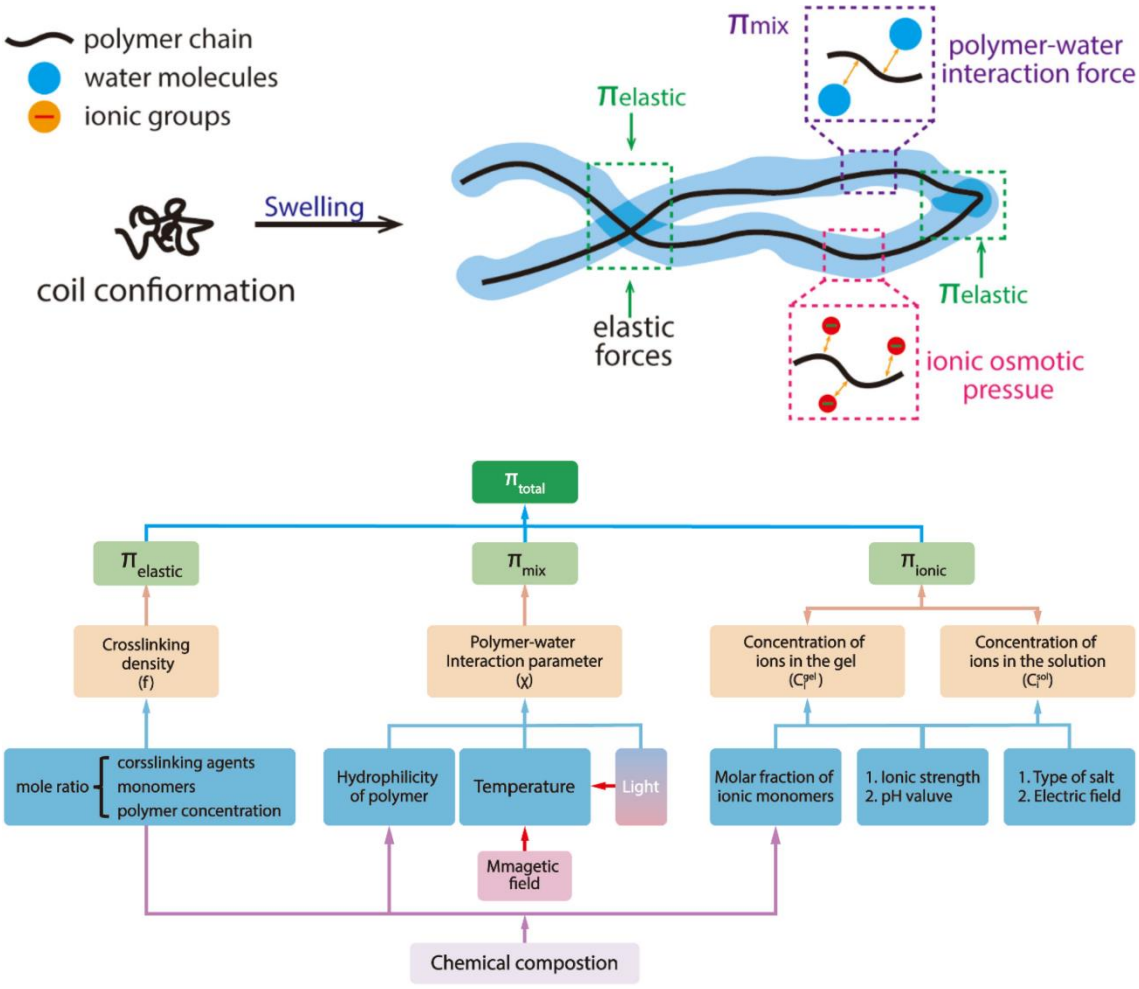


Figure 32 Illustration of the forces, governing the swelling process of hydrogels, together with the influencing factors. These forces are divided into thermodynamic forces of mixing (π_{mix}), elastic forces of the polymer matrix ($\pi_{elastic}$) and ionic swelling pressure (π_{ionic}). Adapted from: [349] under CC BY-ND 4.0 license.

4.3.3.2. Stimuli responsiveness of hydrogels

Hydrogel materials from third generation biomaterials possess the capacity to dynamically alter their physicochemical properties in response to specific environmental triggers. These stimuli-responsive networks undergo reversible structural changes, allowing precise

control over drug release kinetics and matrix mechanics. Three triggers play the most important role in the design of “smart” hydrogels: temperature, pH and light. Other stimuli applied in hydrogel design with examples of applications was broadly described in the published work *Stimuli-responsive delivery systems using carbohydrate polymers: A review* [21].

Thermoresponsive hydrogels represent a prominent class of adaptive materials, defined by their ability to undergo a reversible sol-gel phase transition at specific temperature thresholds. Systems characterized by a Lower Critical Solution Temperature (LCST), such as PNIPAAm, display an inverse temperature response. Below the LCST, strong hydrogen bonding between the polymer chains and water molecules maintains the network in a highly swollen, soluble state. When temperatures exceed the LCST, hydrophobic interactions dominate the thermodynamic environment, causing the polymer chains to dehydrate, collapse and solidify into a gel. This behavior is used to inject therapeutic formulations as liquids at room temperature, which subsequently solidify into stable depots upon reaching physiological body temperature [329]. Other systems, exhibiting Upper Critical Solution Temperature (UCST) behavior, remain fluid at elevated temperatures and transition into a solid gel state upon cooling. PAA and gelatin represent classic examples of this behavior, relying on the disruption of intermolecular hydrogen bonds or physical entanglements at higher temperatures. Below the critical threshold, the kinetic energy of the system decreases sufficiently to allow the polymer chains to re-associate into an ordered, rigid network. This cooling-induced gelation is frequently utilized in bioprinting applications, where heated polymer solutions are extruded and rapidly solidify upon contact with a cooler build plate to maintain structural fidelity [298]. The comparison of LCST and UCST systems was presented in Figure 33.

Other class of stimuli-responsive materials, pH-sensitive hydrogels alter their volume and internal architecture in response to localized fluctuations in acidity or alkalinity. These networks incorporate polyelectrolytes containing weakly acidic or basic pendant groups, such as the carboxylic acid domains in PAA or the amine groups in poly(histidine) [350]. Changes in environmental pH induce the protonation or deprotonation of these functional groups. The resulting electrostatic repulsion between the ionized chains forces the polymer network to expand, thereby increasing the macroscopic swelling ratio. Thanks to such specific interactions, pH-responsive matrices can be used for targeted drug delivery to specific physiological sites. For instance, because tumor microenvironments typically present higher acidity than healthy tissues, pH-sensitive hydrogels can encapsulate chemotherapeutic agents and restrict their release strictly to the acidic tumor site. Similarly, these matrices protect sensitive oral therapeutics from gastric acids, releasing their payload only upon reaching the neutral or alkaline conditions of the intestinal tract [351].

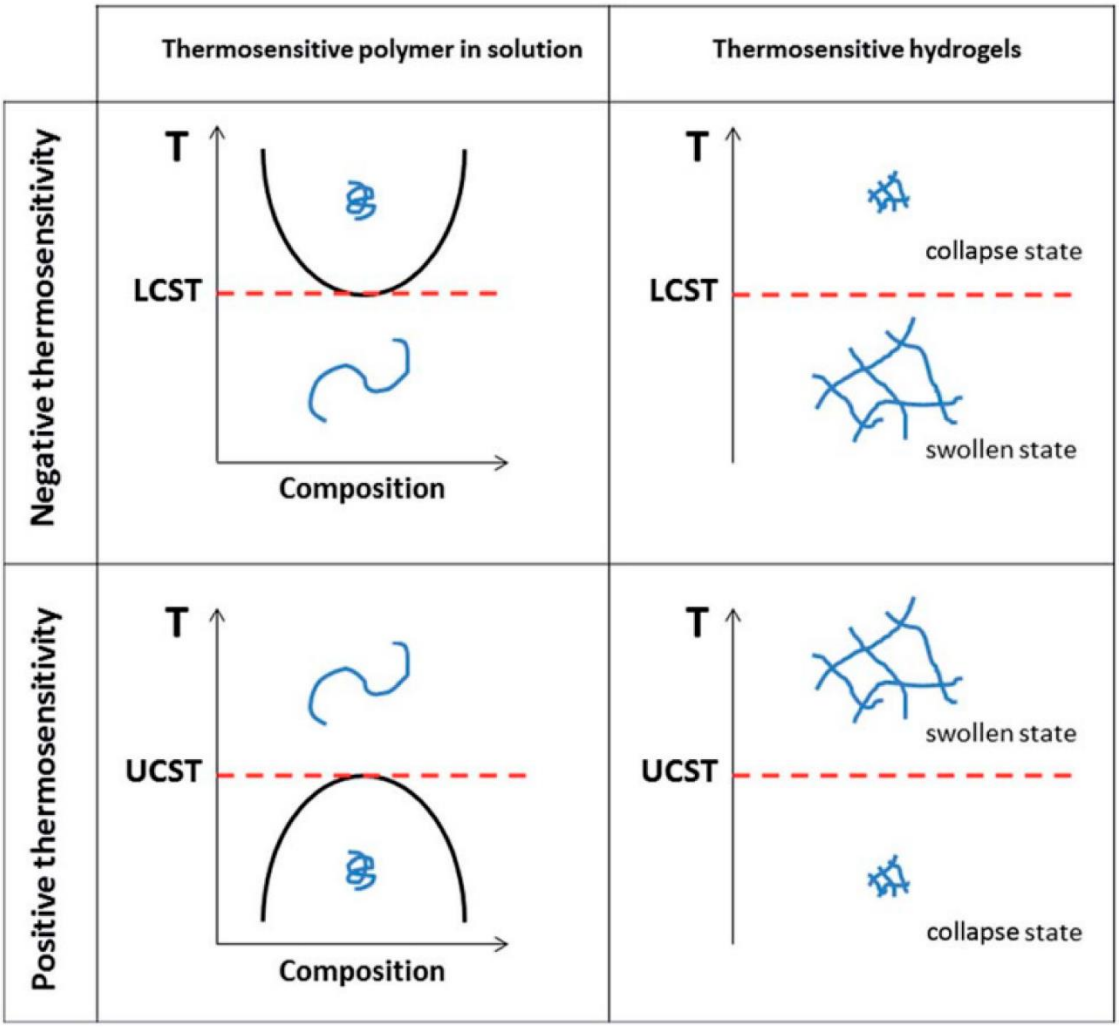


Figure 33 The comparison between behavior of LCST and UCST systems existing as solutions and hydrogels. Adapted from: [352] under CC BY 4.0 license.

In opposition to the two previous classes, light-responsive hydrogels incorporate specific photoreactive moieties directly into their polymer backbone, relying on the external stimulation. Upon exposure to defined wavelengths of light, these functional groups undergo rapid structural conformational changes or initiate secondary crosslinking reactions [316]. This optical activation mechanism grants clinicians non-invasive, remote and highly precise spatial and temporal control over the biomaterial. Because light acts as an external trigger, the activation process remains entirely independent of local physiological variations, such as localized pH shifts or body temperature fluctuations. Furthermore, this controlled exposure allows modify the macroscopic shape and internal stiffness of the hydrogel post-implantation. Recent literature highlights the application of light-sensitive hydrogels in fabricating microlenses, developing advanced biosensors, creating organ-on-a-chip devices and engineering precise drug delivery vehicles [21,23,45].

4.3.3.3. Rheological characteristics

Rheological analysis systematically evaluates the macroscopic mechanical properties and flow behavior of hydrogels when subjected to external physical deformation. Because hydrogels consist of a crosslinked polymer network permeated by an aqueous solvent, they do not behave as purely elastic solids or purely viscous liquids. Instead, they demonstrate a complex viscoelastic nature. This behavior can be quantified by measuring two primary parameters using oscillatory rheology: the storage modulus (G') and the loss modulus (G''). The G' reflects the elastic, solid-like properties of the material, representing the mechanical energy stored within the network during deformation. The G'' reflects the viscous, liquid-like properties, representing the energy dissipated as heat due to internal molecular friction. In a fully formed, stable hydrogel, G' significantly exceeds G'', ensuring that the matrix maintains its structural integrity under static physiological conditions. The comparison of rheological behavior of different types of materials was presented in Figure 34.

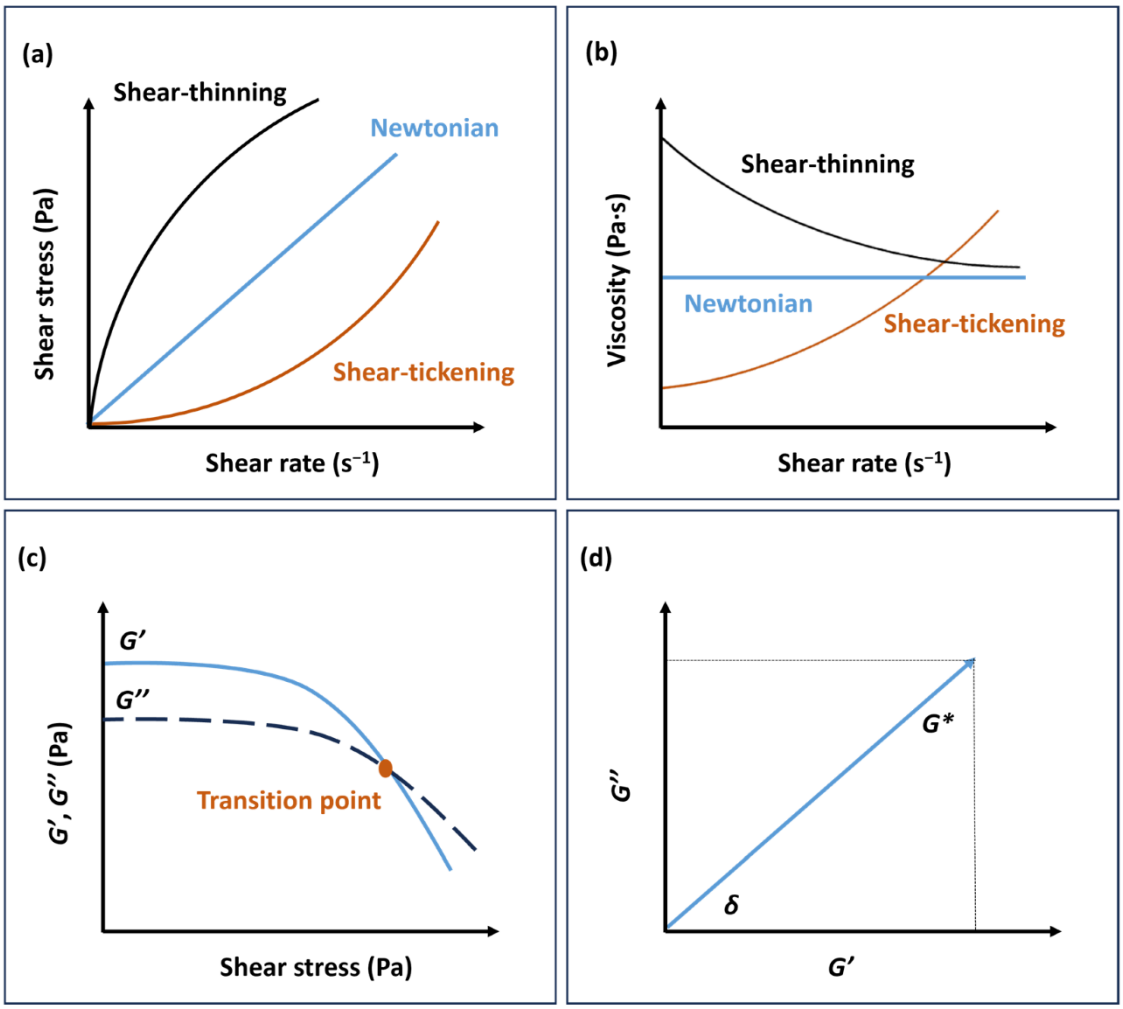


Figure 34 Comparison of Newtonian and non-Newtonian fluids rheological behavior based on a) shear stress and shear rate and b) viscosity and shear rate relations. c) Shear-thinning behavior of non-Newtonian fluid. d) Relationship between the complex shear modulus (G) and G', G''. Adapted from: [353] under CC BY 4.0 license.*

A critical rheological parameter for advanced clinical applications is non-Newtonian shear-thinning behavior. Under static or low-stress environments, shear-thinning hydrogels maintain a robust, solid-like structural configuration [354]. However, when subjected to elevated mechanical shear stress, the internal architecture temporarily yields. This phenomenon occurs primarily in physically crosslinked networks or matrices stabilized by dynamic, reversible covalent bonds. The applied physical force disrupts the transient non-covalent interactions (such as used in physically-crosslinked hydrogels) and forces the entangled polymer chains to align parallel to the direction of flow. This molecular realignment causes a rapid, reversible decrease in macroscopic viscosity, allowing the solid network to liquify and flow smoothly. Once the external shear force stops, the polymer chains lose their forced alignment and the internal dynamic bonds rapidly re-establish. Consequently, the hydrogel autonomously recovers its original elastic storage modulus and stiffness within seconds, a characteristic often referred to as thixotropy or self-healing [145]. However, as depicted in Figure 35, this behavior must be carefully designed to not only allow for extrusion/injection, but also to permit creation of structurally stable constructs/barriers. Additionally, this behavior actively protects encapsulated active substances or cells. If a highly viscous material resists flow, the resulting mechanical shear forces can easily rupture the lipid membranes of encapsulated stem cells or denature therapeutic substances. By liquefying, the shear-thinning hydrogel acts as a protective, low-friction fluid cover during extrusion. After injecting the hydrogel into the specific place, polymer network has to quickly solidify to prevent the unwanted systemic migration of the encapsulated drugs to surrounding tissue [329].

Shear-thinning behavior constitutes a fundamental rheological prerequisite for extrusion-based 3D bioprinting technologies. During the printing process, the dispensing pneumatic or mechanical system extrudes the bioink through a microscopic nozzle. Thus, the bioink must exhibit profound shear-thinning properties to flow continuously and prevent nozzle occlusion. Immediately upon deposition onto the printing bed, the bioink must undergo rapid structural recovery [145]. If the viscosity remains too low, the printed filament will spread, resulting in catastrophic structural collapse and the loss of geometric fidelity. Moreover, bioink must rapidly regain a sufficiently high storage modulus to physically support the weight of subsequent layers stacked above it. Successful design of the hydrogel rheological profile can allow to produce highly complex, computer-generated personalized architectures capable of replacing damaged native tissues [304].

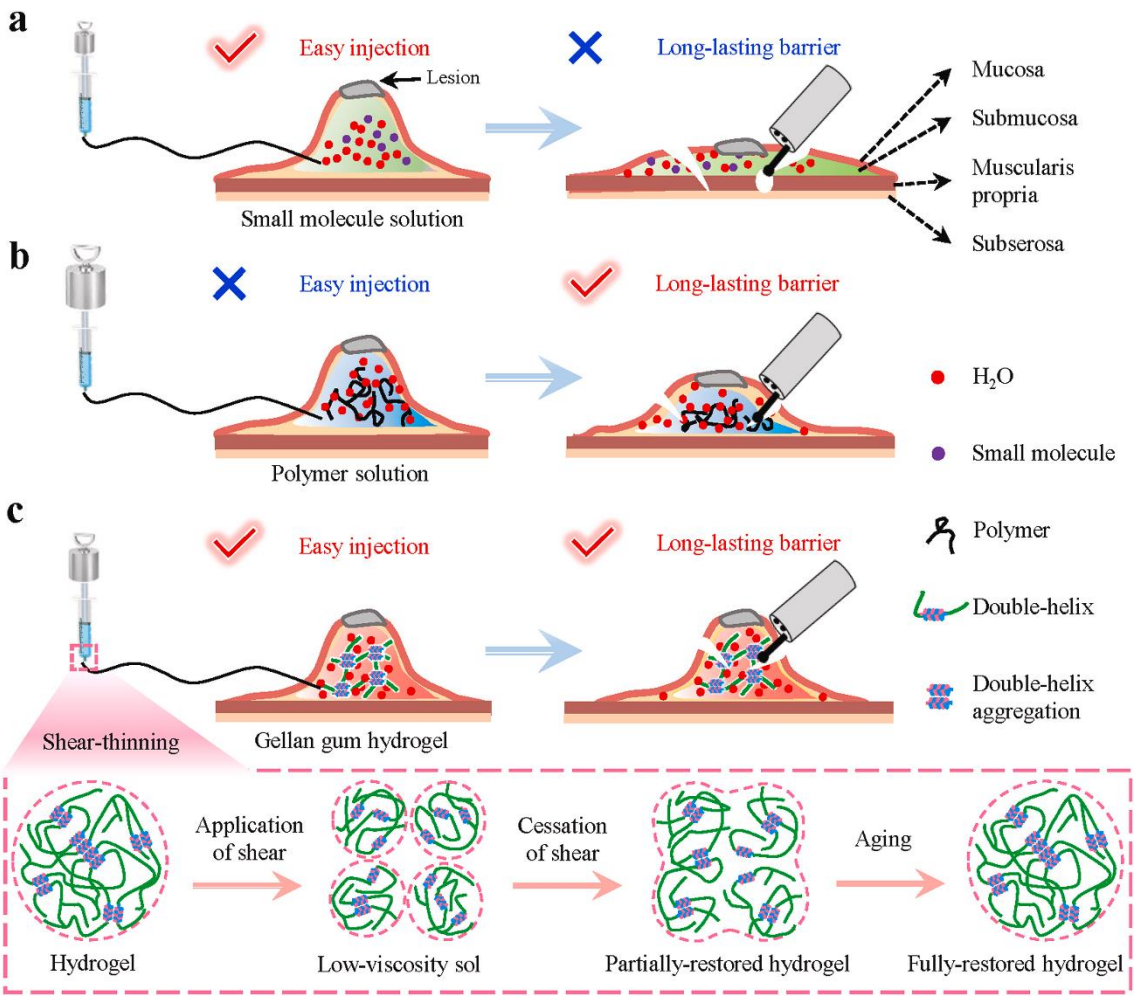


Figure 35 Comparison of different injectable materials: a) Low-viscosity materials, b) Conventional hydrogels, c) Hydrogels with shear-thinning behavior designed for injection applications. Adapted from: [354] under CC BY-ND 4.0 license.

4.3.4.Hydrogels in drug delivery and implantable devices

While their high water content and structural similarity to the native ECM describes hydrogel materials ideal for bulk tissue replacement, the tunable nature of these polymeric matrices make them ideal candidates for sophisticated, dynamic vehicles for controlled drug delivery and as highly functional interfacial coatings for solid medical implants. Specialized devices capable of protecting sensitive therapeutic substances from premature enzymatic degradation within hostile physiological environments can be obtained by strategically modulating source materials, crosslinking density, swelling thermodynamics or stimuli-responsive behaviors [336]. The versatility of hydrogel materials was summarized in Figure 36. Furthermore, when applied to bulk materials, hydrogels address a fundamental challenge in modern surgical practice. Traditional metallic and synthetic prostheses frequently fail due to mechanical stiffness and immediate biological rejection by the host immune system [53]. Thin hydrogel coatings successfully bridge this critical gap by providing a soft, biomimetic exterior that closely mimics the mechanical compliance of surrounding biological tissues. This architectural strategy preserves the required structural strength of the solid implant, while simultaneously shielding it from the

body's aggressive immune system, increasing the biocompatibility of the device. This dual capability defines hydrogels as the one of the most profound examples of third and fourth generations of biomaterials.

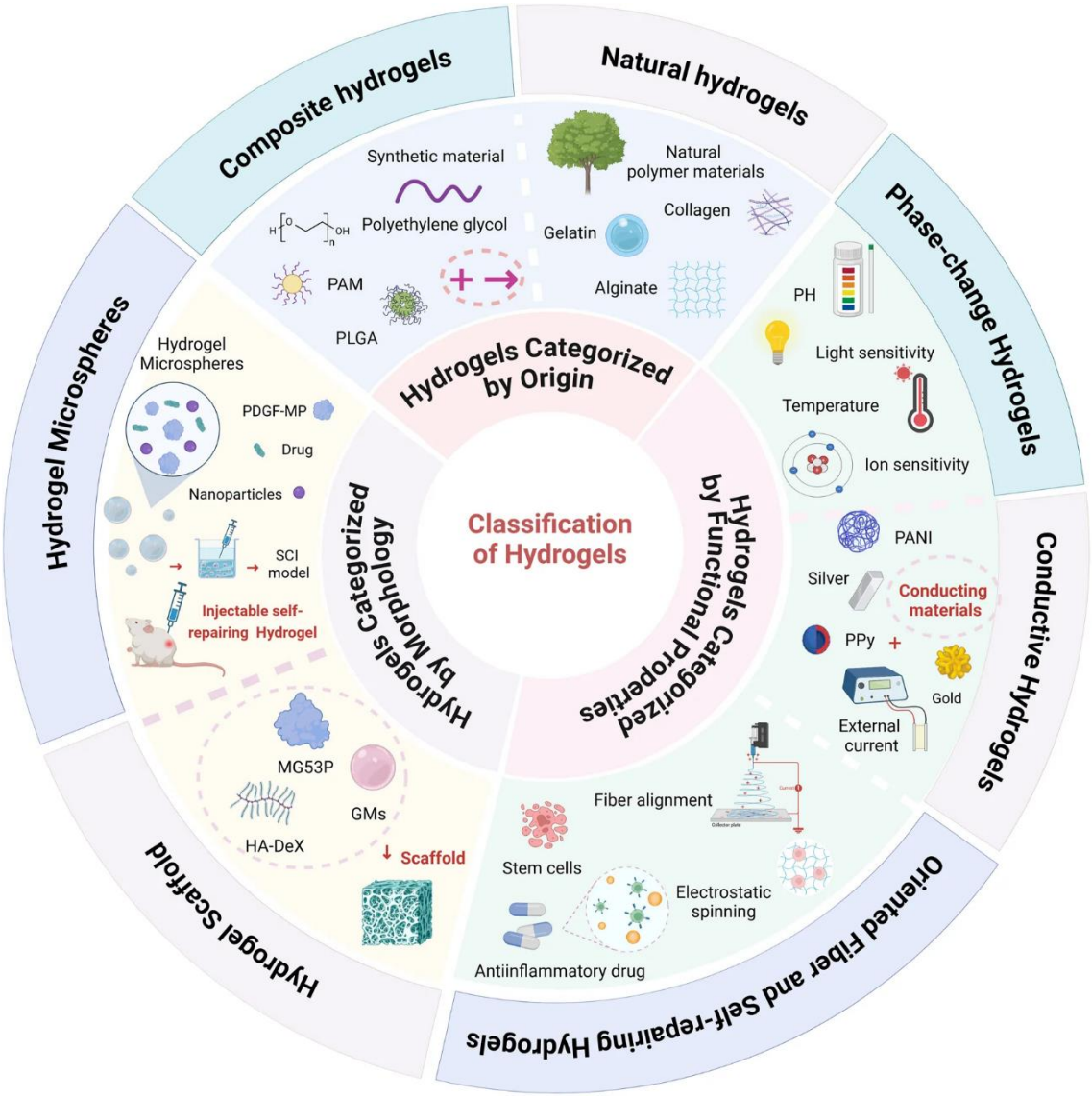


Figure 36 The versatility of possible hydrogel materials design divided into the materials origin, functions and morphology. Adapted from: [355] under CC BY 4.0 license.

4.3.4.1. Mechanisms of active substances transport

Predictable and controlled drug release remains the primary objective of any hydrogel-based delivery system. The movement of encapsulated therapeutic agents out of the polymer matrix and into the surrounding physiological environment is governed by a complex interplay of thermodynamic forces, polymer chain dynamics, physical network constraints and interactions between active substances and polymeric network. There are three fundamental kinetic mechanisms describing this complex interactions: diffusion, swelling and degradation/erosion [347]. Although they can be described individually, in real life all of these mechanisms must be

taken into account because they usually all have the effect on the final DDS performance. The comparison between these release mechanisms was presented in Figure 37.

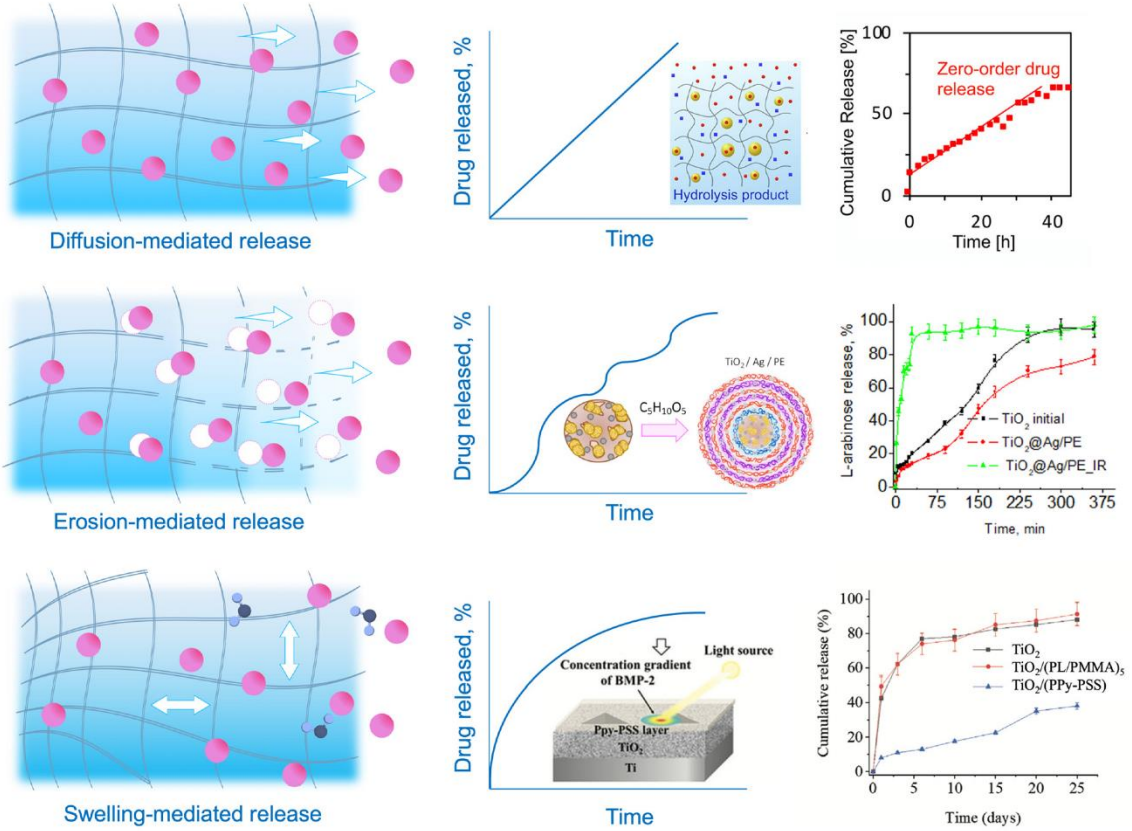


Figure 37 Comparison of release and drug diffusion kinetics. Adapted from: [356] under CC BY 4.0 license.

Diffusion is the most fundamental and extensively modeled pathway. In a purely diffusion-controlled system, the physical mesh size of the crosslinked polymer network strictly dictates the release rate, acting like a sieve [356]. When the hydrodynamic radius of the encapsulated drug is significantly smaller than the hydrogel pores, the drug migrates rapidly out of the matrix unhindered, driven entirely by the macroscopic concentration gradient between the heavily saturated polymer core and the surrounding biological fluid. To accurately predict these profiles, classical Fickian theory can be utilized. In pure Fickian diffusion, the rate of drug release is strictly proportional to the concentration gradient. As the drug exits the hydrogel, the internal concentration drops, meaning the driving force continuously decreases over time [357]. This is frequently characterized by first order kinetics, where the release rate depends directly on the residual concentration remaining inside the matrix. For homogeneous systems, the Higuchi model can be utilized, which simplifies Fick's laws to demonstrate that the cumulative amount of drug released is directly proportional to the square root of time [358]. However, if a therapeutic agent engages in strong interactions with the hydrogel backbone, its release deviates from free-volume diffusion. In these pseudo-second order systems, the rate-limiting step becomes the physical adsorption-desorption exchange between the drug and specific binding sites, resulting in a prolonged release profile independent of pure concentration gradients.

Because hydrogels often undergo significant volumetric expansion concurrently with drug diffusion, pure Fickian models are frequently insufficient to characterize dynamic biological performance. To classify these transitioning systems, researchers employ the Korsmeyer-Peppas semi-empirical power law, which utilizes a specific diffusional release exponent to mathematically identify the underlying transport mechanism [359]. This exponent bridges diffusion-controlled and swelling-controlled kinetics. As previously described, swelling-controlled systems rely heavily on the thermodynamic phase transition of the polymer network itself. In these systems, the hydrogel is administered in a dehydrated state, where the internal mesh size is negligible and the drug is physically locked within a rigid core. When this glassy matrix contacts biological fluids, a sharp penetrating solvent front develops. As water diffuses inward, it acts as a plasticizer, causing the tightly coiled polymer chains to undergo structural relaxation. The matrix systematically opens the interstitial pores and releases the drugs. When the rate of solvent diffusion into the matrix is significantly faster than the rate of polymer chain relaxation, transport is controlled entirely by how quickly the polymer network physically uncoils. This mechanism is termed Case II transport and represents the biomedical ideal for sustained-release implants because it frequently produces zero-order release kinetics [359]. The drug is released at a completely constant, uninterrupted rate governed by the steady swelling. However, in real-life applications, most swellable hydrogels exhibit anomalous or non-Fickian, transport, where the time scales for solvent diffusion and polymer relaxation are roughly equivalent. In anomalous systems, release is governed by a simultaneous interplay of Fickian diffusion through the newly hydrated regions and the continuously shifting internal mesh size caused by ongoing thermodynamic expansion [357].

While diffusion and swelling rely on physical transport mechanisms through an intact matrix, degradation-controlled systems depend entirely on the intentional, progressive erosion of the polymer network. This mechanism is often utilized for the delivery of massive proteins or growth factors, which physically cannot traverse the steric constraints of a tight polymer mesh [344]. Release occurs only as the covalent bonds or physical crosslinks holding the hydrogel together are degraded via hydrolysis or specific enzymatic cleavage. In bulk degradation (homogeneous erosion), the rate at which water penetrates the hydrogel significantly exceeds the rate at which polymer bonds chemically break. Consequently, the entire three-dimensional volume of hydrogel hydrates and degrades simultaneously. Once structural integrity collapses, a burst release of the active substances occurs as the network disintegrates. On the other hand, surface degradation occurs when chemical bond cleavage is significantly faster than internal water diffusion. Common in highly hydrophobic or densely crosslinked networks, this heterogeneous erosion is limited to the outermost material-tissue interface. The exterior surface progressively degrades, leaving the internal core stable. Because the degradation rate is directly proportional to the available surface area, surface-eroding matrices frequently achieve zero-order kinetics, releasing the drugs at a predictable rate as the implant degrades. The effect of different bonds in hydrogel matrix on the degradation kinetics was shown in Figure 38.

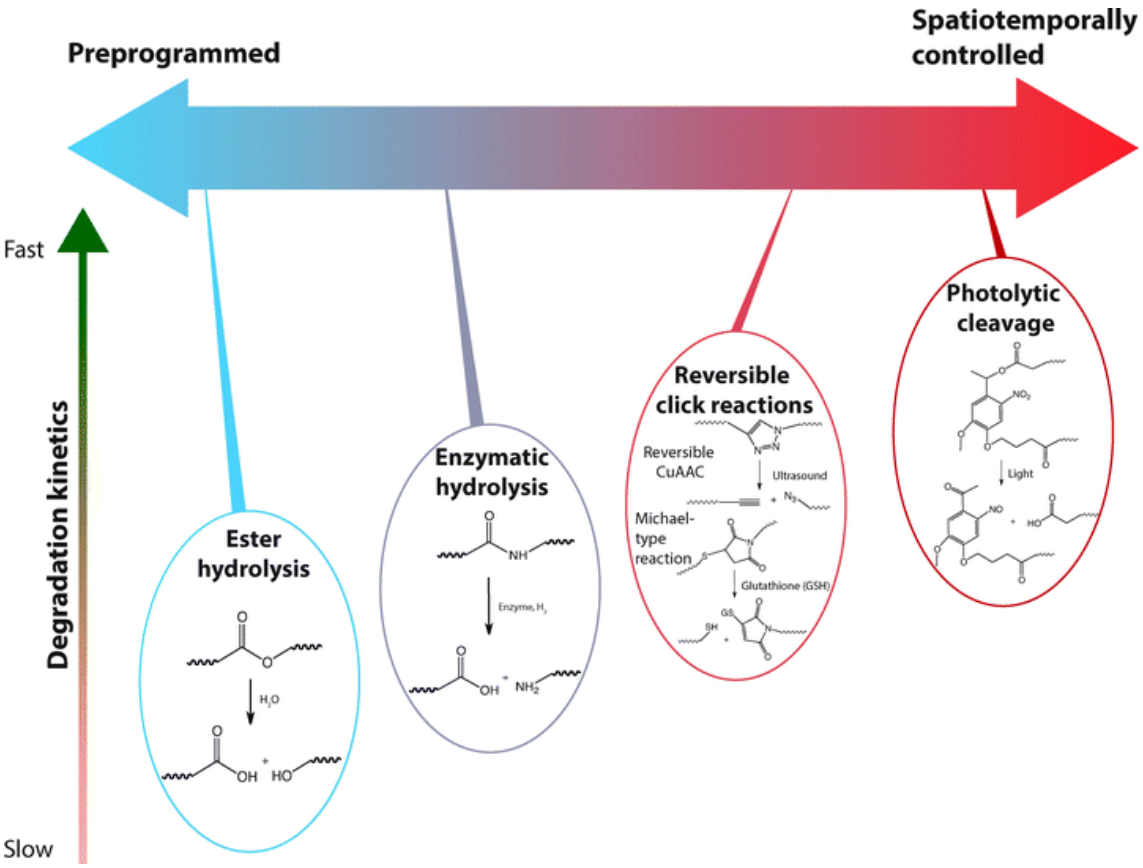


Figure 38 The effect of different bonds in hydrogel matrix on the rate and controllability of the network degradation. Adapted from: [344] under CC BY-NC 3.0 license.

4.3.4.2. Hydrogel coatings for implantable devices

Beyond utilizing hydrogels as localized drug delivery matrices, these highly hydrated polymer networks can be employed as surface coatings to modify conventional medical devices, including endovascular stents, deep brain stimulation electrodes, load-bearing orthopedic prostheses or wound dressings [320,339,341]. For instance, the severe physical mismatch between a rigid metal implant and soft vascular or neural tissue generates chronic shear stress and microscopic friction at the material interface, which results in persistent local inflammation [53]. By covalently grafting a compliant polymer network onto the solid substrate, soft, biomimetic exterior that precisely mimics the ECM can be created.

The most immediate and critical challenge following surgical intervention is the host immune system's attempt to isolate the synthetic device, known as the foreign body response, as described in detail in Section 4.1.2. Hydrogel coatings actively modulate interfacial thermodynamics to prevent the initial stage of protein adsorption. Highly hydrophilic polymer networks, bind tightly to surrounding water molecules via strong hydrogen bonding, generating a dense, highly ordered hydration layer. When circulating proteins approach the implant, the physical compression of this bound water layer creates an intense steric repulsion [295]. This structural evasion minimizes early macrophage activation, averts the formation of foreign body

giant cells and prevents fibrotic encapsulation to ensure the long-term functional viability of the implant.

Pathogenic bacterial infection represents another severe threat that hydrogels successfully mitigate. Bacteria possess a high affinity for synthetic surfaces, rapidly multiplying and forming biofilms upon attachment. Once established, a biofilm makes the bacterial colony exponentially more resistant to both traditional systemic antibiotics and the host immune system. To address this challenge, hydrogel coatings that integrate two distinct, synergistic defense mechanisms – passive and active were design [360].

The passive anti-biofouling strategy relies entirely on the physicochemical properties of the hydrogel surface to prevent the initial bacterial docking phase. The same highly hydrated, sterically repulsive barrier that prevents blood protein adsorption also acts as a formidable shield against bacterial colonization. Furthermore, by imprinting microscopic, biomimetic geometries onto the surface, the hydrogel actively manipulates local fluid shear forces and physically disrupts bacterial settlement patterns, preventing the accumulation of the critical bacterial mass required for biofilm formation (Figure 39).

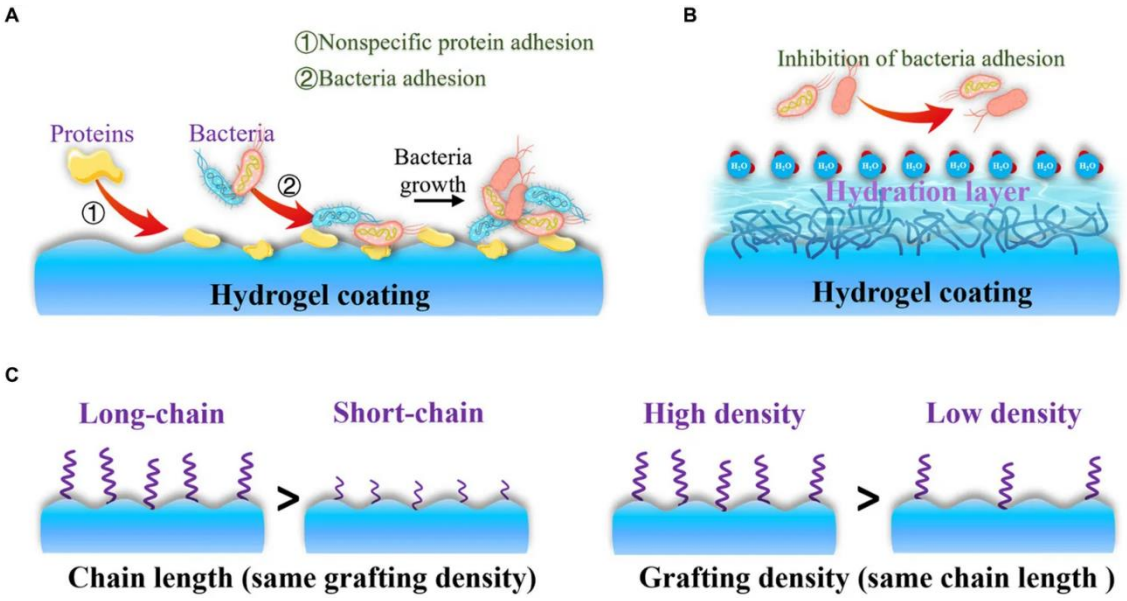


Figure 39 Passive anti-biofouling strategies of hydrogel coatings: A) nonspecific protein adhesion; B) hydration layer; C) bacteria-repelling by chain length and grafting density. Adapted from: [360] under CC BY 4.0 license.

Because overwhelming bacterial loads or direct surgical contamination can occasionally breach passive systems, hydrogels are often modified with active antimicrobial delivery networks. Potent, broad-spectrum bactericidal agents are employed to destroy pathogens that bypass the physical hydration barrier. Such modified matrices provide highly localized, sustained elution of therapeutic active substances directly into the implant-tissue interface. For example, incorporating silver nanoparticles (which continuously release toxic silver ions that aggressively disrupt bacterial cell membranes and generate lethal reactive oxygen species) transforms the hydrogel into a potent contact-killing surface. Alternatively, cationic antimicrobial peptides or conventional

antibiotics that diffuse outward as the hydrogel swells can be introduced into hydrogel matrices. The difference between different active strategies was depicted in Figure 40.

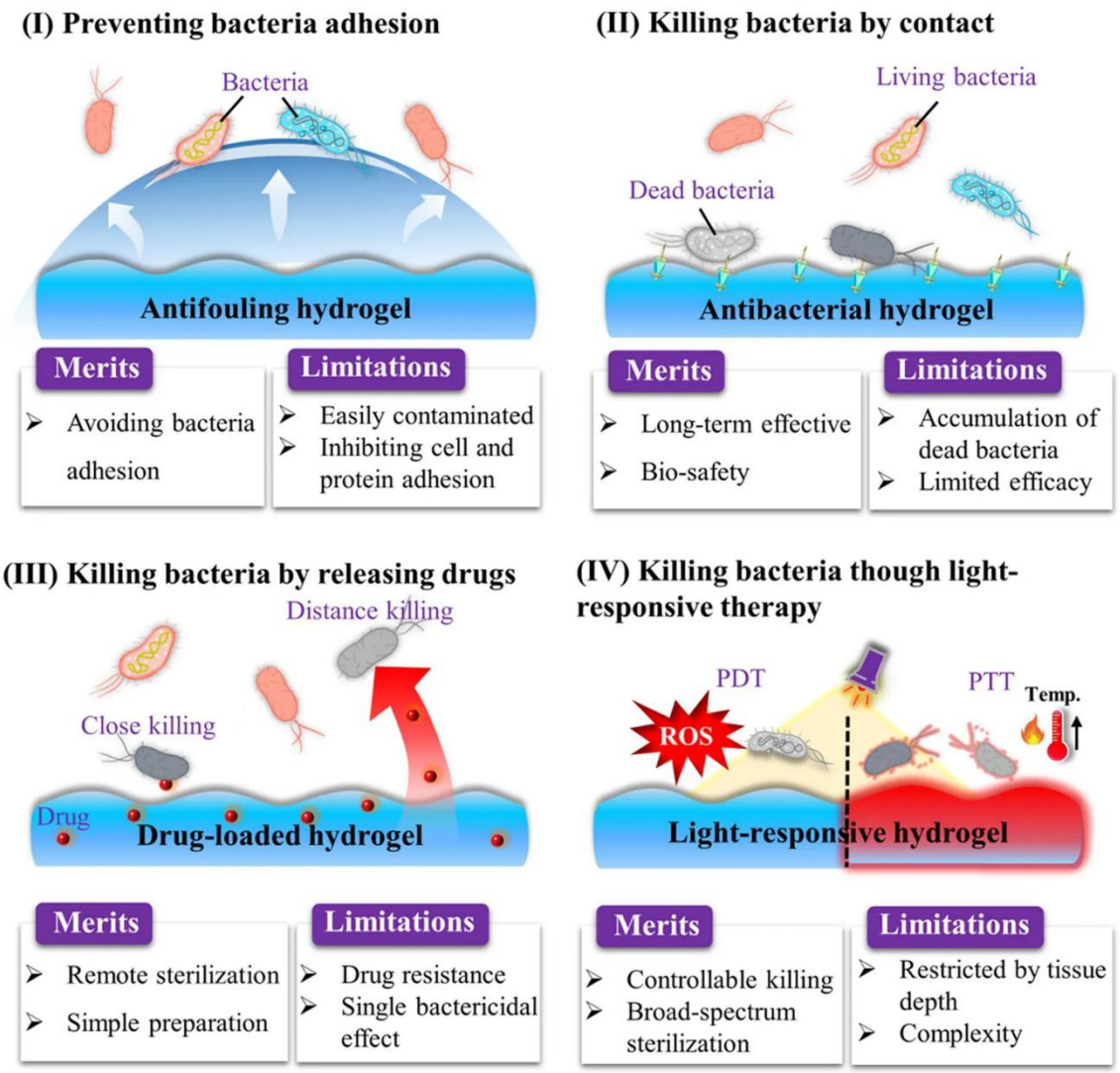


Figure 40 Comparison of different active anti-bacterial strategies to the non-fouling strategy. Adapted from: [360] under CC BY 4.0 license.

This highly localized delivery strategy maintains proper drug concentrations exactly in the microenvironment where the infection risk is highest. Consequently, the hydrogel successfully kills pioneer bacteria before they can establish a biofilm, achieving complete microbial clearance without subjecting the patient to the severe systemic toxicities associated with high-dose intravenous antibiotic therapy.

4.4. Conclusions

The evolution of synthetic biomaterials has progressed from characterizing these materials as purely pharmacologically inert substances to recognizing them as sophisticated systems intended to actively interact with living tissues. Current research positions the discipline within the fourth generation, characterized by smart, autonomous biomaterials that rely on the convergence of materials science, bioelectronics and advanced biofabrication. These advanced systems operate as programmable and reconfigurable devices, executing a broad range of functions without requiring manual external intervention. To advance this domain further, future research must focus on establishing a fifth generation of biomaterials defined by extreme biological complexity and true autonomy. Integrating artificial intelligence and machine learning algorithms will allow researchers to accurately predict cell-material interactions and precisely tailor degradation kinetics, shifting the methodology from trial-and-error experimentation to data-driven engineering. Furthermore, engineering living biomaterials that embed programmable circuits will enable implants to actively manage regeneration by adapting morphologically and biochemically as the host tissue heals.

Polyurethanes represent a highly versatile class of synthetic polymers whose distinct mechanical properties and degradation kinetics derive directly from their microphase-separated morphology. By selectively modulating the ratio and chemical composition of rigid hard segments and flexible soft segments, scaffolds ranging from highly compliant elastomers to rigid structural plastics can be synthesized. Historically, medical-grade PUs relied on aromatic diisocyanates, which degrade *in vivo* into toxic and potentially carcinogenic byproducts. Consequently, modern resorbable implants require aliphatic diisocyanates to ensure the release of strictly non-cytotoxic metabolic intermediates. Future progress in PU engineering necessitates addressing the environmental and occupational hazards associated with traditional synthesis. Researchers must optimize sustainable fabrication routes, such as extracting polyols from renewable resources and developing non-isocyanate polyurethanes through the step-growth polyaddition of cyclic carbonates with aliphatic polyamines. Future developments must also overcome the substantial kinetic limitations of these sustainable pathways, as the aminolysis of cyclic carbonates proceeds at a markedly slower rate than traditional reactions. Additionally, utilizing advanced synthetic routes, such as atom transfer radical polymerization, will enable to build ultra-tough polyurethanes capable of withstanding dynamic mechanical environments in cardiac and muscular tissues.

Hydrogels function as three-dimensional, highly hydrated polymeric networks capable of retaining significant volumes of biological fluids without dissolving. Due to their thermodynamic swelling capacity and structural similarity to the native extracellular matrix, these matrices excel as sophisticated vehicles for controlled drug delivery and as highly functional interfacial coatings for solid medical implants. The stability, porosity and mass transport capabilities of these networks depend strictly on specific physical or chemical crosslinking mechanisms. To expand the clinical utility of hydrogel systems, future developments must overcome the inherent mechanical downsides associated with conventional single-network designs. Engineering interpenetrating

polymer networks offers a strategy to achieve exceptional fracture toughness while preserving the biological activity and diffusivity of the secondary matrix. Furthermore, future drug delivery platforms require enhanced stimuli-responsive capabilities. Precise external triggers, such as specific light wavelengths or localized pH fluctuations, must be utilized to achieve strict spatiotemporal control over the release of encapsulated therapeutic agents.

Modifying base polymers through physical blending, nanoparticle integration and bioactive compound loading remains essential in modern biomaterial design, as single-component materials frequently lack the capacity to simultaneously provide structural rigidity and a bioactive interface. Integrating natural active substances, such as curcumin or propolis, directly into the polymer network provides localized antibacterial and anti-inflammatory activity. While such site-specific delivery aims to reduce initial bacterial colonization, implanting foreign bodies always comes with the risk of biofilm formation, especially when such device starts to degrade, increasing their specific surface. Designing effective implants for the sinonasal cavities requires overcoming distinct organ- and tissue-level challenges. Drug delivery systems contact only small portions of the mucosal tissue, leaving adjacent surfaces prone to inflammatory conditions. Furthermore, the local microenvironment experiences physiological fluctuations, including pH shifts, which can disturb local tissue healing and destabilize bioactive molecules, potentially limiting therapeutic efficacy. Apart from that, natural substances inherently exhibit significant batch-to-batch chemical variability and poor thermal stability, which complicates the rigorous standardization demanded by regulatory agencies. Future research efforts must focus on translating these heterogeneous formulations into highly reproducible, clinically approved composite products that withstand rigorous processing conditions without denaturing the active therapeutic agents.

While robust synthetic polymers offer necessary mechanical support, they often provoke severe foreign body responses and bacterial colonization. On the other hand, highly hydrated biomimetic materials prevent biofouling but lack mechanical durability. The primary objective of this doctoral dissertation directly addresses this specific research void by designing, synthesizing and evaluating a biodegradable, drug eluting implant system combining an aliphatic polyurethane matrix and a curcumin-loaded hydrogel coating for application in regenerative medicine. This system aims to provide localized, controlled release of active substances to accelerate tissue healing and minimize postoperative complications. The hypothesis of this research states that applying a curcumin-loaded, polymer-stabilized hydrogel coating to an aliphatic polyurethane core creates a functional dual-delivery system capable of sequential active substance release. Furthermore, this hypothesis postulates that the composite architecture provides an initial antibacterial release from the hydrogel shell, followed by a sustained release of a secondary pharmacological agent from the degrading polyurethane core, without compromising the mechanical integrity or cytocompatibility of the implant. Because the aliphatic polyurethane exhibits lower initial stiffness than metallic equivalents, it can progressively transfer the

mechanical load to the regenerating host tissue as it degrades, stimulating natural cellular remodeling processes without causing stress shielding.

The proposed research addresses critical limitations across biomaterials design, polyurethane synthesis and hydrogel formulation. Conventional delivery systems often struggle to achieve coordinated, multi-stage therapeutic release. This work resolves this gap by developing a biodegradable core-shell architecture that combines a thermoplastic polyurethane core with hydrogel coating. This design enables dual-drug delivery: an initial antibacterial curcumin release from the hydrogel shell is then followed by sustained corticosteroid elution from the degrading core, preserving mechanical support throughout the healing process. Currently used commercial polyurethanes possess significant biological and functional shortcomings for internal mucosal applications, especially in terms of toxic degradation by-products. This work addresses this research gap by synthesizing custom aliphatic polyurethanes with tailored polyol mixtures. Precise control over the soft segments chemistry allows to precisely tune degradation profile to the targeted application, improving cytocompatibility by avoiding toxic aromatic degradation products and ensuring optimal properties for FDM 3D printing. Incorporating hydrophobic therapeutics into hydrophilic matrices traditionally requires toxic organic solvents that hinder biocompatibility. This work directly addresses this challenge by developing a water-based, green system. Using secondary polymers (specifically poly(vinyl alcohol) and poly(vinylpyrrolidone)) as interfacial mediators, allowed to stabilize hydrophobic curcumin directly within a renewable agar matrix without compromising printability or cytocompatibility.

5. Materials and methods

5.1. Polyurethane synthesis

Syntheses were carried out with different polyol systems based on: poly(ε-caprolactone) (PCL, CAPA 2000, M_w=2000, Sigma-Aldrich, USA), poly(ethylene glycol) (PEG, M_w=2000 g/mol, BASF SE, Poland), α,ω-oligo(ethylene-butylene adipate)diol (POLIOS 55/20, M_w=2000, Purinova, Poland), polytetrahydrofuran (PTMEG, M_w=2000, Cortex, Poland) together with 1,6-hexamethylene diisocyanate (HDI, Sigma Aldrich, Poznań, Poland), dibutyltindilaurate (Sigma-Aldrich, USA) catalyst and 1,4-butanediol (Basf SE, Germany) (BDO) as chain extender. As active substance, Corhydron 25 (hydrocortisone in form of sodium hydrocortisone succinate, Jelfa S.A., Poland) was used.

Polyols were selected to combine hydrolytically degradable polyester soft segments with flexible and oxidation-prone polyethers to systematically tune the degradation rate and matrix hydrophilicity. Varying the ratios of semicrystalline, slow-degrading PCL (ES1) and amorphous POLIOS 55/20 (ES2) alongside hydrophobic PTMEG (ET1) and hydrophilic, highly swelling PEG (ET2) allowed for fine control over drug release kinetics and hydrolytic erosion profiles. As for other substrates, HDI with BDO and a dibutyltin dilaurate catalyst allows to form uniform, crystalline hard segments that provide high mechanical strength, acceptable reaction speed without yielding toxic aromatic degradation byproducts. Hydrocortisone was chosen due to its anti-inflammatory effect, but also due to its specific chemical structure, allowing for potential incorporation into polymer chain, extending its release.

Polyurethanes were synthesized using two-step reaction. The example synthesis scheme: the urethane prepolymer (8 wt % of free isocyanate groups) was obtained in the reaction of PC with HDI in three-necked glass reactor. Polyol was first degassed and dehydrated for 3 h at 80 °C. HDI was added to the reactor and prepolymerization reaction was carried out at 80 °C for 3 h. As a result of this process, a urethane prepolymer called pre-ES1 was obtained. The concentration of unbound isocyanate groups in the obtained prepolymer was performed after 24 hours from the end of its synthesis. About 0.5 g of prepolymer, 3 mL of 0.5 M di-n-butyl amine and 20 mL of acetone were weighed into a 250 cm^3 conical flask. After dissolution of the prepolymer, the mixtures were left for 15 minutes. The unreacted amine was then titrated with 0.1 M HCl using bromophenyl blue as an indicator. The color shift from blue to yellow could be observed. Three determinations were made per one sample and one reference test was made for each polyurethane system, allowing for calculation of the content of %NCO groups (Eq. 3).

$$\%NCO = \frac{V_0 - V_A}{m_N} * 0.42 \qquad (3)$$

where: V_0, V_A - the volume of HCl solution used for the titration of the blank and test sample, respectively [cm^3] and m_N – mass of prepolymer [g].

In the second stage, the prepolymer at 80 °C was mixed using mechanical stirrer with one droplet of the dibutyltindilaurate catalyst. In next step, the calculated BDO amount was added to extend the PU chain. The ratio of free NCO to OH was 1:1.1. The whole mixture was transferred to vacuum vessel to degas the mixture and then was poured into a metal mold placed on a heating plate at 80 °C. After 24 hours of annealing, PU PCL was obtained. Other synthesis with different polyols were proceeded in similar manner (Table 9). If more than one polyol was used, the polyol mixture was always made in equal mass proportions.

Three methods for modifying polyurethane with active substances were investigated. The first method involved modifying the PU during its synthesis, at both the prepolymer formation and chain extension stages. The second method utilized immersing the fabricated models in a solution of the active substance. The third method consisted of coating the 3D printed models with an active substance-loaded hydrogel. The active substances used for the modification included: collagen (OstroVit, Zambrów, Poland), diosmin (Polpharma, Starogard Gdański, Poland), allantoin (Ecospa, Warsaw, Poland), curcumin (Yango, Warsaw, Poland) and Corhydron 25 (hydrocortisone in form of sodium hydrocortisone succinate; Bausch Health Ireland Limited, Dublin, Ireland).

In the first route, PU was synthesized according to the above-described procedure, with the addition of 0.5 % hydrocortisone, which was dissolved either in the polyol mixture or the chain extender (BDO).

In the second route, disc-shaped samples for modification, measuring 3 mm in height and 24 mm in diameter, were first 3D printed using an NX Pellets Pro 3D printer. The obtained models were cleaned in ethanol, dried in a moisture analyzer (RADWAG MAX50/SX) at 40 °C and weighed on an analytical balance (RADWAG AS 220.R2). Subsequently, 1 % solutions of the active substances were prepared (collagen and Corhydron 25 in DMSO; diosmin and allantoin in a mixture of 80% DMSO and 20% THF) and each disc was immersed in the respective solution for 5 minutes at 40 °C. Following the modification, the samples were dried in the moisture analyzer (40 °C) before release studies,

In the third route, the synthesized AG0.6/PVP0.4 hydrogel (synthesis procedure described in Chapter 5.2.) was poured into a Petri dish and placed in a freezer for 24 hours. After this period, the hydrogel was removed, thawed and the excess water was decanted. The hydrogel was then melted using a heated magnetic stirrer and the active substance was added at a concentration of 2.5 wt.% relative to the gel mass at 40 (collagen) or 60 (others) °C. PU discs, prepared identically to those used in the immersion modification, were dipped into the hydrogel and left to dry. Once the hydrogel solidified, the samples were refrigerated for 1 hour before release studies.

Table 9 Polyurethanes prepolymers compositions. Amount of polyol was calculated to obtain 8 wt% of free NCO groups in prepolymer.

Sample name	Used polyol			
	PCL	PEG	PTMEG	POLIOS 55/20
ET1	-	-	+	-
ES1	+	-	-	-
ET2	-	+	-	-
ES2	-	-	-	+
ET2:ES1	+	+	-	-
ET2:ET1	-	+	+	-
ES1:ET1	+	-	+	-
ES1:ES2	+	-	-	+
ES2:ET2	-	+	-	+
ET2:ET1:ES1	+	+	+	-

5.2. Hydrogel synthesis

The synthesis of hydrogel was carried out using: natural polymer: agar E406 (sulphate content: 1.7%, galactose content: 66%, moisture content: 5.1%, ash content: 0.99%, M_w: 397 141 g/mol, M_n: 125 454 g/mol, Đ: 3.16) (Biomus, Lublin, Poland), synthetic polymers: poly(vinylpyrrolidone) (PVP) K15 (M_w 10 000 g/mol) (Sigma-Aldrich Chemie GmbH, Buchs, Switzerland) and poly(vinyl alcohol) (PVA) Mowiol 4-88 (M_w 31 000 g/mol) (Sigma-Aldrich Chemie GmbH, Steinheim, Germany), cross-linking agent: calcium chloride $CaCl_2$ (POCH, Gliwice, Poland), sodium tetraborate (borax) $Na_2B_4O_7$ x 10 H_2O (TechlandLab, Tarnobrzeg, Poland), pH regulator: L-ascorbic acid (Avantor Performance Materials Poland S.A., Gliwice, Poland), active substance: curcumin extract standardized to 95% curcuminoids (Yango, Warsaw, Poland), dimethyl sulfoxide (DMSO) (Merck, Darmstadt, Germany) and 1st class lab water as a solvent and swelling medium.

The hydrogels were obtained by physical crosslinking. Firstly, agar was dissolved in water at a temperature of around 100 °C under rigorous stirring. Then, PVA or PVP was added and dissolved in the same conditions. After that, the water solutions of L-ascorbic acid, borax and $CaCl_2$ were added to the polymer solution and the mixture was left to cool to around 60 °C. Next, DMSO was added, the mixture was rigorously mixed and then poured into petri dishes. To finish the crosslinking, 3 freeze-thawing cycles were performed: freezing at -20 °C for 24 hours, thawing at room temperature for 1 hour and then refrigerating at 4 °C for 24 hours. In the next step hydrogels were first dried using thermobalance MA 50.R (RADWAG, Radom, Poland) to constant mass at 40 °C (mass loss below 1 mg/120 s) and placed in water for 24 hours to remove unreacted compounds. Finished hydrogels were then vacuum packed and stored at 4 °C. 11 hydrogel types were prepared using this procedure (Table 10). Mass of hydrogel samples was controlled

throughout the synthesis and swelling processes using analytical balance AS 110.R2 (RADWAG, Radom, Poland).

For samples modified with curcumin, the solution of set amount of curcumin in DMSO was first prepared. The samples were prepared using the above-mentioned procedure and the solution was added instead of pure DMSO.

Table 10 Hydrogel samples and their compositions.

Sample name	Composition [wt%]								
	Water	DMSO	Agar	PVP	PVA	Calcium chloride	Sodium tetraborate	L-ascorbic acid	Curcumin
AG	92	4	2	0	0	1.6	0.4	0.4	0
AG0.75/PVA0.25	92	4	1.5	0	0.5	1.6	0.4	0.4	0
AG0.6/PVA0.4	92	4	1.2	0	0.8	1.6	0.4	0.4	0
AG0.5/PVA0.5	92	4	1	0	1	1.6	0.4	0.4	0
AG0.75/PVP0.25	92	4	1.5	0.5	0	1.6	0.4	0.4	0
AG0.6/PVP0.4	92	4	1.2	0.8	0	1.6	0.4	0.4	0
AG0.5/PVP0.5	92	4	1	1	0	1.6	0.4	0.4	0
AG/2.5CUR	89.5	4	2	0	0	1.6	0.4	0.4	2.5
AG/5CUR	87	4	2	0	0	1.6	0.4	0.4	5
AG0.6/PVA0.4/2.5CUR	89.5	4	1.2	0	0.8	1.6	0.4	0.4	2.5
AG0.6/PVA0.4/5CUR	87	4	1.2	0	0.8	1.6	0.4	0.4	5
AG0.6/PVP0.4/2.5CUR	89.5	4	1.2	0.8	0	1.6	0.4	0.4	2.5
AG0.6/PVP0.4/5CUR	87	4	1.2	0.8	0	1.6	0.4	0.4	5

5.3. 3D modelling and 3D printing of sinus and septum implants

The 3d models were prepared based on the magnetic resonance imaging (MRI) scan of the human head of one male adult subject without septal deviation. The segmentation process was achieved using 3D Slicer 5.2.1 software. 3D Slicer is an open-source software platform for visualization and medical image computing [361]. By a combination of threshold (43 to 95), scissors, islands (remove smaller than 500 voxels) and smoothing (kernel size 2 mm, 5 mm and 10 mm) tools the septal cartilage model was prepared. The obtained model was exported from the 3D Slicer program in form of STL files. Autodesk Inventor Professional 2023 software was used to process the exported STL files and prepare models suitable for the study of degradation and mechanical analysis.

The models were then subjected to simulated mechanical study consisting of bending and compressing using Stress Analysis tool in Autodesk Inventor Professional 2023 software. Based on literature data corresponding to the properties of human cartilage, a new material was defined and stored in the Inventor material library (Table 11). Next, the newly defined material was assigned to the prepared model of cartilage. For the need to determine the immovable elements necessary for static analysis, the implant was modified by adding supports. Loads of different ranges were applied to the model surface.

Synthesized PUs along with 5 different commercial filaments (Table 12): thermoplastic poly(ester urethane) (TPU) (TPU, DevilDesign, Poland), MediFlex (MediFlex 96, Noctuo, Poland), polylactide (PLA) (Easy PLA, Fiberlogy, Poland), poly-ε-caprolactone (PCL) (PCL, SUNLU, China) and Bioflex (Bioflex, Filoalfa, Poland) were used to produce constructs by FDM 3D printing. For SLA printing, the Zortrax Resin BASIC epoxy resin was used.

NX Pro Pellets (TUMAKER, Irun, Spain), a fused deposition modelling (FDM) 3D printer with Simplify3D V5 slicer (Simplify3D, Cincinnati, USA) were used to print the test elements from PUs. Original Prusa i3 MK3S+ (Prusa Research, Prague, Czech), a FDM 3D printer with PrusaSlicer (2.5.0 version) was used to print the test elements from commercial filaments. For stereolithography (SLA) printing, the Zortrax Inspire printer and Z-SUITE software (2.0 version) were used. The most important FDM 3D printing parameters of all test samples are listed in Table 13. Parameters were established based on the conducted thermal properties evaluation. For SLA printing parameters suggested by manufacturer were used: 0.05 mm layer height, 60 s exposition for first three layers, 9 s exposition for other layers, 100 mm/s platform speed, 1.5 mm support thickness and 45° angle of model tilt.

To evaluate the potential use of the obtained hydrogels as bioinks for extrusion-based 3D bioprinting, a preliminary printability tests were conducted. Selected hydrogel formulations were extruded using an AP24+ 2.4 infusion pump (Ascor, Poland) equipped with a 30 mL syringe connected via a silicone tube to a 1.2 mm diameter needle, dispensing onto a pre-frozen glass Petri dish. To prevent blockages, the silicone tubing was immersed in hot water. The extrusion flow rate was experimentally adjusted to 65 mL/h, with the hydrogel solution temperature

maintained in range of 40-42 °C for unmodified samples and 55-60 °C for samples modified with curcumin. The occlusion pressure was set at 120 kPa and remained below this threshold during the process.

Table 11 Human cartilage properties used in the simulated stress analysis.

Material property	Unit	Value
Young's modulus	MPa	2.72
Poisson's ratio	-	0.26
Shear modulus	MPa	1.9
Density	g/cm^3	1.099
Yield strength	MPa	1
Tensile strength	MPa	1.9

Table 12 Selected properties of commercial filaments. NG – information not given.

Property	Value				
	TPU [362]	**MediFlex** [363]	**PLA** [364]	**PCL** [365]	**Bioflex** [366]
Manufacturer	DevilDesign	Noctuo	Fiberlogy	Sunlu	Filoalfa
Color	Natural	Natural	White	White	White
Density [g/cm^3]	1.23	0.89	1.24	1.28	1.09
Hardness	55 ShD	96 ShA	NG*	NG	27 ShD
Tensile strength at break [MPa]	44	33	53	20	16
Elongation at break [%]	400	>700	NG	560	800
Melting point [°C]	NG	NG	155-160	58-62	185
Glass transition temperature [°C]	NG	NG	55-60	NG	-70

Table 13 FDM 3D printing parameters

Printing parameter	Value					
	TPU	**MediFlex**	**PLA**	**PCL**	**Bioflex**	**PUs**
Extrusion temperature [°C]	215	240	215	180	190	170/220
Bed temperature [°C]	80	80	60	35	60	60
Cooling	Fan on; ramp up from 0 (1st layer) to 100% (3rd layer)					
Layer height [mm]	0.15					
First layer height [mm]	0.2					
Wall thickness	3 contours					
Closing layers (top; bottom)	0; 0					
Infill	20%, gyroidal					
Base printing speed [mm/s]	40 (walls), 50 (infill)					
Retraction length [mm]	4					

5.4. Physico-chemical characterization

5.4.1. Fourier-transform Infrared Spectroscopy (FTIR)

The Fourier-transform infrared spectra of polyurethane samples were obtained with Nicolet iS 10 spectrometer (ThermoFisher, Waltham, USA) in a range of 4000-500 cm^{-1} with a resolution of 4 cm^{-1} and 128 scans per sample at room temperature.

5.4.2. Contact angle

To measure the contact angle goniometer 90-U3-PRO (Rame-Hart, Succasunna, USA) with Drop Image Pro software (Media Cybernetics, Rockville, USA) was used with water, ethylene glycol and diiodomethane (Sigma-Aldrich Saint Louis, USA) as a measuring liquid. Measurements were taken at room temperature. Prior to measurements, pieces of solid materials were pressed on a hot plate heated to melting temperature to obtain thin, flat films.

5.4.3. Mechanical properties

Mechanical analyses were performed using different methods. Tensile, compression and flexural testing was performed on Zwick Z0/20 universal testing machine and compatible TestXpert® II software according to ISO 527 standard. Initial force (F_0) was 1 MPa with initial crosshead speed (V_0) of 5 mm/min. Crosshead speed during the test (V) was 50 mm/min. For flexural strength, a three-point bending test was conducted on 3D printed samples of the nasal septum with added supports. The parameters of the test were based on ISO 178 standard. The study was carried out at room temperature. Distance between supports (L) was 13 mm and initial force (F_0) was 1 N with initial crosshead speed (V_0) of 50 mm/min. Crosshead speed during the test (V) was 60 mm/min. The measurement was conducted up to the maximum length change of 6 mm. Compressive strength testing was performed according to ISO 604 standards. The samples were in the shape of cuboids with dimensions of 10 x 10 x 4 mm. Five samples were

printed for each material with infill along the compression direction and five samples with infill transverse to the compression direction. Initial force (F_0) was 5 N with initial crosshead speed (V_0) of 50 mm/s. Crosshead speed during the test (V) was 1 mm/min. The measurement was conducted up to the maximum length change of 60%.

The dynamic mechanical analysis was performed using the DMA Q800 TA Instruments apparatus. Samples were analyzed in the strain mode with a frequency of 1 Hz. Measurements were performed in the temperature range from −130 to 130 °C with a heating rate of 4 °C/min. Beam-shaped samples with dimensions of 10 mm × 40 mm were used.

5.4.4. Thermal properties

The Differential Scanning Calorimetry (DSC) measurements were performed using a Netzsch 204F1 Pheonix apparatus with Proteus80 software (Netzsch, Selb, Germany) under a nitrogen atmosphere (flow rate 20 mL min^{-1}) at the temperature range of 25/30 – 250 °C. The heating/cooling rate was 10 K min^{-1}.

Thermogravimetry measurements were conducted using TGA2 SF/1100 (Mettler Toledo, Columbus, USA) equipment. Conditions: air, 25-1100 °C, temperature ramp 10 °C/min.

5.4.5. Melt flow rate (MFR) and melt volume rate (MVR)

The MFR and MVR of the studied materials were measured using load plastometer Zwick Roell BMF-001 and TestXpert® II software. The study conditions were based on ISO 1133 standard. The measurement was conducted at printing temperatures under a load of 2.16 kg. Three repetitions were made for each material and the result was presented as an average (n = 3).

5.5. Swelling characteristics

For the swelling examination, three cylindrical samples with a diameter of 24 mm were cut from each type of hydrogel and dried at 40 °C until reaching constant mass (mass loss below 1 mg/120 s), using the thermobalance MA 50.R (RADWAG, Radom, Poland). Next, each of the samples was placed in 20 mL of water at 20 °C, then removed from the medium in the set time intervals, placed on the piece of paper to remove the excess water and finally weighted using an analytical balance AS 110.R2 (RADWAG, Radom, Poland). After obtaining mass, the sample was placed back in the container with water. Swelling values were calculated using Equation 4.

$$W = \frac{m_t - m_0}{m_0} \times 100\%, \quad (4)$$

where: W is swelling [%], m_t and m_0 are the weight [g] of swollen hydrogel after set time (t) and dried hydrogel, respectively.

To analyze the swelling control mechanism, several kinetic models were chosen to fit the experimental data (first order, second order and Korsmeyer-Peppas models), using OriginPro 2018 software (OriginLab Corporation, Northamption, USA). Swelling parameters for different

mathematical models were calculated using average values of swelling (*W*) in a function of time (*t*) for each sample (*n*=3) [367]. In the case of the first–order kinetics (1OK) the swelling value at any time (*t*) is proportional to the uptake of swelling agent, before reaching equilibrium swelling (W_{eq}). The first order kinetics is represented by Equation 5, which can be integrated into the non-linear Equation 6.

$$\frac{dW}{dt} = K_1(W_{eq} - W_t), \tag{5}$$

where: W_{eq} is equilibrium swelling [%], *W* is the swelling at time interval (*t*) [%] and K_1 is the first order swelling kinetics constant [min^{-1}].

$$W = W_{eq}(1 - e^{-K_1 t}), \tag{6}$$

Swelling parameters were also calculated according to the second order kinetics (2OK) using Equation 7, which can be integrated into the non-linear Equation 8 with the assumption that W_0 = W = 0 and t_0 = t = 0.

$$\frac{dW}{dt} = K_2(W_{eq} - W_t)^2, \tag{7}$$

where: W_{eq} is equilibrium swelling [%], *W* is the swelling at set time (*t*) [%] and K_2 is the second order swelling kinetics constant [min^{-1}].

$$W = \frac{K_2 {W_{eq}}^2 t}{1 + K_2 W_{eq} t}, \tag{8}$$

Korsmeyer-Peppas nonlinear diffusion (KPND) model can be applied to investigate the mechanism of water sorption into the hydrogel matrix (Eq. 9). Fickian diffusion and Case II transport are controlled by relaxation of polymer chains and they are expressed by n values equal to 0.5 and 1, respectively. However, when the diffusion exponent is less than 0.5, the diffusion process can be called Quasi-Fickian (DQF) and is characteristic for the diffusion from a non-swelling matrix.

$$W = K_{KP} t^n, \tag{9}$$

where: *W* is swelling [%], K_{KP} is swelling rate constant [min^{-1}], *t* represents the set time interval [min] and *n* is the diffusion exponent.

5.6. Density, average molecular weight between cross-links and crosslinking density

Density of hydrogels was obtained using an analytical balance AS 110.R2 with Density Kit 85 (RADWAG, Radom, Poland) using swollen hydrogel samples. Density was estimated by weighing samples in air and in water. The measurements were carried out at a room temperature of 20 °C.

Based on average density value, average molecular weight between crosslinks and crosslinking density were calculated according to Equations 10-13 [345,346].

$$M_c = -\frac{d_p V_s (V_{2,s}^{\frac{1}{3}} - \frac{V_{2,s}}{2})}{\ln(1 - V_{2,s}) + V_{2,s} + \chi {V_{2,s}}^2}, \tag{10}$$

where: M_c is the average molecular weight between cross-links [g/mol], d_p is the density of hydrogel [g/cm^3], V_s is the molar volume of water [-], $V_{2,s}$ is a volume fraction of hydrogel [-], which can be derived from Equation 11.

$$V_{2,s} = [1 + \frac{d_p}{d_s}\left(\frac{M_a}{M_b} - 1\right)]^{-1}, \quad (11)$$

where: d_p and d_s [g/cm^3] are densities of hydrogel and solvent, respectively and M_a, M_b [g] are masses of swollen and dried hydrogel, respectively.

Furthermore, χ is solvent interaction parameter, which can be calculated knowing the value of $V_{2,s}$ by using Equation 12.

$$\chi = \frac{\ln(1 - V_{2,s}) + V_{2,s}}{{V_{2,s}}^2}, \quad (12)$$

To calculate average density Equation 13 was used.

$$Q_c = \frac{d_p}{M_c}, \quad (13)$$

where Q_c is the average crosslinking density [mol/dm^3], d_p is the density [g/cm^3] and M_c indicates the average molecular weight between cross-links [g/mol].

5.7. Simulated biodegradability and biostability

The short-term degradation studies of obtained samples were performed in selected media: 2 M HCl, 5 M NaOH, 0.01 M PBS. Materials were first cut into round samples with 24 mm diameter, dried and weighed in thermobalance (RADWAG MAX50/SX), set at 60 °C. Nine samples of each studied material were then placed in 24-well cell culture plates filled with selected media: acidic solution of 2 M HCl, alkaline solution of 5 M NaOH or solution of 0.01 M PBS (Sigma-Aldrich Chemie GmbH, Buchs, Switzerland). Samples were incubated in selected media at 37 °C. Sample mass change measurements were as follows: samples were taken out from the container and put into a paper sheet to reduce the medium excess. Samples were then placed in the thermobalance (set at 60 °C), where they were dried to a constant mass and weighed. Mass loss was calculated by Equation 14:

$$S = \left(\frac{m_i - m_0}{m_0} \right) \cdot 100\% \quad (14)$$

where m_i is the sample weight after set days of incubation (g) and m_0 is the sample weight before the test (g). The results were the arithmetic mean of three measurements.

5.8. Optical microscopy

An optical microscope equipped with epifluorescence kit (Delta Optical, model: L-1000) and a digital camera (ToupTek Photonics, model: SCCCD01400KPA) was used in this study coupled with ToupView software. Microscope was used in transmission mode for obtaining standard micrographs and in fluorescence mode a mercury lamp was used together with “U”

bandpass filter employed (band pass: 330–385 nm, dichroic mirror: 400 nm, band absorption: 420 nm).

5.9. Active substance release

Active substance release was studied using UV-vis spectroscopy with UV-5100 spectrophotometer (Biosens, Warsaw, Poland) coupled with MetaSpecPro software (Metash, Shanghai, China). First the calibration curves were obtained by measuring the absorbance at the set wavelengths and concentrations ranges within the applicable range of Beer-Lambert law. The exact parameters of calibrations were given in Table 14.

Table 14 Parameters of calibration curves for selected active substances.

Active substance	Wavelength [nm]	Concentration range [mg/mL]	Calibration curve
Hydrocortisone	247	0.001-0.1	$y = 39.910x + 0.0076$; $R^2=0.9999$
Collagen	208	0.001-1	$y = 30.082x + 0.0224$; $R^2=0.9991$
Diosmin	268	0.001-0.1	$y = 9.1742x + 0.0596$ $R^2=0.9840$
Allantoin	222	0.001-0.05	$y = 5.0008x + 0.0436$ $R^2=0.9975$
Curcumin	436	0.0001-0.01	$y = 0.1622x + 0.0055$ $R^2=0.9997$

Materials were cut into round samples with 24 mm diameter, dried and weighed in thermobalance (RADWAG MAX50/SX), set at 60 °C. Three samples of each studied material were then placed in 12-well cell culture plates filled with 10 mL water in each well and incubated at 37 °C. After set time, 1 mL of the solution was transferred to the measuring cuvette and the absorbance was measured. If the absorption was outside of calibration curve range, the solution was diluted and the result was recalculated for the dilution. The cell culture plates were then refiled with fresh medium and the measured concentrations were included in the calculations for next measurements.

5.10. Antibacterial activity examination

5.10.1. Modified Kirby-Bauer disk diffusion test

Antibacterial activities of the curcumin-modified hydrogels were tested by using Staphylococcus aureus ATCC 25923 and Staphylococcus epidermidis ATCC 12228. Stock cultures were maintained by periodic subculture on nutrient agar slants which were stored at 4 °C. Before each experiment, strains were cultivated on fresh LA plates and incubated for 24 h at 37 °C. For preparation of LA plates, LA medium containing (g/L): casein peptone 10.0; yeast extract 5.0; NaCl 10.0, bacteriological agar 15.0, was dissolved in 1 L of deionized water and then autoclaved (121°C, 1.5 atm, 20 min), cooled to 45 °C and poured into sterile Petri plates. Approximately 25 mL of sterile agar medium was poured into 90 mm disposable, sterile Petri dishes and allowed to solidify. All reagents were supplied by BTL Sp. z o.o., Lodz. Poland.

The startup of the experiments was initiated by inoculating 20 mL of sterile LB medium (Luria-Bertani Broth) with microbial strains from LA plates. Cultivation was carried out in 200 mL Erlenmeyer flasks, on a rotary shaker at 170 rpm at 37 °C for 24 h. LB medium containing, g/L:

casein peptone 10.0; yeast extract 5.0; NaCl 10.0, was dissolved in 1 L of deionized water and then autoclaved (121 °C, 1.5 atm, 20 min) and cooled to room temperature. All reagents were supplied by BTL Sp. z o.o., Lodz. Poland.

After the incubation, 1 mL of each bacterial strain suspension was transferred into 100 mL sterile Erlenmeyer flasks containing 10 mL of the fresh LB medium. The cells were cultivated for 6-8 h at 37 °C on a rotary shaker at 170 rpm to get the log phase of bacteria. For determination of potential antibacterial activities of hydrogels, 100 µL of each bacterial strain suspension was transferred and spread on LA plates with a sterile glass rod. After the incubation of bacterial cultures on LA plates for 24 h at 37 °C, the disk-shaped samples of examined hydrogels were placed over the bacterial cultures on LA plates. For this purpose, each side of hydrogel (1 cm diameter) was exposed to UV radiation for 30 min and then sample was placed with sterile tweezers on LA plates. On each plate, one disk from not modified hydrogel and three disks from curcumin hydrogel were placed. Plates were incubated in 37 °C for 24 h. After the incubation, the presence or absence of zones of bacterial growth inhibition around assayed samples of unmodified and modified hydrogels was checked.

5.10.2. Surface contact method

The study of antibacterial properties of hydrogels with the surface contact method was carried out using liquid cultures of the *Staphylococcus aureus* ATCC 25923 strain. To ensure the required sterility, most of the activities presented below were performed under the MSC-Advantage laminar chamber.

To prepare a liquid culture of bacteria, 1 colony of the tested strain was taken from the Petri dish with LB-agar medium using a sterile loop and transferred to the sterile plastic tube with 15 mL of fresh sterile Mueller-Hinton 2 medium. This stage was repeated 3 times. Next, three tubes with the inoculated medium were placed in a New Brunswick Innova 42 air incubator shaker (Eppendorf, Hamburg, Germany), where it was shaken at 180 RPM for 16 h at 37 °C. After this time, the culture had the value of OD_{600} in range of 1.05 to 0.88. A diluted culture of the tested bacterial strain was then prepared using fresh portions of sterile Mueller-Hinton 2 medium in such a way that the value of OD_{600} was between 0.1 and 0.12, which corresponds to ~10^8 colony-forming units (CFU) per mL.

In the next step, 9 samples were cut from each of the chosen hydrogels, with dimensions of 32x32 mm, divided into three groups and placed in the middle of sterile Petri dishes (Bionovo). In each group, 20 µL of a previously prepared bacterial culture was applied to the gel surface and covered with a sterile glass 22x22 mm coverslip. After that, a sterile vessel containing 1 mL of sterile redistilled water was placed next to the gel sample in each Petri dish for the 1st and 2nd groups. Each Petri dish was then closed with a lid and both parts were tightly and carefully connected with sealing tape for Petri dishes. 1st and 2nd group samples were then placed in the air incubator Stabili Therm (Thermo Scientific) at 37 °C for 3 and 1.5 h, respectively.

3rd group was treated as a control and not placed in the air incubator. Instead, 1 min after covering the gel, the coverslip was removed and rinsed with 0.5 mL of sterile PBS three times. The obtained solution was transferred to the sterile 1.5 mL Eppendorf vial. The surface of hydrogel the was rinsed six times with 0.5 mL of sterile PBS. The obtained solution was transferred to a vial with the solution from the coverslip. The solution was named as 10^0 and used then to make serial dilutions of rinsed bacteria in a sterile PBS solution in the dilution range of 10^{-1} to 10^{-6}. Then, the pour plate technique was used to determine the CFU of each dilution of the tested bacterial strain after the surface contact with each of the analyzed hydrogel samples. To prepare the pour plates, first fresh LB-agar (A&A Biotechnology) solution in the deionized water was prepared with a concentration of 0.04 g/mL and autoclaved (121 °C, 1.5 atm, 20 min). Then, 100 µL of rinsed bacteria dilution was placed on the side of a sterile Petri dish and 20 mL of the fresh autoclaved LB-agar medium cooled to 50 °C was placed on the other side of the dish. Each of the Patri dishes was then gently mixed by 12 plate swirls, left in room temperature to solidify and placed for 16 h at 37 °C in an air incubator. After that time, the plates were removed from incubator and the colonies were counted for dilutions, where total number of colonies was between 10 and 200. Finally, the CFU/mL of the culture was calculated, considering the bacterial dilutions. The obtained CFU values were logarithmized and the mean value and standard deviation were calculated for each group of samples and the type of hydrogel used. The same protocol was used for 1st and 2nd group after set time of incubation.

5.11. Cell culture, cytotoxicity and morphology assessment

The cytotoxicity of the tested materials was determined using the 3-(4,5-dimethylthiazol-2-yl)-2,5 diphenyltetrazolium bromide (MTT) assay on L929 cells (Sigma Aldrich/Merck, St. Louis, MO, USA) according to ISO 10993-5 standard. L929 cells were cultured in medium recommended by the manufacturer: low-glucose Dulbecco's modified Eagle's medium (DMEM LG, Sigma Aldrich/Merck, St. Louis, MO, USA) supplemented with 10% heat-inactivated fetal bovine serum (FBS; Biowest, Nuaille, France), 100 µg/mL streptomycin, 100 U/mL penicillin and 2 mM glutamine (Sigma Aldrich/Merck, St. Louis, MO, USA). Cells were incubated in a humidified atmosphere containing 5% CO_2 at 37 °C. All the experiments were carried out with cells in the exponential phase of growth.

To prepare sample extracts, 1.25 cm^2 of material per 1 mL of culture medium was used. Samples were sterilized for 30 min on each side under UV radiation. Then, 70 mL of extract of the studied samples was prepared by 24 h incubation (37 °C, 5% CO_2) in culture medium DMEM LG supplemented with 10% FBS, 100 U/mL penicillin, 100 µg/mL streptomycin and 2 mM glutamine.

The L929 cells were seeded in 24-well plates with a density of 20,000 cells/well and cultured for 24 h to allow for attachment. Then the cell culture medium was removed and replaced with extract solutions for the next 24, 48 and 72 h. DMEM LG supplemented with FBS and antibiotics was used as a non-toxic control. After the cell cultures were incubated with extract

solutions, the MTT assay was performed. The absorbance of the prepared solutions was measured at λ = 540 nm using an iMark Microplate Absorbance Reader (Bio-Rad, Hercules, CA, USA). The results from three independent experiments (n=3) are shown in the graph as cell viability towards the control (100% of viability). The morphology of L929 cells following treatment with the extract solutions was evaluated using a 20x lens and OLYMPUS IX83 inverted microscope with an XC 50 camera and cellSens Dimension software (Tokyo, Japan).

5.12. Statistical analysis

The statistical analysis was performed with the use of the OriginPro 2018 software (OriginLab Corporation, Northamption, USA). To determine the statistical differences, one-, two- and three-way ANOVA and *post-hoc* Tukey test (α = 0.05, 0.01, 0.001) were used.

6. Development of biodegradable polyurethane matrices

As mentioned in the literature review (Section 4.2.), the primary advantage of PUs lies in their chemical customizability, which enables precise tuning of their physical properties to mimic human tissues. Tailoring these properties, especially high elasticity and controlled degradation profiles, is achieved by selecting and modifying the substrates used for the soft segments. As concluded in the literature review, most of the currently used commercial polyurethanes in medicine possess significant biological and functional shortcomings for internal mucosal applications, especially in terms of toxic degradation by-products. In the presented research, this research gap was addressed by synthesizing custom aliphatic polyurethanes with tailored polyol mixtures. To utilize unique capabilities of PUs, this research concentrated primarily on modifying the soft segments of the polymer chain, as they directly influence the final elasticity and resorption time required by delicate soft tissues. Another aspect of this work was to improve cytocompatibility by avoiding toxic degradation products of aromatic isocyanates and to create drug delivery system, which could be further applied in medicine.

Consequently, the synthesis process utilized four distinct polyols to evaluate their respective physiological effects: two polyesters - PCL (ES1), α,ω-oligo(ethylene-butylene adipate)diol (POLIOS 55/20, ES2) - alongside two polyethers - PTMEG (ET1), PEG (ET2). To complete the macromolecular architecture, linear hexamethylene diisocyanate (HDI) and 1,4-butanediol (BDO) were employed as the essential diisocyanate and chain extender components. The resulting novel polyurethanes aim to overcome the mechanical limitations of current market options, offering an optimized, highly biocompatible material solution for 3D printed patient-specific implants. Part of the presented results was already published in: [25]. For a reference to commercial materials, Bioflex, an aromatic PU-based, 3D printing filament advertised for medical applications was herein presented [26,366].

In Figure 41 and Figure 42 FTIR results for studied samples were presented. In all PU samples, a maximum visible at approx. 3300 cm^{-1}, which can be attributed to the stretching vibrations of the N-H bonds and the local maxima of about 2940 and 2860 cm^{-1}, corresponding to the stretching vibrations of C-H bonds, were observed. Additionally, in region 1750-1680, two signals can be detected – in higher wavelengths from C-O stretching vibrations from ester groups and, in lower wavelengths, stretching vibrations of C=O from urethane bond. Other characteristic signals from urethane groups are appearing at approx. 1540 cm^{-1} (bending vibrations of N-H bonds) and at approx. 1250 cm^{-1} (stretching vibrations of C-N bonds) [15,126]. Ester-based PUs exhibited signals at around 1160 cm^{-1} (stretching vibrations of C-O from ester group) and ether-based PUs exhibited signals at around 1100 cm^{-1}, which can be attributed to stretching vibrations of C-O bond in ether groups [368]. The last signal considered is the maximum at 728 cm^{-1}, which is clearly visible only for Bioflex and may come from C-H vibrations in the aromatic ring, as it is not appearing in HDI-based PUs [369]. In conclusion, the presence of urethane bonds was confirmed for all polyurethanes, together with ether and ester bonds in the specific PUs.

The degradation studies were summarized in Figure 43. The most stable sample was ET1 which showed less than 4% mass loss in all mediums after 56 days. ET2 sample was degrading in all mediums characterized with 75% mass loss in 0.01 M PBS after 56 days and complete degradation 2 M HCl after 35 days and in 5 M NaOH after 56 days. Other quickly degrading samples were: ES2 (complete degradation after 49 days in HCl and NaOH, stable in PBS), ES2:ET2 (complete degradation after 14 days in HCl, ~60% mass loss in NaOH and ~20% mass loss in PBS after 56 days) and ET2:ET1 (complete degradation after 35 days in HCl and after 49 days in NaOH, ~15% mass loss in PBS after 56 days). Generally, all samples based on ET2 (PEG) and ES2 (POLIOS 55/20) were degrading faster in comparison to other samples. It can be concluded they can be used as promotor of degradation in polyurethane compositions. For the application as nasal stent, the degradation of the material cannot be rapid to allow the tissue to regenerate, but also not too long to allow safe expulsion of the implant from the body. In this regard, the highest potential in terms of stability was shown by samples ET2:ES1 and ET2:ET1:ES1, which were characterized by stable, predictable mass loss in all tested environments.

In Figure 44 comparison of FITR spectra and macroscopical appearance of degradation residues after 21 days of simulated hydrolysis were presented on the example of ES1, ES1:ET1 and ES1:ET1:ET2. The main differences could be spotted in deterioration of 1725 cm^{-1} maximum (C=O ester bond) in highly degraded samples (2 M HCl and 5 M NaOH). The difference in intensity of signals at 1730 - 1680 cm^{-1} could be attributed also to appearance of degradation products, which could be seen as signals coming from N=C=O isocyanate stretching bonds or C=O stretching bonds originating from carboxyl, amide or ester functional groups. Based on FTIR spectra it can be assumed that the interactions with simulated hydrolysis environments had effect in both hard and soft segments of synthesized PUs.

In Figure 45 changes in the microstructure of PUs samples after 28 days of accelerated hydrolysis degradation tests were shown on the example of ES1, ES1:ET1 and ES1:ET1:ET2. Prior to degradation, optical microscopy revealed that all neat PU formulations possessed uniform surface morphologies free from macroscopic defects. Following incubation in degradative media, distinct, composition-dependent structural alterations became evident. The ES1 sample exhibited pronounced vulnerability to both the acidic (2 M HCl) and the alkaline environments (5 M NaOH), developing an extensive, interconnected network of deep cracks. In contrast, the incorporation of PTMEG in the binary ES1:ET1 blend altered the degradation profile. It resulted in mitigating deep crack formation in NaOH in favor of a homogeneously roughened, granular surface, but notably eroded surface with severe pitting at the sample edges in HCl. The ternary system containing PCL, PTMEG and hydrophilic PEG (ET2:ET1:ES1) demonstrated the most extreme susceptibility to hydrolytic cleavage across all active media. For this blend, both 2 M HCl and 5 M NaOH environments triggered catastrophic structural breakdown, characterized by massive material loss, severe delamination, macroscopic pitting and profound discoloration. Across all formulations, incubation in 0.01 M PBS represented the mildest degradative condition. While ES1

and ES1:ET1 underwent negligible topographical roughening in the buffer, the inclusion of PEG in the ET2:ET1:ES1 sample facilitated greater aqueous penetration, resulting in distinct surface pitting and the formation of localized granular deposits even in this relatively non-harmful environment.

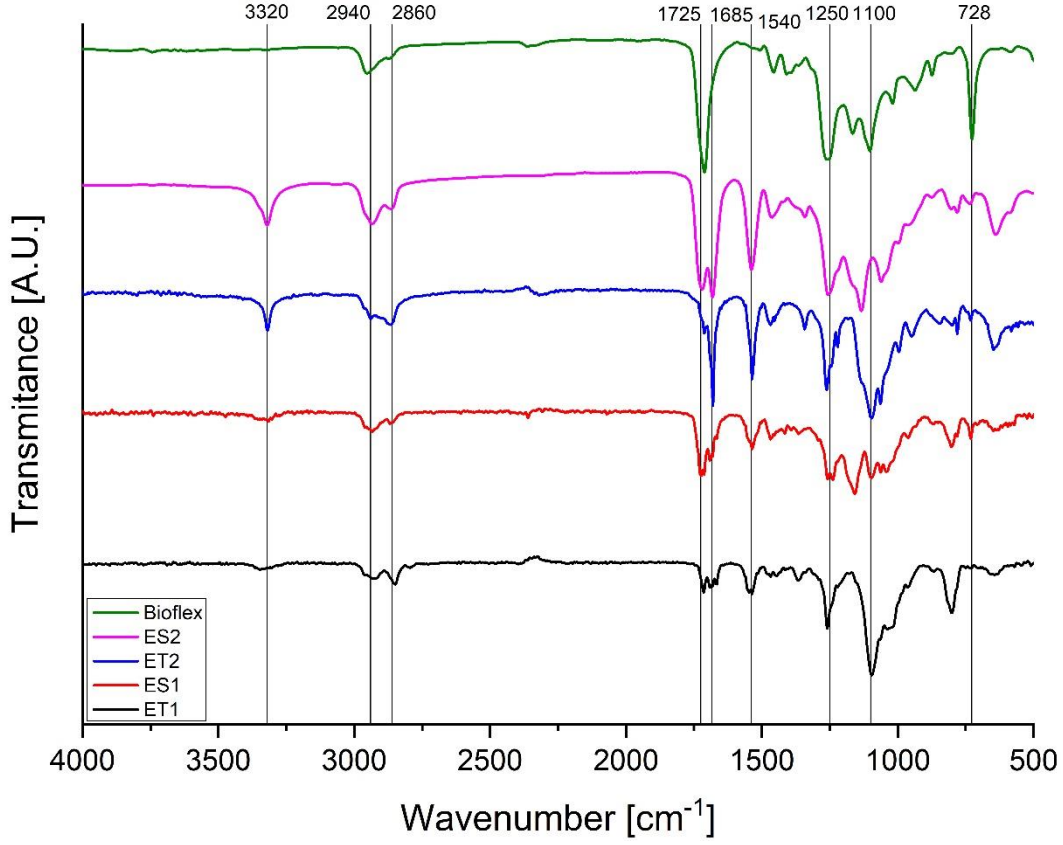


Figure 41 FTIR spectra of the obtained PUs with one type of polyol (ES1, ES2, ET1 and ET2) compared with the Bioflex filament.

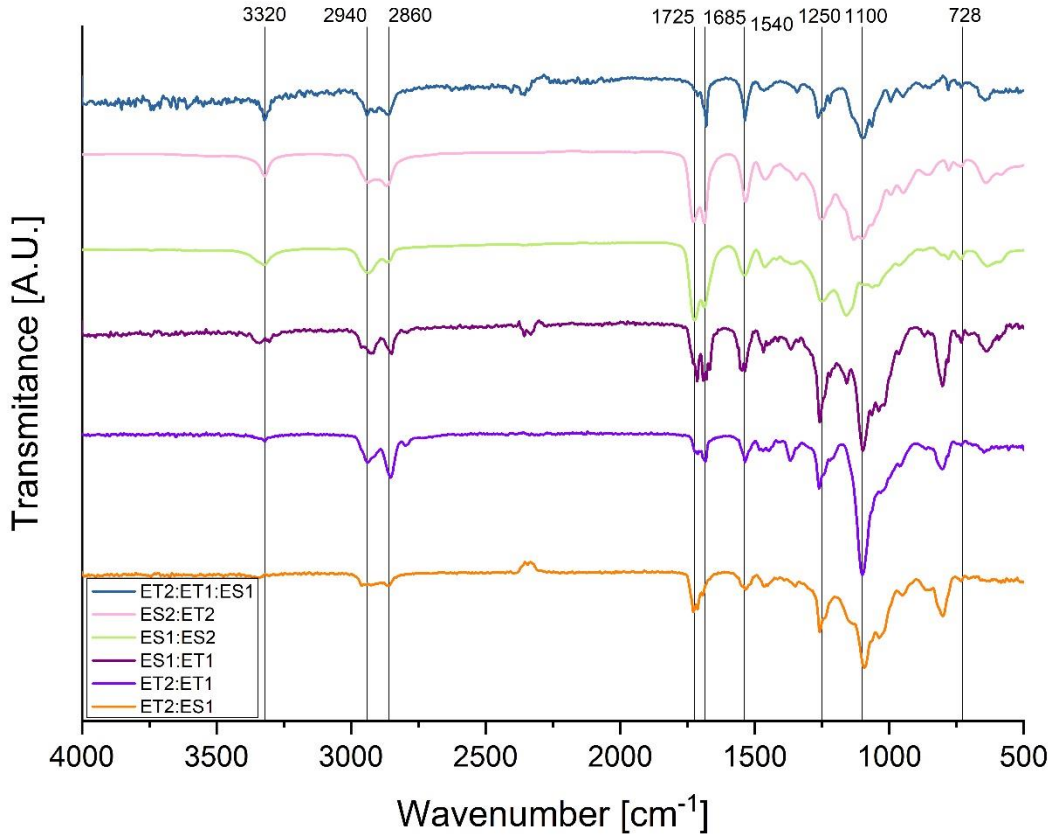


Figure 42 FTIR spectra of the obtained PUs with polyol mixtures: ET2:ES1, ET2:ET1, ES1:ET1, ES1:ES2, ES2:ET2, ET2:ET1:ES1.

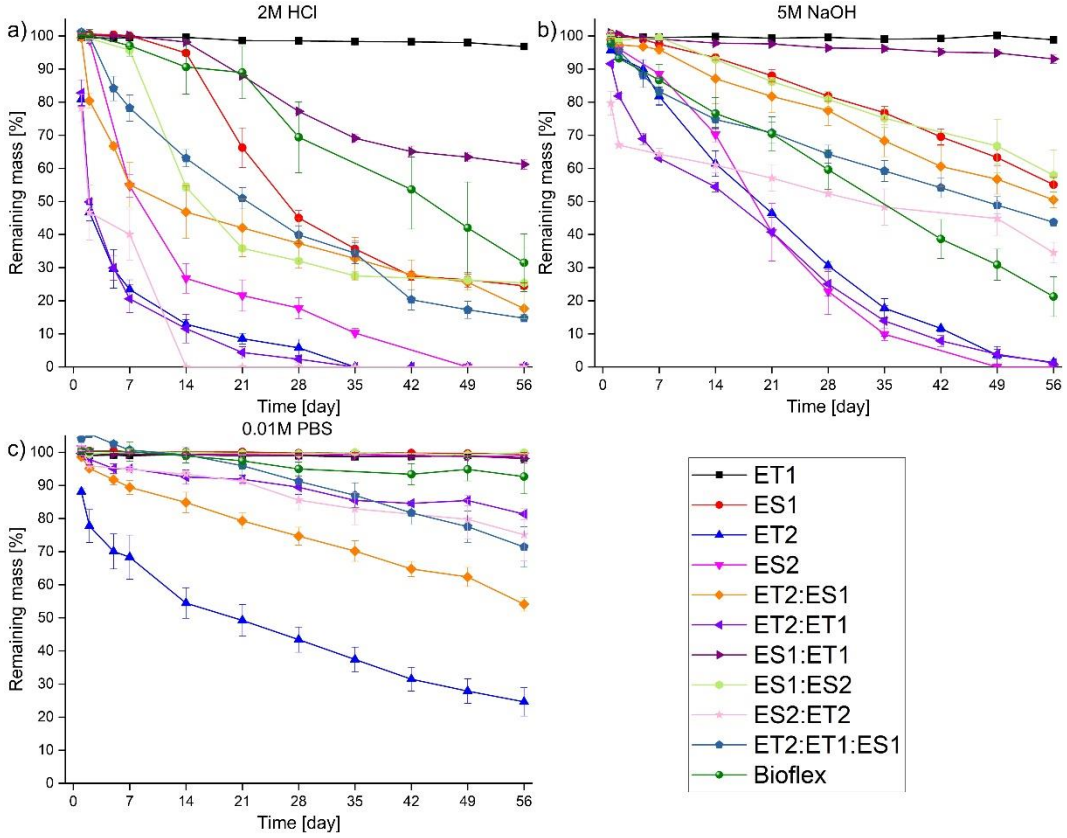


Figure 43 Interactions with wet environment. Accelerated hydrolytic degradation behavior of PUs in a) 2 M HCl, b) 5 M NaOH and c) 0.01 M PBS.

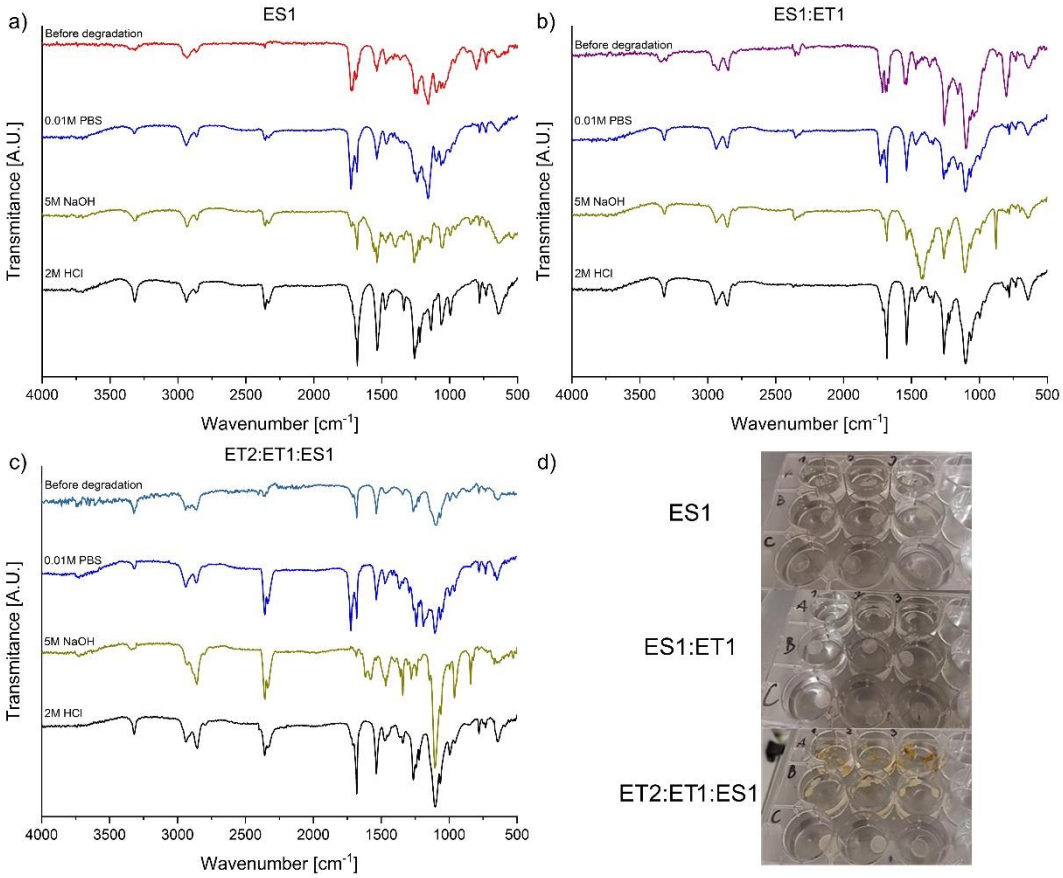


Figure 44 Changes in the PU structure after 21 days of accelerated hydrolytic degradation tests depicted in FTIR spectra for samples: a) ES1, b) ES1:ET1, c) ES1:ET2:ET1 and in d) macroscopical appearance.

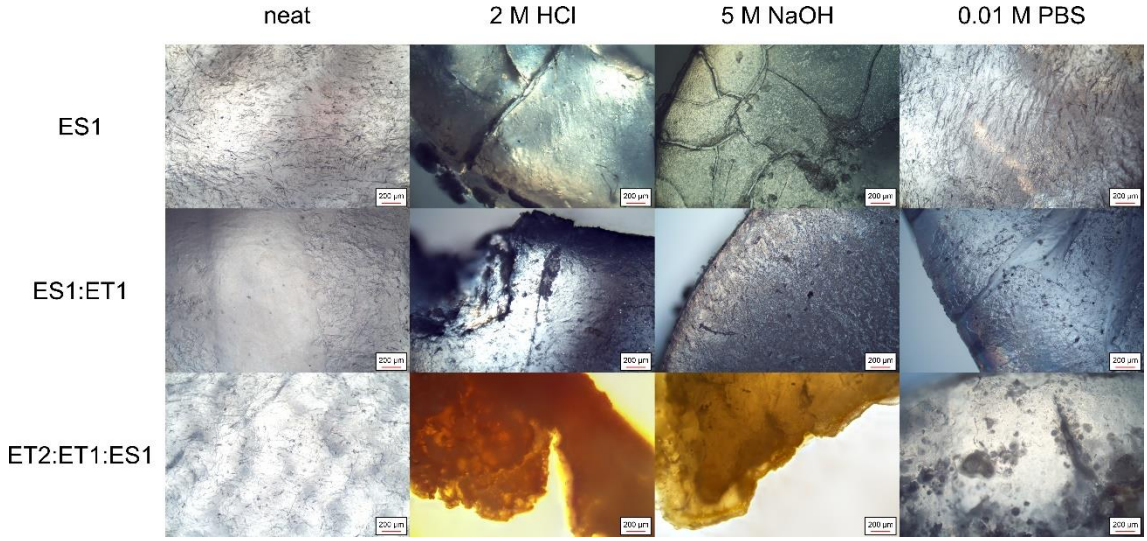


Figure 45 Changes in ES1, ES1:ET1 and ET2:ET1:ES1 PUs microstructure observed after 28 days of accelerated hydrolytic degradation tests in 2 M HCl, 5 M NaOH and 0.01 M PBS. Scale bar = 200 µm.

Tensile testing results were summarized in Figure 46 and Table 15. The behavior of all obtained polyurethanes can be described as typical thermoplastics. Considering the single-polyol PUs, the highest tensile strength and elongation were observed for ES1 (PCL) – 22.6±1.4 MPa, 1375±78 %. Polyether-based PUs offered similar performance, but ET1 (PTMEG) offered lower elongations. ES2-based PU offered the overall lowest tensile strength among single-polyol PUs -

6.00±0.46 MPa with just 136±12 % of elongation. Regarding the mixed-polyol PUs, the clear, synergistic effect is visible for ES1 when mixed with ET1 and ES2 polyols. Overall, the best results were obtained for samples ES1:ET1, ES1:ES2 and ET2:ET1:ES1. Among them, ES1:ET1 offered the highest tensile strength (40.5±1.8 MPa), elongation at break (1615±14) and moderate permanent elongation (44.7±3.3 %). Those results are double in strength than any of the polyols used alone in synthesis (ES1 – 22.6±1.4 MPa, ET1 – 15.4±1.5 MPa). Additionally, despite having the lowest parameters among single-polyol PUs, ES2-based sample – ES1:ES2 – offered the second-best performance reaching 33.5±3.2 MPa tensile strength with elongation at break reaching 1387±126 and permanent elongation of 60.9±3.0 %. The triple-polyol ET2:ET1:ES1 PU offered performance similar to ES1 sample but had significantly lower permanent elongation - 51±12 % vs 225±53 %.

In Figure 47 the results of DMA testing on the synthesized PUs were presented. Analyzing the storage modulus (G') curves reveals a classic, sharp decrease in stiffness during this transition, settling into a rubbery plateau characteristic of an entangled network. Simultaneously, the loss modulus (G'') curves display distinct maxima showing the temperature of maximum viscous energy dissipation as the soft segments acquire mobility. The loss factor (tanδ) graphs display distinct peaks in the range of -50 to -20 °C, corresponding to the glass transition temperature (T_g) of the soft segments. The structural differences among the utilized polyols significantly influence this thermo-mechanical behavior. PEG (ET2), with its highly flexible ether linkages, imparts substantial mobility of segments. This is clearly evidenced by the ET2:ES1 sample, which exhibits the highest tanδ peak, suggesting that the highly mobile PEG chains effectively plasticize the PCL domains. On the other hand, PCL (ES1) is an aliphatic polyester capable of participating in stronger dipole-dipole interactions and forming semi-crystalline regions, which subtly restricts mobility compared to pure polyethers. When these are combined with PTMEG (ET1) (hydrophobic polyether known for excellent low-temperature resistance) the resulting polyurethanes develop complex microphase-separated morphologies. The significant broadness of the tanδ peaks for ternary mixtures like ET2:ET1:ES1 underlines a high degree of phase mixing and overlapping relaxation processes between these diverse soft segments and the HDI/BDO hard domains. While two materials exhibited interesting shape memory properties, the transition temperature near 55 °C (for ET2) and 75 °C (for ES2) remains a significant barrier, restricting their safe, direct use in *in vivo* biomedical applications.

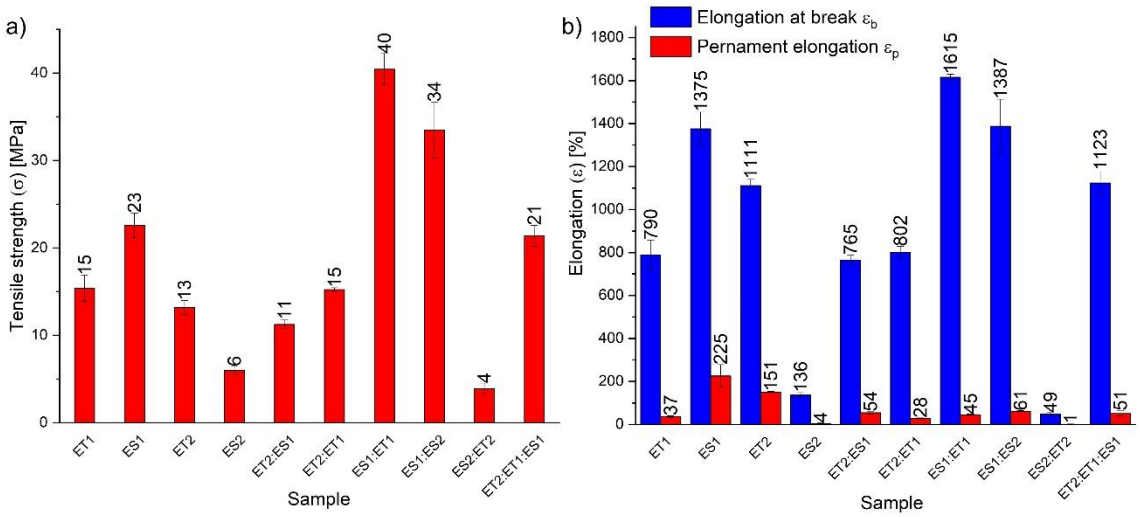


Figure 46 Visualization of tensile testing results on PU samples: a) tensile strength, b) permanent elongation and elongation at break.

Table 15 Summary of the tensile testing results on PU samples

Sample	ε_{break} [%]	± [%]	σ_{max} [MPa]	± [MPa]	E_{Mod} [MPa]	± [MPa]	ε_{perm} [%]	± [%]
ET1	790	68	15.4	1.5	27.1	7.6	36.8	3.7
ES1	1375	78	22.6	1.4	42	10	225	53
ET2	1111	29	13.19	0.80	64.5	4.9	151	2.5
ES2	136	12	6.00	0.46	41.9	2.5	3.7	4.7
ET2:ES1	765	22	11.25	0.51	19.16	0.47	54.3	4.8
ET2:ET1	802	27	15.23	0.22	43.0	2.4	27.9	2.4
ES1:ET1	1615	14	40.5	1.8	38.8	6.3	44.7	3.3
ES1:ES2	1387	126	33.5	3.2	37.6	4.5	60.9	3
ES2:ET2	48.7	6.5	3.89	0.64	43.1	3.7	1.4	1.2
ET2:ET1:ES1	1123	57	21.4	1.2	55.6	4.1	51	12

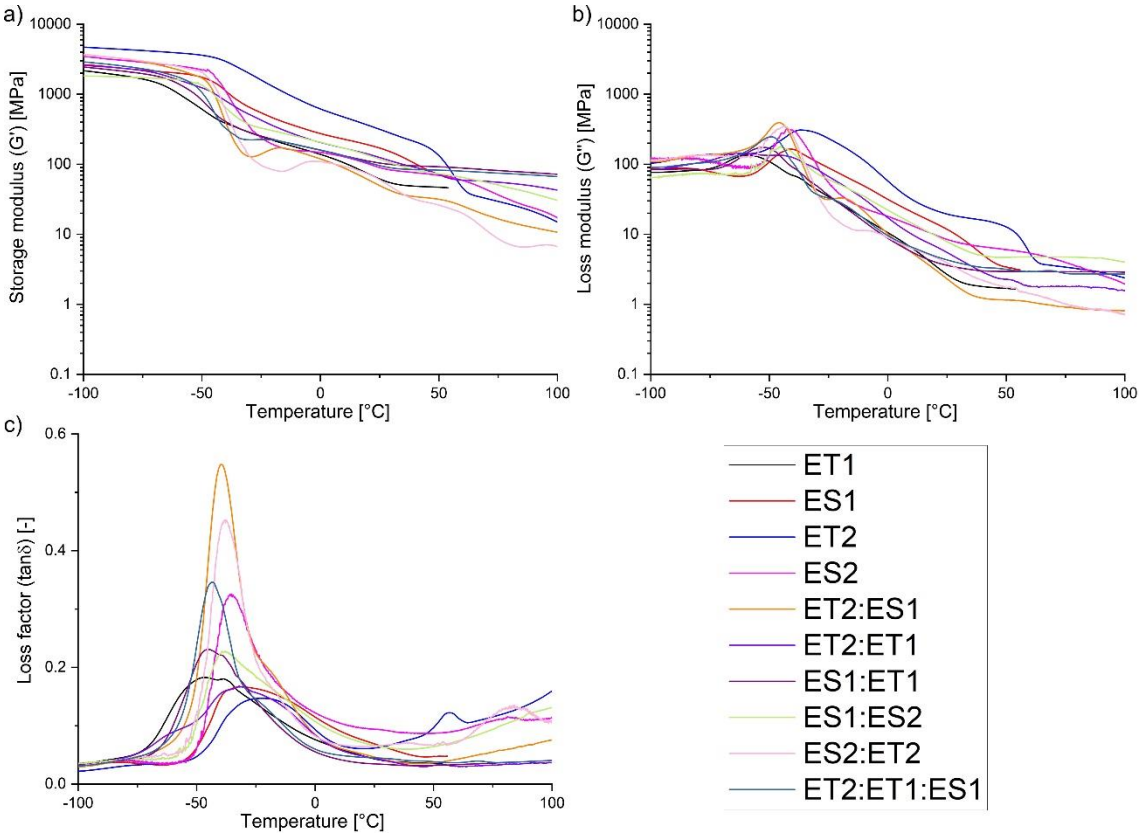


Figure 47 Summary of DMA results: a) storage modulus (G'), b) loss modulus (G''), c) loss factor (tanδ).

Based on the presented results, two compositions exhibited favorable results in all tests, namely ET2:ET1 and ET2:ET1:ES1, offering balance between mechanical strength and predictable susceptibility for degradation. Although other PUs (ES1, ES1:ET1, ES1:ES2) offered higher mechanical strength, they were degrading only in harsh conditions, without pronounced mass loss in 0.01 M PBS. On the other hand, samples with favorable degradation profiles (like ES2:ET2 or ET2:ES1), often lacked the required mechanical strength for the application as cartilage implants. Additionally, it is essential to underline that even 10 to 20 % of mass loss can result in detachment of the implant and expulsion from the body. Thus, the degradation pattern of material selected for use as an implant should allow for full recovery of tissue functions during implant service. If implant degrades too fast, the restored tissue could be misshapen or hollow. On the other hand, if implant stays in its place for too long it can hinder the healing process or lead to tissue overgrowth. Thus, for the further tests the PU based on the ternary mixture was chosen - ET2:ET1:ES1.

The chosen PU was modified using a variety of methods and active substances. First, a set of three naturally derived active substances aimed at accelerating cartilage repair was used. Collagen can improve biocompatibility and cell attachment; allantoin accelerates cellular repair and wound healing and diosmin improves local microcirculation to minimize postoperative edema and inflammation. Initially, surface modification by immersion in active substance solution was used. The efficiency of this modification was verified using a fluorescence microscope and the obtained micrographs were presented in Figure 48. All samples were characterized by the bright,

blue color, confirming successful incorporation of the active substances. Subsequently, the release profiles of these compounds were evaluated and the results were presented in Figure 49. It was observed that all three active substances were rapidly released just after one day of incubation and longer release periods did not result in a significant change in the total amount of the substance released. In the case of diosmin and allantoin the observed release values were close to their maximum solubility in water - ~0.5 mg/mL and ~5 mg/mL, respectively [370]. In the case of collagen, the exact solubility in water depends on many factors such as the degree of hydrolysis and pH, thus it is hard to define precisely. As determining this limit was not within the scope of this study, it can be assumed that the solubility limit was also reached in this case, because no significant increase in release was observed for this substance over time. Coating PU with the modified hydrogel coatings resulted in slightly different release profiles (Figure 50). In case of diosmin, the rapid release on the first day was observed, with the values close to its maximum solubility in water. In case of collagen, similarly to the solvent method, rapid release was observed at the first day, without significant changes in the total amount of the released substance in the next days. However, the total released amount was more than 10 times lower, when compared to solvent method. In the case of allantoin, similar behavior to collagen was observed. However, on the 7th day of incubation the released amount had increased, lowering the difference with solvent method to being around five times lower. Regardless of the specific active substance and introduction method used, it can be concluded that utilized modification strategies were successful in functionalizing the PU surface. Clinically, the rapid release of these naturally derived substances aligns precisely with the immediate postoperative healing window. The early availability of diosmin and allantoin rapidly mitigates swelling and accelerates initial tissue repair, while the immediate presence of collagen promotes early cell adhesion, establishing a strong foundation for the integration of the synthetic implant with native tissues.

In the next step, modification with Corhydron 25 - hydrocortisone in the form of sodium hydrocortisone succinate - was performed. This substance was chosen due to its immediate, localized anti-inflammatory effect, which suppresses the foreign body response and prevents excessive fibrous encapsulation of the polymeric implant. The successful integration of hydrocortisone into the PU structure was confirmed via an FTIR study (Figure 51). Two new signals at approximately 1725 cm^{-1} and 800 cm^{-1} were observed for the modified samples, which can be assigned to C-O stretching vibrations from ester groups and C-H skeleton vibrations of the steroid cyclic structure [371]. In Figure 52, the results of the Corhydron 25 release studies were summarized Similar to the previous study, the observed release was rapid and the total released amount did not change over the course of the studied period. In the case of modification during synthesis, the total amount of released hydrocortisone was above 40 % of the embedded amount in the PU matrix. Specifically, 0.5 % of hydrocortisone introduced during synthesis translates to 5 µg/mg of the modified PU. In a clinical setting, this rapid and localized release of hydrocortisone effectively targets the acute inflammatory phase immediately following surgical implantation. Consequently, mitigating this early foreign body response minimizes the risk of

fibrous encapsulation and implant distortion, ultimately promoting more stable and predictable aesthetic outcomes in nasal reconstructive procedures.

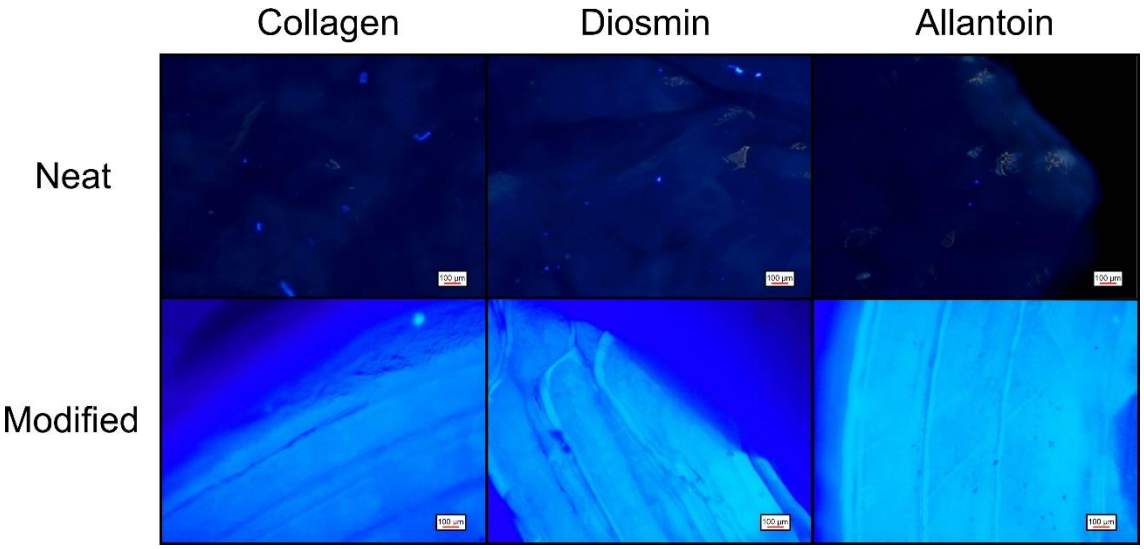


Figure 48 Fluorescence micrographs of ET2:ET1:ES1 PU 3D printed constructs before and after modification with collagen, diosmin and allantoin. Scale bar = 100 µm.

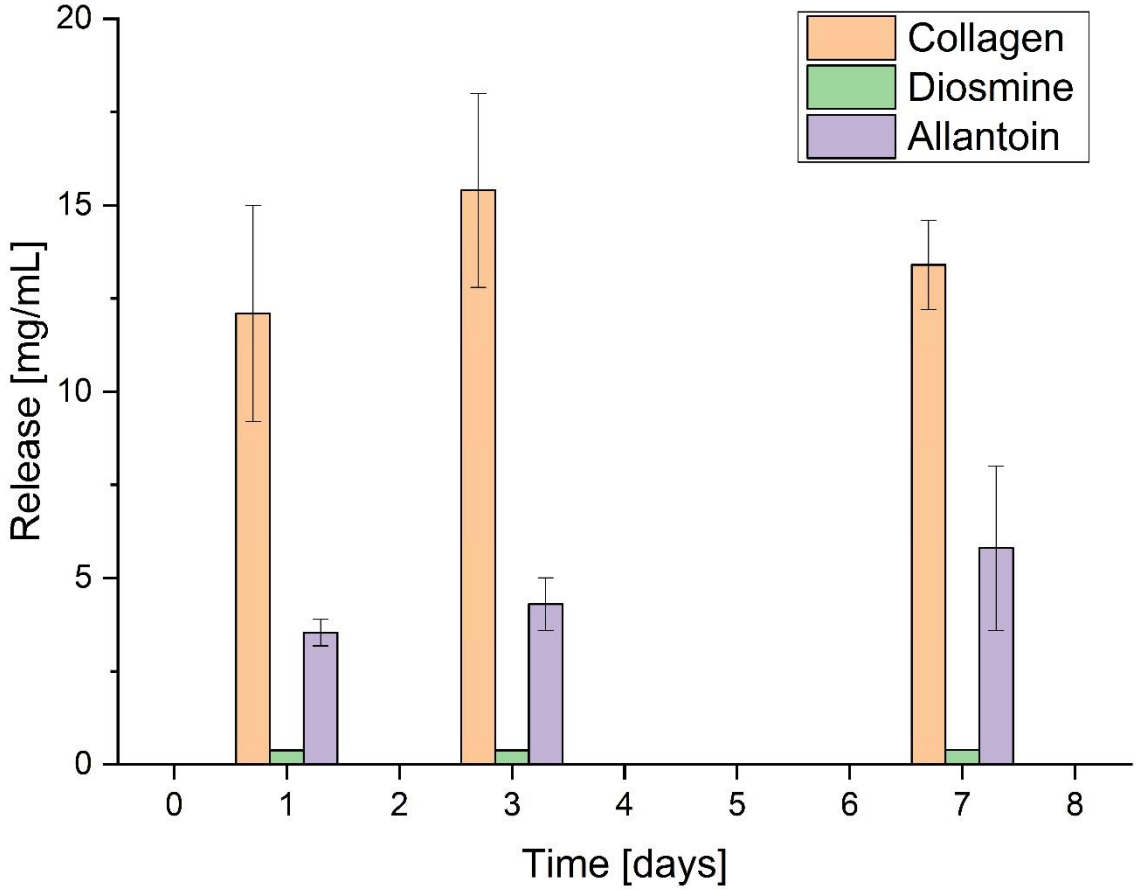


Figure 49 Active substances release profiles form surface-modified ET2:ET1:ES1 PU.

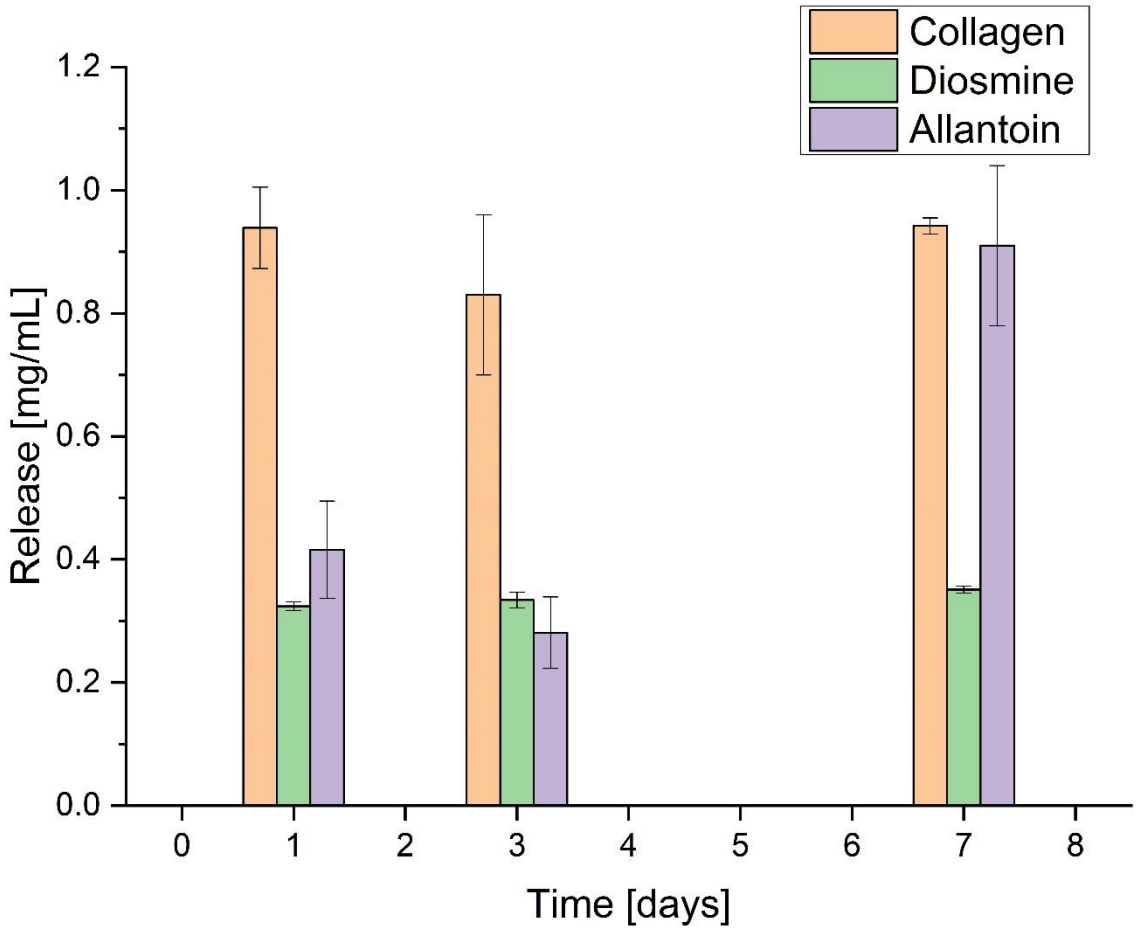


Figure 50 Active substances release profiles form hydrogel-modified ET2:ET1:ES1 PU.

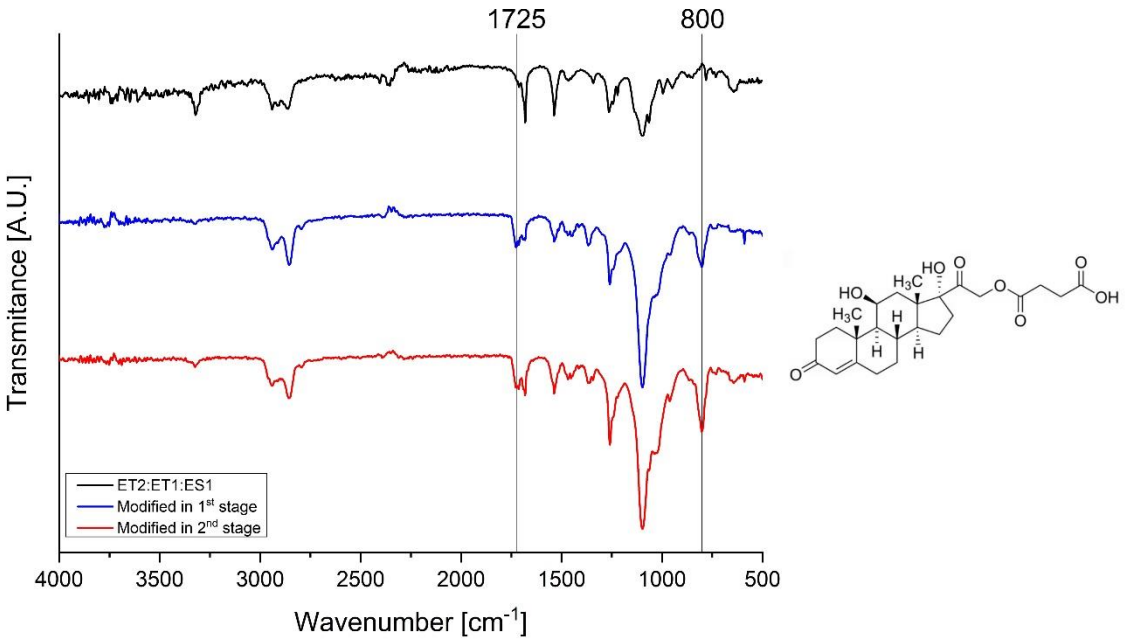


Figure 51 FTIR spectra of ET2:ET1:ES1 PU compared with its derivatives with Corhydron 25 used during 1st and 2nd stage of synthesis. On the right – chemical structure of hydrocortisone succinate.

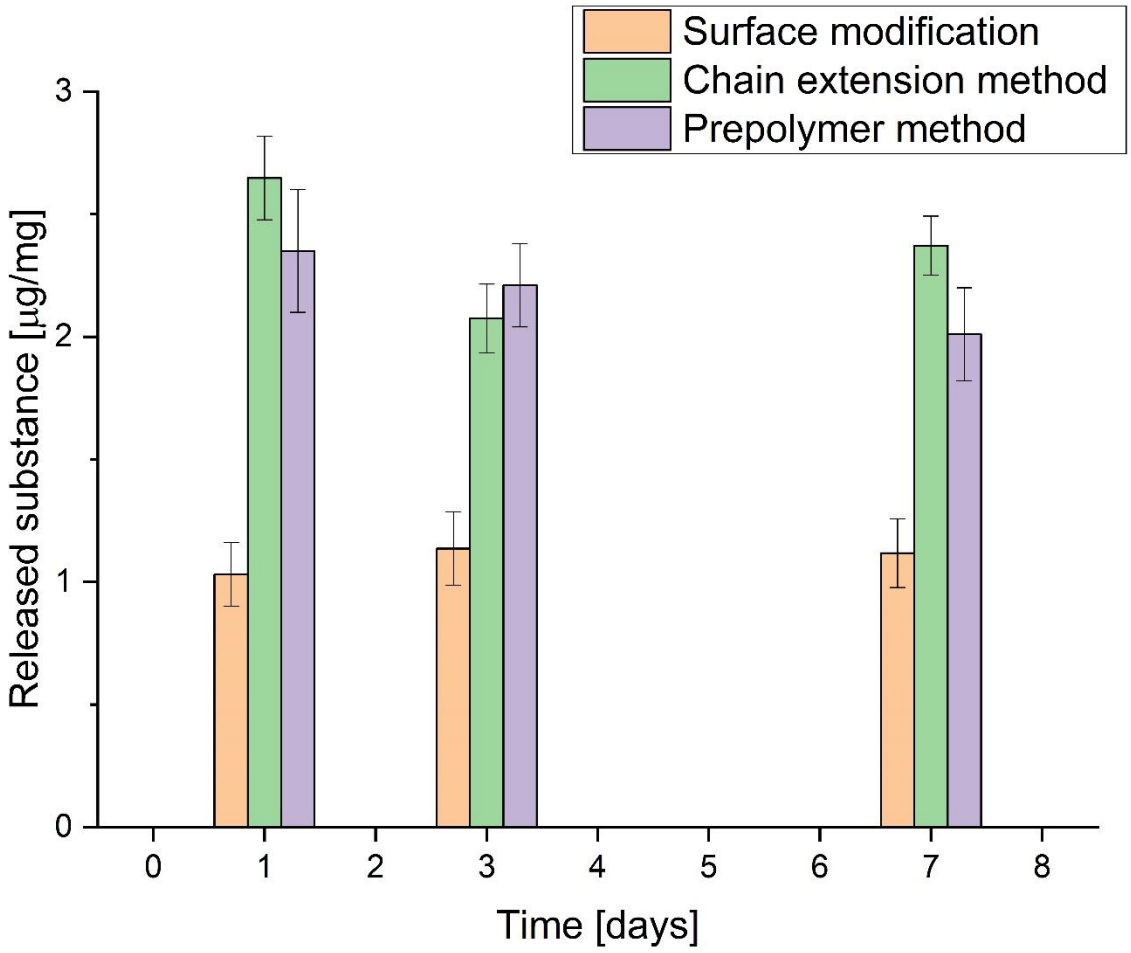


Figure 52 Corhydron 25 release profiles form ET2:ET1:ES1 PU modified during 1st or 2nd stage synthesis and by surface modification.

7. 3D modelling and evaluation of commercial filaments

The successful synthesis and characterization of the novel aliphatic polyurethanes described in Chapter 6 established a foundation of elastomeric polymers with tailored degradation and drug eluting behavior. Translating these custom formulations into functional biomedical devices requires addressing the clinical limitations of conventionally used options. One of the least addressed applications of biomaterials is the soft tissue surgical intervention in facial area. Most of the currently employed protocols is the usage of autologous cartilage grafts to correct structural deviations, limited donor tissue availability and problems with graft stability after surgery restrict their widespread use [372]. Prefabricated synthetic implants offer an alternative, yet they often fail due to excessive rigidity, poor tissue integration and localized stress-induced voids and necrosis resulting from mismatched mechanical compliance, as previously described in Chapter 4.1. [373]. While additive manufacturing enables the production of patient-specific anatomies, the clinical viability of such constructs depends directly on whether the chosen polymer provides sustained elasticity and structural stability. Implants for the nasal septum and paranasal sinuses were thus chosen to serve as an effective benchmark for evaluating novel PU performance because these sites undergo continuous cyclic strain from respiration, soft-tissue tension and facial movement. Satisfying these anatomical challenges requires high mechanical compliance with soft tissue and resilience to prevent extrusion or tissue trauma without sacrificing structural support. Consequently, benchmarking the newly synthesized PUs against standard commercial filaments is essential to identify mechanical deficiencies in existing solutions and establish quantitative targets for degradation, stiffness and print fidelity. Chapter 7 therefore examines commercial filament systems through two complementary stages. Section 7.1 utilizes MRI-derived CAD modeling, stress analysis and different 3D printing techniques to evaluate possibility of manufacturing patient-specific implant designs based on the simulated anatomical loading. On the other hand, Section 7.2 investigates the empirical assessment of commercial materials in terms of mechanical affinity to soft tissue, processability, degradability and biocompatibility to define the baseline criteria that the synthesized polyurethanes must satisfy.

7.1. Case study: Design and stress analysis of patient-specific nasal septum and paranasal sinuses implants using MRI data and CAD modeling.

Surgical correction of nasal septum deviations often utilizes autologous cartilage, but limited tissue availability and harvesting risks drive the need for synthetic alternatives. Currently available prefabricated implants frequently require imprecise manual intraoperative carving, leading to a poor anatomical fit, potential tissue injury and secondary aesthetic complications. Advanced 3D printing combined with computer-aided design can be used to develop patient-specific implants that can perfectly mirror these individual anatomical complexities. However, the

successful implementation of customized solutions depends heavily on the precise reproduction of the nasal septum anatomical details into a functional model. Therefore, this study focuses on the precise geometric modeling of a nasal septum and evaluates its structural integrity through computer simulations of bending and compression.

Based on the MRI scans, three types of stent models were designed and then printed with commercial materials: TPU, Bioflex (FDM) and Resin BASIC (SLA). In Figure 53, the printouts of 1st stent type without post-processing were presented, whereas comparison of support generation on example of 2nd stent type was presented in Figure 54. Models and post-processed printouts of all three types were presented in Figure 55. Overall, the SLA technique using Resin BASIC yielded printouts with far superior visual quality and easily removable supports, closely matching the original 3D models. FDM printing with flexible TPU and Bioflex filaments lacked the precision required for such intricate geometries, especially for projects 1 and 2, where supports had to be used for successful prints. Mechanical cleaning failed to remove all excess support material from the FDM prints, which ultimately complicated the interpretation of the compression tests. During mechanical evaluation, the dome-shaped stent (3rd type) printed via SLA demonstrated the highest compressive strength, reaching approximately 4 200 kPa (Table 16). However, for the ring-shaped designs, FDM materials showed similar and more consistent results between the TPU and Bioflex filaments. While the SLA method provided much better structural accuracy, the Resin BASIC material was ultimately deemed too stiff and brittle for practical medical application as a nasal stent. Although the flexible resins are currently available on the market, the preliminary tested Zortrax Resin FLEXIBLE was not suitable for printing such small details at the time of the study. Thus, it was decided to change the approach and focus on designing the material for nasal septum cartilage repair.

Table 16 Results of compression testing of different types of stent models.

Material	Compression stress [kPa]		
	1st type	2nd type	3rd type
TPU	230±104	109±38	542±76
Bioflex	252±178	145±18	161±16
Resin BASIC	16±12	19±12	4 253±870

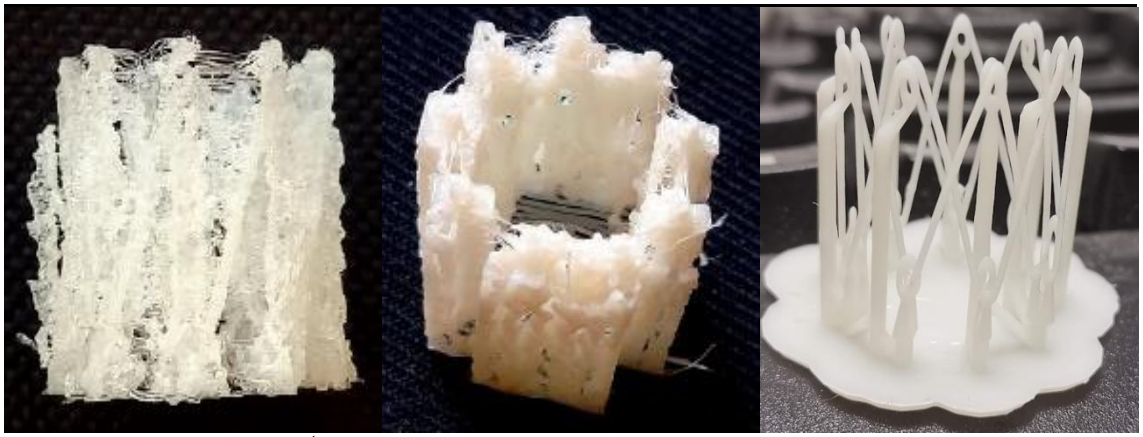


Figure 53 Comparison of 1st stent type printouts without postprocessing. From left: TPU, Bioflex, Resin BASIC. Reproduced with permission of The Licensor through PLSclear from: [24].

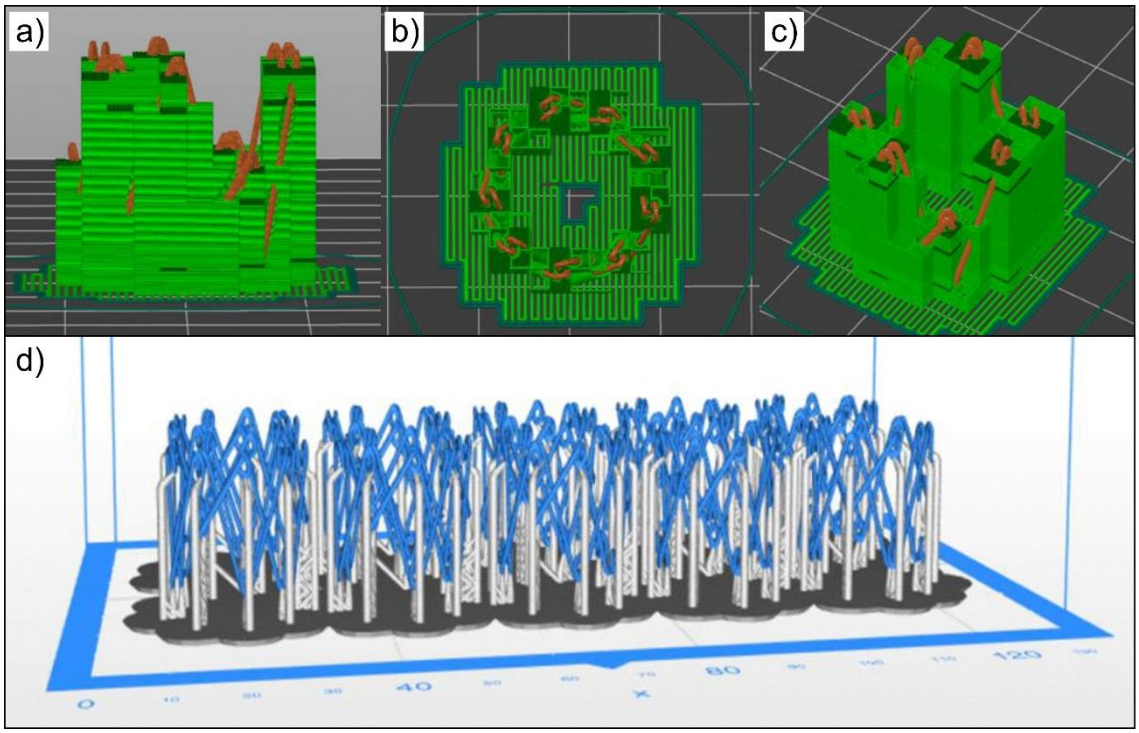
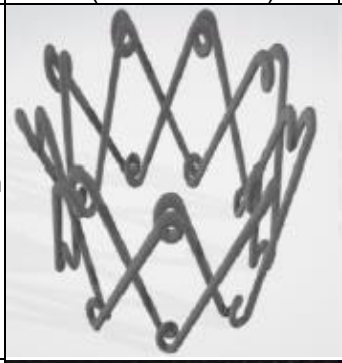


Figure 54 Comparison between FDM and SLA slicers of 2nd project with added supports.

Project	1 (20x20x20 mm)	2 (20x20x20 mm)	3 (20x20x12 mm)
Design			
TPU (FDM)			

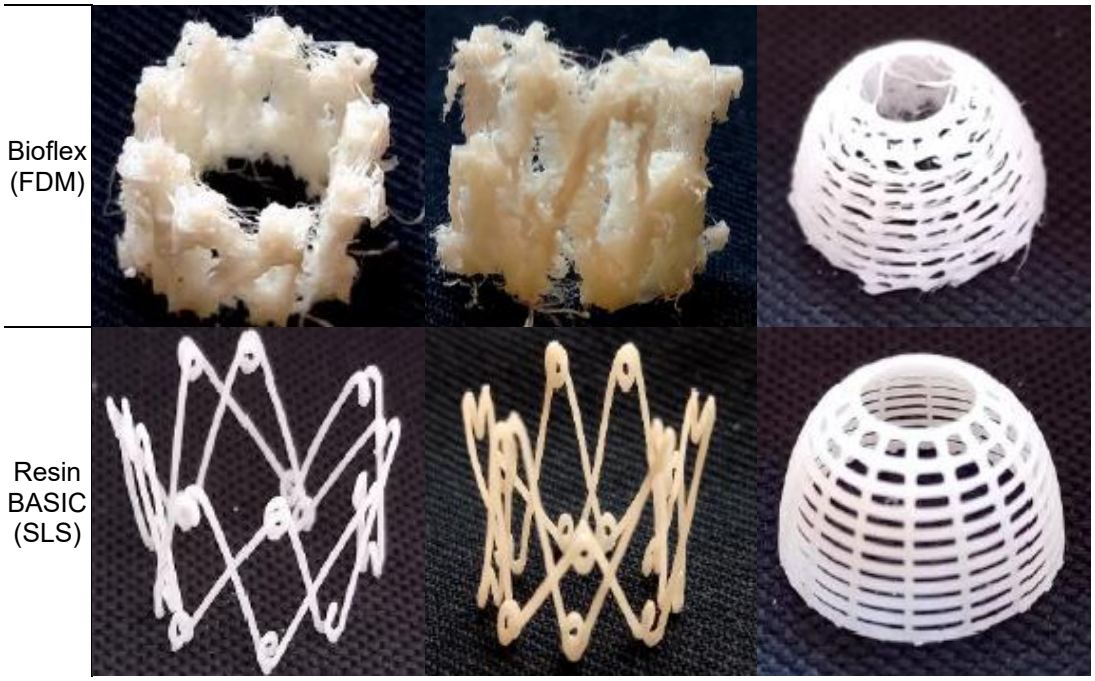


Figure 55 Comparison of the designed and printed stents manufactured using different materials and printing technology. Reproduced with permission of The Licensor through PLSclear from: [24].

The preparation of the anatomical model of nasal septum implant started with segmentation process using 3D Slicer (Figure 56), which was then processed in Autodesk Inventor Professional software. Based on this anatomical model, the synthetic project of nasal septum implant was prepared, together with supports for bending analysis (Figure 57). The proposed project was designed to be around 10% smaller in comparison to human adult septum to allow easy placement and cropping if needed. The model of nasal septum implant was successfully printed using all five selected filaments – standard material in FDM 3D printing – PLA, fast degrading PCL, flexible TPU and two filaments advertised for medical applications – MediFlex and Bioflex (Figure 58). Thus, the designed model was suitable for manufacturing with variety of polymers, from stiff to flexible ones and was chosen for further analysis.

The designed implant was then subjected to compression and bending stress analysis in Autodesk Inventor Professional 2023 with the with the set properties of human septum cartilage (Figure 59, Table 17). Linear responses were observed in both tests, prompting scalability alerts at 7 N (bending) and 90 N (compression). The calculated compressive modulus of 2.28 MPa matches existing literature on human nasal cartilage [374], confirming that the stress analysis is valid for comparisons with the filaments.

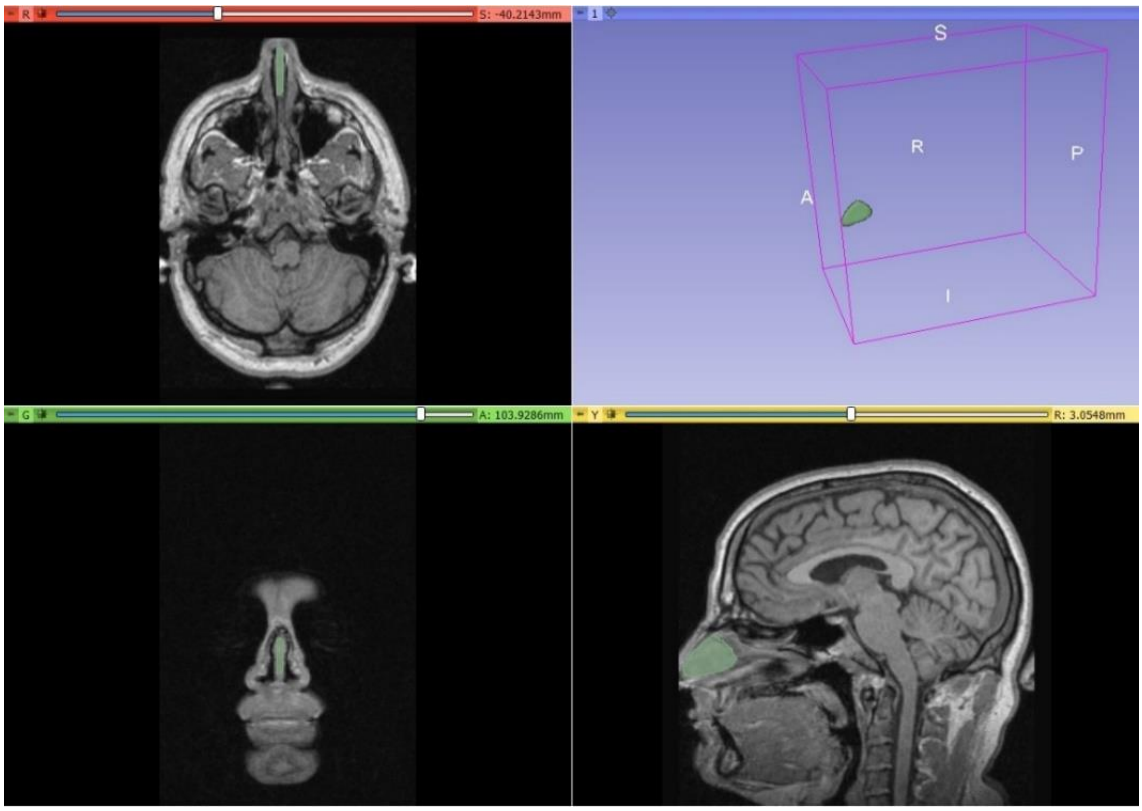


Figure 56 The visualization of the separated nasal septum (top-right) from MRI scan (top-left – top view, bottom-left – front view, bottom-right – left view) in the 3D Slicer program. Adapted from: [26] under CC-BY 4.0 license.

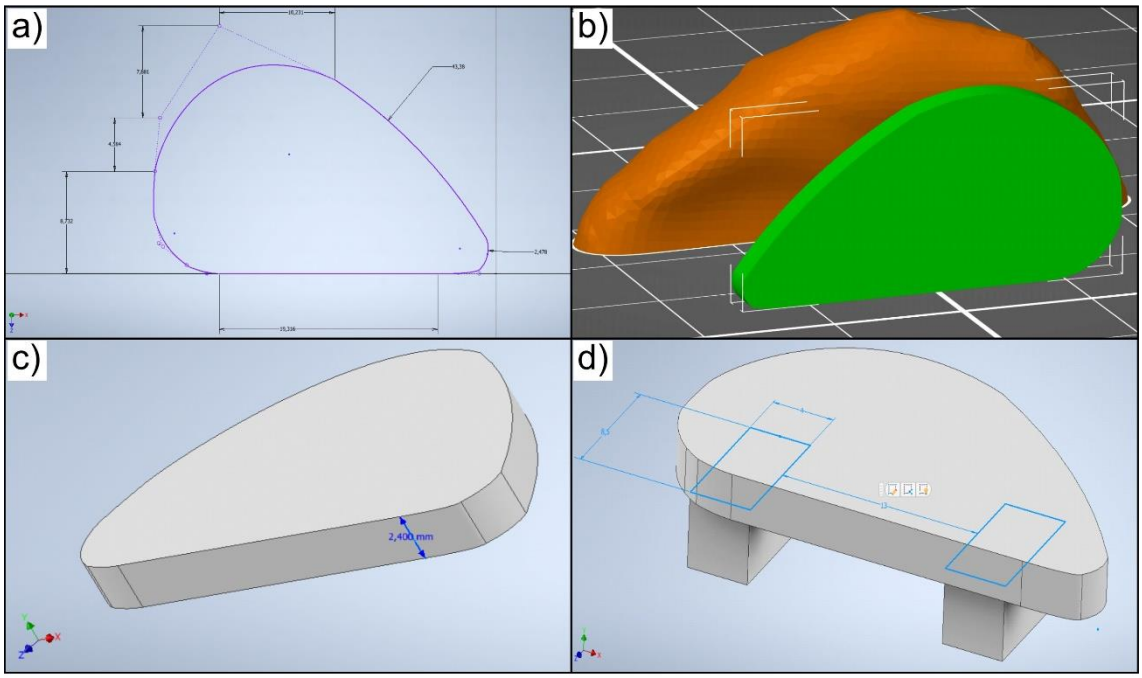


Figure 57 The design of nasal septum cartilage implant: a) technical drawing, b) comparison with the anatomical model extracted from MRI scan, c) 3D model of the implant, d) design of supports for bending test. Adapted from: [26] under CC-BY 4.0 license.

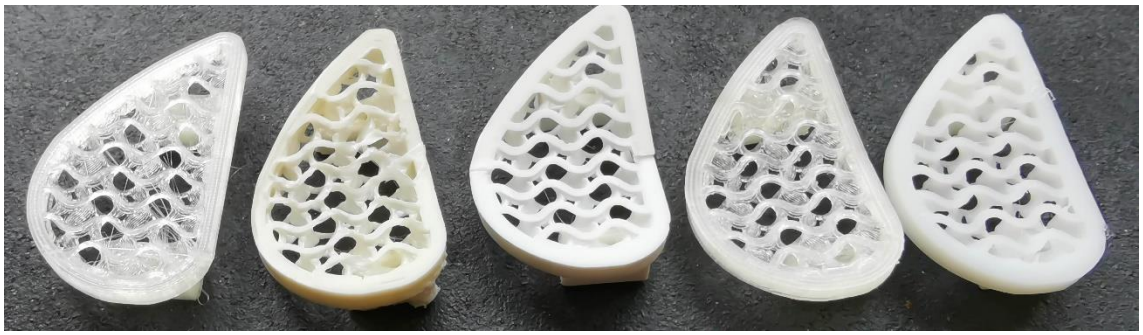


Figure 58 Nasal septum implants with supports for bending testing printed with (from left): MediFlex, PCL, PLA, TPU, Bioflex.

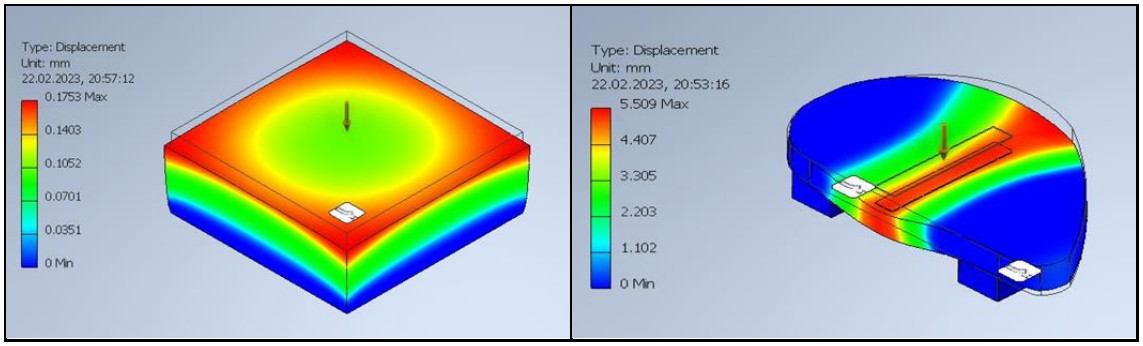


Figure 59 Graphical output of stress simulation on nasal septum cartilage implant. On the left compression study at 10 N of force, on the right bending study at 8 N of force. Adapted from: [26] under CC-BY 4.0 license.

*Table 17 Results of stress simulation on nasal septum cartilage implant. Results with * were obtained with a prompt "The deformation is large compared to the model size. Verify that load and constraint settings are appropriately scaled". Adapted from: [26] under CC-BY 4.0 license.*

Bending analysis		Compression analysis	
Force [N]	**Max. displacement [mm]**	**Force [N]**	**Max. displacement [mm]**
1	0.6886	10	0.1753
2	1.377	20	0.3506
3	2.066	30	0.526
4	2.754	40	0.7013
5	3.443	50	0.8766
6	4.131	60	1.052
7*	4.82	70	1.227
8*	5.509	80	1.403
9*	6.197	90*	1.578
10*	6.886	100*	1.753
		110*	1.929
		120*	2.104
		130*	2.279
		140*	2.454

7.2. Case study: commercial filaments as base materials for nasal implant applications.

A major problem remains in identifying cost-effective polymers that can reliably mimic the specific firmness, flexibility and supportive characteristics of natural human septal cartilage. Consequently, there is a crucial need to systematically evaluate the mechanical suitability of easily accessible, commercial 3D printing filaments for use in nasal reconstructive surgery. Focusing on this material challenge, this study assesses the viability of various market-available filaments for manufacturing cost-effective nasal septum implants by simulating their performance under physiological bending and compression. Chosen filaments (PLA, PCL, TPU, MediFlex and Bioflex) and the printouts were subjected to variety of structural, thermal, mechanical and biological tests. The results of those tests were already described in [26]. Thus, only the most important conclusions from this work will be described in this chapter.

Commercial filament manufacturers typically name only the base polymer type while detailed chemical formulations, specific copolymer ratios, blends and additive packages are not disclosed. Therefore, FTIR analysis was conducted to independently verify and identify the primary polymeric matrices of the tested materials. Based on the FTIR analysis, the type of base polymer used in the four of five filaments was possible to be determined (Figure 60). The FTIR spectra of PLA and PCL filaments were following the expected course for the described polymer types [375,376]. TPU and Bioflex filaments were described as polyurethane-based. More specifically, TPU was determined to be basing on polyester PU due to signals at 3300 cm^{-1} (N-H stretching vibration), 1750-1725 cm^{-1} (C-O stretching vibrations from ester group), 1690 cm^{-1} (stretching vibrations of C=O from urethane bond), 1220 cm^{-1} (stretching vibrations of C-N from urethane bond), 1160 cm^{-1} (stretching vibrations of C-O from ester group) [15,126]. On the other hand, Bioflex was determined to be basing on polyether PU due to lack of polyester-specific signals and the appearance of a strong signal at 1100 cm^{-1}, which can be attributed to stretching vibrations of C-O bond in ether groups [368]. In the case of MediFlex, FTIR analysis suggest the dominant content of aromatic hydrocarbon polymer, e.g., polystyrene, due to lack of signals that can be clearly attributed to bonds other than carbon-carbon or carbon-hydrogen [377].

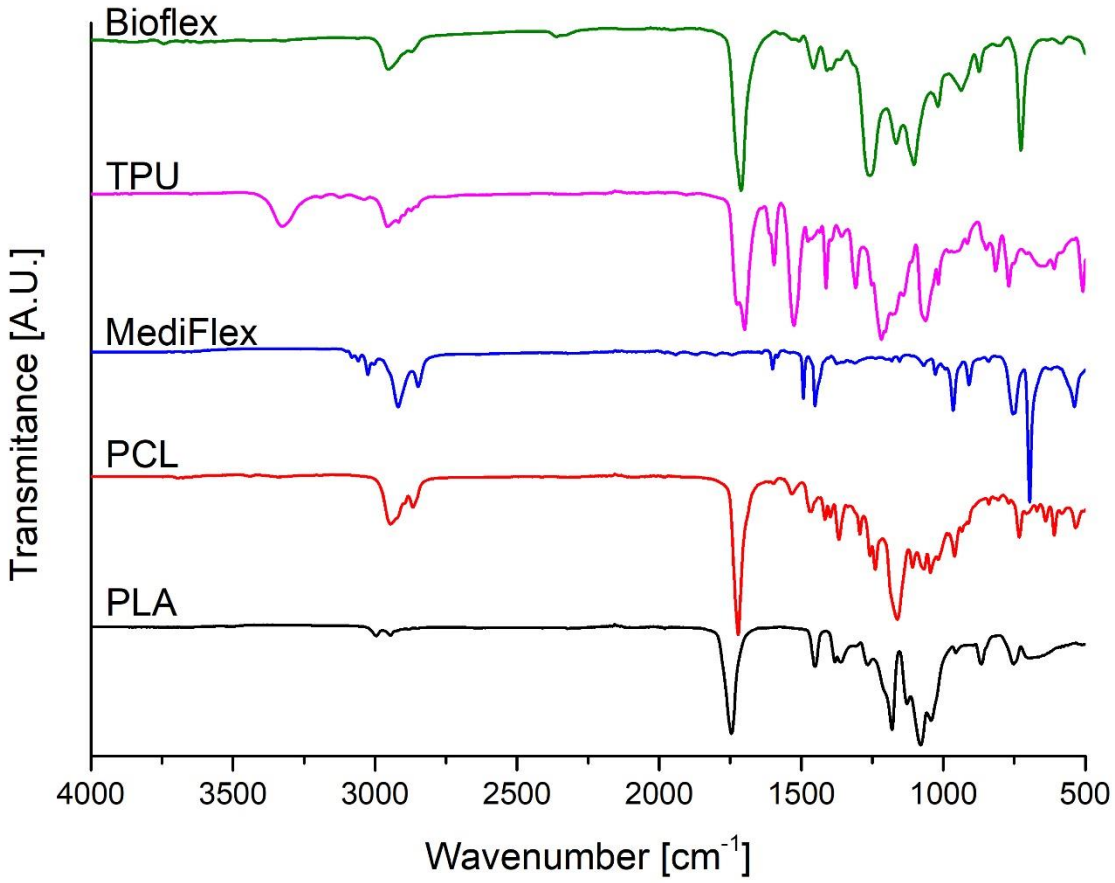


Figure 60 FTIR spectra of the used filaments. Adapted from: [26] under CC-BY 4.0 license.

After determination of the polymer structure, processability of the materials was verified based on flow rates (Table 18) and DSC (Figure 61). The tested materials showed diverse characters – from low-flow, amorphous (MediFlex) to high-flow and crystalline (PCL). The highest flow was observed for PU-based filaments (Bioflex, TPU) and the lowest for MediFlex. However, it must be underlined that the MFR tests were conducted at different temperatures (suggested by manufacturers) and cannot be directly compared. Despite observed differences, all tested materials exhibited MFR in range of 10-80 g/10 min, which is commonly accepted range, allowing decent printing speeds and maintaining dimensional stability [378]. The DSC study allowed to describe phase change temperatures of the tested materials and support the structure description. Bioflex filament exhibited broad signal in range of 105 and 140 °C, characteristic for polyether-based PUs [379]. On the other hand, characteristic melting signal from hard segments of polyester PUs (205-225 °C) was observed for TPU [380]. MediFlex exhibited very discrete signal at around 100°C, characteristic for polystyrene [381]. In PCL thermogram, the typical signal at 55-65 °C can be observed, but also second transition temperature at around 75-90 °C was detected, probably due to impurities. Typical signals for PLA were also observed in this polymer – glass transition at around 60 °C, broad cold crystallization starting at around 110 °C and melting point at around 150 °C. Interestingly, only in case of TPU, the observed phase change temperatures were higher than the recommended printing temperature (215 °C). It is possible that a slightly lower temperature is suggested to maintain dimensional stability during tests and

accelerate the crystallization, as the unmelted phases can act as crystallization nuclei, allowing for higher print speeds.

Table 18 MFR and MVR values of tested filaments under 2.16 kg load and temperatures of print suggested by manufacturers. Adapted from: [26] under CC-BY 4.0 license.

Filament	Temperature [°C]	MFR [g/10 min]	MVR [cm^3/10 min]
Bioflex	190	70.20±0.67	52.57±0.50
TPU	215	51.11±0.93	47.3±1.1
MediFlex	240	10.25±0.31	11.67±0.3
PCL	180	37.13±0.81	34.2±1.3
PLA	215	16.59±0.36	15.01±0.31

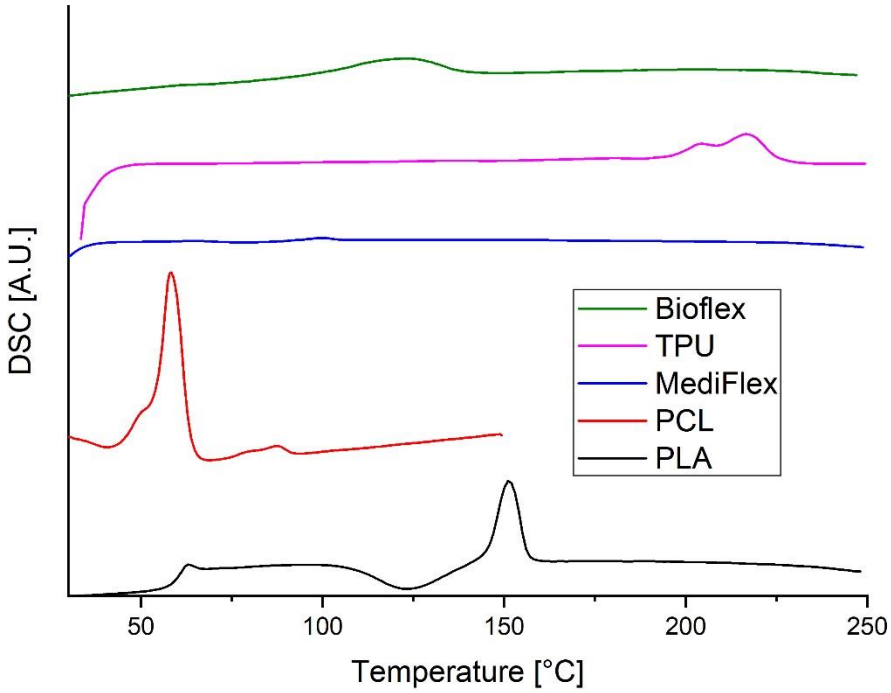


Figure 61 Second heating DSC curves of analyzed filaments. Adapted from: [26] under CC-BY 4.0 license.

The materials were then evaluated in terms of interactions with wet environment. In this regard, hydrophilicity (measured by contact angle) and the susceptibility to degradation was evaluated (Figure 62). Only two of the tested materials were found to be hydrophilic - Bioflex and PLA (61.5±2.2 and 75.52±0.97°, respectively). Other materials were described as hydrophobic, as the measured contact angles were over 90°. Bioflex and PLA were also characterized with the highest surface energies, reaching values above 40 mJ/m^2. In general, materials with high surface energies coupled with contact angle in range of 50-70° are found superior in biological applications, thanks to increased biocompatibility due to enhanced cell adhesion on the printouts [382]. This behavior is also important for *in vivo* degradation, as the hydrolysis is one of the main degradation mechanisms in human body. To influence the hydrophilicity of the filaments, they were surface modified by immersion in collagen, allantoin and diosmin solutions (Figure 63). Generally, no significant changes in contact angle were observed for PCL, PLA and TPU. However, the applied modification strategy had visible effect on MediFlex, where all modifications resulted in contact angles lower than 90° after 2 minutes of water droplet placement. This

discrepancy in results underscores the critical importance of selecting a surface modification method tailored to the inherent chemical characteristics of the specific polymer. Furthermore, successfully transitioning the surface profile to a hydrophilic state is essential for implantable devices, as it actively promotes favorable protein adsorption, enhances cellular adhesion and ultimately facilitates better integration with host tissues.

During accelerated hydrolysis simulation, it was found that only Bioflex exhibited mass losses in all three of the test degradation environments. The lowest remaining mass was noted after 56 days of incubation in 5 M NaOH (21.2±6.0 %), followed by 2 M HCl (31.5±8.7 %). The degradation in the least aggressive environment of phosphate-buffered saline was low, but around 10% of mass loss was noticed just after 42 days of incubation. Similar degradation pattern in acidic and alkaline environment was observed for TPU, although it was faster in 2 M HCl (14±8.3 %) than in 5 M NaOH (58.50±0.50 %), but in both cases mass loss trend could be described as linear. On the other hand, PCL and PLA were found to be extremally prone to degradation in alkali environment – PCL lost nearly 80% of initial mass just after 14 days, whereas PLA completely degraded after just two days. However, PCL exhibited steady degradation in acidic solution (55.0±2.9 % remaining mass after 56 days), whereas PLA was found stable in this environment. At last, MediFlex was found not degradable in the tested conditions, which further supports the previous structural analysis, which did not detect functional groups in this material. The differences in the degradation patterns of these materials have the determining effect on the possibility of application in manufacturing of different implants. It must be underlined that both degradation patterns and interactions with cells should allow the full recovery of tissue functions during service of the device. In this case, the expected operating time of such an implant is determined by the material used for its production and the location of implantation. Additionally, the type of implant must be considered, as even low mass losses (in range of 10-20 %) can result in loss of the ability of stress-bearing, ending with structural collapse and expulsion from the body.

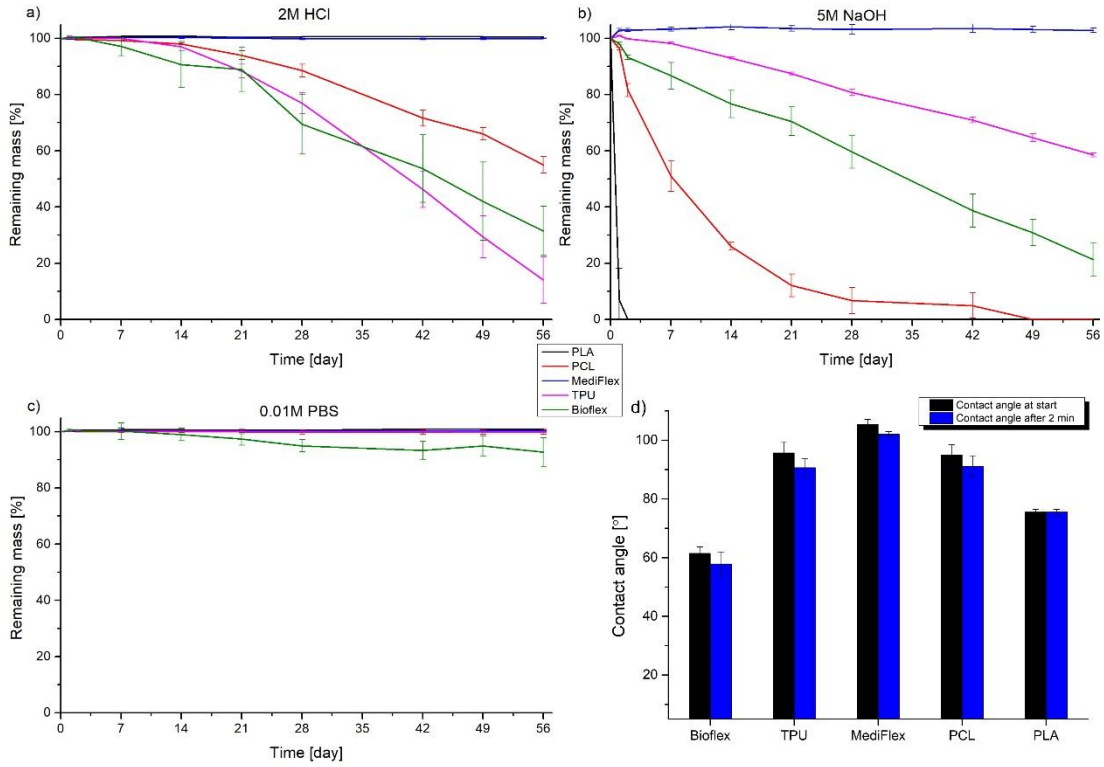


Figure 62 Interactions with wet environment. Accelerated hydrolytic degradation behavior in a) 2 M HCl, b) 5 M NaOH and c) 0.01 M PBS. d) hydrophilicity determination by water contact angle method. Adapted from: [26] under CC-BY 4.0 license.

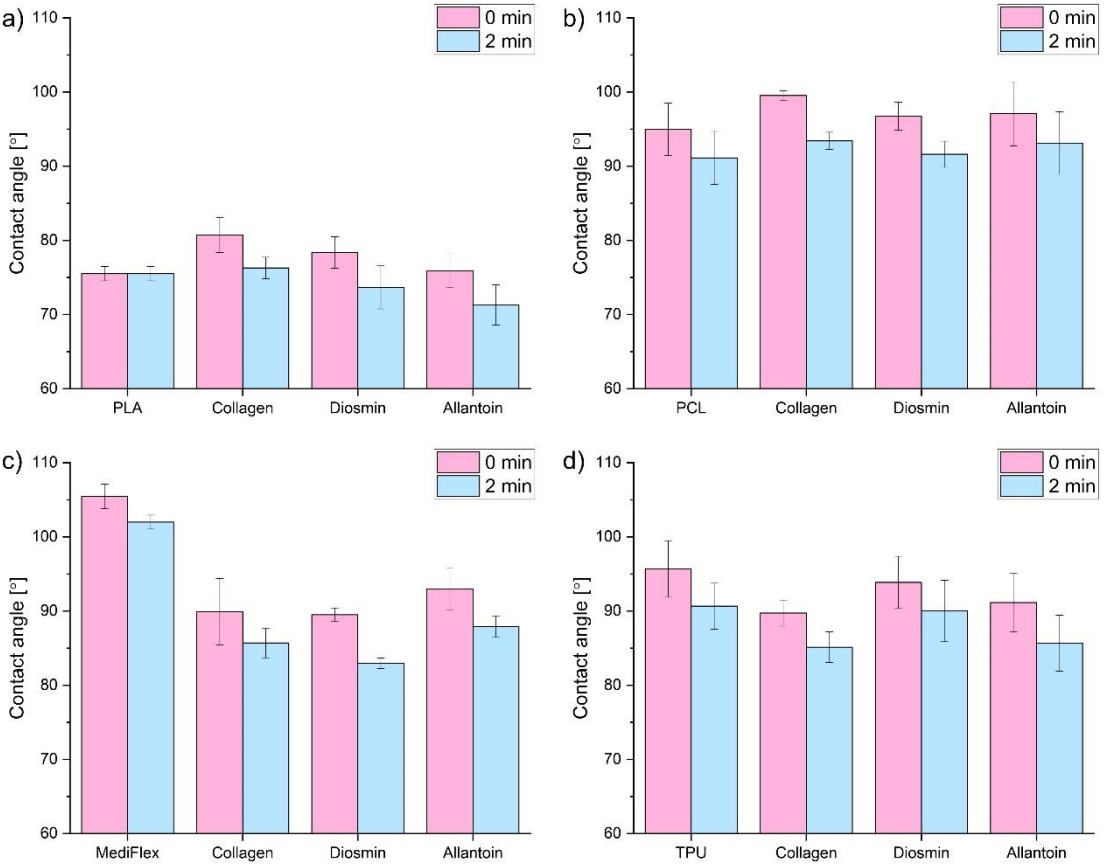


Figure 63 Changes in contact angle after modification with collagen, diosmin and allantoin: a) PLA, b) PCL, c) MediFlex, d) TPU.

The printouts were also evaluated in terms of mechanical properties and the similarity to human cartilage. In compression tests (Figure 64), the closest properties to the simulated nasal septum cartilage were observed for Bioflex and TPU materials, especially in low strain regions (up to ~10 % of deformation), despite the measured Young modulus being higher by two orders of magnitude. It was also observed that the infill direction has a significant impact on the observed compression test results. In general, infill printed longitudinally to stress direction resulted in higher modulus (affecting higher stiffness at lower strains), whereas infill printed transversally to stress direction resulted in higher stiffness at larger strains (up to ~90% higher stress at the end of the test in case of PLA). In Figure 65 the results of bending evaluation of nasal septum implant were presented. Similarly to the compression testing, the closest behavior to the simulated cartilage tissue was observed for Bioflex and TPU materials, with PLA being the stiffest material among all tested ones. Similarly to degradation and hydrophilicity, the mechanical properties of material must be also included when designing the implant. To ensure long-term stability and clinical success, the mechanical profile of an implant should closely mimic that of the host tissue. This alignment promotes even stress distribution and facilitates efficient mechanical loading between the device and the biological site. By minimizing the stiffness mismatch, microscopic shifting at the interface is reduced, which ultimately accelerates the healing process [383]. Interestingly, in terms of mechanical performance, Bioflex and TPU exhibit bending strength comparable to PCL nasal septum implants currently used in clinical practice. Reported literature shows PCL values of 24.10±1.06 MPa (28.9±1.3 N) [384], suggesting that PU-based materials present a competitive alternative for septal reconstruction where similar load-bearing capacities are required.

Bioflex was chosen as the candidate for cytocompatibility analysis due to its favorable characteristics. Previous data highlighted its optimal mechanical compatibility with native septal tissue, hydrophilicity and a degradation profile aligned with the requirements for permanent or long-term implantation. TPU, despite possessing similar properties, was excluded due to lack of degradation in PBS environment. According to the ISO 10993-5 standard, the reduction of cell viability by more than 30% is considered as a cytotoxic effect. Despite the manufacturer’s claims about the biocompatibility of the Bioflex material, following a 24-hour incubation, the 100 % extract concentration induced moderate cytotoxicity (Figure 66). More dilute concentrations remained biocompatible, but by the 48- and 72-hour marks, only the 12.5 % extract maintained cell viability near 80 %, while the 25 % and 50 % concentrations progressed to moderate cytotoxicity. These quantitative findings were supported by morphological analysis of the L-929 cells (Figure 67). Cells exposed to the 12.5% extract remained indistinguishable from the control, while cells treated with the 100 % extract displayed shrinking and detachment, characteristic of cell death.

Although Haryńska et al. previously reported full biocompatibility for Bioflex using CCl 163 cells [369], the discrepancies observed here likely comes from differences in surface-to-volume ratios or cell line sensitivity. Specifically, the use of a 20% gyroidal infill provides a significantly higher contact area than the 85% triangular infill used in their study, potentially

leading to higher leachability. Additionally, the extraction volume was not disclosed, which could have an additional effect on leachability from the material.

Comprehensive evaluation of commercial filaments in terms of mechanical strength, degradation kinetics and surface wettability identified PU-based materials (Bioflex, TPU) as the most promising candidates for nasal septal applications, among the materials tested. Their mechanical profile closely mimics native tissue (particularly within low-strain regions) and they demonstrate both stable degradation and a favorable contact angle. However, TPU was found not degradable in PBS environment and biological assessment revealed that Bioflex's standalone cytocompatibility is currently insufficient for clinical applications. Because few commercial medical-grade elastic filaments exist, there is a clear need for new materials with adjustable properties. Alternatively, future improvements, such as hydrogel coatings, surface functionalization or blending with highly biocompatible polymers, are necessary to meet the rigorous biological standards required for clinical trials. In next chapters these approaches will be explored to obtain systems with suitable properties for utilization in nasal implants.

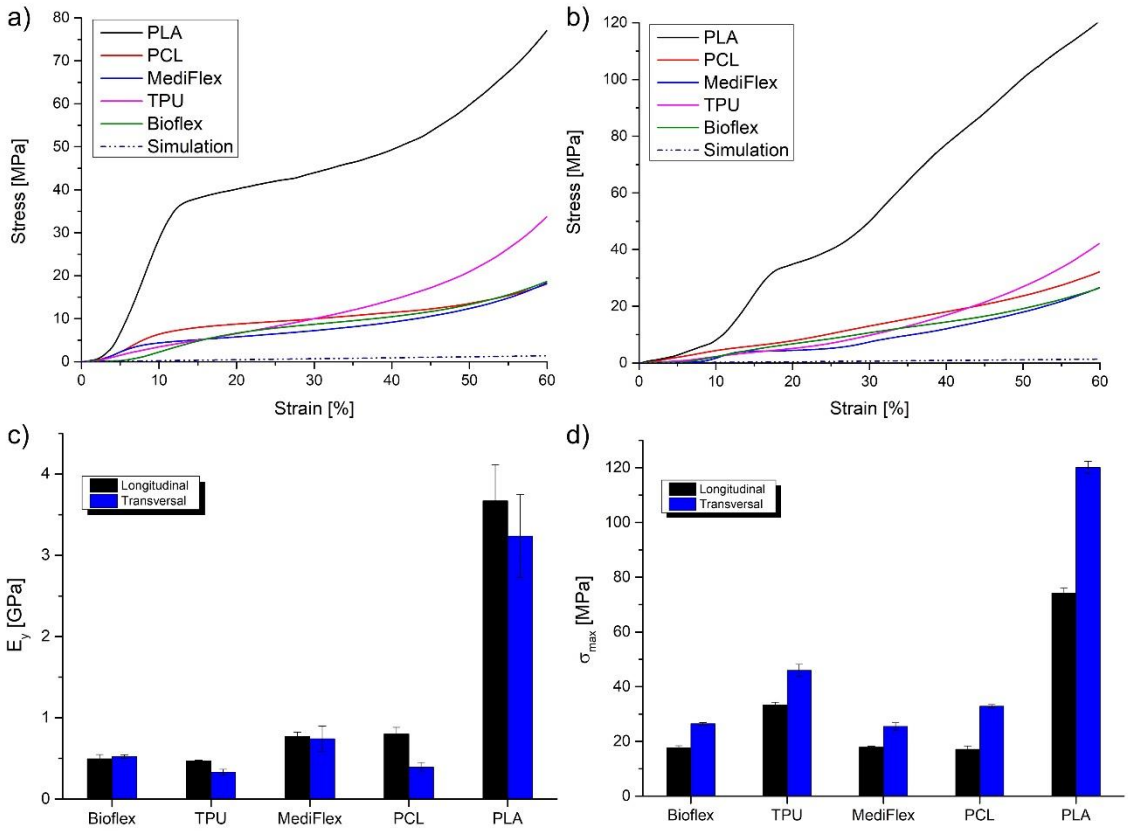


Figure 64 Results of compression mechanical evaluation. Exemplary stress-strain curves in a) longitudinal and b) transversal directions, with respect to the print direction. Comparison of c) Young modulus and d) maximal stress between tested filament types. Adapted from: [26] under CC-BY 4.0 license.

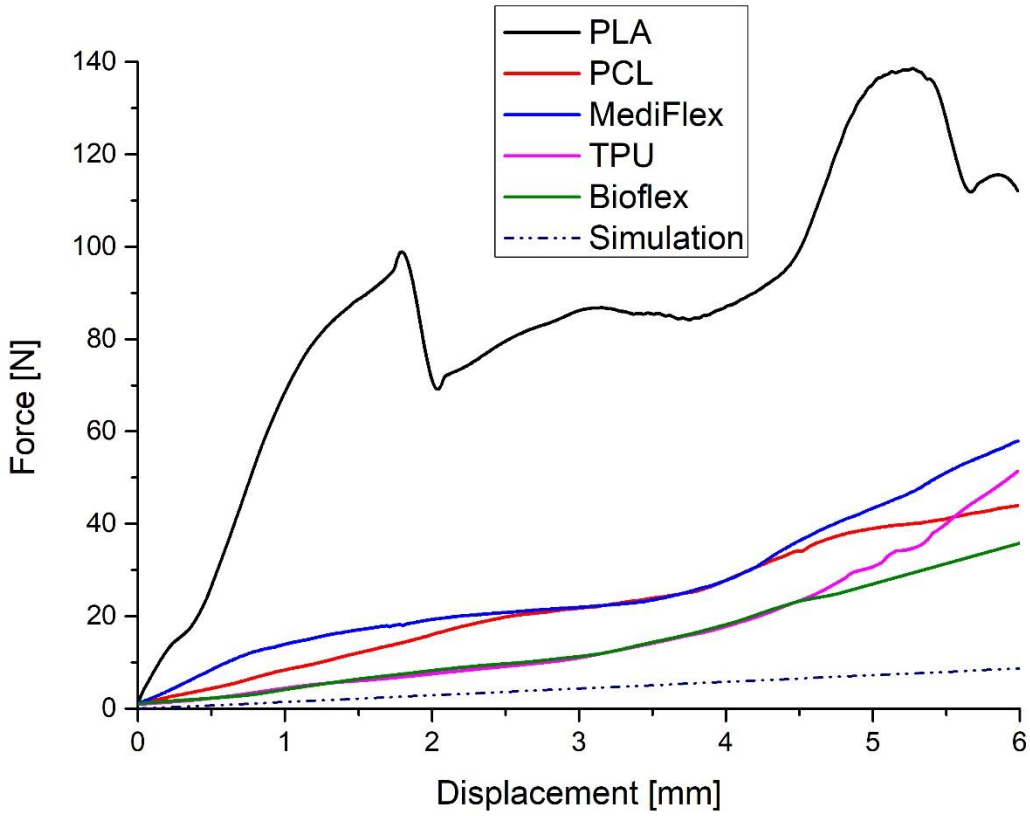


Figure 65 Exemplary bending stress-strain curves for nasal septum implant manufactured with the tested filaments compared with the simulated nasal cartilage behavior. Adapted from: [26] under CC-BY 4.0 license.

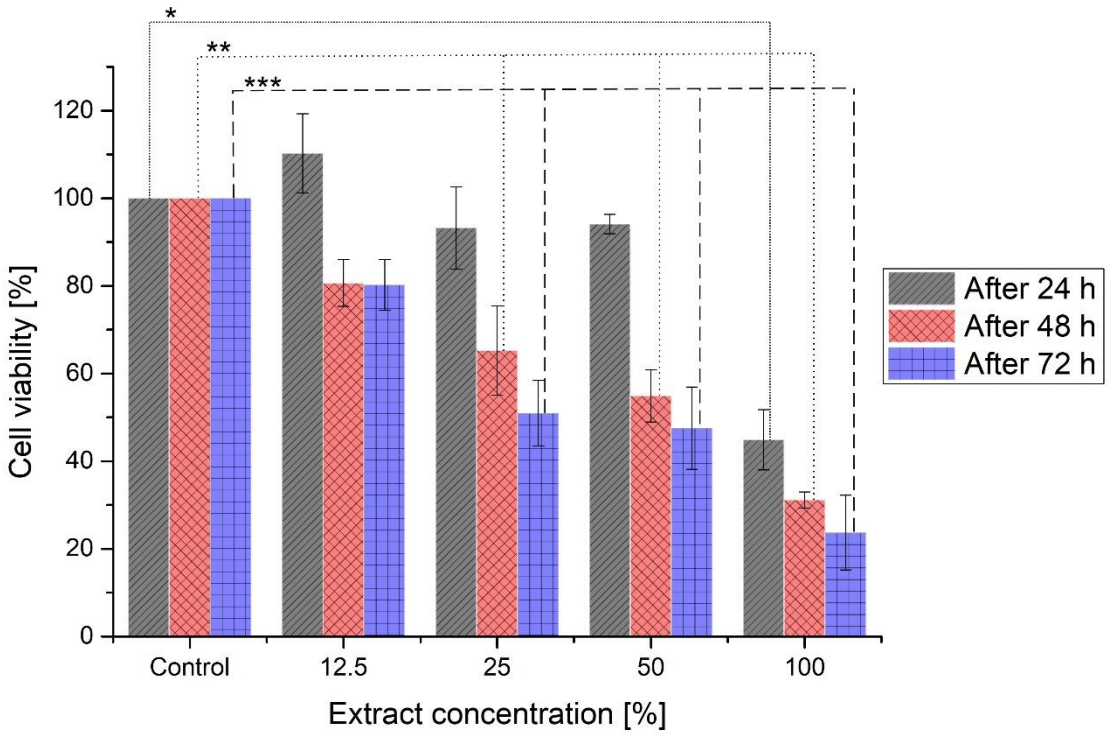


Figure 66 L-929 cell survival rates following Bioflex extract treatment. Cytotoxicity grading: none (>80 % viability), mild (60-80 %), moderate (40-60 %) and severe (<40 %). Statistical significance deviations were identified using a Tukey test at a 0.05 significance level and were denoted by asterisks (, **, ***) relative to the control group at 24, 48 and 72 h, respectively. Adapted from: [26] under CC-BY 4.0 license.*

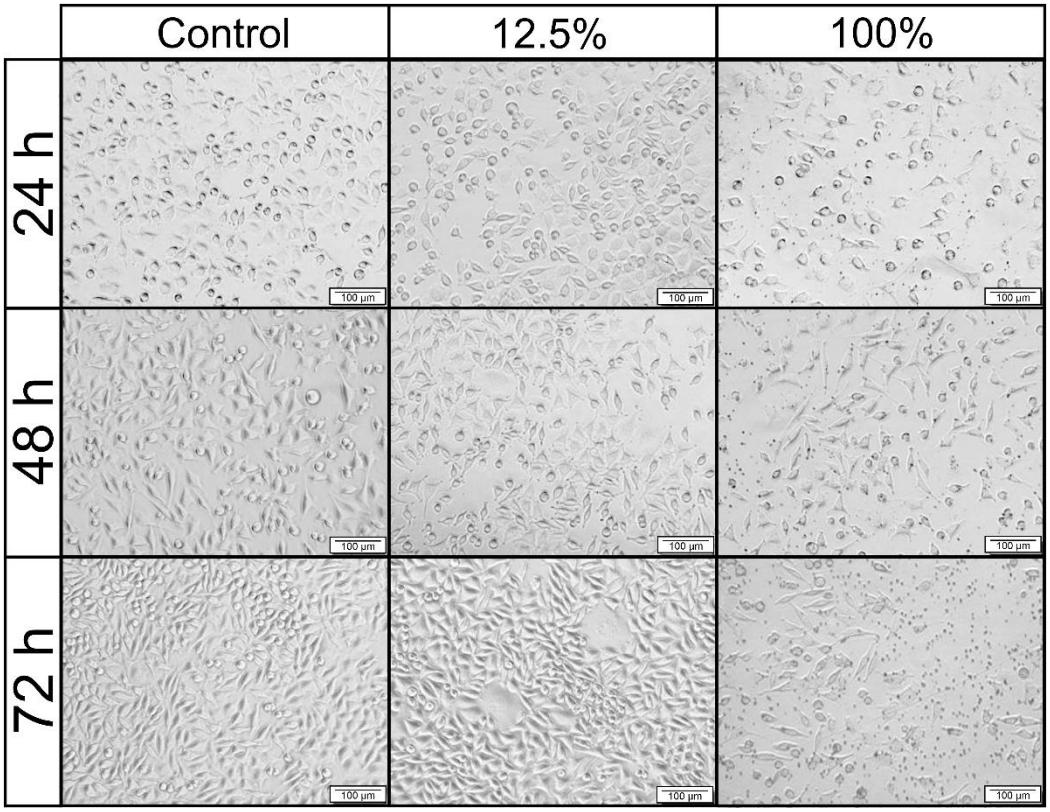


Figure 67 Morphological evaluation of L-929 cells treated with different extract concentrations after 24, 48 and 72 h. Control refers to cells in extract-free medium. Scale bar - 100 µm. Adapted from: [26] under CC-BY 4.0 license.

8. Hydrogel formulation

Although the evaluation of commercial filaments and 3D-modeled constructs established some of the necessary criteria for nasal implants, clinical success of such devices depends equally on long-term surface biocompatibility and infection resistance. Standalone thermoplastic matrices, including commercial filaments and polyurethanes, often present low-level residual cytotoxicity or lack the bioactivity required to prevent localized bacterial colonization within the sinonasal cavity. To mitigate these adverse tissue responses, it was proposed that functionalizing the thermoplastic core with a secondary hydrogel coating can offer an advantageous route to deliver therapeutic agents locally while creating a buffer interface preventing host tissue irritation response. Chapter 8 therefore addresses the formulation and systematic evaluation of multicomponent hydrogel systems designed to act as functional, drug-eluting shell layers. The proposed strategy involved creating hybrid hydrogels composed of natural agar (AG) with synthetic PVA and PVP to combine the inherent biocompatibility and high water retention of polysaccharide networks with the superior mechanical performance, structural stability and higher affinity to hydrophobic active substances.

Seven distinct types of hydrogels based on AG with addition of PVA and PVP in ratios 3:1, 3:2 and 1:2 were successfully synthesized and subjected to a rigorous preliminary evaluation - a critical step necessary to identify the most viable candidates for implant coatings before attempting any active modifications. Because the demanding physiological environment of the human body requires specific material behaviors, this initial screening was essential to ensure that only base matrices demonstrating optimal structural stability, biocompatibility and coating potential were proceeded to the active substance-loading phase. Following this base assessment, pure agar and the blended compositions of 0.6AG/0.4PVA and 0.6AG/0.4PVP emerged as the most suitable candidates and were chosen for curcumin modification. Curcumin, a bioactive compound derived from turmeric, was chosen due to its proven its anti-inflammatory, antioxidant, antiviral, antibacterial, antifungal, antiparasitic and anticancer activities [173,385,386]. The specific ratio of agar to synthetic polymers in these formulations was strategically selected to harness the functional benefits of synthetic materials, such as significantly increased mechanical strength, while deliberately maintaining the predominantly natural, highly biocompatible character of the overall system.

At first, the gelation efficiency of the selected systems was evaluated by mass changes monitoring throughout the preparation steps: after freeze-thaw, 24 hours of soaking and another 24 hours of swelling study (Figure 68). The overall highest gelling efficiency (remaining mass after synthesis) was observed for AG (~57 %), whereas the lowest was detected for samples with the highest ratio of synthetic polymer – 0.5AG/0.5PVA and 0.5AG/0.5PVP. After the synthesis step, the mass of samples oscillated around 95% during the next 24 hours of swelling, supporting the validity of the adopted synthesis methodology. The observed behavior suggests that the selected hybrid crosslinking method was highly efficient for used compositions. The more complex

behavior of the samples was observed after the addition of curcumin. Although the final stability of samples remained very high (observed high deviations are possibly due to manual operations during swelling study, resulting in crumbling of not bonded curcumin), a similar behavior to unmodified samples was observed only for AG/2.5CUR and 0.6AG/0.4PVP/2.5CUR. On the other hand, samples with higher curcumin amount (AG/5CUR and 0.6AG/0.4PVP/5CUR) had noticeably lower stability. In case of the PVA-containing samples the stability of samples during synthesis had significantly increased, especially during soaking (up to 73 %). In these samples, the crumbling phenomenon was also significantly less observed, suggesting greater integration of curcumin into the polymer network.

The appearance of the obtained hydrogels was presented in Figure 69. Generally, the unmodified samples were very similar, thus, only the comparison of curcumin-modified samples was presented. In all samples the evident color change was observed, but the presence of additional synthetic polymer determined the opacity and intensity of orange coloring. The most evident change was observed for 0.6AG/0.4PVA-based samples, where hydrogel became bright orange and opaque. To evaluate the homogeneity of curcumin distribution in the hydrogel samples, optical microscopy was utilized. The micrographs with comparison of the sample appearance of unmodified and modified samples were presented in Figure 70. Interestingly, despite the similar appearance of hydrogels in the unmodified state (1st column), curcumin was incorporated into the hydrogel matrix in different ways, depending on the polymer system used for synthesis. In AG samples, curcumin was dispersed in the form of larger (~150-250 μm) and smaller (< 50 μm) aggregates, without intermediate-sized particles. Increasing amount of curcumin resulted in a significant increase of very small (< 5 μm) curcumin particles in the main structure of the hydrogel, without affecting larger aggregates. The different situation was observed in samples containing PVA – the hydrogel color had changed from slightly yellow to deep red. Additionally, in 0.6AG/0.4PVA/2.5CUR sample, a low amount of small curcumin (< 50 μm) aggregates was detected, whereas in 0.6AG/0.4PVA/5CUR sample, the average particle size was higher, but still lower than observed for AG. Additionally, the smallest fraction of particles was not detected in this case. The appearance of PVP-containing samples seems to lay between two previously described samples. Both 0.6AG/0.4PVP/2.5CUR and 0.6AG/0.4PVP/5CUR contain dispersion of larger and smaller aggregates, similarly to AG samples. However, similarly to PVA-containing samples, the smallest fraction of particles was practically undistinguishable. Additionally, some of the observed particles were well-blended with the hydrogel structure and had a similar, red color to ones observed in the PVA-containing samples. The microscopic evaluation suggests that in case of AG no significant interactions between hydrogel and curcumin are present. In case of synthetic polymers, the lack of the smallest fraction of curcumin was observed, together with the significant color shift from yellowish to deep red. Those changes were the most pronounced in PVA-containing samples.

The experimental values recorded during swelling tests were presented in Figure 71, together with the exemplary runs of fitted models obtained for 0.6AG/0.4PVA and

0.6AG/0.4PVA/2.5CUR hydrogels. Swelling parameters calculated using first order (1OK), second order (2OK) and Korsmeyer-Peppas (KP) were presented in Table 19 and were additionally visualized with the calculations of polymer network parameters in Figure 72.

For further discussions, if not indicated otherwise, only the second order non-linear kinetics model will be considered, as it provided the highest overall R^2 values (over 0.91 for all hydrogels apart from AG0.5/PVP0.5, where it was 0.8998) (Table 19). Overall, the swelling behavior of unmodified samples was found to be comparable. Up to 15 minutes AG sample was characterized with the highest average swelling (460±39%), which is reflected with the highest K values, regardless of used kinetic model. After this point, hydrogels with the addition of synthetic polymer were characterized by higher swelling values. Finally, AG sample had the lowest average swelling (638±27%) among unmodified hydrogels after 24 h of study, whereas the highest swelling was observed for 0.5AG/0.5PVA (858±27%). Interestingly, only AG sample had reached equilibrium swelling during the initial 240 minutes of the test. Swelling of the hydrogels with synthetic polymers has increased by up to 150% between the last two measuring points, which also resulted in significant deviations from the values of W_{eq} predicted by kinetic models. In general, the more synthetic polymer that was added, the slower the swelling rate was. In case of samples with PVA, the observed swelling was also higher with the increasing amount of PVA, but the swelling of AG0.75/PVA0.25 was very similar to AG. Swelling of the samples with PVP was comparable regardless of the synthetic polymer amount and finally higher by around 100% in comparison to AG sample.

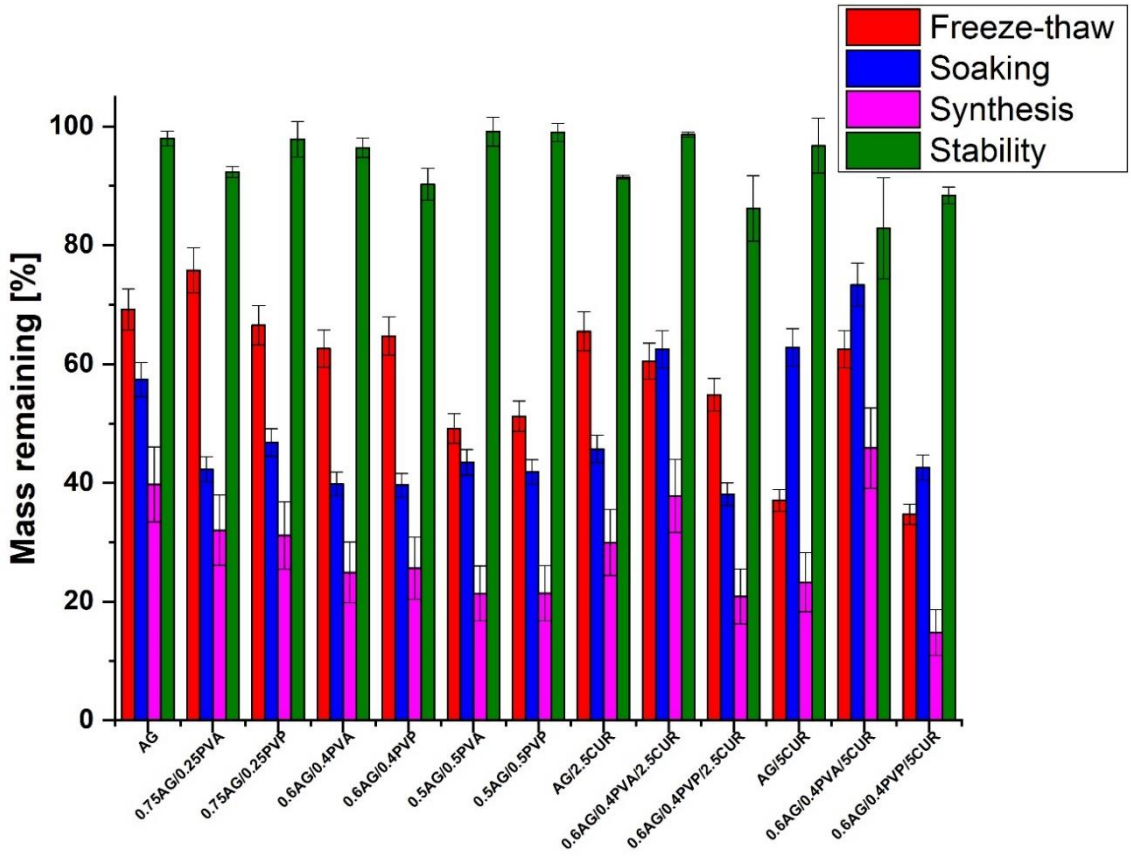


Figure 68 Changes of the hydrogel samples mass during synthesis in relation to the introduced amount of reagents during freeze-thaw process (red columns), after 24 h of soaking in water (blue columns) and after 24 h of swelling test (green columns). Additionally, the change of weight of final samples was denoted as Synthesis (magenta columns).

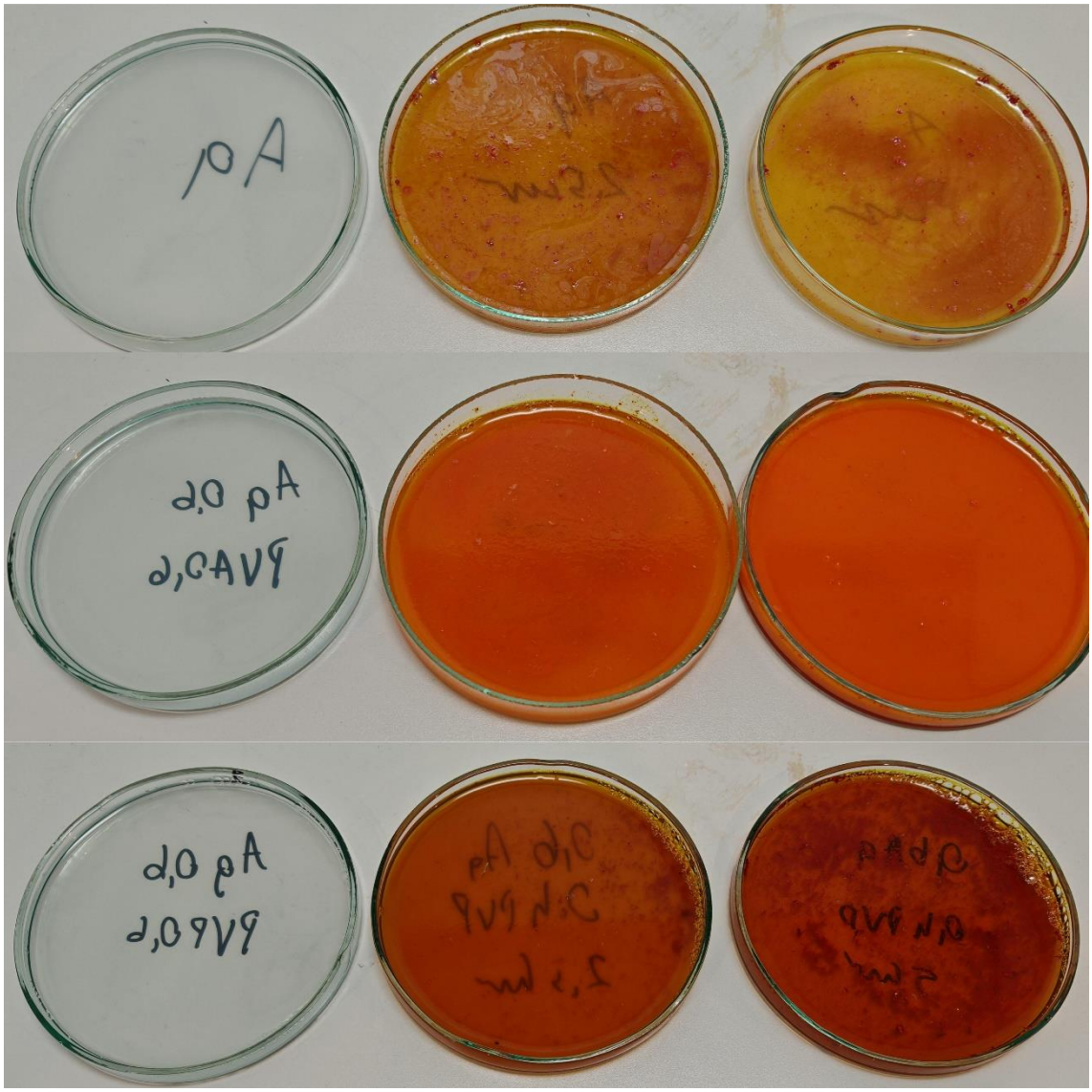


Figure 69 Comparison of macroscopic appearance of hydrogels after synthesis. From the top: samples based on AG, 0.6AG0.4PVA and 0.6AG0.4PVP. From the left: unmodified hydrogels, samples modified with 2.5 % and 5 % curcumin, respectively.

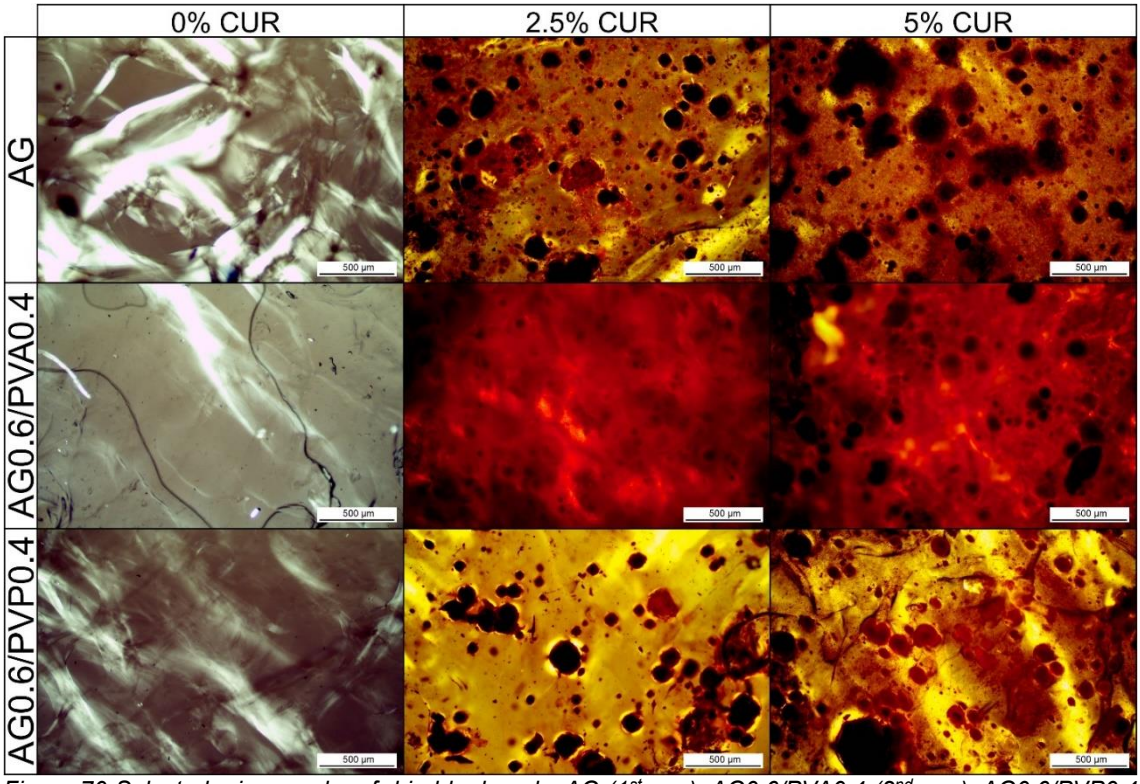


Figure 70 Selected micrographs of dried hydrogels: AG (1st row), AG0.6/PVA0.4 (2nd row), AG0.6/PVP0.4 (3rd row) in their unmodified (1st column) form and modified with 2.5 % (2nd column) and 5 % (3rd column) of curcumin. Scale bar = 500 µm.

The addition of curcumin into hydrogels had a different effect on swelling behavior, depending on the composition of hydrogel. Interestingly, the addition of curcumin did not significantly influence the quick swelling ability, seen for unmodified samples, in the case of 0.6AG/0.4PVP/5CUR resulting in swelling up to 448±21% just after 15 minutes. AG curcumin-modified samples exhibited slightly lower swelling (541±30 for AG/2.5CUR and 593±16% for AG/5CUR), probably due to the presence of hydrophobic curcumin. Although calculated equilibrium swelling was noticeably lower compared to AG, the K_2 parameters did not differ significantly, thus there were no evident interactions between curcumin and the hydrogel network. The presence of non-swelling curcumin in the sample also influences the M_c and Q_c, but together with swelling behavior the obtained values suggest no evident interactions in the network. On the other hand, a compelling difference can be observed for samples with PVA, where addition of curcumin resulted in nearly two-fold decrease of swelling (725±27% for 0.6AG/0.4PVA, 474±37% for 0.6AG/0.4PVA/2.5CUR and 401±36% for 0.6AG/0.4PVA/5CUR), together with significantly faster reaching of equilibrium evidenced by nearly 3 times higher K_2 parameters. It also resulted in nearly 2-fold increase of calculated crosslinking density, suggesting a significant influence of curcumin on the crosslinking process in the obtained hydrogel network.

The observed changes in swelling are in line with the noticed increased stability of the 0.6AG/0.4PVA/2.5CUR and 0.6AG/0.4PVA/5CUR hydrogels during synthesis, which supports the claim of increased crosslinking in PVA systems. A very interesting behavior can be seen for PVP-based samples, where no evident changes in the swelling ability and its kinetics

were observed, despite the addition of hydrophobic curcumin. The proposed explanation of this phenomenon is the lowered crosslinking density of the original polymer network, which was compensated with the mass of non-swelling curcumin, finally resulting in similar values to the unmodified sample. There are three possible forms of curcumin influence in this system: physical expansion of the polymer network by hydrophobic particles, disruption of interactions between polymers and crosslinkers or curcumin interactions with some part of crosslinkers. In the light of the above-mentioned results, the last-mentioned process has probably the highest influence on hydrogel swelling properties, as for samples with AG the expected lowering of swelling ability due to curcumin hydrophobicity was observed.

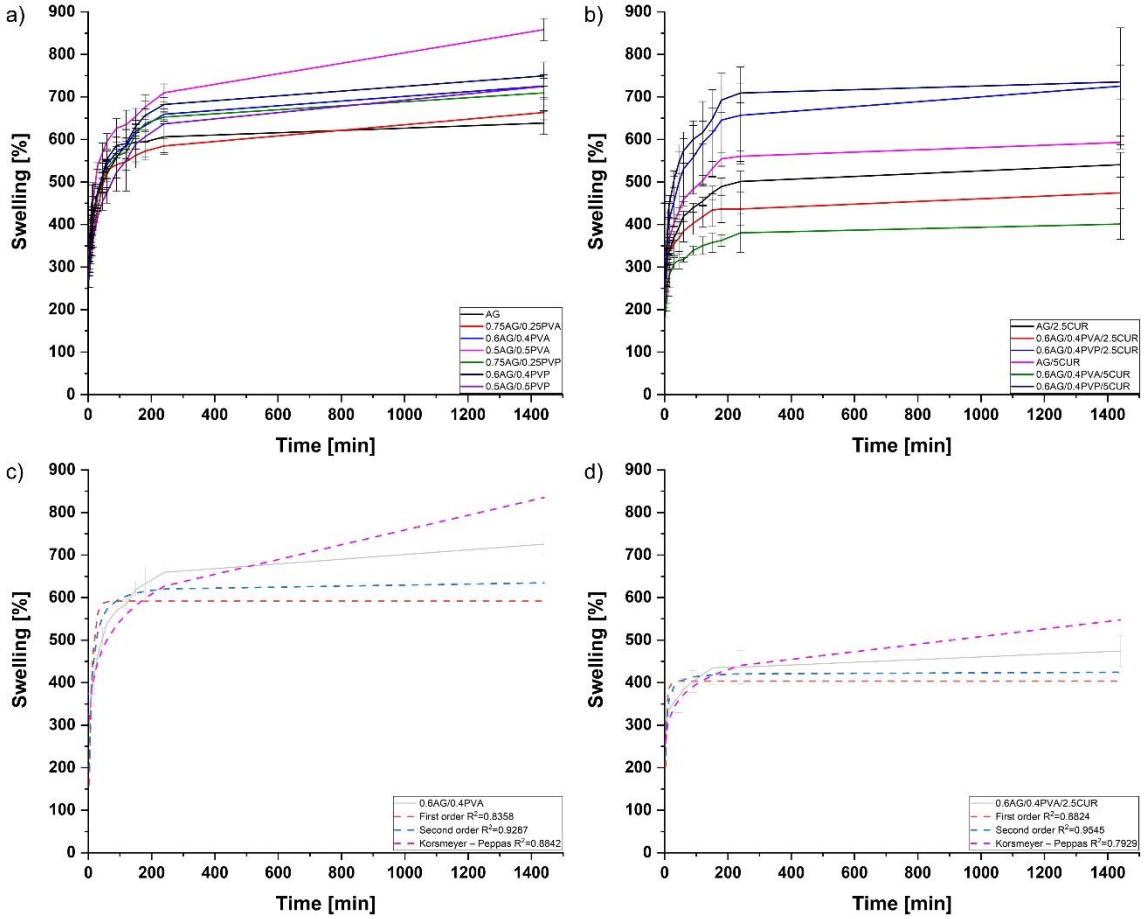


Figure 71 Experimental swelling data of a) unmodified and b) curcumin-modified samples. Experimental swelling data (gray) and curves fitted with first order (red), second order (blue) and Korsmeyer – Peppas (magenta) kinetic models for c) 0.6AG/0.4PVA and d) 0.6AG/0.4PVA/2.5CUR.

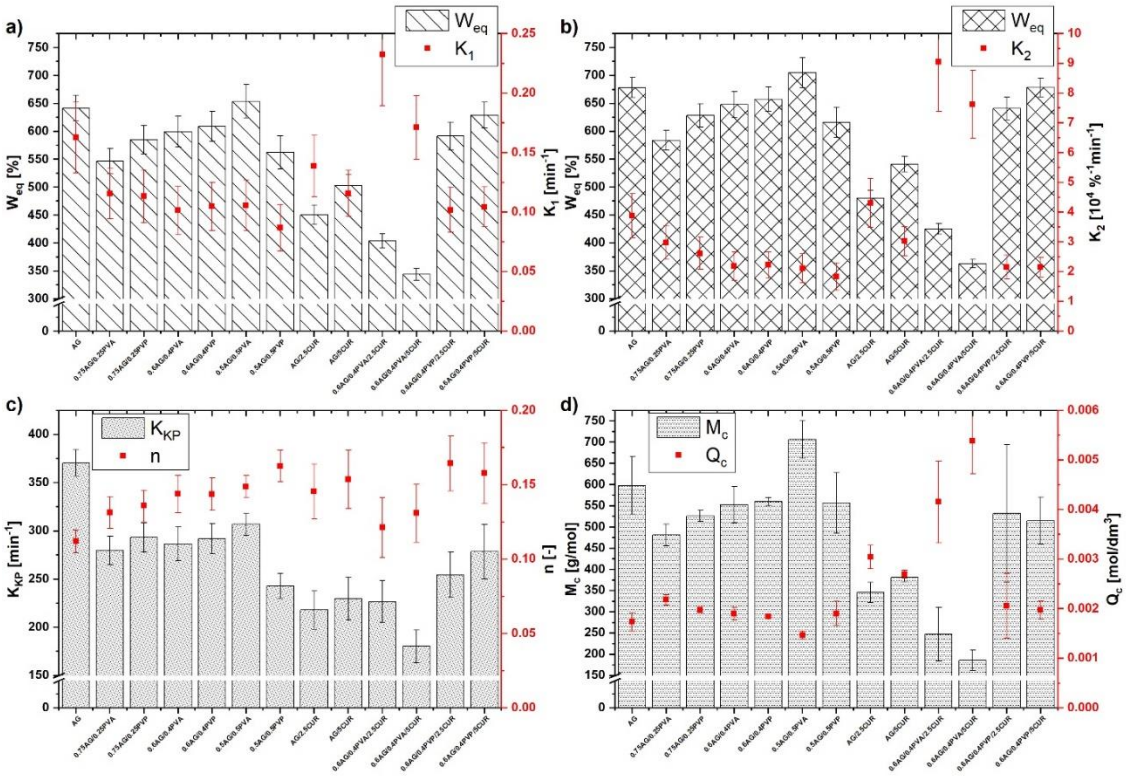


Figure 72 Summary of hydrogel polymer network parameters calculations based on hydrogel swelling. a) First order equilibrium swelling (W_{eq}) and swelling kinetics constant (K_1), b) Second order equilibrium swelling and swelling kinetics constant (K_2), c) Korsmeyer-Peppas swelling kinetics constant (K_{KP}) and diffusion exponent (n), d) Average molecular weight between cross-links (M_c) and average density (Q_c) of hydrogel network.

Table 19 Swelling kinetics parameters of hydrogels calculated using different mathematical models: first and second order and Korsmeyer - Peppas.

Sample name	First order (non-linear)			Second order (non-linear)			Korsmeyer - Peppas		
	W_{eq} [%]	K_1 [min^{-1}]	R^2	W_{eq} [%]	K_2 [$\%^{-1}\ min^{-1}$] × 10^{-4}	R^2	n	K_{KP} [min^{-1}]	R^2
AG	647 ± 24	0.159 ± 0.029*	0.8682	684 ± 18	3.78 ± 0.71*	0.9471	0.137 ± 0.020	329 ± 31	0.8405
AG0.75/PVA0.25	547 ± 23	0.116 ± 0.022	0.8530	584 ± 18	2.98 ± 0.58	0.9399	0.152 ± 0.019	252 ± 24	0.8763
AG0.6/PVA0.4	584 ± 26	0.114 ± 0.023	0.8358	627 ± 21	2.64 ± 0.56	0.9287	0.156 ± 0.019	265 ± 24	0.8842
AG0.5/PVA0.5	592 ± 27	0.105 ± 0.021	0.8376	637 ± 22	2.35 ± 0.49	0.9296	0.160 ± 0.019	261 ± 24	0.8895
AG0.75/PVP0.25	607 ± 27	0.105 ± 0.021	0.8430	656 ± 22	2.24 ± 0.46	0.9330	0.162 ± 0.018	265 ± 24	0.8960
AG0.6/PVP0.4	657 ± 31	0.104 ± 0.022	0.8277	709 ± 27	2.05 ± 0.48	0.9153	0.167 ± 0.017	280 ± 23	0.9175
AG0.5/PVP0.5	562 ± 30	0.087 ± 0.020	0.7950	616 ± 28	1.83 ± 0.47	0.8998	0.178 ± 0.017	224 ± 19	0.9228
AG/2.5CUR	450 ± 18	0.139 ± 0.026	0.8543	481 ± 14	4.31 ± 0.83	0.9412	0.145 ± 0.019	218 ± 20	0.8665
AG/5CUR	503 ± 19	0.116 ± 0.020	0.8781	541 ± 15	3.02 ± 0.50	0.9560	0.154 ± 0.020	230 ± 23	0.8657
AG0.6/PVA0.4/2.5CUR	404 ± 13	0.233 ± 0.044	0.8824	425 ± 10	9.1 ± 1.7	0.9545	0.121 ± 0.021	227 ± 22	0.7929
AG0.6/PVA0.4/5CUR	344 ± 11	0.171 ± 0.027	0.8988	363.2 ± 7.4	7.6 ± 1.2	0.9653	0.131 ± 0.020	180 ± 18	0.8246
AG0.6/PVP0.4/2.5CUR	591 ± 25	0.102 ± 0.019	0.8585	641 ± 21	2.16 ± 0.41	0.9429	0.164 ± 0.019	254 ± 24	0.8929
AG0.6/PVP0.4/5CUR	629 ± 23	0.104 ± 0.017	0.8912	679 ± 18	2.15 ± 0.33	0.9621	0.158 ± 0.021	279 ± 29	0.8635

The structural analysis of unmodified hydrogel samples revealed the dominant influence of agarose signals to the recorded FTIR spectra (Figure 73a). In all samples, a broad band in the 3700-3000 cm^{-1} region can be observed, which can be associated with the stretching vibrations of the O-H groups (υO-H) present in agar and PVA. In the 3000-2800 cm^{-1} region, a broad signal can be distinguished for AG sample, where signals associated with stretching vibrations of CH_2 and CH have overlapped. The signal width also suggests small degree of methylation (O-CH_3) [387]. In hydrogels synthesized with PVA and PVP, small peaks associated with υCH_2 and υCH can be distinguished at around 2920 and 2850 cm^{-1} [388,389]. A common signal for all polymers is also a band near 1640 cm^{-1}, which corresponds mostly to O-H bending vibration (δO-H) from structural water present in the hydrogel network. Weak absorptions observed at approximately 1370 cm^{-1} can be associated with asymmetric stretching of B–O–C bond, suggesting formation of trigonal complexes [390]. The signal observed at 1150 cm^{-1} can be attributed to either to ester-sulfate bond vibrations, C-O stretching vibrations within the pyranose ring or CH-OH stretching vibrations [387,391]. Signals around 1060 cm^{-1} and 930 cm^{-1} are characteristic to agar and are assigned to 3,6-anhydro-galactose bridges [392], while the band near 870 cm^{-1} is typically attributed to galactose sulfate [393]. As the signals characteristic for PVA (e.g., C-O stretching in range of 1200-800 cm^{-1}) [389] and PVP (e.g., υCH_2 of pyrrole ring at around 2950 cm^{-1} or characteristic vibrations of C=N in pyridine ring at around 1600-1500 cm^{-1}) [394] are located in similar regions as previously described agar signals, they are not distinguishable in studied samples. Additionally, the characteristic B–O stretching bond of residual borax ($B(OH)_4^-$) at around 830 cm^{-1} was not observed, which may indicate that limited interactions of borax with polymers in the hydrogels. Physical crosslinking by $CaCl_2$ usually does not result in the appearance of new signals in the FTIR spectrum and no corresponding signals were detected.

FTIR spectra of hydrogels had significantly changed upon addition of curcumin (Figure 73b). Interestingly, those changes were the least pronounced in the case of AG-only samples. In most samples the maximum of broad band in 3700-3000 cm^{-1} region has shifted to higher wavenumbers and several new signals characteristic for curcumin have appeared at lower wavenumbers. For better visibility of changes, the comparison of unmodified and modified samples at 1800-800 cm^{-1} range was presented in Figure 74. Interactions between the synthetic polymers and curcumin may be indicated by spectral changes near 1700 cm^{-1}. In PVA-containing samples, a weak band appears at approximately 1730 cm^{-1}, while PVP-containing samples exhibit a slight extension of 1640 cm^{-1} band toward higher wavenumbers. These features may point to the presence of additional ester or ether linkages. Additionally, the broad band at around 1640 cm^{-1} was split into two sharp peaks: 1625 cm^{-1} (δO-H) and 1580 cm^{-1}, attributed to stretching vibrations of C=C bond present in curcumin [395]. At around 1510 cm^{-1} new sharp peak was found, which can be attributed to vibrations of carbon and oxygen bonds (υC=O or δCC=O) in curcumin compound [396]. The new peak at 1425 cm^{-1}, together with previously observed signal at 1370 cm^{-1} can be attributed to asymmetric stretching signal of B-O-C bond [390,397], suggesting formation of both tetrahedral and trigonal boron complexes and more pronounced intramolecular interactions due to curcumin presence. Another sign of curcumin reaction in the

hydrogel system can be spotted in the 1300-1270 cm^{-1} region. Curcumin is known to exhibit a single, strong signal at around 1280-1260, which is attributed to stretching vibrations of C-O bond in aromatic ring [398]. However, in the obtained spectra two signals can be observed in this region: one at around 1290 cm^{-1} and one at around 1270 cm^{-1}. Signal at higher wavenumbers can be an indication of the boron-curcumin chelate complex, suggesting formation of rosocyanine or rubrocurcumin [399]. This signal can result from hydrogen bond formation between curcumin and hydroxyl groups of PVA and PVP. Additionally, the characteristic signals from residual borax in form of B-H out-of-plane bending vibration at around 963 cm^{-1} [400] and B-O stretching bond at around 830 cm^{-1} [390] were observed, which may indicate increased interactions of borax in the modified hydrogels.

Interestingly, the above-mentioned interactions of borax and curcumin were visible only in samples containing synthetic polymers. In case of lower curcumin loading, described signals were more pronounced in AG0.6/PVA0.4/2.5CUR sample, but for higher amount of active substance, the intensities were comparable. The observed affinity of curcumin to borax in PVA and PVP systems can be described by hydrogen bonding. Curcumin possesses phenolic hydroxyl groups, which can act as electron donors and a β-diketone moiety with several potential acceptor sites (carbonyl oxygens). PVA contains numerous hydroxyl groups (-OH) that can act as both hydrogen bond donors and acceptors and PVP is an effective hydrogen bond acceptor due to the strong polarity of its cyclic carbonyl group. On the other hand, agar, despite having numerous hydroxyl groups (-OH) is not that reactive, probably due to steric hindrance. All this together can lead to increased electron exchange in systems with synthetic polymers, allowing the more pronounced formation of intramolecular bonds. As the most pronounced changes in the structure and swelling properties after modification were observed for AG0.6/PVA0.4, the following rheological, antimicrobial and biological tests were focused on this sample type.

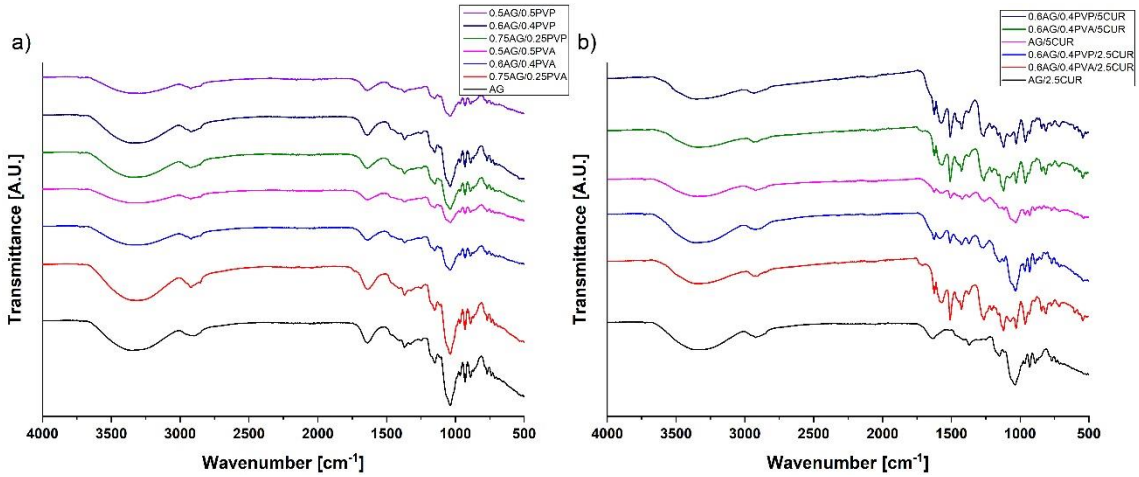


Figure 73 FTIR spectra of a) unmodified and b) curcumin-modified hydrogels.

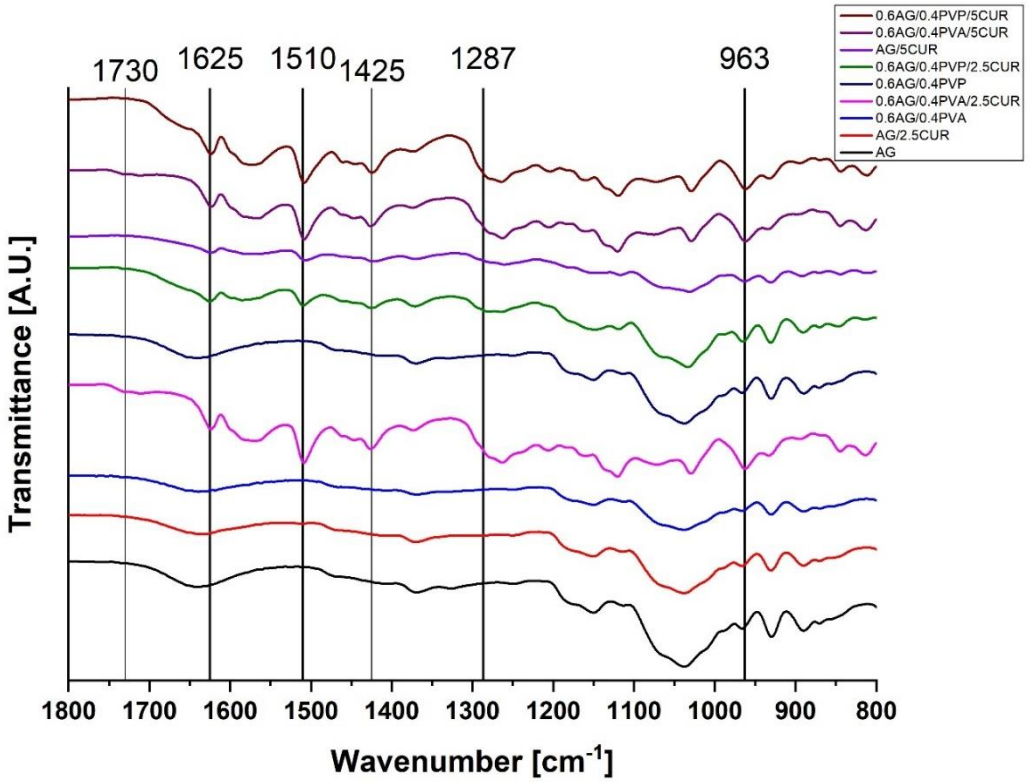


Figure 74 Comparison of FTIR spectra of unmodified and curcumin-modified hydrogels at 1800-800 cm^{-1} range.

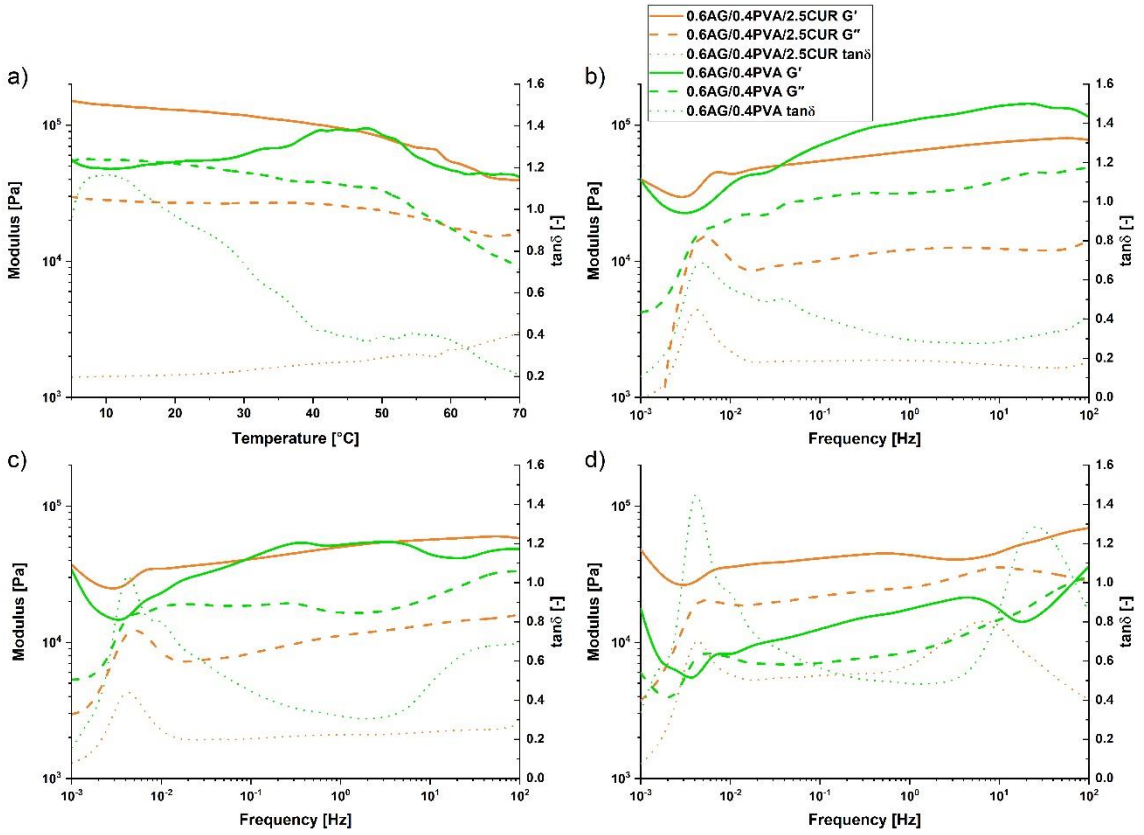


Figure 75 Summary of rheological measurements: a) temperature sweep, b) frequency sweep at 1 % strain, c) frequency sweep at 2.5 % strain, d) frequency sweep at 5 % strain. Storage modulus (G', solid lines), loss modulus (G", dashed lines) and loss factor (tanδ, dotted lines) were presented for AG0.6/PVA0.4 (green) and AG0.6/PVA0.4/2.5CUR (orange) hydrogels.

Viscoelastic properties of selected hydrogels were evaluated using two rheological measurements: temperature and frequency sweep. In these studies, the storage modulus (G'), loss modulus (G'') and loss factor (tanδ) were analyzed as a function of changing temperature and deformation frequency. In addition, frequency sweep tests were conducted utilizing three values of deformation: 1, 2.5 and 5 % to simulate different forces during the extrusion process in 3D printing. The results of these tests were summarized in Figure 75.

In the temperature sweep test, the unmodified sample (AG0.6/PVA0.4 – green lines) exhibited mixed behavior at the lower temperatures, as it was characterized with similar values of G′ and G″. The storage modulus started to dominate in temperatures higher than 30°C, reaching maximum values at around 45°C, while loss modulus remained relatively stable. Observed behavior suggests the reversible, physical crosslinking of this hydrogel, characterized by the appearance of lower critical solution temperature (LCST). Although no dominant viscous behavior or sharp transitions in loss factor were observed throughout the experiment, an indistinct phase transitions in 5-20°C can be spotted, where the tanδ fluctuated around 1, which can be defined as gel point. Such behavior (no dominant viscous behavior) can also be explained by partial chemical crosslinking due to borax. On the other hand, modification of hydrogel with curcumin (AG0.6/PVA0.4/2.5CUR – orange lines) significantly changed the viscoelastic properties. In this case, elastic behavior was dominant (G′>G″) throughout the whole studied temperature range, suggesting chemical crosslinking of the hydrogel, supported by the observed additional signals in FTIR spectra of curcumin-modified sample. This chemical crosslinking is probably responsible for stabilization of the hydrogel polymer network at lower temperatures, where at higher temperatures (>40°C), interactions of physical crosslinking are more pronounced, resulting in a similar storage modulus to the unmodified sample.

Frequency sweep tests (Figure 75 b-d) further support the observations of different crosslinking appearing in the analyzed hydrogel samples. Tests were performed at the temperature of the human body (37 °C), above the observed gelation temperature of AG0.6/PVA0.4. Unmodified sample revealed significant dependency on both frequency and strain in the tested range. At the lowest, 1 % strain, unmodified gel retained mostly elastic behavior in the tested frequency range. At low frequencies (0.002-0.01 Hz) peak of loss factor can be observed, but its maximum value did not reach 1. At moderate strain, slight decrease of both G' and G'' can be observed, with a partial overlap at around 0.003 Hz. Additionally, another peak of loss factor has appeared at frequencies >10 Hz. At the highest strain, significant decrease of both G' and G'' can be observed, together with two apparent transition points into the viscous state at previously observed frequency ranges of tanδ peaks. On the other hand, AG0.6/PVA0.4/2.5CUR remained stable throughout whole range of frequencies and strains studied. In general, modified hydrogel retained dominant elastic behavior (G'>G'') during analysis. However, the viscous behavior was getting more pronounced with increasing strain but did not become predominant. Slight peaks of loss factor can be observed at low frequencies (0.002-0.01 Hz) at all strains and

additional peaks can be observed at 1-10 Hz range at the highest, 5 % strain. Such behavior gives additional support to the presence of additional crosslinking due to curcumin modification.

These observations are in line with the literature reports. The unmodified sample (AG0.6/PVA0.4) exhibits similar properties to agarose-based hydrogels up to 50°C, where in agarose-based hydrogels the transition occurs [401,402], but the herein reported hydrogel structure remains stable, presumably thanks to the presence of PVA and additional crosslinking. The small number of reports on the rheological properties of curcumin-modified gels does not allow for reference to the temperature sweep test, as the frequency and strain sweep tests are usually reported. The observed decrease of storage modulus at higher frequencies and loss modulus at whole frequency range upon curcumin addition was also observed by Ding et al. under the 1 % deformation [403]. They observed the crossing point of storage modulus at around 0.08 Hz (0.5 rad/s), where the G' of PVA-based hydrogel highly modified with curcumin started to fall below the G' of unmodified sample.

Following the observation of favorable rheological properties, hydrogels were subjected to preliminarily evaluation of the extrusion bioprintability utilizing an infusion pump. The resulting constructs were shown in Figure 76. The hydrogels demonstrated potential as base materials for bioinks in extrusion-based 3D bioprinting, enabling layer-by-layer deposition of simple, macroscale three-dimensional structures. Obtained constructs were characterized by satisfactory shape fidelity and reproducibility under the set flow rate and temperature conditions. Furthermore, the constructs remained stable for extended periods when stored vacuum-packed at 4 °C. These findings indicate that the tested compositions could serve as bioinks for extrusion-based 3D bioprinting. The observed characteristics confirm that the material can withstand printing pressures while preserving the dimensional accuracy required for functional tissue constructs. High shape fidelity and structural stability are critical in bioprinting, as they ensure that printed scaffolds maintain the designed open pore architectures necessary for cell survival.

The antibacterial effect of curcumin in hydrogel was assessed using modified Kirby-Bauer disk diffusion test on *Staphylococcus aureus* ATCC 25923 and *Staphylococcus epidermidis* ATCC 12228 bacteria cultures. Photographs of Petri dishes were presented in Figure 77 and micrographs of bacteria growth inhibition zones (BIZs) were presented in Figure 78. The results confirmed that curcumin was being released from hydrogel matrices, but at the same time, the inhibition zone size was limited, probably by hindered diffusion curcumin into agar substrate due to its hydrophobicity. Hence, without micrographs, the BIZs were difficult to observe with the naked eye. In the case of AG0.6/PVA0.4/2.5CUR, the diffusion of the active substance was evidenced by the presence of a zone exhibiting a gradual decrease in color intensity. In this case, size of BIZ cannot be clearly assessed and approximate inhibition distances from the hydrogel disk were estimated to 350 and 500 μm for *S. aureus* and *S. epidermidis*, respectively. On the other hand, in micrographs of AG0.6/PVA0.4/5CUR clear curcumin diffusion front is visible as an orange line, where inhibition of bacteria growth was visible in area close to the hydrogel disk. The calculated inhibition distances from the hydrogel disk were equal to 0.609±0.053 and 1.33±0.12 mm for *S.*

aureus and *S. epidermidis*, respectively. The observed results of Kirby-Bauer disk diffusion test are in line of the literature reports, where extremally small inhibition zones around curcumin-modified hydrogels are usually attributed to hindered diffusion on agar plates [404,405].

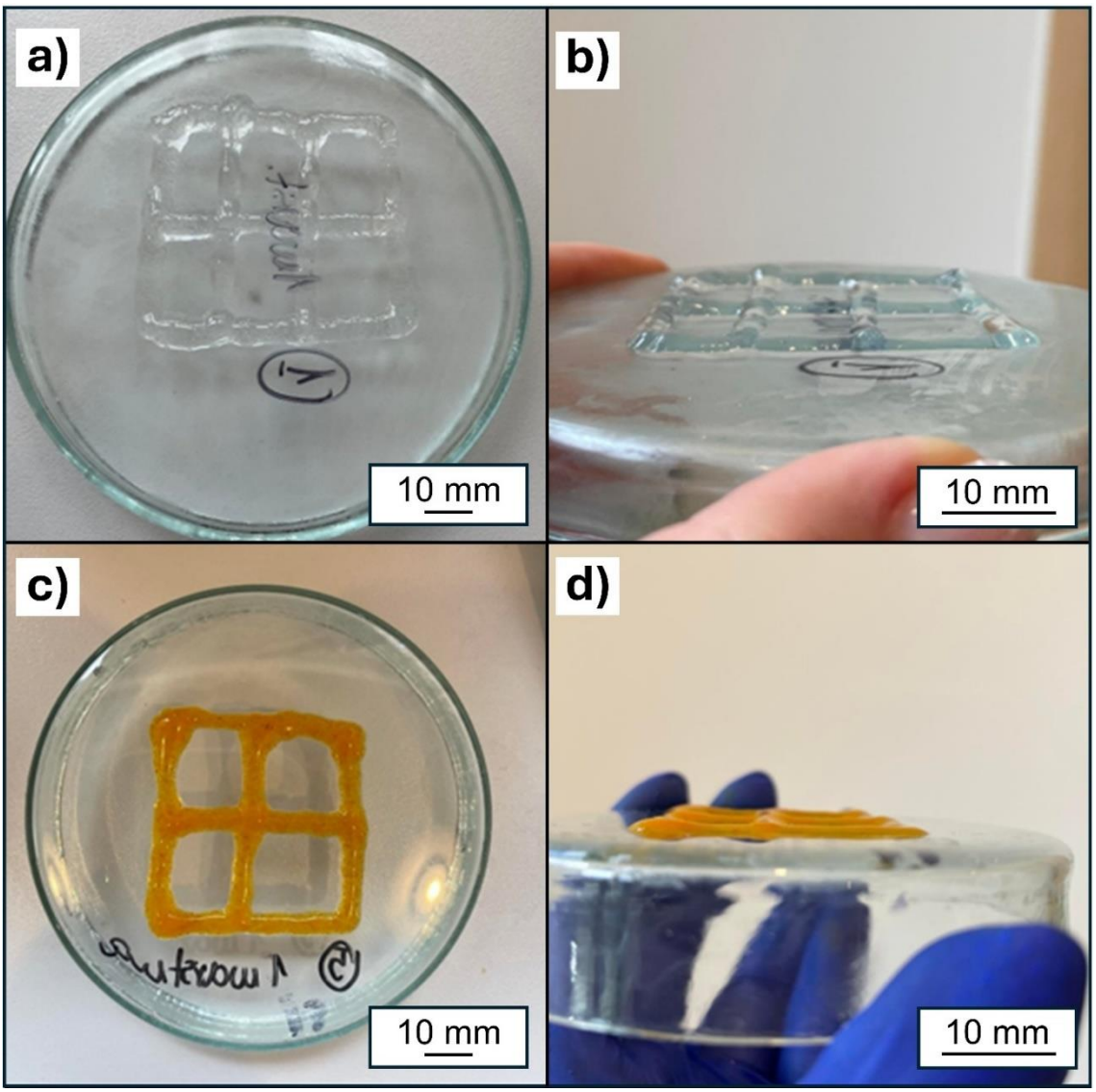


Figure 76 Constructs obtained during preliminary 3D printing tests on: AG0.6/PVA0.4 (a) top view, b) side view) and AG0.6/PVA0.4/2.5CUR (c) top view, d) side view).

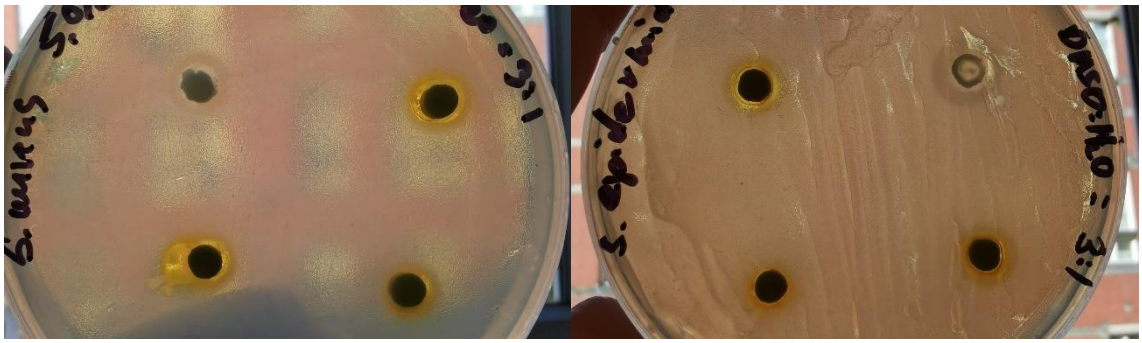


Figure 77 Photographs of Petri dishes after modified Kirby-Bauer disk diffusion test against Staphylococcus aureus ATCC 25923 (on the left) and Staphylococcus epidermidis ATCC 12228 (on the right). White discs (control) - AG0.6/PVA0.4. Other disks - AG0.6/PVA0.4/5CUR.

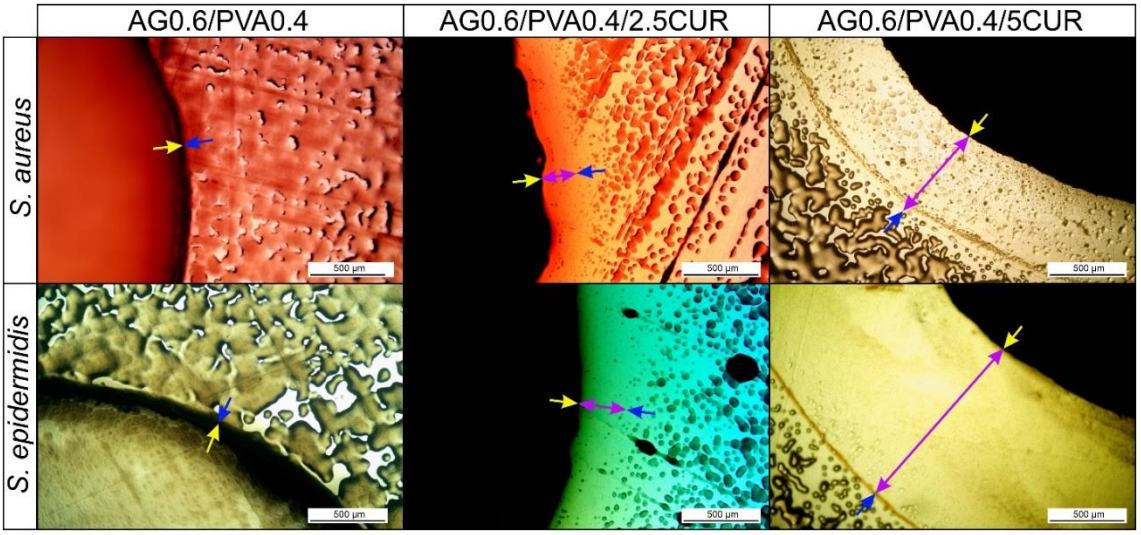


Figure 78 Antimicrobial activity of curcumin-modified hydrogels against S. aureus ATCC 25923 (first row) and S. epidermidis ATCC 12228 (second row) in the modified Kirby-Bauer disk diffusion test. First column: unmodified AG0.6/PVA0.4, second column: AG0.6/PVA0.4/2.5CUR, third column: AG0.6/PVA0.4/5CUR. Yellow arrow indicates the edge of the hydrogel, blue arrow - edge of the inhibition zone/beginning of the intense bacterial growth zone and pink arrows - bacterial growth inhibition zone. Scale bar = 500 µm.

Due to observed problems with assessment of BIZ in modified Kirby-Bauer disk diffusion tests, AG0.6/PVA0.4/2.5CUR was subjected to antibacterial activity examination with contact method, where bacteria were cultivated right on the surface of the hydrogel. The test setup was presented in Figure 79. The effect of a curcumin in hydrogel on the viability of *Staphylococcus aureus ATCC 25923* was assessed after 90 and 180 minutes of incubation. The number of viable bacterial cells was quantified by determining the colony-forming units (CFU) presented in logarithmic scale in Figure 80 and the visual comparison between the number of bacteria colonies grown was presented in Figure 81. The initial number of bacterial cells recovered from both the control and curcumin-loaded hydrogels was comparable, indicating a consistent and reproducible inoculation of the bacterial suspension onto the tested surfaces. After 1.5 hours of incubation, a noticeable increase in the logarithmic value of CFU was observed for *S. aureus* on the surface of the hydrogel without curcumin, suggesting bacterial proliferation. In contrast, the hydrogel containing curcumin exhibited a partial inhibition of bacterial growth, as evidenced by a less pronounced increase in the CFU. A reduction in the CFU for both types of hydrogels was observed at the 3-hour mark compared to the 90 min time point. However, when compared to the initial inoculum (start), the number of CFU on hydrogel without curcumin remained higher. A significant decrease in bacterial viability was noted for the hydrogel with curcumin, where the CFU fell noticeably below the initial count ($p = 0.001$). This finding suggests a time-dependent bactericidal or bacteriostatic effect of the curcumin-loaded hydrogel on the tested *S. aureus* ATCC 25923, as a nearly 10-fold decrease in bacterial colonies was observed compared to the unmodified sample. It means a reduction of viable bacterial cells by ~90% after 180 min of contact with AG0.6/PVA0.4/2.5CUR, with the viability of the bacterial cells tested strain not altered after 90

min of contact with the surface of this hydrogel sample. A similar effect (reduction of viable bacterial cells by ~90% and ~60% in simulated intestinal and gastric fluids, respectively) of curcumin-modified hydrogel on the inhibition of Gram-negative *E. coli* and Gram-positive *S. aureus* growth was reported by Cai et al. [406], although utilizing altered version of herein presented experiment (bacteria contact with hydrogel extract for 30 minutes). The similar antibacterial efficiency (~80% reduction of viable bacterial cells) of curcumin-modified hydrogel in liquid medium was reported by Khaleghi et al., who investigated the activity against *P. aeruginosa* using the broth dilution method [405].

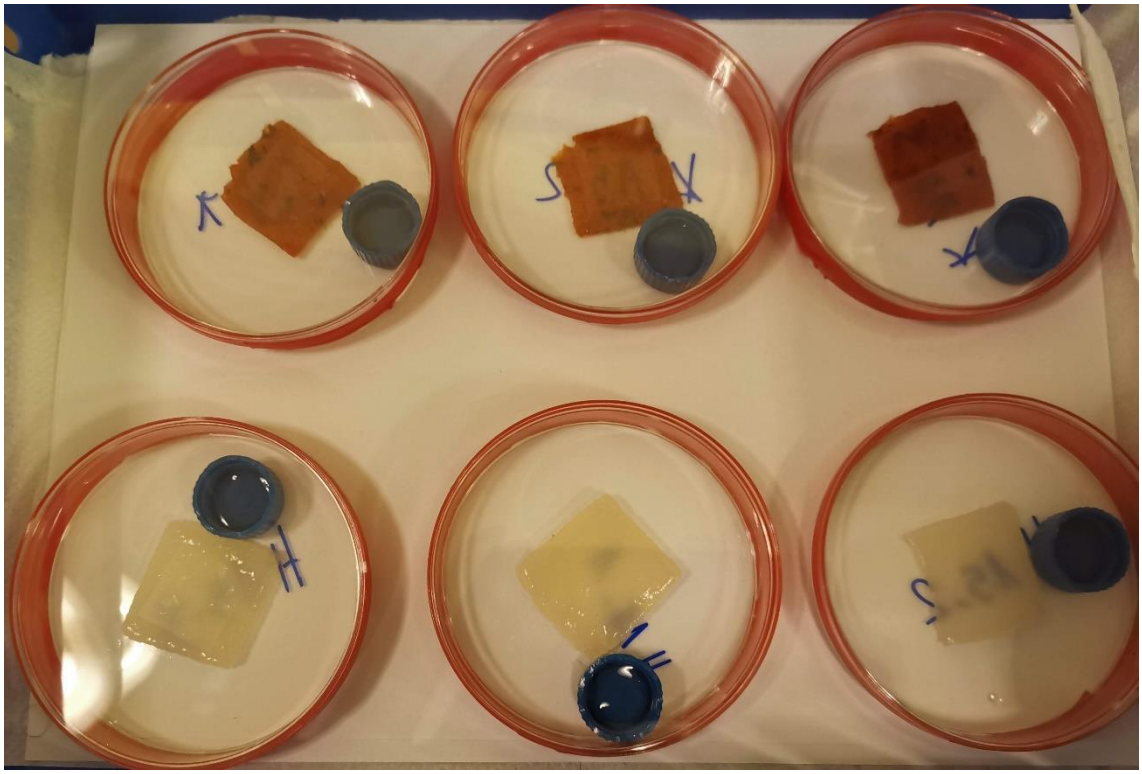


Figure 79 Test setup for antibacterial activity examination with contact method. Bacteria solution was placed on the surface of each hydrogel sample and covered with coverslip.

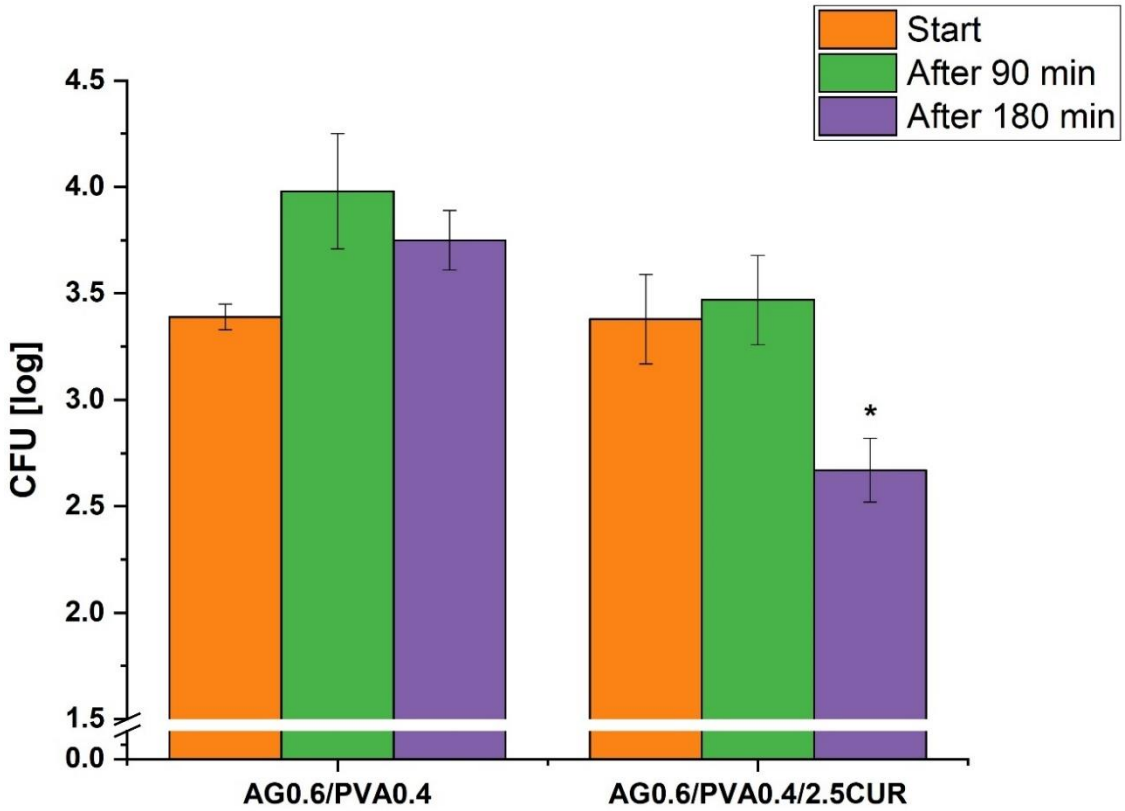


*Figure 80 Antimicrobial activity of AG0.6/PVA0.4/2.5CUR hydrogel against S. aureus ATCC 25923 evaluated using the contact method. Data presented as number of a colony-forming units (CFU) at the start of the test and after 90 and 180 minutes of bacterial cells contact with different hydrogel samples. * - significantly different from corresponding unmodified hydrogel CFU (AG0.6/PVA0.4) at p = 0.001.*

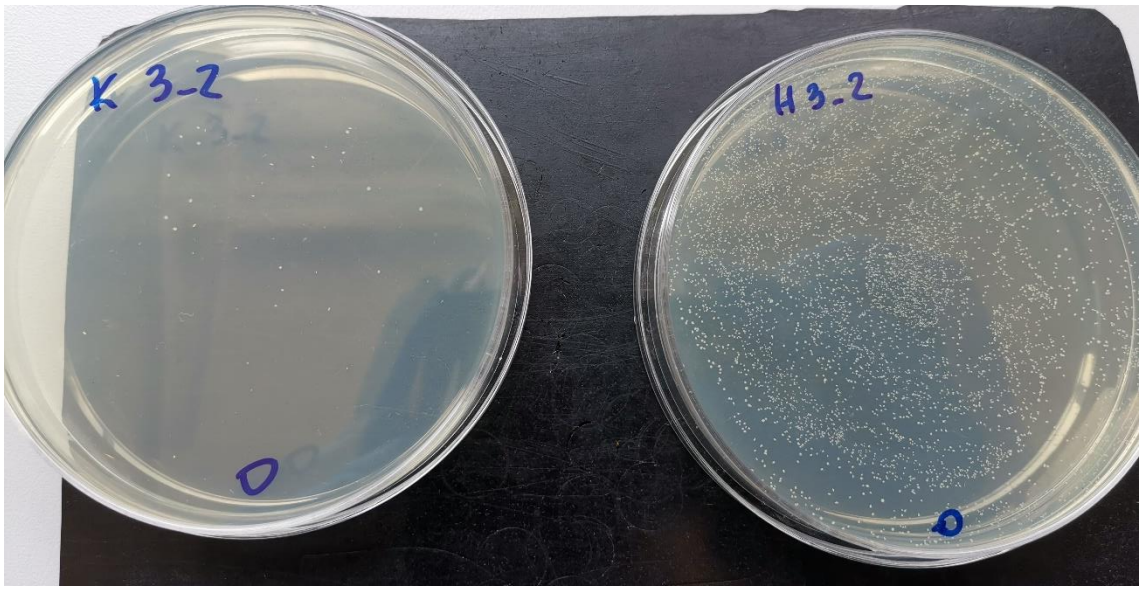


Figure 81 Visual comparison of the grown bacteria colonies from undiluted bacteria solution rinsed from the hydrogel surfaces after 3 hours of contact. On the left - AG0.6/PVA0.4/2.5CUR, on the right - AG0.6/PVA0.4.

9. Composite implant development

The synthesis of custom PU material in Chapter 6, structural optimization of 3D-printed geometries in Chapter 7 and the identification of candidate therapeutic hydrogel coatings in Chapter 8 concentrate into the development of a fully integrated biomedical construct. As demonstrated by the baseline evaluation in Chapter 7, conventional commercial filaments - even when designated as medical grade - can induce localized cytotoxicity, which severely restricts their suitability for prolonged internal tissue contact. To resolve these biological deficiencies, research described in Chapter 9 utilizes the custom synthesized aliphatic thermoplastic PU developed in Chapter 6 (specifically the HDI-based ET2:ET1:ES1 formulation synthesized with PTMEG, PEG and PCL, and modified at 1st stage of synthesis with Corhydron 25) to fabricate patient-specific nasal implant geometries. This tailored polyurethane matrix addresses the cytocompatibility issues of commercial alternatives while providing the compliance and elasticity required for nasal biomechanics. Building on this custom core, the selected AG0.6/PVA0.4/2.5CUR hydrogel from Chapter 8 is applied as a bioactive, antibacterial outer shell to engineer a biodegradable core-shell dual-delivery system. This structured architecture integrates the immediate localized antibacterial and anti-inflammatory activity of the curcumin-loaded hydrogel layer with the sustained release of the hydrocortisone from the underlying PU matrix. Chapter 9 details the fabrication and comprehensive *in vitro* testing of this composite device to validate the overall biocompatibility and therapeutic potential of these novel composite implants.

At first, the chosen PU was evaluated for suitability in FDM 3D printing of geometries, which can be useful in nasal surgeries. Based on the experiences from the nasal case-study presented in Chapter 7, five new models were prepared and printed. The comparison of the newly modelled printouts with the previously developed model is presented in Figure 82. Models 1 and 2 present the previously shown designs (implants based on the MRI scan of septum) with preserved width and height and adapted to surgical placement, respectively. Following consultation with an otolaryngologist, it became evident that a single device could not adequately address the diverse, highly specific needs of septal procedures. Consequently, the initial design was divided into two separate models to target fundamentally different aspects of nasal septum surgery. Model 3 was developed specifically for the partial replacement of septal cartilage, prepared by adjusting thickness and geometry to accurately mimic native tissue biomechanics, thereby ensuring structural stability and restoring natural airflow without adding excessive bulk. On the other hand, Model 4 was engineered to provide post-operative structural support and bacteriostatic protection following septoplasty. This design aims to replace traditional nasal packing (tamponades), which are notoriously painful for patients, restrict breathing and frequently cause mucosal trauma or secondary infections upon removal. The change in the infill pattern was dictated by the insufficient formation of the gyroid infill at such small thicknesses (1 mm), resulting in discontinuities and overall failure of prints. The infill density was experimentally adjusted to 60

% using triangular pattern, offering a good balance between the mechanical strength and ability to be perfused by hydrogel coating (Figure 83).

Models 5 and 6 represent an advanced iteration of the intrasinus stent concepts from Chapter 7, specifically tailored to the capabilities of FDM 3D printing through cylindrical and dome designs, respectively. These models directly address the difficulties in additive production of traditional stent types observed in the case study. Thus, transitioning these designs to an FDM-compatible framework was a necessary step to address the significant anatomical variability of patient sinus cavities. While traditional manufacturing (extrusion, injection and compression molding) limits the ability to produce complex, personalized geometries, FDM allows for the precise fabrication of these structures. Consequently, the cylindrical design can be optimized for robust structural support and drainage, while the dome design seamlessly conforms to natural sinus contours, ultimately preventing tissue damage and ensuring a superior, patient-specific fit.

Following the evaluation of model 4 efficacy as a septoplasty support structure, the research scope was expanded to explore the platform's utility beyond nasal applications (Figure 84). As the developed core-shell dual-delivery system demonstrates significant versatility in encapsulating and releasing active substances, it was necessary to test its adaptability across other critical medical domains where localized therapy is needed. As a natural evolution of this concept, porous structures were developed to serve as active substrates for wound dressings and surgical meshes. Model 7 retains the infill pattern of model 4 to guarantee optimal perfusion of the hydrogel coating, but its macroscopic geometry was adjusted to match standard wound dressing profiles. This adaptation is essential to ensure even distribution of therapeutics over a wound bed, providing mechanical protection while delivering sustained, localized antimicrobial therapy. For model 8, designed as a surgical mesh, the infill was changed to a honeycomb pattern. This structural modification was aimed at soft tissue repair, as it allows for greater multidirectional flexibility, accommodates easier suture placement and significantly reduces the risk of mesh migration or tissue shearing once secured. Finally, to address the complex clinical challenges of orthopedic repair, such as preventing deep-tissue infections and promoting integration, two additional models (models 9 and 10) were developed as compact and loose bone tissue implants. These models are flexible, drug-eluting scaffolds that can be tailored to fill irregular bone voids while actively supporting tissue regeneration.

The suitability of ET2:ET1:ES1 PU modified with Corhydron 25 for FDM 3D printing was successfully validated across all 10 designed model types. This comprehensive testing was necessary to confirm the material's structural versatility across a broad spectrum of clinical applications. The resulting prints exhibited highly accurate reproduction of complex geometries, precise dimensions and excellent surface quality, all of which are essential characteristics for ensuring proper patient fit and facilitating reliable hydrogel adhesion. Additionally, to confirm the scalability of this manufacturing approach, a batch of 36 model 4 implants was printed simultaneously, completing successfully in just 56 minutes (Figure 85). Proving this capacity for rapid batch production is a crucial step as it demonstrates that the proposed system is not only

biologically effective but also practically and economically feasible for real-world, on-demand medical manufacturing.



Figure 82 Comparison of implants models designed for usage as nasal implants: 1 – solid septum implant with supports for bending testing; 2 – previous prototype of porous nasal cartilage implant with supports for bending testing developed in Chapter 7; 3 – next iteration of porous nasal cartilage implant with reduced thickness; 4 – an implant designed to support the cartilage tissue of the nasal septum after surgery; 5, 6 – development of the concept of intrasinus stents from Chapter 7, adapted to the possibilities of FDM printing-cylindrical and dome designs, respectively.

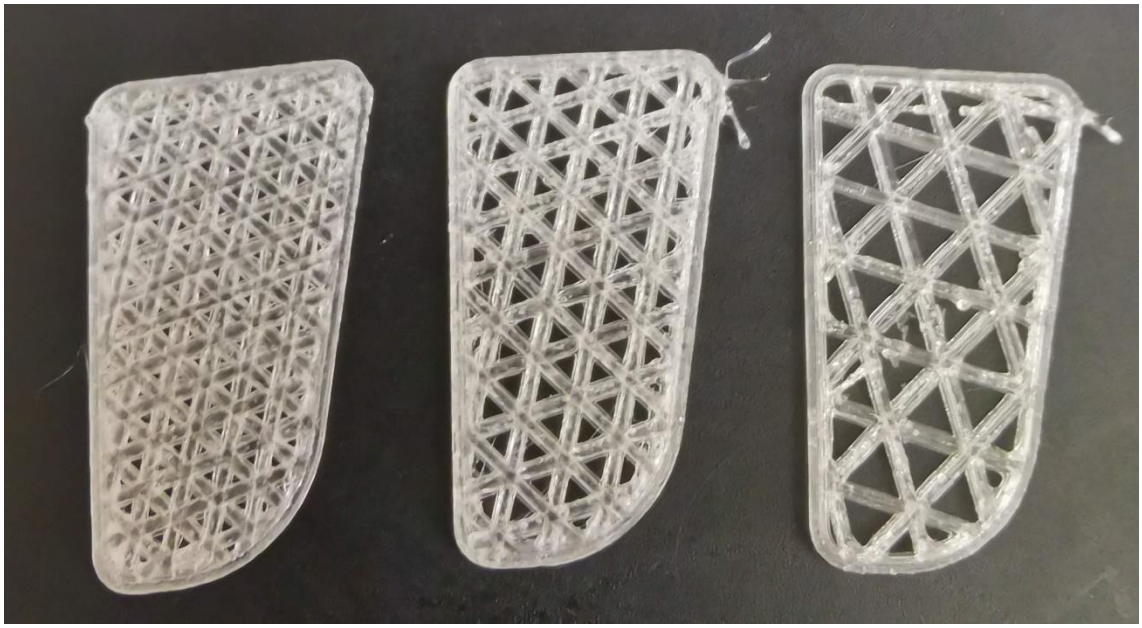


Figure 83 Comparison between different triangular infill density of design 4. From the left: 75, 60 and 45 %.

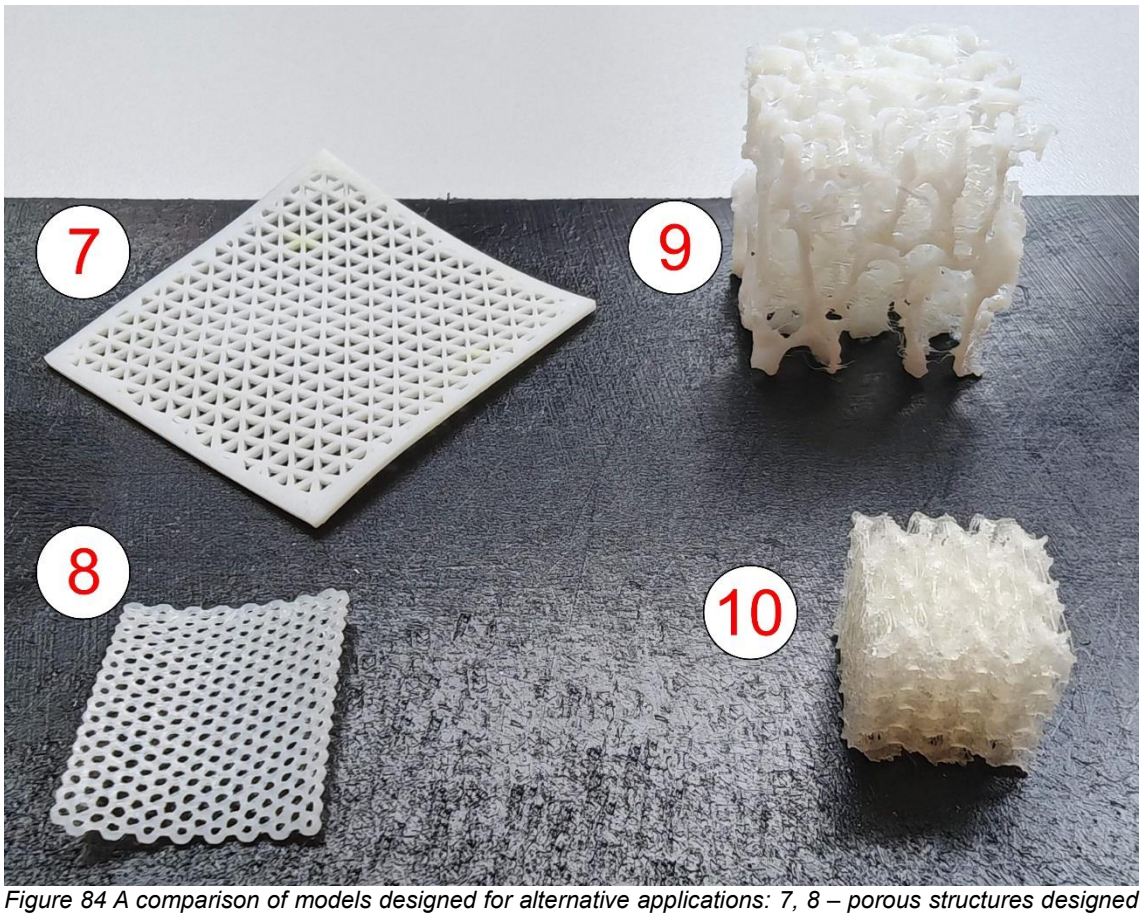
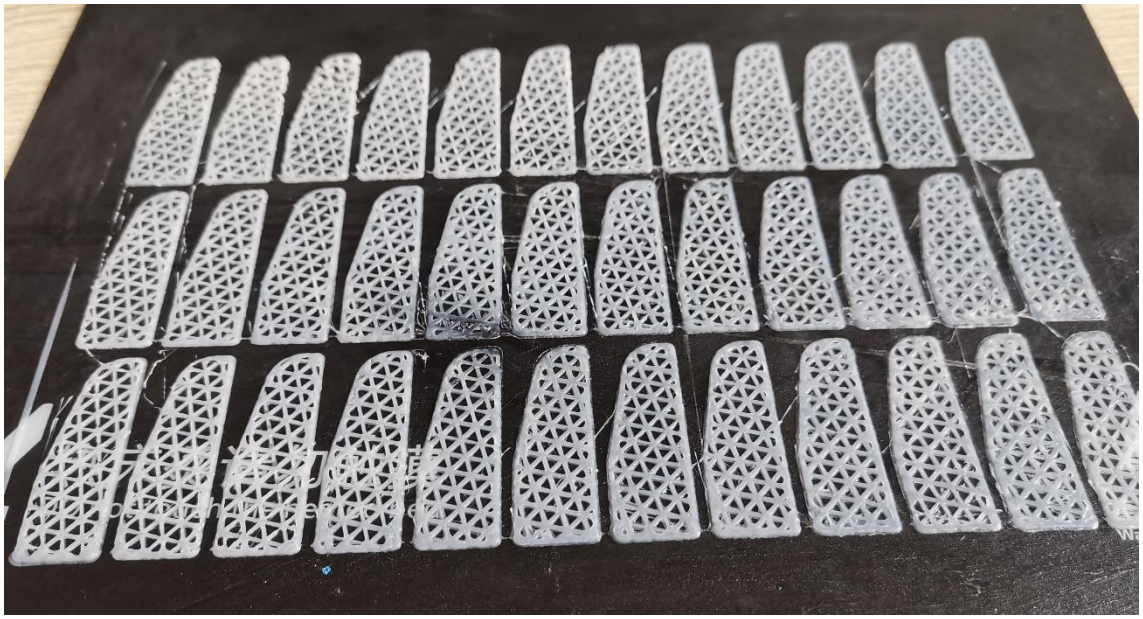


Figure 84 A comparison of models designed for alternative applications: 7, 8 – porous structures designed as substrates for wound dressings and surgical meshes, respectively; 9, 10 – flexible bone fillings (loose and compact, respectively).


Figure 85 Evaluation of batch printing of 36 model 4 implants using ET2:ET1:ES1 PU.

Finally, the complete biodegradable core-shell dual-delivery system based on ET2:ET1:ES1 PU and AG0.6/PVA0.4/2.5CUR was successfully fabricated. The 3D-printed PU constructs were dip-coated in a melted hydrogel maintained at approximately 55 °C. Controlling this specific temperature (previously optimized during preliminary hydrogel 3D printing tests) was essential to induce nearly instantaneous solidification of the hydrogel shell. Rapid gelation is a necessary processing step to prevent the liquid from dripping, thereby ensuring a highly uniform coating thickness across the entire implant, which is strictly required for predictable, controlled drug release kinetics. The resulting composite systems maintained their original geometries while demonstrating a smooth surface and a securely attached hydrogel layer (Figure 86). Furthermore, the process facilitated the penetration of curcumin deep into the PU structure (visible as the yellow coloration of the implant). This deep matrix penetration serves a vital clinical necessity: it embeds a fail-safe layer of antibacterial protection directly within the structural core, guaranteeing sustained therapeutic action even if the external gel layer detaches prematurely.

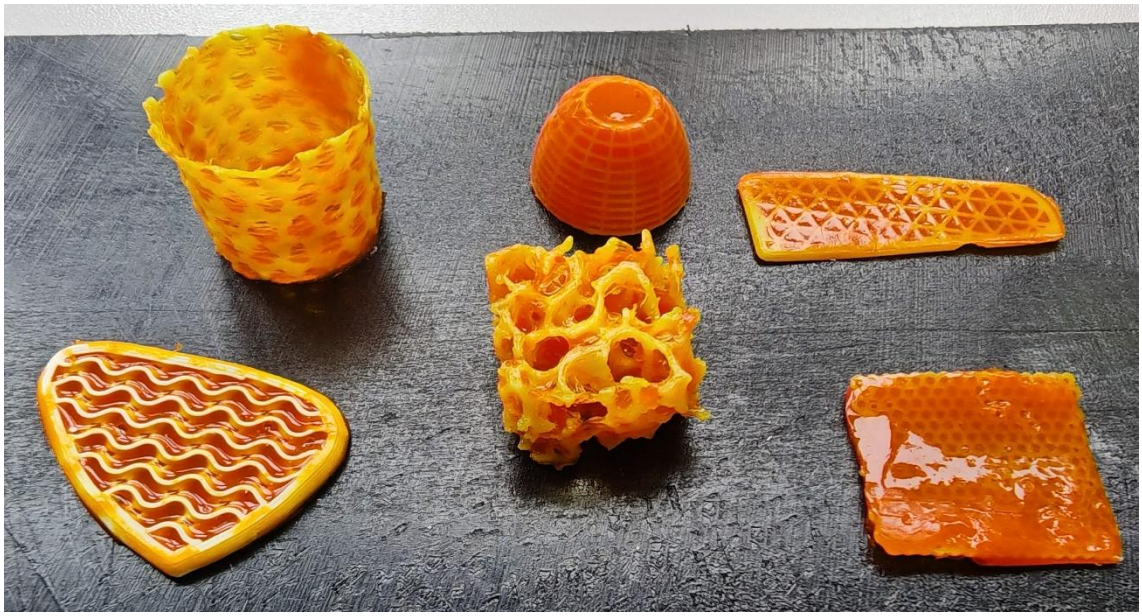


Figure 86 The compete biodegradable core-shell dual-delivery system based on ET2:ET1:ES1 PU modified with Corhydron 25 during 1st step of synthesis manufactured using models 3, 4, 5, 6 8 and 9 and coated with AG0.6/PVA0.4/2.5CUR hydrogel.

To verify the clinical usefulness of the complete composite delivery system, biocompatibility analysis was conducted. To do so, the ET2:ET1:ES1 PU modified with Corhydron 25, AG0.6/PVA0.4, AG0.6/PVA0.4/2.5CUR hydrogels and the composite release system were subjected to cytotoxicity study. Their extracts concentrations at 12.5%, 25%, 50% and 100% (v/v) were used to treat mouse fibroblasts L929 for 24 h and 48 h. The cytotoxic effect was evaluated using MTT assay.

First, the hydrogel formulations were tested (Figure 87). The AG0.6/PVA0.4 was found to be non-toxic to L929 mouse fibroblast cells at all tested extract concentrations after both 24 and 48 hours of incubation. Interestingly, at concentrations up to 50 %, a beneficial effect of the hydrogel extract was observed, as the cell viability was higher than corresponding control

(reaching up to 108.8 ± 2.9 %). Based on this study, the selected unmodified hydrogel can be considered biocompatible. In the case of the curcumin-modified hydrogel, it exhibited had no cytotoxic effect only at concentrations of 12.5 – 50 % after 24 hours and 12.5 – 25 % after 48 hours. After 48 h of exposing mouse fibroblasts to AG0.6/PVA0.4/2.5CUR extracts, the 50% concentration caused mild cytotoxicity, resulting in 65.4 ± 5.5 % viable cells. The 100 % extract concentration was found highly cytotoxic after both exposition times.

For the ET2:ET1:ES1 PU modified with Corhydron 25, the viability analysis showed that standalone PU extracts at all concentrations had no toxic effects on cells after both 24 and 48 hours of incubation (Figure 88). However, it must be noted that the 100 % extract after 48 h caused a decrease in cell viability to 70.2 %. This represents the lower acceptable limit of biocompatibility, since a reduction in cell viability of more than 30 %, in accordance with ISO 10993-5, is considered a cytotoxic effect. Based on this study, the selected PU can be considered biocompatible. The composite release system, based on the ET2:ET1:ES1 PU modified with Corhydron 25 covered with AG0.6/PVA0.4/2.5CUR hydrogel coating, was found to be non-toxic at all extract concentrations after 24 hours of incubation. However, a visible decrease of cell viability can be observed, falling to 73.38 ± 0.58 % after incubation with 100 % extract. After 48 h of exposure to the composite extracts containing curcumin, only 12.5 and 25 % extract concentrations remained non-toxic. The 50% concentration caused mild cytotoxicity, leaving 66.5% of viable cells, while the 100% extract reduced cell viability to 53.4% indicating moderate cytotoxicity.

Despite the observed cytotoxicity, it is important to underline that it was much less severe than both the standalone AG0.6/PVA0.4/2.5CUR hydrogel and the previously evaluated “medical-grade” Bioflex filament (Figure 66). The direct comparison of the presented results with the literature is difficult due to different approaches used for assessing the cytotoxicity of curcumin-modified materials. Some studies report cytotoxicity only in relation to cancer cells [407,408]. Other studies use direct contact method without specifying the contact area [409,410] or use extraction methods with significantly lower extraction ratios than required by ISO 10993-12 standard [406] or even unspecified ratios [411–413], reporting no cytotoxic effect of curcumin-modified hydrogels. Babaluei et al., who used a similar methodology to presented herein (although no specific extract concentration was provided), have tested carboxymethylcellulose/polyacrylamide/polydopamine hydrogels containing vitamin C and curcumin and reported the positive effect of curcumin on the cell viability [329]. These observations underline the need for transparent reporting of experimental conditions for sufficient discussion of obtained results. Considering the above, it can be concluded that the obtained material tested the concentration of extracts up to 50% exhibit similar cytocompatibility to the other hydrogels modified with curcumin reported in the literature. The observed dose- and time-dependent cytotoxic behavior aligns with the known dual biological nature of curcumin. While widely recognized for its cytoprotective, antioxidant and anti-inflammatory properties at lower concentrations, curcumin acts as a pro-oxidant at higher doses [408]. High local concentrations

of curcumin can induce the overproduction of intracellular reactive oxygen species (ROS), disrupt mitochondrial membrane potentials and ultimately trigger apoptosis in fibroblasts. In the standalone AG0.6/PVA0.4/2.5CUR hydrogel, a rapid release of curcumin likely exposes the cells to these toxic thresholds quickly. In the complete composite system, the structural interactions between the PU matrix and the hydrogel coating appear to modulate and slow the release kinetics. This controlled diffusion prevents the immediate accumulation of curcumin to highly cytotoxic levels, which explains the improved cell viability compared to the standalone curcumin hydrogel.

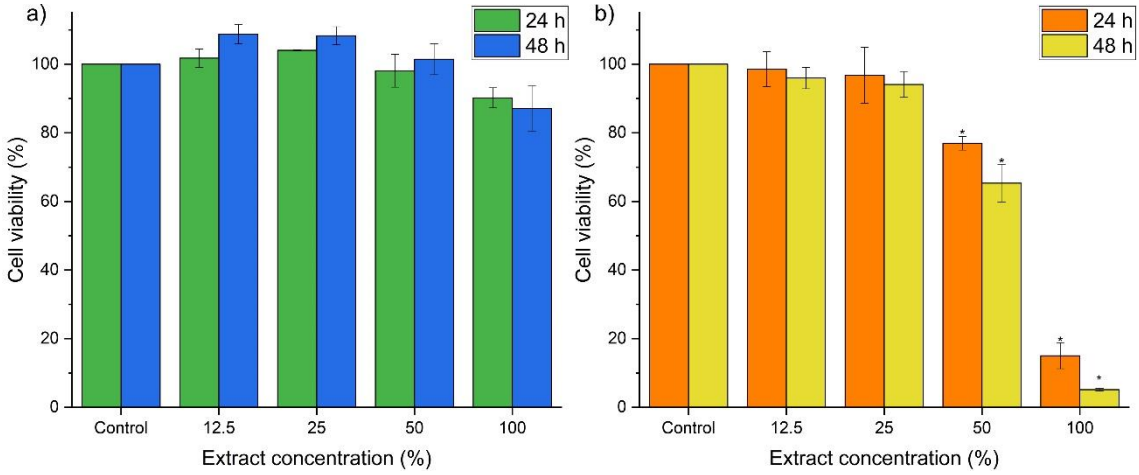


Figure 87 L-929 cell survival rates following a) AG0.6/PVA0.4 and b) AG0.6/PVA0.4/2.5CUR extract treatment. Statistical significance deviations were identified using a Tukey test at a 0.05 significance level and were denoted by asterisks (*) relative to the control group.

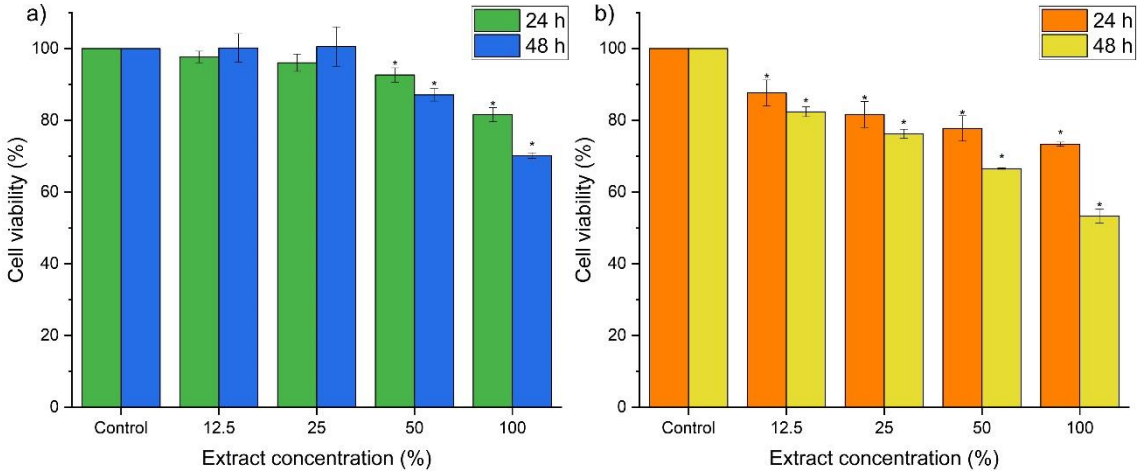


Figure 88 L-929 cell survival rates following ET2:ET1:ES1 PU modified with Corhydron 25 extract treatment: a) standalone PU, b) composite system with AG0.6/PVA0.4/2.5CUR hydrogel coating. Statistical significance deviations were identified using a Tukey test at a 0.05 significance level and were denoted by asterisks (*) relative to the control group.

10. Conclusions and future outlook

The development of custom biodegradable medical implants requires materials that mimic native tissue mechanics while actively supporting local tissue regeneration. Initial evaluations within this study confirmed that commercially available “medical grade” 3D printing filaments exhibit significant biological and functional limitations for mucosal contact applications, establishing a clear necessity for novel, tailored synthetic approaches. The sinonasal cavity is structurally heterogeneous and patient-specific, being composed of different tissue types, including rigid bone, viscoelastic cartilage, dynamic mucosal interfaces and localized lymphoid structures. Each of these tissues possesses unique physicochemical and biomechanical properties, which require particular attention and complicates scaffold matching. The tested filaments failed to address this anatomical diversity, as they mostly lacked the necessary elasticity needed to mimic human cartilage, while the most mechanically close (Bioflex) exhibited cytotoxicity, excluding its further application.

To address this gap, the primary aim of this dissertation was to design, synthesize and evaluate a biodegradable, dual-drug eluting implant system. Specifically, this system combined an aliphatic thermoplastic polyurethane matrix with a curcumin-loaded hydrogel coating to provide localized, sequential delivery of therapeutic agents. According to the current literature, this research represents the first attempt to design biodegradable implant for the simultaneous, sequential delivery of a corticosteroid and curcumin. This research fully accomplished its stated objectives through the successful fabrication and *in vitro* characterization of the proposed core-shell architecture. The synthesis phase yielded a custom aliphatic polyurethane (ET2:ET1:ES1) that demonstrates mechanical flexibility and precise compatibility with FDM manufacturing. Custom design and tailoring of the polyol mixture allowed for match the mechanical properties to human cartilage and achieve appropriate degradability, potentially enabling wound closure and new tissue growth before removing the mechanical support. Concurrently, the formulation of a water-based agar and poly(vinyl alcohol) hydrogel effectively stabilized hydrophobic curcumin without relying on toxic organic solvents.

The most significant findings confirm the hypothesis stated in this work: applying a curcumin-loaded, polymer-stabilized hydrogel coating to an aliphatic polyurethane core created a functional dual-delivery system capable of sequential active substance release. Additionally, the secondary hypothesis was also confirmed, as the composite implant provides immediate antibacterial action from the hydrogel shell alongside sustained hydrocortisone release from the degrading polyurethane core, without compromising the mechanical integrity or cytocompatibility of the implant. Furthermore, structural interactions between the core and the coating strictly modulate the release kinetics of curcumin. This controlled diffusion prevents the accumulation of curcumin to highly cytotoxic levels, maintaining cellular viability while ensuring continuous therapeutic action. Ultimately, this work demonstrates that tailored structural properties and

controlled active substance release offer a scalable, patient-specific alternative to standard postoperative administration methods.

Ideally, the reconstructions of human nasal septum should be performed with autologous cartilage grafts. However, due to its limited availability, it was hypothesized that evaluation of commercially available 3D printing materials could identify appropriate substitutes with applicable properties for this application. Initial survey concerning the type of suitable 3D printing manufacturing process highlighted significant limitations in utilizing FDM for complex, MRI-derived patient-specific geometries. While stereolithography yielded superior visual quality and accuracy, the tested SLA resin was proved to be too stiff and brittle for septal applications. On the other hand, FDM printing lacked the necessary precision for intricate designs and required support structures that were difficult to remove mechanically. This processing bottleneck directly influenced next research phases. To accommodate the inherent structural constraints of FDM while maintaining patient-specific utility, the implant geometries required adaptation into simplified, FDM-compatible designs, such as specific cylindrical and dome-shaped models capable of addressing sinus cavity variability. The mechanical analysis demonstrated that polyurethane-based commercial filaments, specifically Bioflex and TPU, offer compressive profiles that closely mimic native human septal cartilage within low-strain regions. However, the biological assessment revealed a critical shortcoming. Despite “medical-grade” designation, Bioflex exhibited moderate cytotoxicity, reducing cell viability significantly at 100% extract concentrations. Additionally, the study found that TPU failed to degrade in a phosphate-buffered saline environment, rendering it unsuitable for biodegradable implant applications. This baseline assessment confirmed that current off-the-shelf commercial filaments cannot satisfy the complex biological and structural requirements of reconstructive mucosal implants. These specific functional shortcomings provided a strong, validated rationale for the custom synthesis of biofunctionalized aliphatic polyurethanes tailored to precise medical applications.

Therefore, the research on the polyurethanes was based on the hypothesis that precisely tuning the soft segments within an aliphatic polyurethane core would yield a functional matrix capable of sustaining mechanical loads while degrading congruently with tissue regeneration. The primary novelty of this work lies in formulating a ternary polyol blend (ET2:ET1:ES1) utilizing poly(ethylene glycol), poly(tetramethylene ether) glycol and poly(ε-caprolactone). This specific composition resolves the trade-off between mechanical strength and hydrolytic susceptibility observed in single-polyol systems. A direct correlation was observed: formulations relying on PEG ether linkages promoted rapid degradation but lacked structural integrity, whereas PCL and PTMG provided high tensile strength but resisted degradation in physiological buffers. Mixing soft segments produced a synergistic effect, as the optimized ternary matrix achieved a tensile strength of 21.4 MPa alongside reliable elasticity, while maintaining a predictable, steady mass loss profile in different types of hydrolytic degradation environments. This structural balance allows the implant to provide physical support during early healing phases before safely degrading to prevent tissue overgrowth. Furthermore, the customized matrix accommodates both the direct

incorporation of a corticosteroid (hydrocortisone) during the polymerization phase and post-synthetical surface modification. The resulting structure facilitates the rapid, localized release of the active substance to suppress acute postoperative inflammation. By aligning the polymer degradation kinetics with the required therapeutic window and eliminating toxic aromatic byproducts, this custom aliphatic polyurethane provides a highly viable platform for advanced, patient-specific reconstructive devices.

Although the developed PU delivery system is compatible with hydrocortisone, other active substances, especially hydrophobic ones, cannot be easily incorporated into PU network. To further extend the possibilities of utilization PU-based materials in implants, the application of innovative hydrogel coatings acting as secondary drug delivery system of hydrophobic drugs was proposed. As the hydrogels are usually designed to be inherently hydrophilic, the research hypothesized that secondary polymers could act as interfacial mediators to stabilize hydrophobic active substances within a hydrophilic hydrogel network. Specifically, this work formulated aqueous agar-based bioinks containing poly(vinyl alcohol) and poly(vinylpyrrolidone) to encapsulate curcumin without employing toxic organic solvents. This green formulation strategy revealed structure-property correlations depending on the selected secondary polymer. Integrating PVA into the agar matrix (AG0.6/PVA0.4) induced significant intramolecular interactions, likely forming boron-curcumin chelate complexes and hydrogen bonds. Consequently, the AG/PVA/CUR hydrogels exhibited a visually distinct, deep red color and altered rheological properties, maintaining dominantly elastic behavior at physiological temperatures. Interestingly, pure agar networks demonstrated no significant chemical integration of curcumin, displaying simple physical dispersion of aggregates. These structural differences directly influence the swelling kinetics of the hydrogels. The enhanced chemical crosslinking in PVA-containing systems caused a nearly two-fold decrease in swelling capacity upon curcumin addition, alongside a faster rate of reaching equilibrium. In contrast, PVP-based hydrogels maintained their swelling behavior despite the introduction of the hydrophobic agent, suggesting that the non-swelling mass of curcumin compensated for a reduced crosslinking density. Apart from the primary design as the implant coating, the optimized AG0.6/PVA0.4 hydrogel exhibited favorable rheological properties opening the possibility of using them as bioinks for extrusion-based 3D bioprinting. The viability in this application was assessed using simplified setup with infusion pump and the resulting printouts were characterized with robust structural stability for layer-by-layer deposition. Furthermore, contact-based microbiological assays confirmed the time-dependent bactericidal efficacy of the curcumin-modified hydrogels, yielding an approximate 90% reduction in *Staphylococcus aureus* viability after 180 minutes. These findings validate the engineered hydrogel shell as a highly effective matrix for the immediate release of antibacterial agents in composite biomedical implants.

As proven during commercial 3D printing filaments evaluation, their biological and functional limitations establish a strict necessity for custom biomaterials in soft tissue reconstruction. Thus, the thesis evaluated the hypothesis that a dual-delivery composite system,

combining an aliphatic polyurethane core with a curcumin-loaded hydrogel shell, maintains mechanical integrity while preventing severe cytotoxicity. The findings represent the first documented application of a 3D-printed thermoplastic triple-polyol polyurethane coated with an active hydrogel for the sequential release of a corticosteroid and curcumin. This novel core-shell architecture demonstrates significant processing flexibility using FDM 3D printing, which was successfully used to manufacture the custom PU into ten distinct, patient-specific geometries, including porous wound dressings and robust bone scaffolds. A controlled dip-coating process ensured uniform hydrogel adhesion and deep matrix penetration. Structurally, this physical integration directly impacts the biological response. While rapid bursts of curcumin act as a pro-oxidant, the composite matrix modulates the diffusion rate, preventing the active substance from reaching highly toxic cellular thresholds. Consequently, the composite implant exhibits favorable cytocompatibility after 24 hours of cell proliferation, outperforming existing commercial alternatives and confirming its potential for safe, localized pharmacological delivery.

The current study validates the *in vitro* efficacy, dual-release pharmacokinetics and printability of the composite polyurethane-hydrogel system. Even though the proposed solution has its evident advantages, translating this technology to clinical patient care requires long-term, structured progression of *in vivo* evaluations and targeted formulation refinements. Future research must prioritize the optimization of the active substance concentrations within the hydrogel shell. *In vitro* testing indicated that prolonged exposure to high concentrations of curcumin induces a dose-dependent cytotoxic effect, resulting in unsatisfactory cell viability with extract concentrations higher than 50 %, after 48 hours of cell incubation. Consequently, following studies must identify the precise therapeutic window that balances robust antibacterial activity against pathogens like *Staphylococcus aureus* with the maintenance of high cytocompatibility. Simultaneously, the long-term pharmacokinetic profile of the core-shell architecture requires characterization under dynamic physiological conditions. Static *in vitro* models utilized in this work do not fully replicate the fluid shear, enzymatic activity and continuous environment changes and mechanical stress present within the human body. Future dynamic release studies should quantify both the *in vivo* antibacterial effect and the long-term elution of the encapsulated corticosteroid over several months. This analysis will verify whether the aliphatic polyurethane core provides a sustained anti-inflammatory response throughout the critical phases of tissue healing. Further material characterization must also track the long-term mechanical stability and degradation kinetics of the composite system at strict physiological parameters to align strictly with the rate of natural extracellular matrix deposition. A successful implant must provide temporary mechanical support that gradually yields as native cellular structures regenerate. Expanding the manufacturing capabilities constitutes another necessary step toward clinical implementation. While FDM accurately produced macroscale anatomical geometries, future research should optimize printing parameters to fabricate complex microscale architectures. Achieving higher print resolution may enable the development of perfusable porous networks, which typically promote vascularization and tissue integration within the implant. Finally, rigorous *in vivo* animal studies must synthesize these structural and pharmacological findings. These trials will assess the

localized foreign body response, measure systemic clearance of aliphatic degradation byproducts and evaluate *in situ* mechanical performance. Completing these translational steps will establish the safety and clinical viability of the dual-delivery composite system for personalized reconstructive surgery.

Beyond the immediate structural and pharmacological benefits, the clinical translation of this dual-drug eluting composite implant presents substantial pro-health and economic advantages, particularly regarding the optimization of post-operative care. Traditional reconstructive procedures often require prolonged hospitalization, repeated surgical interventions to remove non-degradable supports and systemic administration of antibiotics and anti-inflammatory drugs, which carry elevated risks of systemic toxicity and post-operative complications. By integrating localized, sustained delivery of hydrocortisone and curcumin directly at the surgical site, the developed composite dual-drug delivery system actively mitigates acute inflammation and prevents localized infections. This targeted therapeutic action can significantly accelerate tissue regeneration and reduce the risks associated with the traditional procedures, thereby facilitating a faster, safer transition to patient-oriented care. Consequently, shortening the required recovery periods translates directly to lowered overall treatment costs for healthcare systems and patients alike. Furthermore, the inherent biodegradability of the polyurethane-hydrogel system eliminates the clinical necessity and financial burden of secondary surgeries or procedures for implant removal. In addition, accessible FDM 3D printing for personalized manufacturing reduces reliance on expensive, mass-produced implants and minimizes intraoperative sizing adjustments. Accelerated healing, decreased surgical frequency, localized pharmacological intervention and design versatility of the presented implantable system all together fits into a broader trend of highly cost-effective, patient-oriented therapies in modern reconstructive medicine.

Overall, the findings of this dissertation can be summarized by its contribution to the fields of biomaterials and targeted drug delivery:

- **Development of a biodegradable core-shell dual-delivery system.** This research is the first described composite, biodegradable, implant utilizing custom-designed thermoplastic polyurethane core with a hydrogel shell for the simultaneous, sequential delivery of a corticosteroid and curcumin. The presented results confirm that such approach allows for both immediate antibacterial action and long-term anti-inflammatory therapy critically needed in postoperative care, ultimately reducing the recovery time, medical costs and improving the patients wellbeing.
- **Green formulation of hydrophobic drugs in aqueous inks.** The research introduces a novel, water-based method for incorporating hydrophobic curcumin into hydrophilic agar networks. In opposition to known formulation, usage of PVA and PVP as interfacial mediators allowed to compose hydrogel without usage organic solvents. Presented composite systems had the required water swelling, biocompatibility, printability and shape fidelity for biomedical applications.

- **Influence of processing on release kinetics.** The presented results show that simple dip-coating can be successfully implemented for creation of composite drug-eluting systems without compromising mechanical strength or degradation and drug elution profiles. However, achieving it required precise control on process parameters, which exact values were revealed in rheological assessment of the hydrogels.
- **Medical 3D printing.** This work reveals that some commercial “medical-grade” filaments possess significant biological and functional shortcomings for internal biomedical applications. Additionally, the available selection of elastic filaments and SLA resins suitable for medical applications is largely limited. It underlines the necessity for developing new elastic materials with controlled degradation and sufficient biocompatibility.

11. Scientific achievements

Table 20 Summary of scientific achievements

Parameter	Value
Publications in journals from JCR list	19
Publications in journals outside of JCR list	2
Summarized IF of publications	94.1
Book chapters	4
Scientific conferences participation	16
Patents	2
Patent applications	1
Total citations without self-citations	145
Hirsch index	7

Source: Scopus

List of publications:

- Nagórka, M., Zalewska-Piątek, B., Iwanicki, A., Wityk, P., Jakiela, S., Switlik, W., Bruździak, P., Wieczór, M., Liévin-Le Moal, V., Raczak-Gutknecht, J., **Gnatowski, P.**, Ficek, M., Łepek, A., Narajczyk, M., Piątek, R. (2026) Biophysical and functional characterization of the Escherichia coli Dr fimbrial envelope reveals its importance for pathogenesis and lithogenesis. PLOS Pathogens, 22 e1014588. https://doi.org/10.1371/journal.ppat.1014588. MNiSW: 140, IF: 4.9;
- Sitko, A., **Gnatowski, P.***, Piłat-Wójcik, E., Cieśliński, H., Kosmela, P., Rodak, A., Sienkiewicz, M., Kucińska-Lipka, J. (2025) Small-molecule modification of natural rubber latex: A step toward sustainable and compostable rubber products. Industrial Crops and Products, 236, 121885. https://doi.org/10.1016/j.indcrop.2025.121885. MNiSW: 200, IF: 6.2;
- Piłat, E., Krysiak, N., Gawrycka, P., **Gnatowski, P.**, Kucińska-Lipka, J. (2025) Hydrożelowe Okłady Łagodzące Objawy Migreny. Wiadomości Chemiczne, 79, 7-8. https://doi.org/10.53584/WIADCHEM.2025.07.6. MNiSW: 20;
- Chyzy, A., **Gnatowski, P.**, Piłat, E., Sienkiewicz, M., Wozniak, K., Wojnicka, M., Brzezinski, K., Plonska-Brzezinska, M. E. (2025) Formation and Characterization of Xylitol-Modified Glycidyl Methacrylate-co-Ethyl Methacrylate Matrices for Controlled Release of Antimicrobial Compounds. Molecules, 30, 3083, 10.3390/molecules30153083 MNiSW: 140, IF: 4.6;
- Zawadzka, O., **Gnatowski, P.***, Piłat, E., Kucińska-Lipka, J. (2025) Investigation on the Swelling Kinetics of Gelatin Based Hydrogels. Chemistry & Chemical Technology, 19, 259–269. https://doi.org/10.23939/chcht19.02.259. MNiSW:40, IF: 0.8;
- **Gnatowski, P.**, Ansariaghmiuni, M., Piłat, E., Poostchi, M., Kucińska-Lipka, J., Yazdi, M.K., Ryl, J., Ashrafizadeh, M., Mottaghitalab, F., Farokhi, M., Saeb, M.R., Bączek, T., Chen, C., Lu, Q. (2025) Hydrogel membranes in organ-on-a-chip devices: A review.

Colloids Surfaces B Biointerfaces 251, 114591. https://doi.org/10.1016/j.colsurfb.2025.114591. MNiSW:100, IF: 5.6;

- Gontarek-Castro, E., Pancielejko, A., Baluk, M.A., Kroczewska-Gnatowska, M., **Gnatowski, P.**, Matus, K., Łuczak, J., Zaleska-Medynska, A. (2025) Photocatalytic membranes based on Cu–NH2-MIL-125(Ti) protected by poly(vinylidene fluoride) for high and stable hydrogen production. Mater. Horizons 12, 1504–1515. https://doi.org/10.1039/D4MH01397B. MNiSW:200, IF: 10.7;
- Madineh, H., Mansourinia, F., Zarrintaj, P., Poostchi, M., **Gnatowski, P.***, Kucinska-Lipka, J., Ghaffari, M., Hasanin, M.S., Chapi, S., Yazdi, M.K., Ashrafizadeh, M., Bączek, T., Saeb, M.R., Wang, G. (2025) Stimuli-responsive delivery systems using carbohydrate polymers: A review. Int. J. Biol. Macromol. 310, 142648. https://doi.org/10.1016/j.ijbiomac.2025.142648. MNiSW:100, IF: 8.5;
- Piłat, E., **Gnatowski, P.**, Kurdyn, A., Cieśliński, H., Augustin, E., Kucińska-Lipka, J. (2025) Investigation of bioprintable modified agar-based hydrogels with antimicrobial properties. Int. J. Biol. Macromol. 289, 138707. https://doi.org/10.1016/j.ijbiomac.2024.138707. MNiSW:100, IF: 8.5;
- Szarlej, P., Piłat, E., **Gnatowski, P.***, Cieśliński, H., Sienkiewicz, M., Kucińska-Lipka, J. (2024) Investigation on Swelling of Agar-Based Antibacterial Hydrogels for Hard-To-Heal Wound Dressings. ChemMedChem. e202400042 https://doi.org/10.1002/cmdc.202400042. MNiSW:100, IF: 3.4;
- Sienkiewicz, M., **Gnatowski, P.**, Malus, M., Grzegórska, A., Ipakchi, H., Jouyandeh, M., Kucińska-Lipka, J., Navarro, F.J., Saeb, M.R. (2024) Eco-friendly modification of bitumen: The effects of rubber wastes and castor oil on the microstructure, processability and properties. J. Clean. Prod. 447, 141524. https://doi.org/10.1016/j.jclepro.2024.141524. MNiSW:140, IF: 10;
- Farahani, M.; **Gnatowski, P.**, Najafloo, R., Navaei, T., Piłat, E., Kucińska-Lipka, J., Saeb, M.R., & Mozafari, M. (2024) Enhancing diaphragmatic defect repair and regeneration: How biomaterials leading the way to progress? BMEMat 2, doi:10.1002/bmm2.12070. MNiSW: 5, IF: 15.5;
- **Gnatowski P.**, & Kucińska-Lipka J. (2023) Sustainable polymers targeted at the surgical and otolaryngological applications: Circularity and future. Polymers from Renewable Resources. 14, 289–302. https://doi.org/10.1177/20412479231200317. MNiSW:20;
- Razimowicz, M., **Gnatowski, P.**, Szarlej, P., Piłat, E., Sienkiewicz, M., & Kucińska-Lipka, J. (2023). Developing Materials for Biodegradable Otolaryngological Stents. Chemistry & Chemical Technology, 17, 24-34. https://doi.org/10.23939/chcht17.01.024. MNiSW:40, IF: 0.8;
- **Gnatowski, P.***, Gwizdała, K., Kurdyn, A., Skorek, A., Augustin, E., & Kucińska-Lipka, J. (2023). Investigation on Filaments for 3D Printing of Nasal Septum Cartilage Implant. Materials (Basel), 15, 3534. https://doi.org/10.3390/ma16093534. MNiSW:140, IF: 3.2;
- Gwizdała, K., Szarlej, P., **Gnatowski, P.**, Piłat, E., Sienkiewicz, M., & Kucińska-Lipka, J.

(2023). Determination of Liquid Detergent Pods as a Potential Microplastic Source. Chemistry & Chemical Technology, 17, 365-372. https://doi.org/10.23939/chcht17.02.365. MNiSW:40, IF: 0.8;

- **Gnatowski, P.**, Piłat, E., Kucińska-Lipka, J., Saeb, M., Hamblin, M. R., & Mozafari, M. (2023). Recent advances in 3D bioprinted tumor models for personalized medicine. Translational Oncology, 37, 101750. https://doi.org/10.1016/j.tranon.2023.101750. MNiSW:100, IF: 4.1;
- Carayon, I., Szarlej, P., **Gnatowski, P.***, Piłat, E., Sienkiewicz, M., Glinka, M., Karczewski, J., & Kucińska-Lipka, J. Polyurethane based hybrid ciprofloxacin-releasing wound dressings designed for skin engineering purpose. Adv. Med. Sci. 67, 269–282 (2022). MNiSW:100, IF: 2.6;
- Cemka, Z., Szarlej, P., Piłat, E., **Gnatowski, P.**, Sienkiewicz, M., & Kucińska-Lipka, J. (2022). Hydrogels Based on Natural Polymers for Cardiac Applications. Chemistry & Chemical Technology, 16, 564-572. https://doi.org/10.23939/chcht16.04.564. MNiSW:40, IF: 0.8;
- Szarlej, P., Carayon, I., **Gnatowski, P.**, Glinka, M., Mroczyńska, M., Brillowska-Dąbrowska, A., & Kucińska-Lipka, J. (2021) Composite Polyurethane-Polylactide (PUR/PLA) Flexible Filaments for 3D Fused Filament Fabrication (FFF) of Antibacterial Wound Dressings for Skin Regeneration. Materials (Basel). 14, 6054. https://doi.org/10.3390/ma14206054. MNiSW:140, IF: 3.2.

Book chapters:

- **Gnatowski, P.,** Pacler, M., Kucińska-Lipka, J. & Janik, H. Designing and 3D Printing of Polymer Stents for Chronic Sinusitis. in Advanced Polymer Structures Chemistry for Engineering Applications (eds. Mukbaniani, O., Tatrishvili, T. & Abadie, M. J. M.) (CRC Press, Taylor and Francis Group, Apple Academic Press), ISBN: 9781774913017, https://doi.org/10.1201/9781003352181;
- Kucińska-Lipka, J., Pacler, M., **Gnatowski, P.** & Janik, H. Polymer Stents Used in Chronic Sinusitis. in Advanced Polymer Structures Chemistry for Engineering Applications (eds. Mukbaniani, O., Tatrishvili, T. & Abadie, M. J. M.) (CRC Press, Taylor and Francis Group, Apple Academic Press), ISBN: 9781774913017, https://doi.org/10.1201/9781003352181;
- **Gnatowski P.,** Razimowicz M., Biotechnology in pharmaceutical and polymer industry. in Sustainable Water Treatment and Ecosystem Protection Strategies (eds. Tatrishvili, T.) (CRC Press, Taylor and Francis Group, Apple Academic Press), ISBN: 9781774915189, https://doi.org/10.1201/9781003470014;
- **Gnatowski P,** Gwizdala K, Piłat E, Kucińska-Lipka J. Polymers for burn dressings and skin substitutes. in Polymeric Materials for Biomedical Implants (eds. Sabu Thomas,

Abhimanyu Tharayil) (Woodhead Publishing, Elsevier Publications) ISBN: 9780323996907, https://doi.org/10.1016/B978-0-323-99690-7.00011-X.

Scientific conferences participation:

- 51st International Conference of the Slovak Society of Chemical Engineering, Slovak Society of Chemical Engineering, Jasna, Słowacja, 27-30.05.2025, poster, Biodegradable active substances release systems;
- 30th International Student Scientific Conference, Gdański Uniwersytet Medyczny, Gdańsk, Polska, 10-12.04.2025, poster, Agar-based hydrogels with antimicrobial properties;
- Sustainable approach to green transformation in polymer materials, TMBK Partners, Kielce, Polska, 22-23.05.2024, presentation, Biodegradable packaging made of thermoplastic starch: manufacturing and properties assessment;
- I Warszawskie Sympozjum Chemiczne, Uniwersytet Warszawski, Warszawa, Polska, 27-28.04.2024, poster, Kompostowalne tworzywa skrobiowe – charakterystyka właściwości;
- XX Scientifical-Technical Conference Engineering Polymers and Composites 2023, Stowarzyszenie Wychowanków Politechniki Śląskiej, Wisła, Polska, 24-27.10.2023, presentation, Zrównoważone podejście do odpadów z lateksu kauczuku naturalnego;
- XX Scientifical-Technical Conference Engineering Polymers and Composites 2023, Stowarzyszenie Wychowanków Politechniki Śląskiej, Wisła, Polska, 24-27.10.2023, presentation, Biodegradowalne systemy uwalniania leków oparte na poliuretanach;
- Zastosowanie sprzężonych metod analizy termicznej w badaniach materiałów, Department of Polymer Technlogoly, Faculty of Chemistry, Gdańsk University of Technology and NETZSCH company, Gdańsk, Polska, 15-16.02.2023, poster, Analiza termiczna filamentów przeznaczonych do druku 3D;
- Zastosowanie sprzężonych metod analizy termicznej w badaniach materiałów, Department of Polymer Technlogoly, Faculty of Chemistry, Gdańsk University of Technology and NETZSCH company, Gdańsk, Polska, 15-16.02.2023, poster, Analiza temperaturowa poliuretanów przeznaczonych do druku 3D;
- XIX Scientifical-Technical Conference Engineering Polymers and Composites 2022, Stowarzyszenie Wychowanków Politechniki Śląskiej, Ustroń, Polska, 25-28.10.2022, presentation, Biodegradowalne systemy uwalniania leków oparte na poliuretanach;
- XIX Scientifical-Technical Conference Engineering Polymers and Composites 2022, Stowarzyszenie Wychowanków Politechniki Śląskiej, Ustroń, Polska, 25-28.10.2022, presentation, Ekologiczne podejście w modyfikacji asfaltów;

- XI International Scientific-Technical Conference “Advance in Petroleum and Gas Industry and Petrochemistry” (APGIP-11), Lviv Polytechnic National University, Lviv, Ukraine, 16-20.05.2022, publication in conference materials, Modification of polyurethanes for applications in cardiac surgery;
- XI International Scientific-Technical Conference “Advance in Petroleum and Gas Industry and Petrochemistry” (APGIP-11), Lviv Polytechnic National University, Lviv, Ukraine, 16-20.05.2022, publication in conference materials, Determination of liquid detergent pods as an potential microplastic source;
- XI International Scientific-Technical Conference “Advance in Petroleum and Gas Industry and Petrochemistry” (APGIP-11), Lviv Polytechnic National University, Lviv, Ukraine, 16-20.05.2022, publication in conference materials, Developing materials for biodegradable otolaryngological stents;
- 7th International Caucasian Symposium on Polymers and Advanced Materials, Ivane Javakhishvili Tbilisi State University, Tibilisi, Georgia, 27-30.07.2021, publication in conference materials, Designing and 3D printing of polymer stents for chronic sinusitis;
- 23rd International Conference Materials, Methods & Technologies, International Scientific Events Bulgaria, Burgas, Bulgaria, 19-22.08.2021, poster, Biodegradable polyurethane materials;
- New Vistas in Chemical Research (NVCR-2021), Dwaraka Doss Goverdhan Doss Vainshnav College (Autonomus), e-conference, 27-28.01.2021, presentation, Novel Research on Biomedical Polyurethanes.

Patents:

- Lidia Jasinska-Walc, Robbert Duchateau, Miloud Bouyahyi, Nydia Badillo Sampedro, Maciej Sienkiewicz, Mateusz Malus, **Przemysław Gnatowski**, Johannes Peter Antonius Martens, „Modified bitumen comprising a compatibilizer, a compatibilizer and its use in asphalt, roofing or road applications”, patent no. US 12497513 B2.
- Maciej Sienkiewicz, Justyna Kucinska-Lipka, Robert Szwabis, Piotr Nadolski, Edyta Piłat, **Przemysław Gnatowski**, „Biodegradable protein-carbohydrate composition and method of obtaining it”, patent no. PL 249673 B1

Patent applications:

- Maciej Sienkiewicz, Justyna Kucinska-Lipka, Robert Szwabis, Piotr Nadolski, Edyta Piłat, **Przemysław Gnatowski**, „Biodegradable thermoplastic polymer composition and methods for its manufacture”, filed for protection with the Patent Office of the Republic of Poland on 11/11/2022 and assigned the number WO2024102010 (under the PCT system: PCT/PL2023/050092);

Cooperation with industry:

- Co-author of the project selected for co-financing under the European Funds for Western Pomerania 2021-2027 competition no. FEPZ.01.01-IZ.00/25 "PLASTPOMCoolBioPack - biodegradable container for dynamic cooling and protection of fruit freshness" (FEPZ.01.01-IZ.00-0011/25) with the company PPHU "PLASTPOM" BEATA SZWABIS;
- Co-author of the project selected for funding under the SMART Path, recruitment 1/2024 "BIO-LOPE - ecological biodegradable bubble envelope" (FENG.01.01-IP.02-0123/24) with the company Marcin Wojciechowski FHU MiM;
- Contractor in the NCBiR project, "Development and production of prototypes of ultra-light and safe road barrier bridges made of high-strength steel and an innovative assembly system together with their production technology" (POIR.01.01.01-00-0869/17) with Inter-Metal sp. z o. o.;
- Contractor in the implementation project (CTWT/02/12/2021/L) of patent EP 3064542 B1 with PlastPom sp. z o. o.;
- Contractor in „µGrant B+R dla przedsiębiorstw" 036354 project „Doskonalenie wynalazku PL/EP 3395563 pn. Wielowarstwowa syntetyczno-mineralna wykładzina ochronno-wyrównawcza i/lub uszczelniająca (dostępna na rynku pod nazwą Solidmat)" with GDA sp. z o.o.;
- Contractor in „µGrant B+R dla przedsiębiorstw" 036635 project „Opracowanie prototypu mieszanki lateksu kauczuku naturalnego o zmniejszonym wpływie na środowisko i oceny możliwości zastosowania go w produkcji cienkościennych wyrobów lateksowych" with BELBAL sp. z o.o..

Other achievements:

- IDUB Francium Supporting Outstanding Doctoral Candidates 2022/2023 scholarship in Gdańsk University of Technology;
- PhD student position in the project Opus 18 UMO-2019/35/B/NZ7/04394 „Intensive rearing of poultry - identification of changes occurring in the environment and their impact on human health" in 2021-2022;
- Member of the School Council at the Gdańsk University of Technology in 2022-2024.

12. References

[1] M. Vert, Y. Doi, K.-H. Hellwich, M. Hess, P. Hodge, P. Kubisa, M. Rinaudo, F. Schué, Terminology for biorelated polymers and applications (IUPAC Recommendations 2012), Pure Appl. Chem. 84 (2012) 377–410. https://doi.org/10.1351/PAC-REC-10-12-04.

[2] Y. Zhuo, Y.-G. Zhao, Y. Zhang, Enhancing Drug Solubility, Bioavailability, and Targeted Therapeutic Applications through Magnetic Nanoparticles, Molecules 29 (2024) 4854. https://doi.org/10.3390/molecules29204854.

[3] T.C. Ezike, U.S. Okpala, U.L. Onoja, C.P. Nwike, E.C. Ezeako, O.J. Okpara, C.C. Okoroafor, S.C. Eze, O.L. Kalu, E.C. Odoh, U.G. Nwadike, J.O. Ogbodo, B.U. Umeh, E.C. Ossai, B.C. Nwanguma, Advances in drug delivery systems, challenges and future directions, Heliyon 9 (2023) e17488. https://doi.org/10.1016/j.heliyon.2023.e17488.

[4] M.S. Alqahtani, M. Kazi, M.A. Alsenaidy, M.Z. Ahmad, Advances in Oral Drug Delivery, Front. Pharmacol. 12 (2021) 618411. https://doi.org/10.3389/fphar.2021.618411.

[5] V.P. Chavda, N.R. Gogoi, D.A. Vaghela, P.C. Balar, S. Dawre, D.J. Dave, Parenteral microemulsions for drug delivery: Advances and update, J. Drug Deliv. Sci. Technol. 89 (2023) 104991. https://doi.org/10.1016/j.jddst.2023.104991.

[6] A.J. Hickey, Emerging trends in inhaled drug delivery, Adv. Drug Deliv. Rev. 157 (2020) 63–70. https://doi.org/10.1016/j.addr.2020.07.006.

[7] S.S. Gaikwad, A.L. Zanje, J.D. Somwanshi, Advancements in transdermal drug delivery: A comprehensive review of physical penetration enhancement techniques, Int. J. Pharm. 652 (2024) 123856. https://doi.org/10.1016/j.ijpharm.2024.123856.

[8] K. Huanbutta, V. Puri, A. Sharma, I. Singh, P. Sriamornsak, T. Sangnim, Rise of implantable drugs: A chronicle of breakthroughs in drug delivery systems, Saudi Pharm. J. 32 (2024) 102193. https://doi.org/10.1016/j.jsps.2024.102193.

[9] V. Chernonosova, A. Gostev, I. Murashov, B. Chelobanov, A. Karpenko, P. Laktionov, Assessment of Electrospun Pellethane-Based Scaffolds for Vascular Tissue Engineering, Materials 14 (2021) 3678. https://doi.org/10.3390/ma14133678.

[10] J.C. Audifred-Aguilar, V.H. Pino-Ramos, E. Bucio, Synthesis and characterization of hydrophilically modified Tecoflex® polyurethane catheters for drug delivery, Mater. Today Commun. 26 (2021) 101894. https://doi.org/10.1016/j.mtcomm.2020.101894.

[11] X. Lv, Z. Li, H. Wei, S. Yuan, X. Fu, Z. Li, Preparation of Low-Leachable and Nonhemolytic Antibacterial Thermoplastic Polyurethanes from Synthetic Cationic Polyesters Containing Quaternary Ammonium Salts, ACS Appl. Mater. Interfaces 17 (2025) 47521–47531. https://doi.org/10.1021/acsami.5c11390.

[12] L. Nguyen, L.-C. Xu, E. Yeager, W.J. Weiss, C.A. Siedlecki, In vitro evaluation of blood plasma coagulation responses to four medical-grade polyurethane polymers, J. Biomater. Appl. 38 (2023) 302–310. https://doi.org/10.1177/08853282231191410.

[13] X. Jin, J. Dong, X. Guo, M. Ding, R. Bao, Y. Luo, Current advances in polyurethane biodegradation, Polym. Int. 71 (2022) 1384–1392. https://doi.org/10.1002/pi.6360.

[14] A. Das, P. Mahanwar, A brief discussion on advances in polyurethane applications, Adv. Ind. Eng. Polym. Res. 3 (2020) 93–101. https://doi.org/10.1016/j.aiepr.2020.07.002.

[15] P. Szarlej, I. Carayon, P. Gnatowski, M. Glinka, M. Mroczyńska, A. Brillowska-Dąbrowska, J. Kucińska-Lipka, Composite Polyurethane-Polylactide (PUR/PLA) Flexible Filaments for 3D Fused Filament Fabrication (FFF) of Antibacterial Wound Dressings for Skin Regeneration, Materials 14 (2021) 6054. https://doi.org/10.3390/ma14206054.

[16] S. McMahan, A. Taylor, K.M. Copeland, Z. Pan, J. Liao, Y. Hong, Current advances in biodegradable synthetic polymer based cardiac patches, J. Biomed. Mater. Res. A 108 (2020) 972–983. https://doi.org/10.1002/jbm.a.36874.

[17] M. Dong, D. Jiao, Q. Zheng, Z.L. Wu, Recent progress in fabrications and applications of functional hydrogel films, J. Polym. Sci. 61 (2023) 1026–1039. https://doi.org/10.1002/pol.20220451.

[18] S. Correa, A.K. Grosskopf, H. Lopez Hernandez, D. Chan, A.C. Yu, L.M. Stapleton, E.A. Appel, Translational Applications of Hydrogels, Chem. Rev. 121 (2021) 11385–11457. https://doi.org/10.1021/acs.chemrev.0c01177.

[19] P. Gnatowski, J. Kucińska-Lipka, Sustainable polymers targeted at the surgical and otolaryngological applications: Circularity and future, Polym. Renew. Resour. 14 (2023) 289–302. https://doi.org/10.1177/20412479231200317.

[20] P. Gnatowski, K. Gwizdała, E. Piłat, J. Kucińska-Lipka, Polymers for burn dressings and skin substitutes, in: Polym. Mater. Biomed. Implants, Elsevier, 2024: pp. 319–336. https://doi.org/10.1016/B978-0-323-99690-7.00011-X.
[21] H. Madineh, F. Mansourinia, P. Zarrintaj, M. Poostchi, P. Gnatowski, J. Kucinska-Lipka, M. Ghaffari, M.S. Hasanin, S. Chapi, M.K. Yazdi, M. Ashrafizadeh, T. Bączek, M.R. Saeb, G. Wang, Stimuli-responsive delivery systems using carbohydrate polymers: A review, Int. J. Biol. Macromol. 310 (2025) 142648. https://doi.org/10.1016/j.ijbiomac.2025.142648.
[22] M. Farahani, P. Gnatowski, R. Najafloo, T. Navaei, E. Piłat, J. Kucińska-Lipka, M.R. Saeb, M. Mozafari, Enhancing diaphragmatic defect repair and regeneration: How biomaterials leading the way to progress?, BMEMat 2 (2024) e12070. https://doi.org/10.1002/bmm2.12070.
[23] P. Gnatowski, M. Ansariaghmiuni, E. Piłat, M. Poostchi, J. Kucińska-Lipka, M.K. Yazdi, J. Ryl, M. Ashrafizadeh, F. Mottaghitalab, M. Farokhi, M.R. Saeb, T. Bączek, C. Chen, Q. Lu, Hydrogel membranes in organ-on-a-chip devices: A review, Colloids Surf. B Biointerfaces 251 (2025) 114591. https://doi.org/10.1016/j.colsurfb.2025.114591.
[24] P. Gnatowski, M. Pacler, J. Kucińska-Lipka, H. Janik, Designing and 3d Printing of Polymer Stents for Chronic Sinusitis, in: O. Mukbaniani, T. Tatrishvili, M.J.M. Abadie (Eds.), Adv. Polym. Struct. Chem. Eng. Appl., Apple Academic Press, 2023.
[25] M. Razimowicz, P. Gnatowski, P. Szarlej, E. Piłat, M. Sienkiewicz, J.K. Kucińska-Lipka, Developing Materials for Biodegradable Otolaryngological Stents, Chem. Chem. Technol. 17 (2023) 24–34. https://doi.org/10.23939/chcht17.01.024.
[26] P. Gnatowski, K. Gwizdała, A. Kurdyn, A. Skorek, E. Augustin, J. Kucińska-Lipka, Investigation on Filaments for 3D Printing of Nasal Septum Cartilage Implant, Materials 16 (2023) 3534. https://doi.org/10.3390/ma16093534.
[27] S. Iqbal, M. Sohail, S. Fang, J. Ding, L. Shen, M. Chen, G. Shu, Y.-Z. Du, J. Ji, Biomaterials evolution: from inert to instructive, Biomater. Sci. 11 (2023) 6109–6115. https://doi.org/10.1039/D3BM00322A.
[28] M. Oleksy, K. Dynarowicz, D. Aebisher, Advances in Biodegradable Polymers and Biomaterials for Medical Applications—A Review, Molecules 28 (2023) 6213. https://doi.org/10.3390/molecules28176213.
[29] U. Breine, P.-I. Brånemark, Reconstruction of Alveolar Jaw Bone, Scand. J. Plast. Reconstr. Surg. 14 (1980) 23–48. https://doi.org/10.3109/02844318009105733.
[30] A.S. Hoffman, Introduction: The Diversity and Versatility of Biomaterials, in: Biomater. Sci., Elsevier, 2013: pp. 63–64. https://doi.org/10.1016/B978-0-08-087780-8.00007-3.
[31] E. Ascalone, S.M.S. Sajjadi (eds.), Excavations and Researches at Shahr-i Sokhta, Iranian Center for Archaeological Research, Pishin Pajouh, Tehran, 2022.
[32] R.J. Forbes, Bitumen and Petroleum in Antiquity, E.J. Brill, Leiden, 1936.
[33] C. T. Ambrose, The Conquest of Pus -- a History of Bitumen, Creosote and Carbolic Acid, J. Anc. Dis. Prev. Remedies 06 (2018). https://doi.org/10.4172/2329-8731.1000179.
[34] C. Montoya, Y. Du, A.L. Gianforcaro, S. Orrego, M. Yang, P.I. Lelkes, On the road to smart biomaterials for bone research: definitions, concepts, advances, and outlook, Bone Res. 9 (2021) 12. https://doi.org/10.1038/s41413-020-00131-z.
[35] J.B. Shah, The History of Wound Care, J. Am. Coll. Certif. Wound Spec. 3 (2011) 65–66. https://doi.org/10.1016/j.jcws.2012.04.002.
[36] S. Dumitriu, ed., Polymeric Biomaterials, Revised and Expanded, 0 ed., CRC Press, 2001. https://doi.org/10.1201/9780203904671.
[37] V.J. Vogel, American Indian medicine, 1. paperback print, Univ. of Oklahoma Press, Norman, Okla., 1990.
[38] J.A. Calzonetti, C.J. Laursen, Patents of Charles Goodyear: his international contributions to the rubber industry, Rubber Chem. Technol. 83 (2010) 303–321. https://doi.org/10.5254/1.3525687.
[39] D.R. Ownby, A history of latex allergy, J. Allergy Clin. Immunol. 110 (2002) S27–S32. https://doi.org/10.1067/mai.2002.125336.
[40] J.B. Park, Biomaterials Science and Engineering, Springer US, Boston, MA, 1984. https://doi.org/10.1007/978-1-4613-2769-1.
[41] E.T.J. Chong, J.W. Ng, P.-C. Lee, Classification and Medical Applications of Biomaterials–A Mini Review, BIO Integr. 4 (2023). https://doi.org/10.15212/bioi-2022-0009.
[42] A.G. Tyers, J.R. Collin, Baseball orbital implants: a review of 39 patients., Br. J. Ophthalmol. 69 (1985) 438–442. https://doi.org/10.1136/bjo.69.6.438.

[43] O. Aryasit, D.S. Ng, A.S.C. Goh, K.I. Woo, Y.-D. Kim, Delayed onset porous polyethylene implant-related inflammation after orbital blowout fracture repair: four case reports, BMC Ophthalmol. 16 (2016) 94. https://doi.org/10.1186/s12886-016-0287-0.
[44] R. Sridharan, A.R. Cameron, D.J. Kelly, C.J. Kearney, F.J. O'Brien, Biomaterial based modulation of macrophage polarization: a review and suggested design principles, Mater. Today 18 (2015) 313–325. https://doi.org/10.1016/j.mattod.2015.01.019.
[45] S. Nag, S. Mohanto, M.G. Ahmed, V. Subramaniyan, "Smart" stimuli-responsive biomaterials revolutionizing the theranostic landscape of inflammatory arthritis, Mater. Today Chem. 39 (2024) 102178. https://doi.org/10.1016/j.mtchem.2024.102178.
[46] L.L. Hench, The story of Bioglass®, J. Mater. Sci. Mater. Med. 17 (2006) 967–978. https://doi.org/10.1007/s10856-006-0432-z.
[47] E. Marin, F. Boschetto, G. Pezzotti, Biomaterials and biocompatibility: An historical overview, J. Biomed. Mater. Res. A 108 (2020) 1617–1633. https://doi.org/10.1002/jbm.a.36930.
[48] W. Cao, L.L. Hench, Bioactive materials, Ceram. Int. 22 (1996) 493–507. https://doi.org/10.1016/0272-8842(95)00126-3.
[49] S. Arango-Santander, Bioinspired Topographic Surface Modification of Biomaterials, Materials 15 (2022) 2383. https://doi.org/10.3390/ma15072383.
[50] R.K. Kulkarni, Polylactic Acid for Surgical Implants, Arch. Surg. 93 (1966) 839. https://doi.org/10.1001/archsurg.1966.01330050143023.
[51] G.I. Peterson, A.V. Dobrynin, M.L. Becker, Biodegradable Shape Memory Polymers in Medicine, Adv. Healthc. Mater. 6 (2017) 1700694. https://doi.org/10.1002/adhm.201700694.
[52] J. Kurowiak, T. Klekiel, R. Będziński, Biodegradable Polymers in Biomedical Applications: A Review—Developments, Perspectives and Future Challenges, Int. J. Mol. Sci. 24 (2023) 16952. https://doi.org/10.3390/ijms242316952.
[53] E. Liverani, G. Rogati, S. Pagani, S. Brogini, A. Fortunato, P. Caravaggi, Mechanical interaction between additive-manufactured metal lattice structures and bone in compression: implications for stress shielding of orthopaedic implants, J. Mech. Behav. Biomed. Mater. 121 (2021) 104608. https://doi.org/10.1016/j.jmbbm.2021.104608.
[54] K. Athanasiou, C. Agrawal, F. Barber, S. Burkhart, Orthopaedic applications for PLA-PGA biodegradable polymers, Arthrosc. J. Arthrosc. Relat. Surg. 14 (1998) 726–737. https://doi.org/10.1016/S0749-8063(98)70099-4.
[55] K.Y. Lee, D.J. Mooney, Alginate: Properties and biomedical applications, Prog. Polym. Sci. 37 (2012) 106–126. https://doi.org/10.1016/j.progpolymsci.2011.06.003.
[56] H. Yadav, R. Malviya, N. Kaushik, Chitosan in biomedicine: A comprehensive review of recent developments, Carbohydr. Polym. Technol. Appl. 8 (2024) 100551. https://doi.org/10.1016/j.carpta.2024.100551.
[57] J.E. Davies, Bone bonding at natural and biomaterial surfaces, Biomaterials 28 (2007) 5058–5067. https://doi.org/10.1016/j.biomaterials.2007.07.049.
[58] A.J. Domb, N. Kumar, A. Ezra, eds., Biodegradable Polymers in Clinical Use and Clinical Development, 1st ed., Wiley, 2011. https://doi.org/10.1002/9781118015810.
[59] H. Xing, H. Lee, L. Luo, T.R. Kyriakides, Extracellular matrix-derived biomaterials in engineering cell function, Biotechnol. Adv. 42 (2020) 107421. https://doi.org/10.1016/j.biotechadv.2019.107421.
[60] L. Abdulsalam, S. Abubakar, I. Permatasari, A.A. Lawal, S. Uddin, S. Ullah, I. Ahmad, Advanced Biocompatible and Biodegradable Polymers: A Review of Functionalization, Smart Systems, and Sustainable Applications, Polymers 17 (2025) 2901. https://doi.org/10.3390/polym17212901.
[61] L.A. Smith Callahan, S. Xie, I.A. Barker, J. Zheng, D.H. Reneker, A.P. Dove, M.L. Becker, Directed differentiation and neurite extension of mouse embryonic stem cell on aligned poly(lactide) nanofibers functionalized with YIGSR peptide, Biomaterials 34 (2013) 9089–9095. https://doi.org/10.1016/j.biomaterials.2013.08.028.
[62] E.A. Silantyeva, R.K. Willits, M.L. Becker, Postfabrication Tethering of Molecular Gradients on Aligned Nanofibers of Functional Poly(ε-caprolactone)s, Biomacromolecules 20 (2019) 4494–4501. https://doi.org/10.1021/acs.biomac.9b01264.
[63] Q. Chen, D. Zhang, W. Zhang, H. Zhang, J. Zou, M. Chen, J. Li, Y. Yuan, R. Liu, Dual mechanism β-amino acid polymers promoting cell adhesion, Nat. Commun. 12 (2021) 562. https://doi.org/10.1038/s41467-020-20858-x.
[64] K. Ceonzo, A. Gaynor, L. Shaffer, K. Kojima, C.A. Vacanti, G.L. Stahl, Polyglycolic Acid-Induced Inflammation: Role of Hydrolysis and Resulting Complement Activation, Tissue Eng. 12 (2006) 301–308. https://doi.org/10.1089/ten.2006.12.301.

[65] D. Wienen, T. Gries, S.L. Cooper, D.E. Heath, An overview of polyurethane biomaterials and their use in drug delivery, J. Controlled Release 363 (2023) 376–388. https://doi.org/10.1016/j.jconrel.2023.09.036.
[66] Z. Feng, D. Wang, Y. Zheng, L. Zhao, T. Xu, Z. Guo, M. Irfan Hussain, J. Zeng, L. Lou, Y. Sun, H. Jiang, A novel waterborne polyurethane with biodegradability and high flexibility for 3D printing, Biofabrication 12 (2020) 035015. https://doi.org/10.1088/1758-5090/ab7de0.
[67] X. Zhang, F. Dong, M. Yu, X. Xu, H. Liu, H. Lu, Multifunctional waterborne polyurethane-cellulose nanofiber composite: Realizing ultrarobust, photoluminescence and swift self-healing via multi-dynamic bonding, Chem. Eng. J. 507 (2025) 160302. https://doi.org/10.1016/j.cej.2025.160302.
[68] Z. Feng, Y. Zheng, L. Zhao, Z. Zhang, Y. Sun, K. Qiao, Y. Xie, Y. Wang, W. He, An ultrasound-controllable release system based on waterborne polyurethane/chitosan membrane for implantable enhanced anticancer therapy, Mater. Sci. Eng. C 104 (2019) 109944. https://doi.org/10.1016/j.msec.2019.109944.
[69] X. Xu, A.K. Jha, D.A. Harrington, M.C. Farach-Carson, X. Jia, Hyaluronic acid-based hydrogels: from a natural polysaccharide to complex networks, Soft Matter 8 (2012) 3280. https://doi.org/10.1039/c2sm06463d.
[70] S.A. Bencherif, A. Srinivasan, F. Horkay, J.O. Hollinger, K. Matyjaszewski, N.R. Washburn, Influence of the degree of methacrylation on hyaluronic acid hydrogels properties, Biomaterials 29 (2008) 1739–1749. https://doi.org/10.1016/j.biomaterials.2007.11.047.
[71] Z. Peng, H. Xue, X. Liu, S. Wang, G. Liu, X. Jia, Z. Zhu, M.J. Orvy, Y. Yang, Y. Wang, D. Zhang, L. Tong, Tough, adhesive biomimetic hyaluronic acid methacryloyl hydrogels for effective wound healing, Front. Bioeng. Biotechnol. 11 (2023) 1222088. https://doi.org/10.3389/fbioe.2023.1222088.
[72] Z. Po, M. Xiao, Z. Han, L. Yang, Z. Liang, B. Yanchi, W. YiHu, S. Zhan, W. Jian, J. Fan, Z. Xuesai, Y. Yizhi, X. Xiao, Y. Tengbo, Bioactive multifunctional hydrogel to ameliorate adverse joint microenvironment and enhance cartilage regeneration, Chem. Eng. J. 515 (2025) 163554. https://doi.org/10.1016/j.cej.2025.163554.
[73] I.M. Savić Gajić, I.M. Savić, Z. Svirčev, Preparation and Characterization of Alginate Hydrogels with High Water-Retaining Capacity, Polymers 15 (2023) 2592. https://doi.org/10.3390/polym15122592.
[74] B. Zhu, H. Yin, Alginate lyase: Review of major sources and classification, properties, structure-function analysis and applications, Bioengineered 6 (2015) 125–131. https://doi.org/10.1080/21655979.2015.1030543.
[75] R.M. Desai, S.T. Koshy, S.A. Hilderbrand, D.J. Mooney, N.S. Joshi, Versatile click alginate hydrogels crosslinked via tetrazine–norbornene chemistry, Biomaterials 50 (2015) 30–37. https://doi.org/10.1016/j.biomaterials.2015.01.048.
[76] A. Román-Guerrero, S. Cortés-Camargo, E. Alpizar-Reyes, M.F. Fabela-Morón, J. Cruz-Olivares, S.K. Velázquez-Gutiérrez, C. Pérez-Alonso, Chemically Modified Alginate-Based Hydrogel-Matrices in Drug Delivery, Macromol 5 (2025) 36. https://doi.org/10.3390/macromol5030036.
[77] N.A. Peppas, K.B. Keys, M. Torres-Lugo, A.M. Lowman, Poly(ethylene glycol)-containing hydrogels in drug delivery, J. Controlled Release 62 (1999) 81–87. https://doi.org/10.1016/S0168-3659(99)00027-9.
[78] F. Della Sala, M. Biondi, D. Guarnieri, A. Borzacchiello, L. Ambrosio, L. Mayol, Mechanical behavior of bioactive poly(ethylene glycol) diacrylate matrices for biomedical application, J. Mech. Behav. Biomed. Mater. 110 (2020) 103885. https://doi.org/10.1016/j.jmbbm.2020.103885.
[79] J. Zhu, Bioactive modification of poly(ethylene glycol) hydrogels for tissue engineering, Biomaterials 31 (2010) 4639–4656. https://doi.org/10.1016/j.biomaterials.2010.02.044.
[80] M. Hakim Khalili, R. Zhang, S. Wilson, S. Goel, S.A. Impey, A.I. Aria, Additive Manufacturing and Physicomechanical Characteristics of PEGDA Hydrogels: Recent Advances and Perspective for Tissue Engineering, Polymers 15 (2023) 2341. https://doi.org/10.3390/polym15102341.
[81] U. Hersel, C. Dahmen, H. Kessler, RGD modified polymers: biomaterials for stimulated cell adhesion and beyond, Biomaterials 24 (2003) 4385–4415. https://doi.org/10.1016/S0142-9612(03)00343-0.
[82] X. Liang, H.-J. Zhong, H. Ding, B. Yu, X. Ma, X. Liu, C.-M. Chong, J. He, Polyvinyl Alcohol (PVA)-Based Hydrogels: Recent Progress in Fabrication, Properties, and Multifunctional Applications, Polymers 16 (2024) 2755. https://doi.org/10.3390/polym16192755.

[83] H. Adelnia, R. Ensandoost, S. Shebbrin Moonshi, J.N. Gavgani, E.I. Vasafi, H.T. Ta, Freeze/thawed polyvinyl alcohol hydrogels: Present, past and future, Eur. Polym. J. 164 (2022) 110974. https://doi.org/10.1016/j.eurpolymj.2021.110974.
[84] N.Q. Vu, T.M. Le, A.N.B. Ngo, M.H.T. Nguyen, Y.-C. Liao, T.T. Tran, Engineering Functional PVA: A Comprehensive Review of Chemical Modifications and Prospective Developments, ACS Polym. Au 6 (2026) 33–60. https://doi.org/10.1021/acspolymersau.5c00133.
[85] M.K. Egbo, A fundamental review on composite materials and some of their applications in biomedical engineering, J. King Saud Univ. - Eng. Sci. 33 (2021) 557–568. https://doi.org/10.1016/j.jksues.2020.07.007.
[86] S.-J. Wang, Z.-Z. Zhang, D. Jiang, Y.-S. Qi, H.-J. Wang, J.-Y. Zhang, J.-X. Ding, J.-K. Yu, Thermogel-Coated Poly(ε-Caprolactone) Composite Scaffold for Enhanced Cartilage Tissue Engineering, Polymers 8 (2016) 200. https://doi.org/10.3390/polym8050200.
[87] J.D. Friedl, V. Nele, G. De Rosa, A. Bernkop-Schnürch, Bioinert, Stealth or Interactive: How Surface Chemistry of Nanocarriers Determines Their Fate In Vivo, Adv. Funct. Mater. 31 (2021) 2103347. https://doi.org/10.1002/adfm.202103347.
[88] A. Vashist, A. Vashist, Y.K. Gupta, S. Ahmad, Recent advances in hydrogel based drug delivery systems for the human body, (2014) 147–166. https://doi.org/10.1039/c3tb21016b.
[89] P.R. Turner, E. Murray, C.J. McAdam, M.A. McConnell, J.D. Cabral, Peptide Chitosan/Dextran Core/Shell Vascularized 3D Constructs for Wound Healing, ACS Appl. Mater. Interfaces 12 (2020) 32328–32339. https://doi.org/10.1021/acsami.0c07212.
[90] K. Miao, Y. Zhou, X. He, Y. Xu, X. Zhang, H. Zhao, X. Zhou, Q. Gu, H. Yang, X. Liu, L. Huang, Q. Shi, Microenvironment-responsive bilayer hydrogel microspheres with gelatin-shell for osteoarthritis treatment, Int. J. Biol. Macromol. 261 (2024) 129862. https://doi.org/10.1016/j.ijbiomac.2024.129862.
[91] A.R. Akkineni, J. Spangenberg, M. Geissler, S. Reichelt, H. Buechner, A. Lode, M. Gelinsky, Controlled and Local Delivery of Antibiotics by 3D Core/Shell Printed Hydrogel Scaffolds to Treat Soft Tissue Infections, Pharmaceutics 13 (2021) 2151. https://doi.org/10.3390/pharmaceutics13122151.
[92] A. Kirillova, T.R. Yeazel, D. Asheghali, S.R. Petersen, S. Dort, K. Gall, M.L. Becker, Fabrication of Biomedical Scaffolds Using Biodegradable Polymers, Chem. Rev. 121 (2021) 11238–11304. https://doi.org/10.1021/acs.chemrev.0c01200.
[93] S. Zhu, H. Sun, T. Mu, A. Richel, Research Progress in 3D Printed Biobased and Biodegradable Polyester/Ceramic Composite Materials: Applications and Challenges in Bone Tissue Engineering, ACS Appl. Mater. Interfaces 17 (2025) 2791–2813. https://doi.org/10.1021/acsami.4c15719.
[94] M. Subramaniyan, S. Karuppan, S. Helaili, I. Ahmad, Structural, mechanical, and in-vitro characterization of hydroxyapatite loaded PLA composites, J. Mol. Struct. 1306 (2024) 137862. https://doi.org/10.1016/j.molstruc.2024.137862.
[95] X. Luo, D. Barbieri, R. Duan, H. Yuan, J.D. Bruijn, Strontium-containing apatite/polylactide composites enhance bone formation in osteopenic rabbits, Acta Biomater. 26 (2015) 331–337. https://doi.org/10.1016/j.actbio.2015.07.044.
[96] A. Sharipova, O. Bakina, A. Lozhkomoev, M. Lerner, E. Gutmanas, A. Sosnik, Drug-eluting biodegradable metals and metal-ceramic composites, Materialia 28 (2023) 101756. https://doi.org/10.1016/j.mtla.2023.101756.
[97] Y. Zhang, J. Hu, R. Xie, Y. Yang, J. Cao, Y. Tu, Y. Zhang, T. Qin, X. Zhao, A programmable, fast-fixing, osteo-regenerative, biomechanically robust bone screw, Acta Biomater. 103 (2020) 293–305. https://doi.org/10.1016/j.actbio.2019.12.017.
[98] C. Vidal, P. Alves, M.M. Alves, M.J. Carmezim, M.H. Fernandes, L. Grenho, P.L. Inácio, F.B. Ferreira, T.G. Santos, C. Santos, Fabrication of a biodegradable and cytocompatible magnesium/nanohydroxyapatite/fluorapatite composite by upward friction stir processing for biomedical applications, J. Mech. Behav. Biomed. Mater. 129 (2022) 105137. https://doi.org/10.1016/j.jmbbm.2022.105137.
[99] X. Liu, P. Huo, X. Wang, H. Jiang, O. Yue, Next-generation electroactive biomaterials-integrated bioelectronics for advanced healthcare management, Trends Biotechnol. 44 (2026) 710–723. https://doi.org/10.1016/j.tibtech.2025.07.023.
[100] G. De Marzo, V.M. Mastronardi, M.T. Todaro, L. Blasi, V. Antonaci, L. Algieri, M. Scaraggi, M. De Vittorio, Sustainable electronic biomaterials for body-compliant devices: Challenges and perspectives for wearable bio-mechanical sensors and body energy harvesters, Nano Energy 123 (2024) 109336. https://doi.org/10.1016/j.nanoen.2024.109336.

[101] M. Levin, G. Pezzulo, J.M. Finkelstein, Endogenous Bioelectric Signaling Networks: Exploiting Voltage Gradients for Control of Growth and Form, Annu. Rev. Biomed. Eng. 19 (2017) 353–387. https://doi.org/10.1146/annurev-bioeng-071114-040647.
[102] W. Zhang, X. Zeng, X. Deng, F. Yang, X. Ma, W. Gao, Smart biomaterials: as active immune modulators to shape pro-regenerative microenvironments, Front. Cell Dev. Biol. 13 (2025) 1669399. https://doi.org/10.3389/fcell.2025.1669399.
[103] S. Dutta, S. Havanagi, P. Mishra, D. Sharma, B.N. Singh, From inert to intelligent: smart biomaterials reshaping the landscape of bioengineering, Int. J. Smart Nano Mater. 16 (2025) 845–877. https://doi.org/10.1080/19475411.2025.2570535.
[104] J.M. Dodda, M. F. Kunrath, L.Z. Zhao, M. Bodaghi, A. Yousefi, N. Ashammakhi, Autonomous Implants, Adv. Mater. 37 (2025) e10702. https://doi.org/10.1002/adma.202510702.
[105] A. Raheem, K. Mandal, S. Biswas, A. Ahari, A. Hassani Najafabadi, N. Farhadi, F. Zehtabi, A. Gangrade, M. Mecwan, S. Maity, S. Sharma, J.N. Arputharaj, P.A. Khan, A. Udduttula, N.H. Kouchehbaghi, D. Khorsandi, R. Vasita, R. Haghniaz, R.D. Herculano, J.V. John, H. Kim, M.R. Dokmeci, K.C. Popat, Y. Zhu, G. Manivasagam, Smart biomaterials in healthcare: Breakthroughs in tissue engineering, immunomodulation, patient-specific therapies, and biosensor applications, Appl. Phys. Rev. 12 (2025) 011333. https://doi.org/10.1063/5.0238817.
[106] T. Dayyoub, A.V. Maksimkin, O.V. Filippova, V.V. Tcherdyntsev, D.V. Telyshev, Shape Memory Polymers as Smart Materials: A Review, Polymers 14 (2022) 3511. https://doi.org/10.3390/polym14173511.
[107] T. Tadge, S. Garje, V. Saxena, A.M. Raichur, Application of Shape Memory and Self-Healable Polymers/Composites in the Biomedical Field: A Review, ACS Omega 8 (2023) 32294–32310. https://doi.org/10.1021/acsomega.3c04569.
[108] F. Mokhtari, R.W. Symes, Ž. Simon, B. Dharmasiri, L.C. Henderson, M.W. Joosten, R.J. Varley, An energy efficient and sustainable approach to structural health monitoring in carbon fiber composites: harnessing sound-induced vibration with $Ti_3C_2T_x$ MXene/AgNPs modified P(VDF-TrFE) sensors, J. Mater. Chem. A 13 (2025) 6482–6492. https://doi.org/10.1039/D4TA07797K.
[109] E.R. Ruskowitz, C.A. DeForest, Photoresponsive biomaterials for targeted drug delivery and 4D cell culture, Nat. Rev. Mater. 3 (2018) 17087. https://doi.org/10.1038/natrevmats.2017.87.
[110] Z. Wang, S. Zhang, J. Zeng, Z. Yin, M. Yang, Y. Liu, Z. Qin, J. Zhang, Z. Wu, X. Cui, Q. Xu, B. Zhou, W. Hu, Recent advances in self-powered implantable medical devices: Energy harvesting, conversion and therapeutic applications, Rev. Mater. Res. 1 (2025) 100087. https://doi.org/10.1016/j.revmat.2025.100087.
[111] J. Yong, C.-H. Toh, Rethinking coagulation: from enzymatic cascade and cell-based reactions to a convergent model involving innate immune activation, Blood 142 (2023) 2133–2145. https://doi.org/10.1182/blood.2023021166.
[112] C.W. Shields, M.A. Evans, L.L.-W. Wang, N. Baugh, S. Iyer, D. Wu, Z. Zhao, A. Pusuluri, A. Ukidve, D.C. Pan, S. Mitragotri, Cellular backpacks for macrophage immunotherapy, Sci. Adv. 6 (2020) eaaz6579. https://doi.org/10.1126/sciadv.aaz6579.
[113] Y. Zhang, Y. Fu, T. Sun, W. Li, L. Yu, J. Ding, Skin Relevant Biomaterials from Wound Healing, Medical Aesthetics, Flexible Electronics to Artificial Intelligence and Beyond, Adv. Mater. (2025) e12919. https://doi.org/10.1002/adma.202512919.
[114] C. Ligorio, A. Mata, Functional Biomaterials Through Biocooperation, Adv. Mater. (2026) e15925. https://doi.org/10.1002/adma.202515925.
[115] G. Chakrapani, V. Vijay Kumar, M. Zare, Next-Generation Biomaterials: Design Strategies, Clinical Translation, and the Rise of Intelligent Therapeutic Platforms, ACS Omega 10 (2025) 46272–46293. https://doi.org/10.1021/acsomega.5c06034.
[116] M. Mozafari, How artificial intelligence shapes the future of biomaterials?, Mater. 7 (2025) 100381. https://doi.org/10.1016/j.nxmate.2024.100381.
[117] C. Lu, Y. Huang, J. Cui, J. Wu, C. Jiang, X. Gu, Y. Cao, S. Yin, Toward Practical Applications of Engineered Living Materials with Advanced Fabrication Techniques, ACS Synth. Biol. 13 (2024) 2295–2312. https://doi.org/10.1021/acssynbio.4c00259.
[118] M.J.T. Tan, H.R. Kasireddy, A.B. Satriya, H. Abdul Karim, N. AlDahoul, Health is beyond genetics: on the integration of lifestyle and environment in real-time for hyper-personalized medicine, Front. Public Health 12 (2025) 1522673. https://doi.org/10.3389/fpubh.2024.1522673.

[119] A. Kumar, S.S. Han, PVA-based hydrogels for tissue engineering: A review, Int. J. Polym. Mater. Polym. Biomater. 66 (2017) 159–182. https://doi.org/10.1080/00914037.2016.1190930.
[120] V.S. Shtol, A.D. Tsareva, K.A. Arsentiev, S.P. Konovalova, S.A. Tlimahova, D.V. Klinov, D.A. Ivanov, P.E. Musienko, Polylactide/Polycaprolactone Nanofiber Scaffold Enhances Primary Cortical Neuron Growth, Polymers 18 (2026) 294. https://doi.org/10.3390/polym18020294.
[121] H. Fujimaki, H. Matsumine, H. Osaki, Y. Ueta, W. Kamei, M. Shimizu, K. Hashimoto, K. Fujii, T. Kazama, T. Matsumoto, Y. Niimi, M. Miyata, H. Sakurai, Dedifferentiated fat cells in polyglycolic acid-collagen nerve conduits promote rat facial nerve regeneration, Regen. Ther. 11 (2019) 240–248. https://doi.org/10.1016/j.reth.2019.08.004.
[122] J. Luo, L. Qin, L. Zhao, L. Gui, M.W. Ellis, Y. Huang, M.H. Kural, J.A. Clark, S. Ono, J. Wang, Y. Yuan, S.-M. Zhang, X. Cong, G. Li, M. Riaz, C. Lopez, A. Hotta, S. Campbell, G. Tellides, A. Dardik, L.E. Niklason, Y. Qyang, Tissue-Engineered Vascular Grafts with Advanced Mechanical Strength from Human iPSCs, Cell Stem Cell 26 (2020) 251-261.e8. https://doi.org/10.1016/j.stem.2019.12.012.
[123] C.-H. Cho, K.-C. Bae, D.-H. Kim, Biomaterials Used for Suture Anchors in Orthopedic Surgery, Clin. Orthop. Surg. 13 (2021) 287. https://doi.org/10.4055/cios20317.
[124] J. Holländer, N. Genina, H. Jukarainen, M. Khajeheian, A. Rosling, E. Mäkilä, N. Sandler, Three-Dimensional Printed PCL-Based Implantable Prototypes of Medical Devices for Controlled Drug Delivery, J. Pharm. Sci. 105 (2016) 2665–2676. https://doi.org/10.1016/j.xphs.2015.12.012.
[125] M. Saidi, A. Dabbaghi, S. Rahmani, Swelling and drug delivery kinetics of click - synthesized hydrogels based on various combinations of PEG and star - shaped PCL : influence of network parameters on swelling and release behavior, Polym. Bull. 77 (2020) 3989–4010. https://doi.org/10.1007/s00289-019-02948-z.
[126] A. Haryńska, J. Kucinska-Lipka, A. Sulowska, I. Gubanska, M. Kostrzewa, H. Janik, Medical-grade PCL based polyurethane system for FDM 3D printing-characterization and fabrication, Materials 16 (2019) 887. https://doi.org/10.3390/ma12060887.
[127] A. Hasan, S. Soliman, F. El Hajj, Y.-T. Tseng, H.C. Yalcin, H.E. Marei, Fabrication and In Vitro Characterization of a Tissue Engineered PCL-PLLA Heart Valve, Sci. Rep. 8 (2018) 8187. https://doi.org/10.1038/s41598-018-26452-y.
[128] P. Li, Y. Wang, X. Jin, J. Dou, X. Han, X. Wan, J. Yuan, J. Shen, Fabrication of PCL/keratin composite scaffolds for vascular tissue engineering with catalytic generation of nitric oxide potential, J. Mater. Chem. B 8 (2020) 6092–6099. https://doi.org/10.1039/D0TB00857E.
[129] V. Hasirci, D. Arslantunali, T. Dursun, D. Yucel, N. Hasirci, Peripheral nerve conduits: technology update, Med. Devices Evid. Res. (2014) 405. https://doi.org/10.2147/MDER.S59124.
[130] C. Cristallini, G. Vaccari, N. Barbani, E. Cibrario Rocchietti, R. Barberis, M. Falzone, K. Cabiale, G. Perona, E. Bellotti, R. Rastaldo, S. Pascale, P. Pagliaro, C. Giachino, Cardioprotection of PLGA/gelatine cardiac patches functionalised with adenosine in a large animal model of ischaemia and reperfusion injury: A feasibility study, J. Tissue Eng. Regen. Med. 13 (2019) 1253–1264. https://doi.org/10.1002/term.2875.
[131] K. Huang, D. Zhu, J. Soto, S. Hu, J. Fang, J. Huang, X. Zhang, J. Li, Y. Li, P. Tasoudis, S. Liu, X. Mei, T. Hoffman, T.G. Caranasos, C. Yu, Z. Gu, S. Li, K. Cheng, Immunomodulatory microneedle patch for cardiac repair in rodent and porcine models of myocardial infarction, Cell Biomater. 1 (2025) 100152. https://doi.org/10.1016/j.celbio.2025.100152.
[132] T.M.B.K. Dos Santos, C. Merlini, Á. Aragones, M.C. Fredel, Manufacturing and characterization of plates for fracture fixation of bone with biocomposites of poly (lactic acid-co-glycolic acid) (PLGA) with calcium phosphates bioceramics, Mater. Sci. Eng. C 103 (2019) 109728. https://doi.org/10.1016/j.msec.2019.05.013.
[133] H. Kotturi, A. Abuabed, H. Zafar, E. Sawyer, B. Pallipparambil, H. Jamadagni, M. Khandaker, Evaluation of Polyethylene Glycol Diacrylate-Polycaprolactone Scaffolds for Tissue Engineering Applications, J. Funct. Biomater. 8 (2017) 39. https://doi.org/10.3390/jfb8030039.
[134] W.S. Al-Arjan, M.U.A. Khan, H.H. Almutairi, S.M. Alharbi, S.I.A. Razak, pH-Responsive PVA/BC-f-GO Dressing Materials for Burn and Chronic Wound Healing with Curcumin Release Kinetics, Polymers 14 (2022) 1949. https://doi.org/10.3390/polym14101949.

[135] K.M. El Salmawi, Application of polyvinyl alcohol (PVA)/carboxymethyl cellulose (CMC) hydrogel produced by conventional crosslinking or by freezing and thawing., J Macromol Sci Part Pure Appl Chem 44 (2007) 619–624. https://doi.org/10.1080/10601320701285045.
[136] E. Dattola, E.I. Parrotta, S. Scalise, G. Perozziello, T. Limongi, P. Candeloro, M.L. Coluccio, C. Maletta, L. Bruno, M.T. De Angelis, G. Santamaria, V. Mollace, E. Lamanna, E. Di Fabrizio, G. Cuda, Development of 3D PVA scaffolds for cardiac tissue engineering and cell screening applications, RSC Adv. 9 (2019) 4246–4257. https://doi.org/10.1039/C8RA08187E.
[137] J. Patterson, R. Siew, S.W. Herring, A.S.P. Lin, R. Guldberg, P.S. Stayton, Hyaluronic acid hydrogels with controlled degradation properties for oriented bone regeneration, Biomaterials 31 (2010) 6772–6781. https://doi.org/10.1016/j.biomaterials.2010.05.047.
[138] X. Wang, J. He, Y. Wang, F.-Z. Cui, Hyaluronic acid-based scaffold for central neural tissue engineering, Interface Focus 2 (2012) 278–291. https://doi.org/10.1098/rsfs.2012.0016.
[139] Y. Dong, M. Cui, J. Qu, X. Wang, S.H. Kwon, J. Barrera, N. Elvassore, G.C. Gurtner, Conformable hyaluronic acid hydrogel delivers adipose-derived stem cells and promotes regeneration of burn injury, Acta Biomater. 108 (2020) 56–66. https://doi.org/10.1016/J.ACTBIO.2020.03.040.
[140] T.A. Ahmed, B.M. Aljaeid, Preparation, characterization, and potential application of chitosan, chitosan derivatives, and chitosan metal nanoparticles in pharmaceutical drug delivery, Drug Des. Devel. Ther. 10 (2016) 483–507. https://doi.org/10.2147/DDDT.S99651.
[141] H. Chopra, S. Bibi, Y.K. Mohanta, T. Kumar Mohanta, S. Kumar, I. Singh, M. Saad Khan, P. Ranjan Rauta, A. Alshammari, M. Alharbi, A. F. Alasmari, In Vitro and In Silico Characterization of Curcumin-Loaded Chitosan–PVA Hydrogels: Antimicrobial and Potential Wound Healing Activity, Gels 9 (2023) 394. https://doi.org/10.3390/gels9050394.
[142] W. Kruczkowska, J. Gałęziewska, K.H. Grabowska, P. Gromek, K. Czajkowska, M. Rybicki, M. Kciuk, K.K. Kłosiński, From Molecules to Mind: The Critical Role of Chitosan, Collagen, Alginate, and Other Biopolymers in Neuroprotection and Neurodegeneration, Molecules 30 (2025) 1017. https://doi.org/10.3390/molecules30051017.
[143] C. Ceccaldi, S.G. Fullana, C. Alfarano, O. Lairez, D. Calise, D. Cussac, A. Parini, B. Sallerin, Alginate Scaffolds for Mesenchymal Stem Cell Cardiac Therapy: Influence of Alginate Composition, Cell Transplant. 21 (2012) 1969–1984. https://doi.org/10.3727/096368912X647252.
[144] M. Cavo, M. Caria, I. Pulsoni, F. Beltrame, M. Fato, S. Scaglione, A new cell-laden 3D Alginate-Matrigel hydrogel resembles human breast cancer cell malignant morphology, spread and invasion capability observed “in vivo,” Sci. Rep. 8 (2018) 5333. https://doi.org/10.1038/s41598-018-23250-4.
[145] J. Xu, S. Zheng, X. Hu, L. Li, W. Li, R. Parungao, Y. Wang, Y. Nie, T. Liu, K. Song, Advances in the Research of Bioinks Based on Natural Collagen, Polysaccharide and Their Derivatives for Skin 3D Bioprinting, Polymers 12 (2020) 1237. https://doi.org/10.3390/polym12061237.
[146] Z. Khodabandeh, N. Tanideh, F.S. Aslani, I. Jamhiri, S. Zare, N. Alizadeh, A. Safari, N. Farshidfar, M. Dara, M. Zarei, A comparative in vitro and in vivo study on bone tissue engineering potential of the collagen/nano-hydroxyapatite scaffolds loaded with ginger extract and curcumin, Mater. Today Commun. 31 (2022) 103339. https://doi.org/10.1016/J.MTCOMM.2022.103339.
[147] A.B. Shekhter, A.L. Fayzullin, M.N. Vukolova, T.G. Rudenko, V.D. Osipycheva, P.F. Litvitsky, Medical Applications of Collagen and Collagen-Based Materials, Curr. Med. Chem. 26 (2017) 506–516. https://doi.org/10.2174/0929867325666171205170339.
[148] Z. Zhang, X. Wang, Y. Wang, J. Hao, Rapid-Forming and Self-Healing Agarose-Based Hydrogels for Tissue Adhesives and Potential Wound Dressings, Biomacromolecules 19 (2018) 980–988. https://doi.org/10.1021/acs.biomac.7b01764.
[149] C. Cheng, X. Peng, L. Xi, C. Wan, S. Shi, Y. Wang, X. Yu, An agar-polyvinyl alcohol hydrogel loaded with tannic acid with efficient hemostatic and antibacterial capacity for wound dressing, Food Funct. 13 (2022) 9622–9634. https://doi.org/10.1039/d2fo02251f.
[150] E. Piłat, P. Gnatowski, A. Kurdyn, H. Cieśliński, E. Augustin, J. Kucińska-Lipka, Investigation of bioprintable modified agar-based hydrogels with antimicrobial properties, Int. J. Biol. Macromol. 289 (2025) 138707. https://doi.org/10.1016/j.ijbiomac.2024.138707.
[151] M.A. Salati, J. Khazai, A.M. Tahmuri, A. Samadi, A. Taghizadeh, M. Taghizadeh, P. Zarrintaj, J.D. Ramsey, S. Habibzadeh, F. Seidi, M.R. Saeb, M. Mozafari, Agarose-Based

biomaterials: Opportunities and challenges in cartilage tissue engineering, Polymers 12 (2020) 1150. https://doi.org/10.3390/POLYM12051150.
[152] P. Szarlej, E. Piłat, P. Gnatowski, H. Cieśliński, M. Sienkiewicz, J. Kucińska-Lipka, Investigation on Swelling of Agar-Based Antibacterial Hydrogels for Hard-to-Heal Wound Dressings, ChemMedChem 20 (2025). https://doi.org/10.1002/cmdc.202400042.
[153] P. Zarrintaj, S. Manouchehri, Z. Ahmadi, M.R. Saeb, A.M. Urbanska, D.L. Kaplan, M. Mozafari, Agarose-based biomaterials for tissue engineering, Carbohydr. Polym. 187 (2018) 66–84. https://doi.org/10.1016/j.carbpol.2018.01.060.
[154] S. Zheng, H. Wei, H. Cheng, Y. Qi, Y. Gu, X. Ma, J. Sun, F. Ye, F. Guo, C. Cheng, Advances in nerve guidance conduits for peripheral nerve repair and regeneration, Am. J. Stem Cells 12 (2023) 112–123.
[155] O. Bayer, Das Di-Isocyanat-Polyadditionsverfahren (Polyurethane), Angew. Chem. 59 (1947) 257–272. https://doi.org/10.1002/ange.19470590901.
[156] S. Azarmgin, B. Torabinejad, R. Kalantarzadeh, H. Garcia, C.A. Velazquez, G. Lopez, M. Vazquez, G. Rosales, B.S. Heidari, S.M. Davachi, Polyurethanes and Their Biomedical Applications, ACS Biomater. Sci. Eng. 10 (2024) 6828–6859. https://doi.org/10.1021/acsbiomaterials.4c01352.
[157] S. Singh, K. Kumar Paswan, A. Kumar, V. Gupta, M. Sonker, M. Ashhar Khan, A. Kumar, N. Shreyash, Recent Advancements in Polyurethane-based Tissue Engineering, ACS Appl. Bio Mater. 6 (2023) 327–348. https://doi.org/10.1021/acsabm.2c00788.
[158] G. Dang, J. Gu, J. Song, Z. Li, J. Hao, Y. Wang, C. Wang, T. Ye, F. Zhao, Y.-F. Zhang, F.R. Tay, L. Niu, L. Xia, Multifunctional polyurethane materials in regenerative medicine and tissue engineering, Cell Rep. Phys. Sci. 5 (2024) 102053. https://doi.org/10.1016/j.xcrp.2024.102053.
[159] F.M. De Souza, P.K. Kahol, R.K. Gupta, Introduction to Polyurethane Chemistry, in: R.K. Gupta, P.K. Kahol (Eds.), ACS Symp. Ser., American Chemical Society, Washington, DC, 2021: pp. 1–24. https://doi.org/10.1021/bk-2021-1380.ch001.
[160] H. Fałtynowicz, H. Janik, J. Kucinska-Lipka, M. Sienkiewicz, Polyurethanes, in: Handb. Thermoset Plast., Elsevier, 2022: pp. 231–262. https://doi.org/10.1016/B978-0-12-821632-3.00007-5.
[161] A. Mouren, L. Avérous, Sustainable cycloaliphatic polyurethanes: from synthesis to applications, Chem. Soc. Rev. 52 (2023) 277–317. https://doi.org/10.1039/D2CS00509C.
[162] A.G. Morena, I. Stefanov, K. Ivanova, S. Pérez-Rafael, M. Sánchez-Soto, T. Tzanov, Antibacterial polyurethane foams with incorporated lignin-capped silver nanoparticles for chronic wound treatment, Ind. Eng. Chem. Res. 59 (2020) 4504–4514. https://doi.org/10.1021/acs.iecr.9b06362.
[163] Y. Ding, Z. Sun, R. Shi, H. Cui, Y. Liu, H. Mao, B. Wang, D. Zhu, F. Yan, Integrated Endotoxin Adsorption and Antibacterial Properties of Cationic Polyurethane Foams for Wound Healing, ACS Appl. Mater. Interfaces 11 (2019) 2860–2869. https://doi.org/10.1021/acsami.8b19746.
[164] N. Namviriyachote, V. Lipipun, Y. Akkhawattanangkul, P. Charoonrut, G.C. Ritthidej, Development of polyurethane foam dressing containing silver and asiaticoside for healing of dermal wound, Asian J. Pharm. Sci. 14 (2019) 63–77. https://doi.org/10.1016/j.ajps.2018.09.001.
[165] E.H. Song, S.H. Jeong, J.U. Park, S. Kim, H.E. Kim, J. Song, Polyurethane-silica hybrid foams from a one-step foaming reaction, coupled with a sol-gel process, for enhanced wound healing, Mater. Sci. Eng. C 79 (2017) 866–874. https://doi.org/10.1016/j.msec.2017.05.041.
[166] H. Choe, J.H. Kim, Reactivity of isophorone diisocyanate in fabrications of polyurethane foams for improved acoustic and mechanical properties, J. Ind. Eng. Chem. 69 (2019) 153–160. https://doi.org/10.1016/j.jiec.2018.09.025.
[167] I. Carayon, P. Szarlej, P. Gnatowski, E. Piłat, M. Sienkiewicz, M. Glinka, J. Karczewski, J. Kucińska-Lipka, Polyurethane based hybrid ciprofloxacin-releasing wound dressings designed for skin engineering purpose, Adv. Med. Sci. 67 (2022) 269–282. https://doi.org/10.1016/j.advms.2022.05.003.
[168] M. Khattab, N. Abdel Hady, Y. Dahman, Green Biodegradable Polylactide-Based Polyurethane Triblock Copolymers Reinforced with Cellulose Nanowhiskers, J. Funct. Biomater. 14 (2023) 118. https://doi.org/10.3390/jfb14030118.
[169] E. Shams, H. Yeganeh, H. Naderi-Manesh, R. Gharibi, Z. Mohammad Hassan, Polyurethane/siloxane membranes containing graphene oxide nanoplatelets as antimicrobial

wound dressings: in vitro and in vivo evaluations, J. Mater. Sci. Mater. Med. 28 (2017). https://doi.org/10.1007/s10856-017-5881-z.
[170] I. Gubanska, J. Kucinska-Lipka, H. Janik, The influence of amorphous macrodiol, diisocyanate type and L-ascorbic acid modifier on chemical structure, morphology and degradation behavior of polyurethanes for tissue scaffolds fabrication, Polym. Degrad. Stab. 163 (2019) 52–67. https://doi.org/10.1016/j.polymdegradstab.2019.02.025.
[171] C. Yu, M. Salzano De Luna, A. Russo, I. Adamiano, F. Scherillo, Z. Wang, X. Zhang, H. Xia, M. Lavorgna, Role of Diisocyanate Structure on Self-Healing and Anticorrosion Properties of Waterborne Polyurethane Coatings, Adv. Mater. Interfaces 8 (2021) 2100117. https://doi.org/10.1002/admi.202100117.
[172] P. Król, Ł. Uram, B. Król, K. Pielichowska, M. Walczak, Study of chemical, physico-mechanical and biological properties of 4,4′-methylenebis(cyclohexyl isocyanate)-based polyurethane films, Mater. Sci. Eng. C 93 (2018) 483–494. https://doi.org/10.1016/j.msec.2018.07.082.
[173] Y. Feng, K. Xiao, Y. He, B. Du, J. Hong, H. Yin, D. Lu, F. Luo, Z. Li, J. Li, H. Tan, Q. Fu, Tough and biodegradable polyurethane-curcumin composited hydrogel with antioxidant, antibacterial and antitumor properties, Mater. Sci. Eng. C 121 (2021) 111820. https://doi.org/10.1016/j.msec.2020.111820.
[174] N. Firoozi, A.H. Rezayan, S.J. Tabatabaei Rezaei, M. Mir-Derikvand, M.R. Nabid, J. Nourmohammadi, J. Mohammadnejad Arough, Synthesis of poly(ε-caprolactone)-based polyurethane semi-interpenetrating polymer networks as scaffolds for skin tissue regeneration, Int. J. Polym. Mater. Polym. Biomater. 66 (2017) 805–811. https://doi.org/10.1080/00914037.2016.1276059.
[175] C. Iga, T. Agata, Ł. Marcin, F. Natalia, K.-L. Justyna, Ciprofloxacin-Modified Degradable Hybrid Polyurethane-Polylactide Porous Scaffolds Developed for Potential Use as an Antibacterial Scaffold for Regeneration of Skin, Polymers 12 (2020) 171. https://doi.org/10.3390/polym12010171.
[176] A. Shababdoust, M. Zandi, M. Ehsani, P. Shokrollahi, R. Foudazi, Controlled curcumin release from nanofibers based on amphiphilic-block segmented polyurethanes, Int. J. Pharm. 575 (2020) 118947. https://doi.org/10.1016/j.ijpharm.2019.118947.
[177] S.S. Hosseini Salekdeh, H. Daemi, M. Zare-Gachi, S. Rajabi, F. Bazgir, N. Aghdami, M.S. Nourbakhsh, H. Baharvand, Assessment of the Efficacy of Tributylammonium Alginate Surface-Modified Polyurethane as an Antibacterial Elastomeric Wound Dressing for both Noninfected and Infected Full-Thickness Wounds, ACS Appl. Mater. Interfaces 12 (2020) 3393–3406. https://doi.org/10.1021/acsami.9b18437.
[178] J. Kucinska-Lipka, I. Gubanska, A. Lewandowska, A. Terebieniec, A. Przybytek, H. Cieśliński, Antibacterial polyurethanes, modified with cinnamaldehyde, as potential materials for fabrication of wound dressings, Polym. Bull. 76 (2019) 2725–2742. https://doi.org/10.1007/s00289-018-2512-x.
[179] M. Shafiq, M.T.Z. Butt, S.M. Khan, Synthesis of Mono Ethylene Glycol (MEG)-Based Polyurethane and Effect of Chain Extender on Its Associated Properties, Polymers 13 (2021) 3436. https://doi.org/10.3390/polym13193436.
[180] S.A.A. Najafabadi, A. Mohammadi, A.Z. Kharazi, Polyurethane nanocomposite impregnated with chitosan-modified graphene oxide as a potential antibacterial wound dressing, Mater. Sci. Eng. C 115 (2020) 110899. https://doi.org/10.1016/j.msec.2020.110899.
[181] F. Zhang, C. Hu, Q. Kong, R. Luo, Y. Wang, Peptide-/Drug-Directed Self-Assembly of Hybrid Polyurethane Hydrogels for Wound Healing, ACS Appl. Mater. Interfaces 11 (2019) 37147–37155. https://doi.org/10.1021/acsami.9b13708.
[182] D.K. Patel, V. Gupta, A. Dwivedi, S.K. Pandey, V.K. Aswal, D. Rana, P. Maiti, Superior biomaterials using diamine modified graphene grafted polyurethane, Polymer 106 (2016) 109–119. https://doi.org/10.1016/j.polymer.2016.10.060.
[183] I. Olazabal, A. González, S. Vallejos, I. Rivilla, C. Jehanno, H. Sardon, Upgrading Polyurethanes into Functional Ureas through the Asymmetric Chemical Deconstruction of Carbamates, ACS Sustain. Chem. Eng. 11 (2023) 332–342. https://doi.org/10.1021/acssuschemeng.2c05647.
[184] I. Yilgor, E. Yilgor, I.G. Guler, T.C. Ward, G.L. Wilkes, FTIR investigation of the influence of diisocyanate symmetry on the morphology development in model segmented polyurethanes, Polymer 47 (2006) 4105–4114. https://doi.org/10.1016/j.polymer.2006.02.027.

[185] J. Qin, Y. Chen, X. Guo, Y. Huang, G. Chen, Q. Zhang, G. He, S. Zhu, X. Ruan, H. Zhu, Regulation of Hard Segment Cluster Structures for High-performance Poly(urethane-urea) Elastomers, Adv. Sci. 11 (2024) 2400255. https://doi.org/10.1002/advs.202400255.
[186] S. Wendels, L. Avérous, Biobased polyurethanes for biomedical applications, Bioact. Mater. 6 (2021) 1083–1106. https://doi.org/10.1016/j.bioactmat.2020.10.002.
[187] S. Mondal, D. Martin, Hydrolytic degradation of segmented polyurethane copolymers for biomedical applications, Polym. Degrad. Stab. 97 (2012) 1553–1561. https://doi.org/10.1016/j.polymdegradstab.2012.04.008.
[188] L.H. Chan-Chan, R. Solis-Correa, R.F. Vargas-Coronado, J.M. Cervantes-Uc, J.V. Cauich-Rodríguez, P. Quintana, P. Bartolo-Pérez, Degradation studies on segmented polyurethanes prepared with HMDI, PCL and different chain extenders, Acta Biomater. 6 (2010) 2035–2044. https://doi.org/10.1016/j.actbio.2009.12.010.
[189] J. Mystkowska, M. Mazurek-Budzyńska, E. Piktel, K. Niemirowicz, W. Karalus, P. Deptuła, K. Pogoda, D. Łysik, J.R. Dąbrowski, G. Rokicki, R. Bucki, Assessment of aliphatic poly(ester-carbonate-urea-urethane)s potential as materials for biomedical application, J. Polym. Res. 24 (2017) 144. https://doi.org/10.1007/s10965-017-1296-2.
[190] Y.W. Tang, R.S. Labow, J.P. Santerre, Enzyme-induced biodegradation of polycarbonate polyurethanes: Dependence on hard-segment concentration, J. Biomed. Mater. Res. 56 (2001) 516–528. https://doi.org/10.1002/1097-4636(20010915)56:4%3C516::AID-JBM1123%3E3.0.CO;2-B.
[191] E.M. Christenson, J.M. Anderson, A. Hiltner, Oxidative mechanisms of poly(carbonate urethane) and poly(ether urethane) biodegradation: *In vivo* and *in vitro* correlations, J. Biomed. Mater. Res. A 70A (2004) 245–255. https://doi.org/10.1002/jbm.a.30067.
[192] F. Sadeghi, Y. Zamani, K.L. Bear, A. Kheradvar, Material characterization and biocompatibility of polycarbonate-based polyurethane for biomedical implant applications, RSC Adv. 15 (2025) 8839–8850. https://doi.org/10.1039/D5RA00568J.
[193] J. Nicolas, S. Magli, L. Rabbachin, S. Sampaolesi, F. Nicotra, L. Russo, 3D Extracellular Matrix Mimics: Fundamental Concepts and Role of Materials Chemistry to Influence Stem Cell Fate, Biomacromolecules 21 (2020) 1968–1994. https://doi.org/10.1021/acs.biomac.0c00045.
[194] N. Watcharajittanont, C. Putson, P. Pripatnanont, Ji. Meesane, Electrospun polyurethane fibrous membranes of mimicked extracellular matrix for periodontal ligament: Molecular behavior, mechanical properties, morphology, and osseointegration, J. Biomater. Appl. 34 (2020) 753–762. https://doi.org/10.1177/0885328219874601.
[195] H. Sardon, A. Pascual, D. Mecerreyes, D. Taton, H. Cramail, J.L. Hedrick, Synthesis of Polyurethanes Using Organocatalysis: A Perspective, Macromolecules 48 (2015) 3153–3165. https://doi.org/10.1021/acs.macromol.5b00384.
[196] R. Devendra, N.R. Edmonds, T. Söhnel, Computational and experimental investigations of the urethane formation mechanism in the presence of organotin(IV) carboxylate catalysts, J. Mol. Catal. Chem. 366 (2013) 126–139. https://doi.org/10.1016/j.molcata.2012.09.015.
[197] A.J. Bloodworth, A.G. Davies, 975. Organometallic reactions. Part I. The addition of tin alkoxides to isocyanates, J. Chem. Soc. Resumed (1965) 5238. https://doi.org/10.1039/jr9650005238.
[198] Hans.R. Kricheldorf, S.M. Weidner, About the Toxicity of Polymerization Catalysts and Polymer Additives Based on Tin(II) Salts and Tin(IV) Compounds, ACS Chem. Health Saf. 32 (2025) 677–689. https://doi.org/10.1021/acs.chas.5c00105.
[199] M. Hatanaka, DFT Analysis of Catalytic Urethanation, Bull. Chem. Soc. Jpn. 84 (2011) 933–935. https://doi.org/10.1246/bcsj.20110144.
[200] H.Q. Waleed, M. Csécsi, V. Konyhás, Z.R. Boros, B. Viskolcz, Z. Fejes, B. Fiser, Aliphatic tertiary amine catalysed urethane formation – a combined experimental and theoretical study, Phys. Chem. Chem. Phys. 24 (2022) 20538–20545. https://doi.org/10.1039/D2CP00728B.
[201] D. Grzęda, G. Węgrzyk, A. Nowak, G. Komorowska, L. Szczepkowski, J. Ryszkowska, Effect of Different Amine Catalysts on the Thermomechanical and Cytotoxic Properties of 'Visco'-Type Polyurethane Foam for Biomedical Applications, Materials 16 (2023) 1527. https://doi.org/10.3390/ma16041527.
[202] J. Alsarraf, F. Robert, H. Cramail, Y. Landais, Latent catalysts based on guanidine templates for polyurethane synthesis, Polym. Chem. 4 (2013) 904. https://doi.org/10.1039/c2py21006a.
[203] C.O. Adetunji, O.T. Olaniyan, O.A. Anani, A. Inobeme, J.T. Mathew, Environmental Impact of Polyurethane Chemistry, in: R.K. Gupta, P.K. Kahol (Eds.), ACS Symp. Ser., American

Chemical Society, Washington, DC, 2021: pp. 393–411. https://doi.org/10.1021/bk-2021-1380.ch014.
[204] A. Stras, S. Mannaert, M. Canfyn, T. Weytjens, E. Deconinck, B. Desmedt, T. Vanhaecke, Quantitative Risk Assessment of Diisocyanates Leaching From Wound Dressings Under Physiological Conditions, Contact Dermatitis 94 (2026) 245–258. https://doi.org/10.1111/cod.70061.
[205] C. Xu, Y. Hong, Rational design of biodegradable thermoplastic polyurethanes for tissue repair, Bioact. Mater. 15 (2022) 250–271. https://doi.org/10.1016/j.bioactmat.2021.11.029.
[206] J.P. Santerre, K. Woodhouse, G. Laroche, R.S. Labow, Understanding the biodegradation of polyurethanes: From classical implants to tissue engineering materials, Biomaterials 26 (2005) 7457–7470. https://doi.org/10.1016/j.biomaterials.2005.05.079.
[207] P. Dicesare, W.M. Fox, M.J. Hill, G.R. Krishnan, S. Yang, D. Sarkar, Cell–material interactions on biphasic polyurethane matrix, J. Biomed. Mater. Res. A 101A (2013) 2151–2163. https://doi.org/10.1002/jbm.a.34515.
[208] R. Guidoin, M. Sigot, M. King, M.-F. Sigot-Luizard, Biocompatibility of the Vascugraft ®: evaluation of a novel polyester methane vascular substitute by an organotypic culture technique, Biomaterials 13 (1992) 281–288. https://doi.org/10.1016/0142-9612(92)90051-O.
[209] M.-F. Sigot-Luizard, M. Sigot, R. Guidoin, M. King, W.W. Von Maltzahn, R. Kowligi, R.C. Eberhart, A Novel Microporous Polyurethane Blood Conduit: Biocompatibility Assessment of the UTA Arterial Prosthesis by an Organo-typic Culture Technique, J. Invest. Surg. 6 (1993) 251–271. https://doi.org/10.3109/08941939309141616.
[210] Z. Miri, S. Farè, Q. Ma, H.J. Haugen, Updates on polyurethane and its multifunctional applications in biomedical engineering, Prog. Biomed. Eng. 5 (2023) 042001. https://doi.org/10.1088/2516-1091/acef84.
[211] J. Zhang, S. Lv, X. Zhao, S. Ma, F. Zhou, Surface functionalization of polyurethanes: A critical review, Adv. Colloid Interface Sci. 325 (2024) 103100. https://doi.org/10.1016/j.cis.2024.103100.
[212] A.D. Gholap, R.P. Said, P.R. Khuspe, S.R. Pardeshi, P.L. Pingale, K.M. Bhandari, J.K. Kale, J.S. Gupta, N.T. Hatvate, P.S. Giram, Recent Advances in Polyurethane Polymer for Biomedical Applications, Mol. Pharm. 22 (2025) 7155–7197. https://doi.org/10.1021/acs.molpharmaceut.5c00538.
[213] Y.J. Du, J.L. Brash, G. McClung, L.R. Berry, P. Klement, A.K.C. Chan, Protein adsorption on polyurethane catheters modified with a novel antithrombin-heparin covalent complex, J. Biomed. Mater. Res. A 80A (2007) 216–225. https://doi.org/10.1002/jbm.a.30977.
[214] H. Wang, Y. Hu, D. Lynch, M. Young, S. Li, H. Cong, F.-J. Xu, G. Cheng, Zwitterionic Polyurethanes with Tunable Surface and Bulk Properties, ACS Appl. Mater. Interfaces 10 (2018) 37609–37617. https://doi.org/10.1021/acsami.8b10450.
[215] A.T. Speidel, P.R.A. Chivers, C.S. Wood, D.A. Roberts, I.P. Correia, A.S. Caravaca, Y.K.V. Chan, C.S. Hansel, J. Heimgärtner, E. Müller, J. Ziesmer, G.A. Sotiriou, P.S. Olofsson, M.M. Stevens, Tailored Biocompatible Polyurethane-Poly(ethylene glycol) Hydrogels as a Versatile Nonfouling Biomaterial, Adv. Healthc. Mater. 11 (2022) 2201378. https://doi.org/10.1002/adhm.202201378.
[216] I. Francolini, F. Crisante, A. Martinelli, L. D'Ilario, A. Piozzi, Synthesis of biomimetic segmented polyurethanes as antifouling biomaterials, Acta Biomater. 8 (2012) 549–558. https://doi.org/10.1016/j.actbio.2011.10.024.
[217] A. Vasilescu, S. Gáspár, M. Gheorghiu, C. Polonschii, R.M. Banciu, S. David, E. Gheorghiu, J.-L. Marty, Promising Solutions to Address the Non-Specific Adsorption in Biosensors Based on Coupled Electrochemical-Surface Plasmon Resonance Detection, Chemosensors 13 (2025) 92. https://doi.org/10.3390/chemosensors13030092.
[218] J.L. Cohen, J.J. Van Aartsen, The hydrolytic degradation of polyurethanes, J. Polym. Sci. Polym. Symp. 42 (1973) 1325–1338. https://doi.org/10.1002/polc.5070420333.
[219] H.J. Griesser, Degradation of polyurethanes in biomedical applications—A review, Polym. Degrad. Stab. 33 (1991) 329–354. https://doi.org/10.1016/0141-3910(91)90080-B.
[220] S. Piatnitskaia, G. Rafikova, A. Bilyalov, S. Chugunov, I. Akhatov, V. Pavlov, J. Kzhyshkowska, Modelling of macrophage responses to biomaterials in vitro: state-of-the-art and the need for the improvement, Front. Immunol. 15 (2024) 1349461. https://doi.org/10.3389/fimmu.2024.1349461.
[221] G. Gallagher, A. Padsalgikar, E. Tkatchouk, C. Jenney, C. Iacob, J. Runt, Environmental stress cracking performance of polyether and PDMS-based polyurethanes in an *in vitro*

oxidation model, J. Biomed. Mater. Res. B Appl. Biomater. 105 (2017) 1544–1558. https://doi.org/10.1002/jbm.b.33691.
[222] B.D. Ratner, K.W. Gladhill, T.A. Horbett, Analysis of *in vitro* enzymatic and oxidative degradation of polyurethanes, J. Biomed. Mater. Res. 22 (1988) 509–527. https://doi.org/10.1002/jbm.820220607.
[223] C. Gamerith, E. Herrero Acero, A. Pellis, A. Ortner, R. Vielnascher, D. Luschnig, B. Zartl, K. Haernvall, S. Zitzenbacher, G. Strohmeier, O. Hoff, G. Steinkellner, K. Gruber, D. Ribitsch, G.M. Guebitz, Improving enzymatic polyurethane hydrolysis by tuning enzyme sorption, Polym. Degrad. Stab. 132 (2016) 69–77. https://doi.org/10.1016/j.polymdegradstab.2016.02.025.
[224] T.A. Lewandowski, A.W. Hayes, B.D. Beck, Risk evaluation of occupational exposure to methylene dianiline and toluene diamine in polyurethane foam, Hum. Exp. Toxicol. 24 (2005) 655–662. https://doi.org/10.1191/0960327105ht587oa.
[225] P.T. Knight, J.T. Kirk, J.M. Anderson, P.T. Mather, In vivo kinetic degradation analysis and biocompatibility of aliphatic polyester polyurethanes, J. Biomed. Mater. Res. A 94 (2010) 333–343. https://doi.org/10.1002/jbm.a.32806.
[226] F. Oveissi, S. Naficy, A. Lee, D.S. Winlaw, F. Dehghani, Materials and manufacturing perspectives in engineering heart valves: a review, Mater. Today Bio 5 (2020) 100038. https://doi.org/10.1016/j.mtbio.2019.100038.
[227] P. Boloori Zadeh, S.C. Corbett, H. Nayeb-Hashemi, In-vitro calcification study of polyurethane heart valves, Mater. Sci. Eng. C 35 (2014) 335–340. https://doi.org/10.1016/j.msec.2013.11.015.
[228] S. Daebritz, B. Fausten, B. Hermanns, J. Schroeder, J. Groetzner, R. Autschbach, B. Messmer, J. Sachweh, Introduction of a flexible polymeric heart valve prosthesis with special design for aortic position1, Eur. J. Cardiothorac. Surg. 25 (2004) 946–952. https://doi.org/10.1016/j.ejcts.2004.02.040.
[229] M. Bil, E. Kijeńska-Gawrońska, E. Głodkowska-Mrówka, A. Manda-Handzlik, P. Mrówka, Design and in vitro evaluation of electrospun shape memory polyurethanes for self-fitting tissue engineering grafts and drug delivery systems, Mater. Sci. Eng. C 110 (2020) 110675. https://doi.org/10.1016/J.MSEC.2020.110675.
[230] S. Velankar, S.L. Cooper, Microphase Separation and Rheological Properties of Polyurethane Melts. 1. Effect of Block Length, Macromolecules 31 (1998) 9181–9192. https://doi.org/10.1021/ma9811472.
[231] S. Velankar, S.L. Cooper, Microphase Separation and Rheological Properties of Polyurethane Melts. 2. Effect of Block Incompatibility on the Microstructure, Macromolecules 33 (2000) 382–394. https://doi.org/10.1021/ma990817g.
[232] M. Asensio, V. Costa, A. Nohales, O. Bianchi, C.M. Gómez, Tunable Structure and Properties of Segmented Thermoplastic Polyurethanes as a Function of Flexible Segment, Polymers 11 (2019) 1910. https://doi.org/10.3390/polym11121910.
[233] R.Y.H. Tan, C.S. Lee, M.R. Pichika, S.F. Cheng, K.Y. Lam, PH Responsive Polyurethane for the Advancement of Biomedical and Drug Delivery, Polymers 14 (2022) 1672. https://doi.org/10.3390/polym14091672.
[234] S. Yu, C. He, J. Ding, Y. Cheng, W. Song, X. Zhuang, X. Chen, pH and reduction dual responsive polyurethane triblock copolymers for efficient intracellular drug delivery, Soft Matter 9 (2013) 2637. https://doi.org/10.1039/c2sm27616j.
[235] J. Zhao, J. Zhu, J. Zhang, Z. Huang, D. Qi, Review of research on thermoplastic self-healing polyurethanes, React. Funct. Polym. 199 (2024) 105886. https://doi.org/10.1016/j.reactfunctpolym.2024.105886.
[236] C. Yu, J. Choi, J. Lee, S. Lim, Y. Park, S.M. Jo, J. Ahn, S.Y. Kim, T. Chang, C. Boyer, M.S. Kwon, Functional Thermoplastic Polyurethane Elastomers with *α, ω* -Hydroxyl End-Functionalized Polyacrylates, Adv. Mater. 36 (2024) 2403048. https://doi.org/10.1002/adma.202403048.
[237] D.-B. Ju, J.-C. Lee, S.-K. Hwang, C.-S. Cho, H.-J. Kim, Progress of Polysaccharide-Contained Polyurethanes for Biomedical Applications, Tissue Eng. Regen. Med. 19 (2022) 891–912. https://doi.org/10.1007/s13770-022-00464-2.
[238] N. Nan, W. Hu, J. Wang, Lignin-Based Porous Biomaterials for Medical and Pharmaceutical Applications, Biomedicines 10 (2022) 747. https://doi.org/10.3390/biomedicines10040747.

[239] S. Wendels, R. Balahura, S. Dinescu, M. Costache, L. Avérous, Synthesis and properties of biobased polyurethane tissue adhesives from bacterial polyester, Sustain. Mater. Technol. 34 (2022) e00515. https://doi.org/10.1016/j.susmat.2022.e00515.
[240] G. Satchanska, S. Davidova, P.D. Petrov, Natural and Synthetic Polymers for Biomedical and Environmental Applications, Polymers 16 (2024) 1159. https://doi.org/10.3390/polym16081159.
[241] Y.L. Uscátegui, L.E. Díaz, J.A. Gómez-Tejedor, A. Vallés-Lluch, G. Vilariño-Feltrer, M.A. Serrano, M.F. Valero, Candidate polyurethanes based on castor oil (ricinus communis), with polycaprolactone diol and chitosan additions, for use in biomedical applications, Molecules 24 (2019). https://doi.org/10.3390/molecules24020237.
[242] K.M. Zia, F. Zia, M. Zuber, S. Rehman, M.N. Ahmad, Alginate based polyurethanes: A review of recent advances and perspective, Int. J. Biol. Macromol. 79 (2015) 377–387. https://doi.org/10.1016/j.ijbiomac.2015.04.076.
[243] M. Movahedi, A. Asefnejad, M. Rafienia, M.T. Khorasani, Potential of novel electrospun core-shell structured polyurethane/starch (hyaluronic acid) nanofibers for skin tissue engineering: In vitro and in vivo evaluation, Int. J. Biol. Macromol. 146 (2020) 627–637. https://doi.org/10.1016/j.ijbiomac.2019.11.233.
[244] A. Ruiz, K.R. Rathnam, K.S. Masters, Effect of hyaluronic acid incorporation method on the stability and biological properties of polyurethane–hyaluronic acid biomaterials, J. Mater. Sci. Mater. Med. 25 (2014) 487–498. https://doi.org/10.1007/s10856-013-5092-1.
[245] M. Sheikholeslam, M.E.E. Wright, N. Cheng, H.H. Oh, Y. Wang, A.K. Datu, J.P. Santerre, S. Amini-Nik, M.G. Jeschke, Electrospun Polyurethane-Gelatin Composite: A New Tissue-Engineered Scaffold for Application in Skin Regeneration and Repair of Complex Wounds, ACS Biomater. Sci. Eng. 6 (2020) 505–516. https://doi.org/10.1021/acsbiomaterials.9b00861.
[246] H. Zhao, Y. Liu, Y. Jiang, eds., Advances in the Preparation, Properties and Application of Polyurethane, Cellulose and Their Composites, MDPI, 2024. https://doi.org/10.3390/books978-3-7258-0184-8.
[247] W.-F. Su, C.-C. Ho, T.-H. Shih, C.-H. Wang, C.-H. Yeh, Exceptional biocompatibility of 3D fibrous scaffold for cardiac tissue engineering fabricated from biodegradable polyurethane blended with cellulose, Int. J. Polym. Mater. Polym. Biomater. 65 (2016) 703–711. https://doi.org/10.1080/00914037.2016.1157802.
[248] D. Filip, D. Macocinschi, C.G. Tuchilus, S. Vlad, M.F. Zaltariov, C.D. Varganici, Chloramphenicol-based poly(ester-ether)urethane bioconjugates with antibacterial properties for biomedical applications, Polym. Bull. 75 (2018) 701–727. https://doi.org/10.1007/s00289-017-2064-5.
[249] X. Chen, R. Zhao, X. Wang, X. Li, F. Peng, Z. Jin, X. Gao, J. Yu, C. Wang, Electrospun mupirocin loaded polyurethane fiber mats for anti-infection burn wound dressing application, J. Biomater. Sci. Polym. Ed. 28 (2017) 162–176. https://doi.org/10.1080/09205063.2016.1262158.
[250] S. Kolay, S. Dey, T. Mondal, S. Sk, S. Haldar, B. Giri, M.R. Molla, Surface Charge-Switchable Doxorubicin-Containing Polyurethane Prodrug Nanoparticles for Targeted Cancer Therapy, ACS Appl. Nano Mater. 8 (2025) 21912–21921. https://doi.org/10.1021/acsanm.5c03950.
[251] M. Borowska, M. Glinka, N. Filipowicz, A. Terebieniec, P. Szarlej, A. Kot-Wasik, J. Kucińska-Lipka, Polymer biodegradable coatings as active substance release systems for urological applications, Monatshefte Für Chem. - Chem. Mon. 150 (2019) 1697–1702. https://doi.org/10.1007/s00706-019-02474-8.
[252] M. Singh, M. Anees, A. Afreen, D. Kalyanasundaram, N. Bhatnagar, H. Singh, Development of iodine based sustained release antimicrobial coatings for polyurethane voice prostheses, J. Mater. Chem. B 12 (2024) 5907–5916. https://doi.org/10.1039/D4TB00439F.
[253] Jie Luo, Ying Deng, Yuyu Sun, Antimicrobial Activity and Biocompatibility of Polyurethane—Iodine Complexes, J. Bioact. Compat. Polym. 25 (2010) 185–206. https://doi.org/10.1177/0883911509359980.
[254] A. Eskandarinia, A. Kefayat, M. Agheb, M. Rafienia, M. Amini Baghbadorani, S. Navid, K. Ebrahimpour, D. Khodabakhshi, F. Ghahremani, A Novel Bilayer Wound Dressing Composed of a Dense Polyurethane/Propolis Membrane and a Biodegradable Polycaprolactone/Gelatin Nanofibrous Scaffold, Sci. Rep. 10 (2020) 1–15. https://doi.org/10.1038/s41598-020-59931-2.

[255] D. Khodabakhshi, A. Eskandarinia, A. Kefayat, M. Rafienia, S. Navid, S. Karbasi, J. Moshtaghian, In vitro and in vivo performance of a propolis-coated polyurethane wound dressing with high porosity and antibacterial efficacy, Colloids Surf. B Biointerfaces 178 (2019) 177–184. https://doi.org/10.1016/j.colsurfb.2019.03.010.
[256] H.S. Sofi, T. Akram, A.H. Tamboli, A. Majeed, N. Shabir, F.A. Sheikh, Novel lavender oil and silver nanoparticles simultaneously loaded onto polyurethane nanofibers for wound-healing applications, Int. J. Pharm. 569 (2019). https://doi.org/10.1016/j.ijpharm.2019.118590.
[257] A. Manikandan, M.P. Mani, S.K. Jaganathan, R. Rajasekar, M. Jagannath, Formation of functional nanofibrous electrospun polyurethane and murivenna oil with improved haemocompatibility for wound healing, Polym. Test. 61 (2017) 106–113. https://doi.org/10.1016/j.polymertesting.2017.05.008.
[258] Z. Alborzi, H. Izadi-Vasafi, F. Ghayoumi, Wound dressings based on chitosan and gelatin containing starch, sesame oil and banana peel powder for the treatment of skin burn wounds, J. Polym. Res. 28 (2021) 1–16. https://doi.org/10.1007/S10965-021-02427-Y.
[259] S.K. Jaganathan, M. Prasath Mani, A.Z.M. Khudzari, A. Fauzi bin Ismail, Physicochemical assessment of tailor made fibrous polyurethane scaffolds incorporated with turmeric oil for wound healing applications, Int. J. Polym. Anal. Charact. 24 (2019) 752–762. https://doi.org/10.1080/1023666X.2019.1676010.
[260] S.A.B. Nordin, M.P. Mani, S.K. Jaganathan, A.Z.M. Khudzari, A.F. Ismail, Fabrication and characterization of a novel wound scaffold based on polyurethane added with Channa striatus for wound dressing applications, Int. J. Polym. Anal. Charact. 25 (2020) 126–133. https://doi.org/10.1080/1023666X.2020.1766786.
[261] M. Li, Q. Dong, Y. Xiao, Q. Du, C. Huselsteind, T. Zhang, X. He, W. Tian, Y. Chen, A biodegradable soy protein isolate-based waterborne polyurethane composite sponge for implantable tissue engineering, J. Mater. Sci. Mater. Med. 31 (2020) 120. https://doi.org/10.1007/s10856-020-06451-0.
[262] M. Staji, N. Sadeghzadeh, S. Zamanlui, M. Azarani, A. Golchin, M. Soleimani, A. Ardeshirylajimi, A. Khojasteh, S. Hosseinzadeh, Evaluation of dermal growth of keratinocytes derived from foreskin in co-culture condition with mesenchymal stem cells on polyurethane/gelatin/amnion scaffold, Int. J. Polym. Mater. Polym. Biomater. 72 (2023) 386–396. https://doi.org/10.1080/00914037.2021.2018316.
[263] B. Pant, M. Park, G.P. Ojha, D.-U. Kim, H.-Y. Kim, S.-J. Park, Electrospun salicylic acid/polyurethane composite nanofibers for biomedical applications, Int. J. Polym. Mater. Polym. Biomater. 67 (2018) 739–744. https://doi.org/10.1080/00914037.2017.1376200.
[264] N. Dehghan-Manshadi, S. Fattahi, M. Hadizadeh, H. Nikukar, S.M. Moshtaghioun, B. Aflatoonian, The influence of elastomeric polyurethane type and ratio on the physicochemical properties of electrospun polyurethane/silk fibroin hybrid nanofibers as potential scaffolds for soft and hard tissue engineering, Eur. Polym. J. 121 (2019) 109294. https://doi.org/10.1016/j.eurpolymj.2019.109294.
[265] J.I. Kim, H.R. Pant, H.-J. Sim, K.M. Lee, C.S. Kim, Electrospun propolis/polyurethane composite nanofibers for biomedical applications, Mater. Sci. Eng. C 44 (2014) 52–57. https://doi.org/10.1016/j.msec.2014.07.062.
[266] S. Rezaei Hosseinabadi, A. Parsapour, S. Nouri Khorasani, S.M. Razavi, B. Hashemibeni, F. Heidari, S. Khalili, Wound dressing application of castor oil- and CAPA-based polyurethane membranes, Polym. Bull. 77 (2020) 2945–2964. https://doi.org/10.1007/s00289-019-02891-z.
[267] N. Namviriyachote, P. Muangman, K. Chinaroonchai, C. Chuntrasakul, G.C. Ritthidej, Polyurethane-biomacromolecule combined foam dressing containing asiaticoside: fabrication, characterization and clinical efficacy for traumatic dermal wound treatment, Int. J. Biol. Macromol. 143 (2020) 510–520. https://doi.org/10.1016/j.ijbiomac.2019.10.166.
[268] L.-G. Dai, N.-T. Dai, T.-Y. Chen, L.-Y. Kang, S. Hsu, A bioprinted vascularized skin substitute with fibroblasts, keratinocytes, and endothelial progenitor cells for skin wound healing, Bioprinting 28 (2022) e00237. https://doi.org/10.1016/j.bprint.2022.e00237.
[269] R. Pathak, S. Bierman, P. d'Arnaud, Inhibition of bacterial attachment and biofilm formation by a novel intravenous catheter material using an in vitro percutaneous catheter insertion model, Med. Devices Evid. Res. Volume 11 (2018) 427–432. https://doi.org/10.2147/MDER.S183409.
[270] A. Mahomed, D.W.L. Hukins, S.N. Kukureka, D.E.T. Shepherd, Effect of accelerated aging on the viscoelastic properties of Elast-Eon™: A polyurethane with soft

poly(dimethylsiloxane) and poly(hexamethylene oxide) segments, Mater. Sci. Eng. C 30 (2010) 1298–1303. https://doi.org/10.1016/j.msec.2010.07.014.
[271] D. Atherton, V. Sreetharan, A. Mosahebi, S. Prior, J. Willis, J. Bishop, P. Dziewulski, A randomised controlled trial of a double layer of Allevyn™ compared to Jellonet and proflavin as a tie-over dressing for small skin grafts, J. Plast. Reconstr. Aesthet. Surg. 61 (2008) 535–539. https://doi.org/10.1016/j.bjps.2007.01.004.
[272] M. Jenks, J. Craig, W. Green, N. Hewitt, M. Arber, A. Sims, Tegaderm CHG IV Securement Dressing for Central Venous and Arterial Catheter Insertion Sites: A NICE Medical Technology Guidance, Appl. Health Econ. Health Policy. 14 (2016) 135–149. https://doi.org/10.1007/s40258-015-0202-5.
[273] R. Rajaram, M. Zhang, G. Premaratne, S. Ng, Novosorb® BTM- history, production and application in challenging wounds, Front. Bioeng. Biotechnol. 12 (2024) 1450973. https://doi.org/10.3389/fbioe.2024.1450973.
[274] G.T. Szoradi, A.M. Feier, S.G. Zuh, O.M. Russu, T.S. Pop, Polymethyl Methacrylate Bone Cement Polymerization Induced Thermal Necrosis at the Cement–Bone Interface: A Narrative Review, Appl. Sci. 14 (2024) 11651. https://doi.org/10.3390/app142411651.
[275] J. Lim, A. Jariwala, C. Wigderowitz, T. Drew, The Use of Bone Adhesive for Fracture Fixation in Long Bones – A Biomechanical Study, Front. Biol. Life Sci. 2 (2014) 29. https://doi.org/10.12966/fbls.06.03.2014.
[276] M. Dm, H. S, P. A, M. A, P. Bj, T. Bc, Artelon as a Bio-Scaffold to Augment Collateral Ligament Repair after Knee Dislocation, Malays. Orthop. J. 16 (2022) 110–118. https://doi.org/10.5704/MOJ.2207.014.
[277] I. Rykowska, I. Nowak, R. Nowak, Drug-Eluting Stents and Balloons—Materials, Structure Designs, and Coating Techniques: A Review, Molecules 25 (2020) 4624. https://doi.org/10.3390/molecules25204624.
[278] H. Xiang, D. Verrico, T. Hafiz, E. He, G.E. Wnek, K. Hu, G. Liu, Y. Wei, J. Ji, Antimicrobial and breathable membranes with printed carbon nanotube-silver composite conductive layers for electronic sensing, Chem. Sci. 16 (2025) 20344–20354. https://doi.org/10.1039/D5SC05696A.
[279] D. Kowalczuk, M. Miazga-Karska, A. Gładysz, P. Warda, A. Barańska, B. Drop, Characterization of Ciprofloxacin-Bismuth-Loaded Antibacterial Wound Dressing, Mol. Basel Switz. 25 (2020). https://doi.org/10.3390/molecules25215096.
[280] P. Losi, T. Al Kayal, M. Buscemi, I. Foffa, A. Cavallo, G. Soldani, Bilayered fibrin-based electrospun-sprayed scaffold loaded with platelet lysate enhances wound healing in a diabetic mouse model, Nanomaterials 10 (2020) 1–11. https://doi.org/10.3390/nano10112128.
[281] C. Luo, W. Liu, B. Luo, J. Tian, W. Wen, M. Liu, C. Zhou, Antibacterial activity and cytocompatibility of chitooligosaccharide-modified polyurethane membrane via polydopamine adhesive layer, Carbohydr. Polym. 156 (2017) 235–243. https://doi.org/10.1016/j.carbpol.2016.09.036.
[282] T.Y. Jasim, M.A. Najim, A.R. Jabur, Improving the mechanical properties of (chitosan/polyurethane) electrospun blend scaffold used for skin regeneration, AIP Conf. Proc. 2123 (2019) 0–7. https://doi.org/10.1063/1.5116969.
[283] I. Herrmann, E. Supriyanto, S.K. Jaganathan, A. Manikandan, Advanced nanofibrous textile-based dressing material for treating chronic wounds, Bull. Mater. Sci. 41 (2018) 18. https://doi.org/10.1007/s12034-017-1543-5.
[284] S.K. Jaganathan, M.P. Mani, P. Prabhakaran, E. Supriyanto, A.F. Ismail, Production, blood compatibility and cytotoxicity evaluation of a single stage non-woven multicomponent electrospun scaffold mixed with sesame oil, honey and propolis for skin tissue engineering, Int. J. Polym. Anal. Charact. 24 (2019) 457–474. https://doi.org/10.1080/1023666X.2019.1602919.
[285] M.P. Mani, S.K. Jaganathan, Physicochemical and blood compatibility characteristics of garlic incorporated polyurethane nanofibrous scaffold for wound dressing applications, J. Text. Inst. 110 (2019) 1615–1623. https://doi.org/10.1080/00405000.2019.1610145.
[286] M.P. Mani, S.K. Jaganathan, A.F. Ismail, Appraisal of electrospun textile scaffold comprising polyurethane decorated with ginger nanofibers for wound healing applications, J. Ind. Text. 49 (2019) 648–662. https://doi.org/10.1177/1528083718795911.
[287] M.P. Mani, S.K. Jaganathan, Fabrication and characterization of electrospun polyurethane blended with dietary grapes for skin tissue engineering, J. Ind. Text. 50 (2020) 655–674. https://doi.org/10.1177/1528083719840628.

[288] P. Sagitha, C.R. Reshmi, S.P. Sundaran, A. Binoy, N. Mishra, A. Sujith, In-vitro evaluation on drug release kinetics and antibacterial activity of dextran modified polyurethane fibrous membrane, Int. J. Biol. Macromol. 126 (2019) 717–730. https://doi.org/10.1016/j.ijbiomac.2018.12.155.
[289] Y.J. Seol, H. Lee, J.S. Copus, H.W. Kang, D.W. Cho, A. Atala, S.J. Lee, J.J. Yoo, 3D bioprinted biomask for facial skin reconstruction, Bioprinting 10 (2018) 1–6. https://doi.org/10.1016/j.bprint.2018.e00028.
[290] S. Currie, F.J. Shariatzadeh, H. Singh, S. Logsetty, S. Liu, Highly Sensitive Bacteria-Responsive Membranes Consisting of Core–Shell Polyurethane Polyvinylpyrrolidone Electrospun Nanofibers for In Situ Detection of Bacterial Infections, ACS Appl. Mater. Interfaces 12 (2020) 45859–45872. https://doi.org/10.1021/acsami.0c14213.
[291] H. Singh, W. Li, M.R. Kazemian, R. Yang, C. Yang, S. Logsetty, S. Liu, Lipase-Responsive Electrospun Theranostic Wound Dressing for Simultaneous Recognition and Treatment of Wound Infection, ACS Appl. Bio Mater. 2 (2019) 2028–2036. https://doi.org/10.1021/acsabm.9b00076.
[292] Y. Guo, S. Pan, F. Jiang, E. Wang, L. Miinea, N. Marchant, M. Cakmak, Anisotropic swelling wound dressings with vertically aligned water absorptive particles, RSC Adv. 8 (2018) 8173–8180. https://doi.org/10.1039/C7RA13764H.
[293] P. Mistry, R. Chhabra, S. Muke, A. Narvekar, S. Sathaye, R. Jain, P. Dandekar, Fabrication and characterization of starch-TPU based nanofibers for wound healing applications, Mater. Sci. Eng. C 119 (2021) 111316. https://doi.org/10.1016/j.msec.2020.111316.
[294] M.P. Drupitha, K. Bankoti, P. Pal, B. Das, R. Parameswar, S. Dhara, G.B. Nando, K. Naskar, Morphology-induced physico-mechanical and biological characteristics of TPU–PDMS blend scaffolds for skin tissue engineering applications, J. Biomed. Mater. Res. - Part B Appl. Biomater. 107 (2019) 1634–1644. https://doi.org/10.1002/jbm.b.34256.
[295] J.R. Clegg, K. Adebowale, Z. Zhao, S. Mitragotri, Hydrogels in the clinic: An update, Bioeng. Transl. Med. 9 (2024) e10680. https://doi.org/10.1002/btm2.10680.
[296] J.M. Van Bemmelen, Das Hydrogel und das krystallinische Hydrat des Kupferoxyds, Z. Für Anorg. Chem. 5 (1894) 466–483. https://doi.org/10.1002/zaac.18940050156.
[297] O. Wichterle, D. Lim, Hydrophilic gels for biological use, Nature (1960) 117–118. https://doi.org/10.1038/185117a0.
[298] A. GhavamiNejad, N. Ashammakhi, X.Y. Wu, A. Khademhosseini, Crosslinking Strategies for 3D Bioprinting of Polymeric Hydrogels, Small 16 (2020) 2002931. https://doi.org/10.1002/smll.202002931.
[299] K.L.M. Taaca, E.I. Prieto, M.R. Vasquez, Current Trends in Biomedical Hydrogels: From Traditional Crosslinking to Plasma-Assisted Synthesis, Polymers 14 (2022) 2560. https://doi.org/10.3390/polym14132560.
[300] R.A. Christian, K.J. Stabile, A.K. Gupta, B.D. Leckey, D.M. Cardona, R.J. Nowinski, J.D. Kelly, A.P. Toth, Histologic Analysis of Porcine Dermal Graft Augmentation in Treatment of Rotator Cuff Tears, Am. J. Sports Med. 49 (2021) 3680–3686. https://doi.org/10.1177/03635465211049434.
[301] B. Jadach, Z. Mielcarek, T. Osmałek, Use of Collagen in Cosmetic Products, Curr. Issues Mol. Biol. 46 (2024) 2043–2070. https://doi.org/10.3390/cimb46030132.
[302] L. Zaulyanov, R.S. Kirsner, A review of a bi-layered living cell treatment (Apligraf□) in the treatment of venous leg ulcers and diabetic foot ulcers, Clin. Interv. Aging 2 (2007) 93–98. https://doi.org/10.2147/ciia.2007.2.1.93.
[303] Y. Lu, M. Zhao, Y. Peng, S. He, X. Zhu, C. Hu, G. Xia, T. Zuo, X. Zhang, Y. Yun, W. Zhang, X. Shen, A physicochemical double-cross-linked gelatin hydrogel with enhanced antibacterial and anti-inflammatory capabilities for improving wound healing, J. Nanobiotechnology 20 (2022) 426. https://doi.org/10.1186/s12951-022-01634-z.
[304] S. Asim, T.A. Tabish, U. Liaqat, I.T. Ozbolat, M. Rizwan, Advances in Gelatin Bioinks to Optimize Bioprinted Cell Functions, Adv. Healthc. Mater. 12 (2023) 2203148. https://doi.org/10.1002/adhm.202203148.
[305] J. Ma, S. Gan, R. Shu, L. Zhou, S. Chen, Efficacy and safety assessment of gelatin hemostatic matrix in a burr hole neurosurgical beagle model, Sci. Rep. 15 (2025) 44374. https://doi.org/10.1038/s41598-025-28075-6.
[306] K. Nomura, M. Yoshida, M. Okada, Y. Nakamura, K. Yawatari, E. Nakayama, Effectiveness of a Gelatin–Thrombin Matrix Sealant (Floseal®) for Reducing Blood Loss During Microendoscopic Decompression Surgery for Lumbar Spinal Canal Stenosis: A

Retrospective Cohort Study, Glob. Spine J. 13 (2023) 764–770. https://doi.org/10.1177/21925682211008835.
[307] C.J. Gassel, E. Nasyrov, D.A. Wenzel, B. Voykov, XEN45 gel stent in the treatment of pigmentary glaucoma: A two-year follow-up, Eur. J. Ophthalmol. 35 (2025) 172–180. https://doi.org/10.1177/11206721241261093.
[308] K. Jia, J. You, Y. Zhu, M. Li, S. Chen, S. Ren, S. Chen, J. Zhang, H. Wang, Y. Zhou, Platelet-rich fibrin as an autologous biomaterial for bone regeneration: mechanisms, applications, optimization, Front. Bioeng. Biotechnol. 12 (2024) 1286035. https://doi.org/10.3389/fbioe.2024.1286035.
[309] J.K. Gandhi, F. Mano, R. Iezzi, S.A. LoBue, B.H. Holman, M.P. Fautsch, T.W. Olsen, J.S. Pulido, A.D. Marmorstein, Fibrin hydrogels are safe, degradable scaffolds for sub-retinal implantation, PLOS ONE 15 (2020) e0227641. https://doi.org/10.1371/journal.pone.0227641.
[310] J.R. Bagó, G.J. Pegna, O. Okolie, S.D. Hingtgen, Fibrin matrices enhance the transplant and efficacy of cytotoxic stem cell therapy for post-surgical cancer, Biomaterials 84 (2016) 42–53. https://doi.org/10.1016/j.biomaterials.2016.01.007.
[311] J. Kim, J. Park, S.-Y. Song, E. Kim, Advanced Therapy medicinal products for autologous chondrocytes and comparison of regulatory systems in target countries, Regen. Ther. 20 (2022) 126–137. https://doi.org/10.1016/j.reth.2022.04.004.
[312] L.N. Trinh, A. Gupta, Hyaluronic Acid Fillers for Midface Augmentation: A Systematic Review, Facial Plast. Surg. 37 (2021) 576–584. https://doi.org/10.1055/s-0041-1724122.
[313] J. Peck, A. Slovek, P. Miro, N. Vij, B. Traube, C. Lee, A.A. Berger, H. Kassem, A.D. Kaye, W.F. Sherman, A. Abd-Elsayed, A Comprehensive Review of Viscosupplementation in Osteoarthritis of the Knee, Orthop. Rev. 13 (2021). https://doi.org/10.52965/001c.25549.
[314] D.L. Mann, R.J. Lee, A.J.S. Coats, G. Neagoe, D. Dragomir, E. Pusineri, M. Piredda, L. Bettari, B.-A. Kirwan, R. Dowling, M. Volterrani, S.D. Solomon, H.N. Sabbah, A. Hinson, S.D. Anker, One-Year Follow-Up Results from AUGMENT-HF: A Multicentre Randomized Controlled Clinical Trial of the Efficacy of Left Ventricular Augmentation with Algisyl in the Treatment of Heart Failure, Eur. J. Heart Fail. 18 (2016) 314–325. https://doi.org/10.1002/ejhf.449.
[315] Y.J. Lee, K.S. Park, D.Y. Kim, H.-S. Shim, Evaluating Effectiveness of Medical Grade Honey-Containing Alginate Dressing in Patients with Chronic Lower Extremity Wounds, J. Wound Manag. Res. 17 (2021) 178–186. https://doi.org/10.22467/jwmr.2021.01557.
[316] M.S. Chellathurai, L.Y. Chung, A.R. Hilles, Z.M. Sofian, S. Singha, K. Ghosal, S. Mahmood, Pharmaceutical chitosan hydrogels: A review on its design and applications, Int. J. Biol. Macromol. 280 (2024) 135775. https://doi.org/10.1016/j.ijbiomac.2024.135775.
[317] H. Azargoon, B.J. Williams, E.S. Solomon, H.P. Kessler, J. He, R. Spears, Assessment of Hemostatic Efficacy and Osseous Wound Healing Using HemCon Dental Dressing, J. Endod. 37 (2011) 807–811. https://doi.org/10.1016/j.joen.2011.02.023.
[318] M. Steinwachs, N. Cavalcanti, S. Mauuva Venkatesh Reddy, C. Werner, D. Tschopp, H.N. Choudur, Arthroscopic and open treatment of cartilage lesions with BST-CARGEL scaffold and microfracture: A cohort study of consecutive patients, The Knee 26 (2019) 174–184. https://doi.org/10.1016/j.knee.2018.11.015.
[319] A.R. Li, B. Taylor, A.N. Snyder, T. Schlesinger, Algeness—What do we know about this filler, Dermatol. Rev. 4 (2023) 100–104. https://doi.org/10.1002/der2.184.
[320] I. Gibas, H. Janik, Review: Synthetic Polymer Hydrogels for Biomedical Applications, Chem. Chem. Technol. 4 (2010) 297–304. https://doi.org/10.23939/chcht04.04.297.
[321] S. Sun, Y. Cui, B. Yuan, M. Dou, G. Wang, H. Xu, J. Wang, W. Yin, D. Wu, C. Peng, Drug delivery systems based on polyethylene glycol hydrogels for enhanced bone regeneration, Front. Bioeng. Biotechnol. 11 (2023) 1117647. https://doi.org/10.3389/fbioe.2023.1117647.
[322] R.D. Machiele, A. Guduru, L.W. Herndon, Hydrogel Sealant for Closure of Clear Corneal Incisions in Combined Glaucoma Procedures, Clin. Ophthalmol. Volume 16 (2022) 861–865. https://doi.org/10.2147/OPTH.S354531.
[323] H. Grewal, R. Kedar, G. Dhillon, G. Sidhu, R. Kashyap, K. Sailagundala, SpaceOAR hydrogel complications in prostate cancer, Br. J. Radiol. 96 (2023) 20230717. https://doi.org/10.1259/bjr.20230717.
[324] M.A. Shiffman, Introduction to Wound Dressings, in: M.A. Shiffman, M. Low (Eds.), Chronic Wounds Wound Dress. Wound Heal., Springer International Publishing, Cham, 2018: pp. 181–184. https://doi.org/10.1007/15695_2018_135.

[325] A. Jeremic, R. Abussa, Cartiva or fusion for Hallux Rigidus? A systematic review and meta-analysis, J. Foot Ankle Surg. (2026) S1067251626000785. https://doi.org/10.1053/j.jfas.2026.03.003.
[326] M. Kurakula, G.S.N.K. Rao, Pharmaceutical assessment of polyvinylpyrrolidone (PVP): As excipient from conventional to controlled delivery systems with a spotlight on COVID-19 inhibition, J. Drug Deliv. Sci. Technol. 60 (2020). https://doi.org/10.1016/j.jddst.2020.102046.
[327] X. Lin, X. Guan, Y. Wu, S. Zhuang, Y. Wu, L. Du, J. Zhao, J. Rong, J. Zhao, M. Tu, An alginate/poly(N-isopropylacrylamide)-based composite hydrogel dressing with stepwise delivery of drug and growth factor for wound repair, Mater. Sci. Eng. C 115 (2020). https://doi.org/10.1016/J.MSEC.2020.111123.
[328] F. Tajik, N. Eslahi, A. Rashidi, M.M. Rad, Hybrid antibacterial hydrogels based on PVP and keratin incorporated with lavender extract, J. Polym. Res. 28 (2021). https://doi.org/10.1007/s10965-021-02681-0.
[329] M. Babaluei, F. Mottaghitalab, A. Seifalian, M. Farokhi, Injectable multifunctional hydrogel based on carboxymethylcellulose/polyacrylamide/polydopamine containing vitamin C and curcumin promoted full-thickness burn regeneration, Int. J. Biol. Macromol. 236 (2023) 124005. https://doi.org/10.1016/j.ijbiomac.2023.124005.
[330] A.-E. Segneanu, L.E. Bejenaru, C. Bejenaru, A. Blendea, G.D. Mogoşanu, A. Biţă, E.R. Boia, Advancements in Hydrogels: A Comprehensive Review of Natural and Synthetic Innovations for Biomedical Applications, Polymers 17 (2025) 2026. https://doi.org/10.3390/polym17152026.
[331] J. Zhao, M. Marczynski, M. Henkel, O. Lieleg, Agarose-based hydrogels with tunable, charge-selective permeability properties, J. Appl. Polym. Sci. 140 (2023) e54303. https://doi.org/10.1002/app.54303.
[332] J. Pasek, S. Szajkowski, G. Cieślar, A Double-Blind Study on the Effectiveness of Polarized Light Therapy in the Treatment of Venous leg Ulcers—Pilot Study, Int. J. Low. Extrem. Wounds (2024) 15347346241264602. https://doi.org/10.1177/15347346241264602.
[333] K. Theodoridis, M.E. Manthou, E. Aggelidou, A. Kritis, *In Vivo* Cartilage Regeneration with Cell-Seeded Natural Biomaterial Scaffold Implants: 15-Year Study, Tissue Eng. Part B Rev. 28 (2022) 206–245. https://doi.org/10.1089/ten.teb.2020.0295.
[334] M.M. Schreiner, M. Raudner, P. Szomolanyi, K. Ohel, L. Ben-Zur, V. Juras, V. Mlynarik, R. Windhager, S. Trattnig, Chondral and Osteochondral Femoral Cartilage Lesions Treated with GelrinC: Significant Improvement of Radiological Outcome Over Time and Zonal Variation of the Repair Tissue Based on T_2 Mapping at 24 Months, CARTILAGE 13 (2021) 604S-616S. https://doi.org/10.1177/1947603520926702.
[335] K.N. Mangang, P. Thakran, J. Halder, K.S. Yadav, G. Ghosh, D. Pradhan, G. Rath, V.K. Rai, PVP-microneedle array for drug delivery: mechanical insight, biodegradation, and recent advances, J. Biomater. Sci. Polym. Ed. 34 (2023) 986–1017. https://doi.org/10.1080/09205063.2022.2155778.
[336] M.M. Rana, H. De La Hoz Siegler, Evolution of Hybrid Hydrogels: Next-Generation Biomaterials for Drug Delivery and Tissue Engineering, Gels 10 (2024) 216. https://doi.org/10.3390/gels10040216.
[337] Y. Choi, H.Y. Koh, J.Y. Han, S. Seo, Synthesis of Hydrogel-Based Microgels and Nanogels Toward Therapeutic and Biomedical Applications, Appl. Sci. 15 (2025) 1368. https://doi.org/10.3390/app15031368.
[338] D.-Z. Ma, Z.-Z. Hu, P. Zhang, W.-M. Xie, X.-Y. Lin, F.-F. Wu, X.-M. Sha, Z.-C. Tu, Enhanced gelling properties in fish gelatin by refined and semi-refined κ-carrageenan, Curr. Res. Food Sci. 12 (2026) 101338. https://doi.org/10.1016/j.crfs.2026.101338.
[339] X. Gan, X. Wang, Y. Huang, G. Li, H. Kang, Applications of Hydrogels in Osteoarthritis Treatment, Biomedicines 12 (2024) 923. https://doi.org/10.3390/biomedicines12040923.
[340] F. Seidi, W. Zhao, H. Xiao, Y. Jin, M.R. Saeb, C. Zhao, Radical polymerization as a versatile tool for surface grafting of thin hydrogel films, Polym. Chem. 11 (2020) 4355–4381. https://doi.org/10.1039/D0PY00787K.
[341] P. Sánchez-Cid, M. Jiménez-Rosado, A. Romero, V. Pérez-Puyana, Novel Trends in Hydrogel Development for Biomedical Applications: A Review, Polymers 14 (2022) 3023. https://doi.org/10.3390/polym14153023.
[342] C. Cona, K. Bailey, E. Barker, Characterization Methods to Determine Interpenetrating Polymer Network (IPN) in Hydrogels, Polymers 16 (2024) 2050. https://doi.org/10.3390/polym16142050.

[343] J.-Y. Sun, X. Zhao, W.R.K. Illeperuma, O. Chaudhuri, K.H. Oh, D.J. Mooney, J.J. Vlassak, Z. Suo, Highly stretchable and tough hydrogels, Nature 489 (2012) 133–136. https://doi.org/10.1038/nature11409.
[344] P.M. Kharkar, K.L. Kiick, A.M. Kloxin, Designing degradable hydrogels for orthogonal control of cell microenvironments, Chem Soc Rev 42 (2013) 7335–7372. https://doi.org/10.1039/C3CS60040H.
[345] P.J. Flory, J. Rehner, Statistical Mechanics of Cross-Linked Polymer Networks II. Swelling, J. Chem. Phys. 11 (1943) 521–526. https://doi.org/10.1063/1.1723792.
[346] P.J. Flory, J. Rehner, Statistical Mechanics of Cross-Linked Polymer Networks I. Rubberlike Elasticity, J. Chem. Phys. 11 (1943) 512–520. https://doi.org/10.1063/1.1723791.
[347] N.R. Richbourg, N.A. Peppas, The swollen polymer network hypothesis: Quantitative models of hydrogel swelling, stiffness, and solute transport, Prog. Polym. Sci. 105 (2020) 101243. https://doi.org/10.1016/j.progpolymsci.2020.101243.
[348] K. Chaturvedi, K. Ganguly, M.N. Nadagouda, T.M. Aminabhavi, Polymeric hydrogels for oral insulin delivery, J. Controlled Release 165 (2013) 129–138. https://doi.org/10.1016/j.jconrel.2012.11.005.
[349] R. Wang, C. Cheng, H. Wang, D. Wang, Swollen hydrogel nanotechnology: Advanced applications of the rudimentary swelling properties of hydrogels, ChemPhysMater 3 (2024) 357–375. https://doi.org/10.1016/j.chphma.2024.07.006.
[350] M. Bustamante-Torres, D. Romero-Fierro, B. Arcentales-Vera, K. Palomino, H. Magaña, E. Bucio, Hydrogels Classification According to the Physical or Chemical Interactions and as Stimuli-Sensitive Materials, Gels 7 (2021). https://doi.org/10.3390/GELS7040182.
[351] X. Li, X. Xu, M. Xu, Z. Geng, P. Ji, Y. Liu, Hydrogel systems for targeted cancer therapy, Front. Bioeng. Biotechnol. 11 (2023) 1140436. https://doi.org/10.3389/fbioe.2023.1140436.
[352] L. Li, J. Guo, C. Kang, LCST-UCST Transition Property of a Novel Retarding Swelling and Thermosensitive Particle Gel, Materials 16 (2023) 2761. https://doi.org/10.3390/ma16072761.
[353] R.V. Barrulas, M.C. Corvo, Rheology in Product Development: An Insight into 3D Printing of Hydrogels and Aerogels, Gels 9 (2023) 986. https://doi.org/10.3390/gels9120986.
[354] Y. Tang, M. Hu, F. Tang, R. Huang, H. Wang, D. Wu, P. Lan, Easily-injectable shear-thinning hydrogel provides long-lasting submucosal barrier for gastrointestinal endoscopic surgery, Bioact. Mater. 15 (2022) 44–52. https://doi.org/10.1016/j.bioactmat.2021.11.026.
[355] C. Han, J. Jiao, C. Gong, J. Li, M. Zhao, X. Lu, Multidimensional exploration of hydrogels as biological scaffolds for spinal cord regeneration: mechanisms and future perspectives, Front. Bioeng. Biotechnol. 13 (2025) 1576524. https://doi.org/10.3389/fbioe.2025.1576524.
[356] F.V. Lavrentev, V.V. Shilovskikh, V.S. Alabusheva, V.Yu. Yurova, A.A. Nikitina, S.A. Ulasevich, E.V. Skorb, Diffusion-Limited Processes in Hydrogels with Chosen Applications from Drug Delivery to Electronic Components, Molecules 28 (2023) 5931. https://doi.org/10.3390/molecules28155931.
[357] A. Pareek, S. Maheshwari, S. Cherlo, R.S.R. Thavva, V. Runkana, Modeling drug release through stimuli responsive polymer hydrogels, Int. J. Pharm. 532 (2017) 502–510. https://doi.org/10.1016/j.ijpharm.2017.09.001.
[358] T. Higuchi, Mechanism of sustained-action medication. Theoretical analysis of rate of release of solid drugs dispersed in solid matrices, J. Pharm. Sci. 52 (1963) 1145–1149. https://doi.org/10.1002/jps.2600521210.
[359] R.W. Korsmeyer, R. Gurny, E. Doelker, P. Buri, N.A. Peppas, Mechanisms of solute release from porous hydrophilic polymers, Int. J. Pharm. 15 (1983) 25–35. https://doi.org/10.1016/0378-5173(83)90064-9.
[360] M. Wang, Y. Zheng, C. Yin, S. Dai, X. Fan, Y. Jiang, X. Liu, J. Fang, B. Yi, Q. Zhou, T. Wang, Recent Progress in antibacterial hydrogel coatings for targeting biofilm to prevent orthopedic implant-associated infections, Front. Microbiol. 14 (2023) 1343202. https://doi.org/10.3389/fmicb.2023.1343202.
[361] A. Fedorov, R. Beichel, J. Kalpathy-Cramer, J. Finet, J.-C. Fillion-Robin, S. Pujol, C. Bauer, D. Jennings, F. Fennessy, M. Sonka, J. Buatti, S. Aylward, J.V. Miller, S. Pieper, R. Kikinis, 3D Slicer as an image computing platform for the Quantitative Imaging Network, Magn. Reson. Imaging 30 (2012) 1323–1341. https://doi.org/10.1016/j.mri.2012.05.001.
[362] DevilDesign, TPU product card, (n.d.).
[363] Noctuo, Mediflex product card, (n.d.).
[364] Fiberlogy, EasyPLA technical data sheet, (n.d.).

[365] SUNLU, PCL product card, (n.d.). https://3dsunlu.com/en/PCL-PG7435739 (accessed April 17, 2023).
[366] Filoalfa, Bioflex technical data sheet, (n.d.).
[367] N. Bouklas, R. Huang, Swelling kinetics of polymer gels: comparison of linear and nonlinear theories, Soft Matter 8 (2012) 8194. https://doi.org/10.1039/c2sm25467k.
[368] M. Włoch, J. Datta, K. Błażek, The Effect of High Molecular Weight Bio-based Diamine Derivative of Dimerized Fatty Acids Obtained from Vegetable Oils on the Structure, Morphology and Selected Properties of Poly(ether-urethane-urea)s, J. Polym. Environ. 26 (2018) 1592–1604. https://doi.org/10.1007/s10924-017-1059-5.
[369] A. Haryńska, I. Carayon, P. Kosmela, K. Szeliski, M. Łapiński, M. Pokrywczyńska, J. Kucińska-Lipka, H. Janik, A comprehensive evaluation of flexible FDM/FFF 3D printing filament as a potential material in medical application, Eur. Polym. J. 138 (2020) 109958. https://doi.org/10.1016/j.eurpolymj.2020.109958.
[370] The Merck Index Online - chemicals, drugs and biologicals, (n.d.). https://merckindex.rsc.org/?access=ft (accessed May 8, 2026).
[371] C. Rosado, C. Silva, C.P. Reis, Hydrocortisone-loaded poly(ε-caprolactone) nanoparticles for atopic dermatitis treatment, Pharm. Dev. Technol. 18 (2013) 710–718. https://doi.org/10.3109/10837450.2012.712537.
[372] T. Zan, W. Wang, H. Li, C. Liu, H. Zhu, Y. Xie, S. Zhou, Y. Gao, X. Huang, S. Gu, K. Liu, B. Gu, F. Xie, L.L.Q. Pu, Q. Li, Autologous Tissue Repair and Total Face Restoration, JAMA Otolaryngol. Neck Surg. 150 (2024) 695. https://doi.org/10.1001/jamaoto.2024.1572.
[373] M. Kauke-Navarro, L. Knoedler, H. Baecher, K. Sherwani, S. Knoedler, O. Allam, F. Diatta, M. Alperovich, A.-F. Safi, A systematic review of implant materials for facial reconstructive and aesthetic surgery, Front. Surg. 12 (2025) 1548597. https://doi.org/10.3389/fsurg.2025.1548597.
[374] M.F. Griffin, Y. Premakumar, A.M. Seifalian, M. Szarko, P.E.M. Butler, Biomechanical characterisation of the human nasal cartilages; implications for tissue engineering, J. Mater. Sci. Mater. Med. 27 (2016) 1–6. https://doi.org/10.1007/S10856-015-5619-8/TABLES/1.
[375] E.M. Abdelrazek, A.M. Hezma, A. El-khodary, A.M. Elzayat, Spectroscopic studies and thermal properties of PCL/PMMA biopolymer blend, Egypt. J. Basic Appl. Sci. 3 (2016) 10–15. https://doi.org/10.1016/j.ejbas.2015.06.001.
[376] R. Li, Y. Wu, Z. Bai, J. Guo, X. Chen, Effect of molecular weight of polyethylene glycol on crystallization behaviors, thermal properties and tensile performance of polylactic acid stereocomplexes, RSC Adv. 10 (2020) 42120–42127. https://doi.org/10.1039/D0RA08699A.
[377] D. Olmos, E.V. Martín, J. González-Benito, New molecular-scale information on polystyrene dynamics in PS and PS–BaTiO 3 composites from FTIR spectroscopy, Phys Chem Chem Phys 16 (2014) 24339–24349. https://doi.org/10.1039/C4CP03516J.
[378] S. Wang, L. Capoen, D.R. D'hooge, L. Cardon, Can the melt flow index be used to predict the success of fused deposition modelling of commercial poly(lactic acid) filaments into 3D printed materials?, Plast. Rubber Compos. 47 (2018) 9–16. https://doi.org/10.1080/14658011.2017.1397308.
[379] X. Jin, N. Guo, Z. You, Y. Tan, Design and Performance of Polyurethane Elastomers Composed with Different Soft Segments, Materials 13 (2020) 4991. https://doi.org/10.3390/ma13214991.
[380] A. Haryńska, I. Carayon, P. Kosmela, A. Brillowska-Dąbrowska, M. Łapiński, J. Kucińska-Lipka, H. Janik, Processing of Polyester-Urethane Filament and Characterization of FFF 3D Printed Elastic Porous Structures with Potential in Cancellous Bone Tissue Engineering, Materials 13 (2020) 4457. https://doi.org/10.3390/ma13194457.
[381] J. Momanyi, M. Herzog, P. Muchiri, Analysis of Thermomechanical Properties of Selected Class of Recycled Thermoplastic Materials Based on Their Applications, Recycling 4 (2019) 33. https://doi.org/10.3390/recycling4030033.
[382] J. Kucińska-Lipka, I. Gubanska, A. Skwarska, Microporous polyurethane thin layer as a promising scaffold for tissue engineering, Polymers 9 (2017) 1–16. https://doi.org/10.1023/B:WATE.0000026525.82039.ef.
[383] U. Sharma, D. Concagh, L. Core, Y. Kuang, C. You, Q. Pham, G. Zugates, R. Busold, S. Webber, J. Merlo, R. Langer, G.M. Whitesides, M. Palasis, The development of bioresorbable composite polymeric implants with high mechanical strength, Nat. Mater. 17 (2018) 96–103. https://doi.org/10.1038/nmat5016.
[384] D.H. Kim, W.-S. Yun, J.-H. Shim, K.-H. Park, D. Choi, M.I. Park, S.H. Hwang, S.W. Kim, Clinical Application of 3-Dimensional Printing Technology for Patients With Nasal Septal

Deformities, JAMA Otolaryngol. Neck Surg. 144 (2018) 1145. https://doi.org/10.1001/jamaoto.2018.2054.
[385] B.S. Caldas, C.S. Nunes, M.R. Panice, D.B. Scariot, C.V. Nakamura, E.C. Muniz, Manufacturing micro/nano chitosan/chondroitin sulfate curcumin-loaded hydrogel in ionic liquid: A new biomaterial effective against cancer cells, Int. J. Biol. Macromol. 180 (2021) 88–96. https://doi.org/10.1016/j.ijbiomac.2021.02.194.
[386] L. Zhang, X. Ren, P. Zhou, F. Wu, L. Liu, Z. Hai, Sequential self-assembly and disassembly of curcumin hydrogel effectively alleviates inflammatory bowel disease, Biomater. Sci. 10 (2022) 6517–6524. https://doi.org/10.1039/D2BM01120D.
[387] P. Guerrero, A. Etxabide, I. Leceta, M. Peñalba, K. De La Caba, Extraction of agar from Gelidium sesquipedale (Rodhopyta) and surface characterization of agar based films, Carbohydr. Polym. 99 (2014) 491–498. https://doi.org/10.1016/j.carbpol.2013.08.049.
[388] L.K. Mireles, M.-R. Wu, N. Saadeh, L. Yahia, E. Sacher, Physicochemical Characterization of Polyvinyl Pyrrolidone: A Tale of Two Polyvinyl Pyrrolidones, ACS Omega 5 (2020) 30461–30467. https://doi.org/10.1021/acsomega.0c04010.
[389] H.S. Mansur, C.M. Sadahira, A.N. Souza, A.A.P. Mansur, FTIR spectroscopy characterization of poly (vinyl alcohol) hydrogel with different hydrolysis degree and chemically crosslinked with glutaraldehyde, Mater. Sci. Eng. C 28 (2008) 539–548. https://doi.org/10.1016/J.MSEC.2007.10.088.
[390] S. Spoljaric, A. Salminen, N.D. Luong, J. Seppälä, Stable, self-healing hydrogels from nanofibrillated cellulose, poly(vinyl alcohol) and borax via reversible crosslinking, Eur. Polym. J. 56 (2014) 105–117. https://doi.org/10.1016/j.eurpolymj.2014.03.009.
[391] E. Gómez-Ordóñez, P. Rupérez, FTIR-ATR spectroscopy as a tool for polysaccharide identification in edible brown and red seaweeds, Food Hydrocoll. 25 (2011) 1514–1520. https://doi.org/10.1016/j.foodhyd.2011.02.009.
[392] K. Sharma, V. Kumar, C. Swart-Pistor, B. Chaudhary, H.C. Swart, Synthesis, characterization, and anti-microbial activity of superabsorbents based on agar–poly(methacrylic acid-glycine), J. Bioact. Compat. Polym. 32 (2016) 74–91. https://doi.org/10.1177/0883911516653148.
[393] E.A. El-hefian, M.M. Nasef, A.H. Yahaya, Preparation and Characterization of Chitosan/Agar Blended Films: Part 1. Chemical Structure and Morphology, J. Chem. 9 (2012) 1431–1439. https://doi.org/10.1155/2012/781206.
[394] H.M. Zidan, E.M. Abdelrazek, A.M. Abdelghany, A.E. Tarabiah, Characterization and some physical studies of PVA/PVP filled with MWCNTs, J. Mater. Res. Technol. 8 (2019) 904–913. https://doi.org/10.1016/j.jmrt.2018.04.023.
[395] F. Meng, A. Trivino, D. Prasad, H. Chauhan, Investigation and correlation of drug polymer miscibility and molecular interactions by various approaches for the preparation of amorphous solid dispersions, Eur. J. Pharm. Sci. 71 (2015) 12–24. https://doi.org/10.1016/j.ejps.2015.02.003.
[396] P.R.K. Mohan, G. Sreelakshmi, C.V. Muraleedharan, R. Joseph, Water soluble complexes of curcumin with cyclodextrins: Characterization by FT-Raman spectroscopy, Vib. Spectrosc. 62 (2012) 77–84. https://doi.org/10.1016/j.vibspec.2012.05.002.
[397] E. Al-Emam, H. Soenen, J. Caen, K. Janssens, Characterization of polyvinyl alcohol-borax/agarose (PVA-B/AG) double network hydrogel utilized for the cleaning of works of art, Herit. Sci. 8 (2020) 106. https://doi.org/10.1186/s40494-020-00447-3.
[398] S. Faham, R. Ghavami, H. Golmohammadi, G. Khayatian, Spectrophotometric and visual determination of zoledronic acid by using a bacterial cell-derived nanopaper doped with curcumin, Microchim. Acta 186 (2019) 719. https://doi.org/10.1007/s00604-019-3815-9.
[399] S. Wanninger, V. Lorenz, A. Subhan, F.T. Edelmann, Metal complexes of curcumin – synthetic strategies, structures and medicinal applications, Chem. Soc. Rev. 44 (2015) 4986–5002. https://doi.org/10.1039/C5CS00088B.
[400] M. Huang, Y. Hou, Y. Li, D. Wang, L. Zhang, High performances of dual network PVA hydrogel modified by PVP using borax as the structure-forming accelerator, Des. Monomers Polym. 20 (2017) 505–513. https://doi.org/10.1080/15685551.2017.1382433.
[401] E. Fernández, D. López, C. Mijangos, M. Duskova-Smrckova, M. Ilavsky, K. Dusek, Rheological and thermal properties of agarose aqueous solutions and hydrogels, J. Polym. Sci. Part B Polym. Phys. 46 (2008) 322–328. https://doi.org/10.1002/polb.21370.
[402] D. Nordqvist, T.A. Vilgis, Rheological Study of the Gelation Process of Agarose-Based Solutions, Food Biophys. 6 (2011) 450–460. https://doi.org/10.1007/s11483-011-9225-0.

[403] P. Ding, X. Ding, J. Li, W. Guo, O.V. Okoro, M. Mirzaei, Y. Sun, G. Jiang, A. Shavandi, L. Nie, Facile preparation of self-healing hydrogels based on chitosan and PVA with the incorporation of curcumin-loaded micelles for wound dressings, Biomed. Mater. 19 (2024) 025021. https://doi.org/10.1088/1748-605X/ad1df9.
[404] N. Rashid, S.H. Khalid, I. Ullah Khan, Z. Chauhdary, H. Mahmood, A. Saleem, M. Umair, S. Asghar, Curcumin-Loaded Bioactive Polymer Composite Film of PVA/Gelatin/Tannic Acid Downregulates the Pro-inflammatory Cytokines to Expedite Healing of Full-Thickness Wounds, ACS Omega 8 (2023) 7575–7586. https://doi.org/10.1021/acsomega.2c07018.
[405] M. Khaleghi, F. Haghi, M. Gholami, H. Hourfar, F. Shahi, A. Mir Mousavi Zekoloujeh, F. Aliakbari, E. Ahmadi, D. Morshedi, A fabricated hydrogel of hyaluronic acid/curcumin shows super-activity to heal the bacterial infected wound, AMB Express 13 (2023) 29. https://doi.org/10.1186/s13568-023-01533-y.
[406] J. Cai, H. Zhong, W. Tang, F. Wen, Y. Lv, X. Huang, J. Luo, P. Li, Multiple response behaviors of curcumin-loaded ammonium alginate/polyvinyl alcohol hydrogel and its application, Biomass Convers. Biorefinery 14 (2024) 16121–16139. https://doi.org/10.1007/s13399-023-03787-9.
[407] M. Pourmadadi, S.E. Gerami, N. Ajalli, F. Yazdian, A. Rahdar, S. Fathi-karkan, M.A. Aboudzadeh, Novel pH-responsive hybrid hydrogels for controlled delivery of curcumin: Overcoming conventional constraints and enhancing cytotoxicity in MCF-7 cells, Hybrid Adv. 6 (2024) 100210. https://doi.org/10.1016/j.hybadv.2024.100210.
[408] R. Raveendran, G. Bhuvaneshwar, C.P. Sharma, In vitro cytotoxicity and cellular uptake of curcumin-loaded Pluronic/Polycaprolactone micelles in colorectal adenocarcinoma cells, J. Biomater. Appl. 27 (2013) 811–827. https://doi.org/10.1177/0885328211427473.
[409] E.-R.S. Kenawy, E.A. Kamoun, Z.S. Ghaly, A.M. Shokr, M.A. El-Meligy, Y.A.-G. Mahmoud, Novel Physically Cross-Linked Curcumin-Loaded PVA/Aloe vera Hydrogel Membranes for Acceleration of Topical Wound Healing: In Vitro and In Vivo Experiments, Arab. J. Sci. Eng. 48 (2023) 497–514. https://doi.org/10.1007/s13369-022-07283-6.
[410] K.C. Aye, T. Rojanarata, T. Ngawhirunpat, P. Opanasopit, C. Pornpitchanarong, P. Patrojanasophon, Development and characterization of curcumin nanosuspension-embedded genipin-crosslinked chitosan/polyvinylpyrrolidone hydrogel patch for effective wound healing, Int. J. Biol. Macromol. 274 (2024) 133519. https://doi.org/10.1016/j.ijbiomac.2024.133519.
[411] A.A. Shefa, T. Sultana, M.K. Park, S.Y. Lee, J.-G. Gwon, B.-T. Lee, Curcumin incorporation into an oxidized cellulose nanofiber-polyvinyl alcohol hydrogel system promotes wound healing, Mater. Des. 186 (2020) 108313. https://doi.org/10.1016/j.matdes.2019.108313.
[412] J.P.F. Carvalho, M.C. Teixeira, N.S. Lameirinhas, F.S. Matos, J.L. Luís, L. Pires, H. Oliveira, M. Oliveira, A.J.D. Silvestre, C. Vilela, C.S.R. Freire, Hydrogel Bioinks of Alginate and Curcumin-Loaded Cellulose Ester-Based Particles for the Biofabrication of Drug-Releasing Living Tissue Analogs, ACS Appl. Mater. Interfaces 15 (2023) 40898–40912. https://doi.org/10.1021/acsami.3c07077.
[413] G. Guo, X. Li, X. Ye, J. Qi, R. Fan, X. Gao, Y. Wu, L. Zhou, A. Tong, EGF and curcumin co-encapsulated nanoparticle/hydrogel system as potent skin regeneration agent, Int. J. Nanomedicine Volume 11 (2016) 3993–4009. https://doi.org/10.2147/IJN.S104350.

List of figures

Figure 1 The summary of the dissertation work cycle – from research gaps identification to validation of the research hypothesis. Created with Canva. 15
Figure 2 Schematic representation of biomaterials evolution through generations. 17
Figure 3 Evolution of research interest in biomaterials. Data base: Scopus within Article title, abstract and keywords. Search query: (“biomaterial*” OR “biomedical material*”). 17
Figure 4 Evolution of biomaterials generations depicted by the changing research interest. Data base: Scopus within Article title, abstract and keywords. Search queries: 1st generation: (“biomaterial*” OR “biomedical material*”) AND (“first generation” OR “1st generation” OR “bioinert*” OR “inert*” OR “minimal host response” OR “biocompatible”). 2nd generation: (“biomaterial*” OR “biomedical material*”) AND (“second generation” OR “2nd generation” OR “bioactive” OR “bioresorbable” OR “biodegradable” OR “bioglass” OR “hydroxyapatite” OR “calcium phosphate” OR “osteo*” OR “osseo*”). 3rd generation: (“biomaterial*” OR “biomedical material*”) AND (“third generation” OR “3rd generation” OR “biointeractive” OR “regenerative” OR “biomimetic” OR “tissue engineering” OR “scaffold*” OR “extracellular matrix” OR “ECM” OR “molecular signaling” OR “stem cell*” OR “cellular response”). 4th generation: (“biomaterial*” OR “biomedical material*”) AND (“fourth generation” OR “4th generation” OR “smart” OR “electronic*” OR “autonomous” OR “programmable” OR “stimuli-responsive” OR “Theranostic*” OR “nano” OR “cyber” OR “piezoelectric*” OR “sensor” OR “shape-memory” OR “shape memory”). 18
Figure 5 The progression of biomaterials smartness level – from inert materials to fully autonomous systems with closed cycle of sense-response-adapt interactions. Adapted from: [34] under CC BY 4.0 license. 19
Figure 6 The evolution of host biological response to inert implants. Following inert biomaterial implantation, vascular protein adsorption triggers the recruitment and adhesion of innate immune cells like macrophages and platelets. These cells secrete signaling molecules that recruit fibroblasts and stem cells, ultimately leading to collagen deposition and fibrous encapsulation of the implant. Adapted from: [44] under CC BY-NC-ND 4.0 license. 21
Figure 7 Second generation of biomaterials can adapt dynamically to various stimuli, including pH, light, ultrasound and enzymatic triggers, highlighting their responsive behavior in both internal and external environments. Adapted from: [45] under CC BY-NC-ND 4.0 license. 22
Figure 8 The strategies of surface modifications/ used to improve the degree of interactions on the host-biomaterial interface. Adapted from: [34] under CC BY 4.0 license. 23
Figure 9 Mechanisms of cellular adhesion on surfaces functionalized with RGD peptides, KRSR sequences and β-amino acid polymers. Adapted from: [63] under CC BY 4.0 license. 25
Figure 10 Examples of HA-MA hydrogels usage in biointeractive materials. a) Schematic representation of HA-MA/ poly(N-hydroxyethyl acrylamide) hydrogel synthesis for wound dressing applications. The insets provide the chemical structures for the HEAA monomer, HA-MA biomacromolecules and the I-2959 photoinitiator, alongside the resulting network architecture. Adapted from: [71] under CC BY 4.0 license. b) RGD-modified HA-MA hydrogel co-loaded with

cartilaginous inducer Kartogenin (KGN) and anti-aging protein Klotho (HAMA-RGD@KGN/Klotho, HRKK) hydrogel to ameliorate the adverse joint microenvironment and enhance cartilage regeneration. Adapted from: [72] under CC BY 4.0 license. 26
Figure 11 Emerging strategies for optimizing nanocarrier stealth emphasizing PEG conformation (e.g., linear vs. branched), terminal group functionalization and the development of “sheddable” coatings to balance long circulation with efficient cellular uptake. Adapted from: [87] under CC BY-NC-ND 4.0 license. 28
Figure 12 The composite screw prepared utilizing PU as base material, HA as an osseointegrating agent and RGD modification for improved cell signaling. a) schematic visualization of screw components. b) SEM surface images revealing surface size development due to the even distribution of the composite components neat polymer. c) Histological investigation of the screws after implantation showing lower number of inflammatory cells in case of composite screw. Reprinted from Acta Biomaterialia, 103, Yuanchi Zhang, Jinlian Hu, Ruiqi Xie, Yuhe Yang, Jie Cao, Yunhu Tu, Yi Zhang, Tingwu Qin, Xin Zhao, A programmable, fast-fixing, osteo-regenerative, biomechanically robust bone screw, Pages 293-305, Copyright (2020), with permission from Elsevier [97]. 30
Figure 13 Recent trends in biomaterials research. a) Six major focus areas to guide future development of biomaterials: novel materials. Adapted from: [113]. b) Future direction towards the design of stimuli responsive materials with help of machine learning. c) Representation of main material types utilized in modern biomaterials research. Adapted from: [103]. d) The evolution of biocooperation level through the integration of rationally designed synthetic materials with natural agents. Adapted from: [114]. e) Implantable self-powered medical devices (SIMDs) for biomedical applications. Adapted from: [110]. All images were adapted under applicable Creative Commons license. 33
Figure 14 Evolution the polyurethanes share in biomaterials generations depicted by the changing research interest. Data base: Scopus within Article title, abstract and keywords. Search queries: 1st generation: (“biomaterial*” OR “biomedical material*”) AND (“polyurethane*” OR “polyesterurethane*” OR “polyetherurethane*” OR “thermoplastic polyurethane*”) AND (“first generation” OR “1st generation” OR “bioinert*” OR “inert*” OR “minimal host response” OR “biocompatible”). 2nd generation: (“biomaterial*” OR “biomedical material*”) AND (“polyurethane*” OR “polyesterurethane*” OR “polyetherurethane*” OR “thermoplastic polyurethane*”) AND (“second generation” OR “2nd generation” OR “bioactive” OR “bioresorbable” OR “biodegradable” OR “bioglass” OR “hydroxyapatite” OR “calcium phosphate” OR “osteo*” OR “osseo*”). 3rd generation: (“biomaterial*” OR “biomedical material*”) AND (“polyurethane*” OR “polyesterurethane*” OR “polyetherurethane*” OR “thermoplastic polyurethane*”) AND (“third generation” OR “3rd generation” OR “biointeractive” OR “regenerative” OR “biomimetic” OR “tissue engineering” OR “scaffold*” OR “extracellular matrix” OR “ECM” OR “molecular signaling” OR “stem cell*” OR “cellular response”). 4th generation: (“biomaterial*” OR “biomedical material*”) AND (“polyurethane*” OR “polyesterurethane*” OR “polyetherurethane*” OR “thermoplastic polyurethane*”) AND (“fourth generation” OR “4th generation” OR “smart” OR “electronic*” OR

“autonomous” OR “programmable” OR “stimuli-responsive” OR “Theranostic*” OR “nano” OR “cyber” OR “piezoelectric*” OR “sensor” OR “shape-memory” OR “shape memory”). 42
Figure 15 The summary of commonly used raw materials in synthesizing PUs for each of the main materials groups: diisocyanates, catalysts, polyols and chain extenders. 43
Figure 16 The summary of the most common reactions between isocyanate and H-labile groups. Adapted from: [161] under CC BY 3.0 license. 44
Figure 17 Mechanisms of polyurethane synthesis in the a) absence of catalyst, b) presence of a base (nucleophilic) catalyst, c) presence of an acid (electrophilic) catalyst. Adapted from: [195] under ACS AuthorChoice License. 53
Figure 18 Scheme of polyurethane synthesis reaction catalyzed by organotin. Adapted from: [195] under ACS AuthorChoice License. 55
Figure 19 The main strategies of counteracting non-specific adsorption of proteins: a) surface hydrophobization, b) attachment of long, hydrophilic polymers, c) usage of zwitterionic polymers, d) creating steric hindrance or e) surface negatively charging. Adapted from: [217] under CC BY 4.0 license. 57
Figure 20 Schematic representation of the most important biodegradation reactions of polyurethanes: a) polyol ester bond hydrolysis, b) polyol ether bond oxidation, c) urethane bond hydrolysis. 58
Figure 21 Comparison of calcification susceptibility of different polyurethane heart valves. A) polyether-based polyurethane Angioflex® and it’s bisphosphonate-modified version valves before and after calcification. B) (i) Polycarbonate-based polyurethane (ADIAM®) after 20 weeks of implantation, (ii) porcine-based Mosaic® after 10 days and (iii) bovine-based Perimount® after 30 days (animals died after the indicated time for ii and iii implants). Adapted from: [226] under CC BY-NC-ND 4.0 license. 59
Figure 22 Four main groups of most used polyurethane modification methods useful in biomaterials manufacturing: natural polymers, bioactive compounds, drugs and nanoparticles. For each group, the mostly used compounds were described. 60
Figure 23 Examples of polyurethane structure tuning and modifications. On the left there are presented structural designs and on the right the exemplary features. Modifications for: A) electrical conductivity, B) temperature induced shape-memory, C) solubility in water, D) enzymatic degradation susceptibility, E) antibacterial properties, F) reduction of thrombogenesis, G) reduction degradation susceptibility. Adapted from: [205], under CC BY-NC-ND 4.0 license. ... 63
Figure 24 Graphical representation of main fabrication methods for small-scale manufacturing of PU-based blends and composites useful in tissue engineering: hydrogels formation, film casting, SC/PL, electrospinning, foaming and bioprinting. 65
Figure 25 Evolution the hydrogels share in biomaterials generations depicted by the changing research interest. Data base: Scopus within Article title, abstract and keywords. Search queries: 1st generation: (“biomaterial*” OR “biomedical material*”) AND (“hydrogel*” OR “microgel*” OR “nanogel*” OR “polymeric gel*”) AND (“first generation” OR “1st generation” OR “bioinert*” OR “inert*” OR “minimal host response” OR “biocompatible”). 2nd generation: (“biomaterial*” OR

“biomedical material*”) AND (“hydrogel*” OR “microgel*” OR “nanogel*” OR “polymeric gel*”) AND (“second generation” OR “2nd generation” OR “bioactive” OR “bioresorbable” OR “biodegradable” OR “bioglass” OR “hydroxyapatite” OR “calcium phosphate” OR “osteo*” OR “osseo*”). 3rd generation: (“biomaterial*” OR “biomedical material*”) AND (“hydrogel*” OR “microgel*” OR “nanogel*” OR “polymeric gel*”) AND (“third generation” OR “3rd generation” OR “biointeractive” OR “regenerative” OR “biomimetic” OR “tissue engineering” OR “scaffold*” OR “extracellular matrix” OR “ECM” OR “molecular signaling” OR “stem cell*” OR “cellular response”). 4th generation (“biomaterial*” OR “biomedical material*”) AND (“hydrogel*” OR “microgel*” OR “nanogel*” OR “polymeric gel*”) AND (“fourth generation” OR “4th generation” OR “smart” OR “electronic*” OR “autonomous” OR “programmable” OR “stimuli-responsive” OR “Theranostic*” OR “nano” OR “cyber” OR “piezoelectric*” OR “sensor” OR “shape-memory” OR “shape memory”). 75
Figure 26 The most popular natural and synthetic polymers used for development of hybrid hydrogels. Adapted from: [336] under CC BY 4.0 license. 82
Figure 27 Comparison of different approaches for hydrogel crosslinking: physical, chemical and combined. Adapted from: [337] under CC BY 4.0 license. 83
Figure 28 Physical crosslinking methods of hydrogels. Adapted from: [339] under CC BY 4.0 license. 85
Figure 29 Main chemical crosslinking methods of hydrogels: A) enzymatic crosslinking, B) chemical reaction promoted by a cross-linking agent, C) high-energy radiation, D) free-radical polymerization and E) click reactions. Adapted from: [341] under CC BY 4.0 license. 87
Figure 30 Interactions in interpenetrating polymer networks. Adapted from: [342] under CC BY 4.0 license. 88
Figure 31 Structure-property relations in hydrogel design. Adapted from: [344] under CC BY-NC 3.0 license. 89
Figure 32 Illustration of the forces, governing the swelling process of hydrogels, together with the influencing factors. These forces are divided into thermodynamic forces of mixing (π_{mix}), elastic forces of the polymer matrix ($\pi_{elastic}$) and ionic swelling pressure (π_{ionic}). Adapted from: [349] under CC BY-ND 4.0 license. 91
Figure 33 The comparison between behavior of LCST and UCST systems existing as solutions and hydrogels. Adapted from: [352] under CC BY 4.0 license. 93
Figure 34 Comparison of Newtonian and non-Newtonian fluids rheological behavior based on a) shear stress and shear rate and b) viscosity and shear rate relations. c) Shear-thinning behavior of non-Newtonian fluid. d) Relationship between the complex shear modulus (G*) and G′, G″. Adapted from: [353] under CC BY 4.0 license. 94
Figure 35 Comparison of different injectable materials: a) Low-viscosity materials, b) Conventional hydrogels, c) Hydrogels with shear-thinning behavior designed for injection applications. Adapted from: [354] under CC BY-ND 4.0 license. 96
Figure 36 The versatility of possible hydrogel materials design divided into the materials origin, functions and morphology. Adapted from: [355] under CC BY 4.0 license. 97

Figure 37 Comparison of release and drug diffusion kinetics. Adapted from: [356] under CC BY 4.0 license. 98
Figure 38 The effect of different bonds in hydrogel matrix on the rate and controllability of the network degradation. Adapted from: [344] under CC BY-NC 3.0 license. 100
Figure 39 Passive anti-biofouling strategies of hydrogel coatings: A) nonspecific protein adhesion; B) hydration layer; C) bacteria-repelling by chain length and grafting density. Adapted from: [360] under CC BY 4.0 license. 101
Figure 40 Comparison of different active anti-bacterial strategies to the non-fouling strategy. Adapted from: [360] under CC BY 4.0 license. 102
Figure 41 FTIR spectra of the obtained PUs with one type of polyol (ES1, ES2, ET1 and ET2) compared with the Bioflex filament. 123
Figure 42 FTIR spectra of the obtained PUs with polyol mixtures: ET2:ES1, ET2:ET1, ES1:ET1, ES1:ES2, ES2:ET2, ET2:ET1:ES1. 124
Figure 43 Interactions with wet environment. Accelerated hydrolytic degradation behavior of PUs in a) 2 M HCl, b) 5 M NaOH and c) 0.01 M PBS. 124
Figure 44 Changes in the PU structure after 21 days of accelerated hydrolytic degradation tests depicted in FTIR spectra for samples: a) ES1, b) ES1:ET1, c) ES1:ET2:ET1 and in d) macroscopical appearance. 125
Figure 45 Changes in ES1, ES1:ET1 and ET2:ET1:ES1 PUs microstructure observed after 28 days of accelerated hydrolytic degradation tests in 2 M HCl, 5 M NaOH and 0.01 M PBS. Scale bar = 200 μm. 125
Figure 46 Visualization of tensile testing results on PU samples: a) tensile strength, b) permanent elongation and elongation at break. 127
Figure 47 Summary of DMA results: a) storage modulus (G'), b) loss modulus (G''), c) loss factor (tanδ). 128
Figure 48 Fluorescence micrographs of ET2:ET1:ES1 PU 3D printed constructs before and after modification with collagen, diosmin and allantoin. Scale bar = 100 μm. 130
Figure 49 Active substances release profiles form surface-modified ET2:ET1:ES1 PU. 130
Figure 50 Active substances release profiles form hydrogel-modified ET2:ET1:ES1 PU. 131
Figure 51 FTIR spectra of ET2:ET1:ES1 PU compared with its derivatives with Corhydron 25 used during 1st and 2nd stage of synthesis. On the right – chemical structure of hydrocortisone succinate. 131
Figure 52 Corhydron 25 release profiles form ET2:ET1:ES1 PU modified during 1st or 2nd stage synthesis and by surface modification. 132
Figure 53 Comparison of 1st stent type printouts without postprocessing. From left: TPU, Bioflex, Resin BASIC. Reproduced with permission of The Licensor through PLSclear from: [24]. 134
Figure 54 Comparison between FDM and SLA slicers of 2nd project with added supports. 135
Figure 55 Comparison of the designed and printed stents manufactured using different materials and printing technology. Reproduced with permission of The Licensor through PLSclear from: [24]. 136

Figure 56 The visualization of the separated nasal septum (top-right) from MRI scan (top-left – top view, bottom-left – front view, bottom-right – left view) in the 3D Slicer program. Adapted from: [26] under CC-BY 4.0 license. 137
Figure 57 The design of nasal septum cartilage implant: a) technical drawing, b) comparison with the anatomical model extracted from MRI scan, c) 3D model of the implant, d) design of supports for bending test. Adapted from: [26] under CC-BY 4.0 license. 137
Figure 58 Nasal septum implants with supports for bending testing printed with (from left): MediFlex, PCL, PLA, TPU, Bioflex. 138
Figure 59 Graphical output of stress simulation on nasal septum cartilage implant. On the left compression study at 10 N of force, on the right bending study at 8 N of force. Adapted from: [26] under CC-BY 4.0 license. 138
Figure 60 FTIR spectra of the used filaments. Adapted from: [26] under CC-BY 4.0 license... 140
Figure 61 Second heating DSC curves of analyzed filaments. Adapted from: [26] under CC-BY 4.0 license. 141
Figure 62 Interactions with wet environment. Accelerated hydrolytic degradation behavior in a) 2 M HCl, b) 5 M NaOH and c) 0.01 M PBS. d) hydrophilicity determination by water contact angle method. Adapted from: [26] under CC-BY 4.0 license. 143
Figure 63 Changes in contact angle after modification with collagen, diosmin and allantoin: a) PLA, b) PCL, c) MediFlex, d) TPU. 143
Figure 64 Results of compression mechanical evaluation. Exemplary stress-strain curves in a) longitudinal and b) transversal directions, with respect to the print direction. Comparison of c) Young modulus and d) maximal stress between tested filament types. Adapted from: [26] under CC-BY 4.0 license. 145
Figure 65 Exemplary bending stress-strain curves for nasal septum implant manufactured with the tested filaments compared with the simulated nasal cartilage behavior. Adapted from: [26] under CC-BY 4.0 license. 146
Figure 66 L-929 cell survival rates following Bioflex extract treatment. Cytotoxicity grading: none (>80 % viability), mild (60-80 %), moderate (40-60 %) and severe (<40 %). Statistical significance deviations were identified using a Tukey test at a 0.05 significance level and were denoted by asterisks (*, **, ***) relative to the control group at 24, 48 and 72 h, respectively. Adapted from: [26] under CC-BY 4.0 license. 146
Figure 67 Morphological evaluation of L-929 cells treated with different extract concentrations after 24, 48 and 72 h. Control refers to cells in extract-free medium. Scale bar - 100 µm. Adapted from: [26] under CC-BY 4.0 license. 147
Figure 68 Changes of the hydrogel samples mass during synthesis in relation to the introduced amount of reagents during freeze-thaw process (red columns), after 24 h of soaking in water (blue columns) and after 24 h of swelling test (green columns). Additionally, the change of weight of final samples was denoted as Synthesis (magenta columns). 151

Figure 69 Comparison of macroscopic appearance of hydrogels after synthesis. From the top: samples based on AG, 0.6AG0.4PVA and 0.6AG0.4PVP. From the left: unmodified hydrogels, samples modified with 2.5 % and 5 % curcumin, respectively. 151
Figure 70 Selected micrographs of dried hydrogels: AG (1st row), AG0.6/PVA0.4 (2nd row), AG0.6/PVP0.4 (3rd row) in their unmodified (1st column) form and modified with 2.5 % (2nd column) and 5 % (3rd column) of curcumin. Scale bar = 500 μm. 152
Figure 71 Experimental swelling data of a) unmodified and b) curcumin-modified samples. Experimental swelling data (gray) and curves fitted with first order (red), second order (blue) and Korsmeyer – Peppas (magenta) kinetic models for c) 0.6AG/0.4PVA and d) 0.6AG/0.4PVA/2.5CUR. 153
Figure 72 Summary of hydrogel polymer network parameters calculations based on hydrogel swelling. a) First order equilibrium swelling (W_{eq}) and swelling kinetics constant (K_1), b) Second order equilibrium swelling and swelling kinetics constant (K_2), c) Korsmeyer-Peppas swelling kinetics constant (K_{KP}) and diffusion exponent (n), d) Average molecular weight between cross-links (M_c) and average density (Q_c) of hydrogel network. 154
Figure 73 FTIR spectra of a) unmodified and b) curcumin-modified hydrogels. 157
Figure 74 Comparison of FTIR spectra of unmodified and curcumin-modified hydrogels at 1800-800 cm^{-1} range. 158
Figure 75 Summary of rheological measurements: a) temperature sweep, b) frequency sweep at 1 % strain, c) frequency sweep at 2.5 % strain, d) frequency sweep at 5 % strain. Storage modulus (G′, solid lines), loss modulus (G″, dashed lines) and loss factor (tanδ, dotted lines) were presented for AG0.6/PVA0.4 (green) and AG0.6/PVA0.4/2.5CUR (orange) hydrogels. 158
Figure 76 Constructs obtained during preliminary 3D printing tests on: AG0.6/PVA0.4 (a) top view, b) side view) and AG0.6/PVA0.4/2.5CUR (c) top view, d) side view). 161
Figure 77 Photographs of Petri dishes after modified Kirby-Bauer disk diffusion test against Staphylococcus aureus ATCC 25923 (on the left) and Staphylococcus epidermidis ATCC 12228 (on the right). White discs (control) - AG0.6/PVA0.4. Other disks - AG0.6/PVA0.4/5CUR. 161
Figure 78 Antimicrobial activity of curcumin-modified hydrogels against S. aureus ATCC 25923 (first row) and S. epidermidis ATCC 12228 (second row) in the modified Kirby-Bauer disk diffusion test. First column: unmodified AG0.6/PVA0.4, second column: AG0.6/PVA0.4/2.5CUR, third column: AG0.6/PVA0.4/5CUR. Yellow arrow indicates the edge of the hydrogel, blue arrow - edge of the inhibition zone/beginning of the intense bacterial growth zone and pink arrows - bacterial growth inhibition zone. Scale bar = 500 μm. 162
Figure 79 Test setup for antibacterial activity examination with contact method. Bacteria solution was placed on the surface of each hydrogel sample and covered with coverslip. 163
Figure 80 Antimicrobial activity of AG0.6/PVA0.4/2.5CUR hydrogel against S. aureus ATCC 25923 evaluated using the contact method. Data presented as number of a colony-forming units (CFU) at the start of the test and after 90 and 180 minutes of bacterial cells contact with different hydrogel samples. * - significantly different from corresponding unmodified hydrogel CFU (AG0.6/PVA0.4) at p = 0.001. 164

Figure 81 Visual comparison of the grown bacteria colonies from undiluted bacteria solution rinsed from the hydrogel surfaces after 3 hours of contact. On the left - AG0.6/PVA0.4/2.5CUR, on the right - AG0.6/PVA0.4. 164
Figure 82 Comparison of implants models designed for usage as nasal implants: 1 – solid septum implant with supports for bending testing; 2 – previous prototype of porous nasal cartilage implant with supports for bending testing developed in Chapter 7; 3 – next iteration of porous nasal cartilage implant with reduced thickness; 4 – an implant designed to support the cartilage tissue of the nasal septum after surgery; 5, 6 – development of the concept of intrasinus stents from Chapter 7, adapted to the possibilities of FDM printing- cylindrical and dome designs, respectively. 167
Figure 83 Comparison between different triangular infill density of design 4. From the left: 75, 60 and 45 %..... 167
Figure 84 A comparison of models designed for alternative applications: 7, 8 – porous structures designed as substrates for wound dressings and surgical meshes, respectively; 9, 10 – flexible bone fillings (loose and compact, respectively). 168
Figure 85 Evaluation of batch printing of 36 model 4 implants using ET2:ET1:ES1 PU. 168
Figure 86 The compete biodegradable core-shell dual-delivery system based on ET2:ET1:ES1 PU modified with Corhydron 25 during 1st step of synthesis manufactured using models 3, 4, 5, 6 8 and 9 and coated with AG0.6/PVA0.4/2.5CUR hydrogel. 169
Figure 87 L-929 cell survival rates following a) AG0.6/PVA0.4 and b) AG0.6/PVA0.4/2.5CUR extract treatment. Statistical significance deviations were identified using a Tukey test at a 0.05 significance level and were denoted by asterisks (*) relative to the control group..... 171
Figure 88 L-929 cell survival rates following ET2:ET1:ES1 PU modified with Corhydron 25 extract treatment: a) standalone PU, b) composite system with AG0.6/PVA0.4/2.5CUR hydrogel coating. Statistical significance deviations were identified using a Tukey test at a 0.05 significance level and were denoted by asterisks (*) relative to the control group. 171

List of tables

Table 1 Key advantages, disadvantages, applications and modification methods of the selected most popular polymeric biomaterials 35
Table 2 Common diisocyanates in polyurethane synthesis 47
Table 3 Common chain extenders in polyurethane synthesis 48
Table 4 Common polyols in polyurethane synthesis 51
Table 5 Examples of polyurethane-based biomaterials modified with natural active substances. 68
Table 6 Commercially available polyurethanes and their chemical modification, processing and targeted application in skin engineering. 72
Table 7 Commercially available PU wound dressings (films or foams) found on the WoundSource, an annual wound care product reference guide. 73
Table 8 Overview of materials utilized in the fabrication hydrogels depending on the source material origin. Originally published in [23]. PAA: poly(acrylic acid), PAAm: polyacrylamide, PNIPAAm: poly(N-isopropylacrylamide), Gel-MA: gelatin methacrylate, PEG-DA: poly(ethylene glycol)-diacrylate. 79
Table 9 Polyurethanes prepolymers compositions. Amount of polyol was calculated to obtain 8 wt% of free NCO groups in prepolymer. 108
Table 10 Hydrogel samples and their compositions. 110
Table 11 Human cartilage properties used in the simulated stress analysis. 112
Table 12 Selected properties of commercial filaments. NG – information not given. 112
Table 13 FDM 3D printing parameters 113
Table 14 Parameters of calibration curves for selected active substances. 117
Table 15 Summary of the tensile testing results on PU samples 127
Table 16 Results of compression testing of different types of stent models. 134
Table 17 Results of stress simulation on nasal septum cartilage implant. Results with * were obtained with a prompt “The deformation is large compared to the model size. Verify that load and constraint settings are appropriately scaled”. Adapted from: [26] under CC-BY 4.0 license. ... 138
Table 18 MFR and MVR values of tested filaments under 2.16 kg load and temperatures of print suggested by manufacturers. Adapted from: [26] under CC-BY 4.0 license. 141
Table 19 Swelling kinetics parameters of hydrogels calculated using different mathematical models: first and second order and Korsmeyer - Peppas. 155
Table 20 Summary of scientific achievements 178